MEASUREMENT AND MODELLING OF INTERFACIAL TENSION AND VISCOSITY OF RESERVOIR FLUIDS

by

Khalil Kashefi

Submitted for the degree of Doctor of Philosophy

In

Petroleum Engineering

Heriot-Watt University

Institute of Petroleum Engineering

January 2012

ABSTRACT

The knowledge of reservoir fluids physical properties is crucial in upstream and downstream processes of petroleum industry. Viscosity and interfacial tension are among the most influential parameters on fluid behaviour. These properties have considerable effects on fluid flow characteristics and consequently in many oil and gas production and processing aspects from porous media to surface facilities. Hence, accurate estimation of the mentioned fluid properties plays a significant role in reservoir development. However, experimental data are scarce at high pressure and high temperature (HPHT) conditions. The work presented in this thesis is an integrated experimental and modelling investigation of viscosity and interfacial tension of petroleum reservoir fluids over a wide range of pressure and temperature conditions.

Several series of experimental data on the viscosity of reservoir fluids were generated at high pressure and high temperature conditions (up to 20,000 psia and 200 °C). Experiments were conducted on three binary hydrocarbon systems and three synthetic and real multi-component mixtures, in addition to investigating the effect of dissolved water on the viscosity of the above fluids. Besides, the influence of oil-based mud filtrate on the viscosity of various dead oil samples also was studied as part of this thesis. The effect of different salt concentrations on the interfacial tension of gas-brine systems over a wide range of pressure and temperature conditions also was studied experimentally.

The experimental data generated were employed to evaluate, improve and propose predictive models to estimate the mentioned physical properties. A new approach to retrieve the viscosity of original fluid (clean dead oil) from contaminated sample was introduced. Also a novel technique for predicting the gas-water (brine) interfacial tension was outlined. The proposed techniques and models were evaluated against independent experimental data generated in this work and the data gathered from open sources. Predictions of the developed methods were in good agreement with the experimental data.

Dedicated to my wife, Soheila

Without her patience and understanding, this would have never been written.

ACKNOWLEDGMENTS

This thesis is submitted in partial fulfilment of the requirements for the Ph.D. degree at Heriot-Watt University. This work has been conducted at the Institute of Petroleum Engineering from February 2008 to November 2011 under the supervision of Professor Bahman Tohidi and Dr. Antonin Chapoy.

The project has been financed by grants by a Joint Industrial Project (JIP) conducted at the Institute of Petroleum Engineering, Heriot-Watt University. The JIP is supported by Total, Marathon Oil Corporation and Schlumberger, which is gratefully acknowledged.

I would like to thank my advisor, Professor Bahman Tohidi for providing me the opportunity to work with such a scientifically interesting and challenging project in the Reservoir Fluid Study group, and would like to express my sincere gratitude for his help and guidance throughout this project. Special and countless thanks go to Dr. Antonin Chapoy for all his continuous help and support, his inspiring discussions, and his huge enthusiasm during the time we worked together. Also in this regard, I would like to thank my colleague Mr. Keith Bell for his close collaboration. Additionally, I greatly appreciate the help from Mr. Rod Burgess and all the colleagues making my stay in Edinburgh very pleasant and provided me with any help needed. I wish to express my thanks to the Institute of Petroleum Engineering, Heriot-Watt University.

Khalil Kashefi

ACADEMIC REGISTRY
Research Thesis Submission

Name*:*	**Khalil Kashefi**		
School/PGI:	**Institute of Petroleum Engineering**		
Version: *(i.e. First, Resubmission, Final)*	Final	Degree Sought (Award **and** Subject area)	**PhD in Petroleum Engineering**

Declaration

In accordance with the appropriate regulations I hereby submit my thesis and I declare that:

1) the thesis embodies the results of my own work and has been composed by myself
2) where appropriate, I have made acknowledgement of the work of others and have made reference to work carried out in collaboration with other persons
3) the thesis is the correct version of the thesis for submission and is the same version as any electronic versions submitted*.
4) my thesis for the award referred to, deposited in the Heriot-Watt University Library, should be made available for loan or photocopying and be available via the Institutional Repository, subject to such conditions as the Librarian may require
5) I understand that as a student of the University I am required to abide by the Regulations of the University and to conform to its discipline.

* *Please note that it is the responsibility of the candidate to ensure that the correct version of the thesis is submitted.*

Signature of Candidate*:*		Date:	

Submission

Submitted By *(name in capitals):*	**KHALIL KASHEFI**
Signature of Individual Submitting:	
Date Submitted:	

For Completion in the Student Service Centre (SSC)

Received in the SSC by *(name in capitals):*			
Chapter 1Method of Submission *(Handed in to SSC; posted through internal/external mail):*			
Chapter 2*E-thesis Submitted* ***(mandatory for final theses)***			
Signature:		Date:	

TABLE OF CONTENTS

LISTS OF TABLES

LISTS OF FIGURES

LIST OF PUBLICATIONS BY THE CANDIDATE

Kashefi, K., Chapoy, A., Tohidi, B., *Prediction of gas-water interfacial tensions: a new approach using gas solubility*, Energy and Fuels, Submitted paper.

Kashefi, K., Chapoy, A., Bell, K., Tohidi, B., *Viscosity of binary and multicomponent hydrocarbon fluids at high pressure and high temperature conditions: measurements and predictions*, Journal of Petroleum Science and Engineering, Submitted paper.

Kashefi, K., Chapoy, A., Tohidi, B., *Prediction of gas-water interfacial tensions: a new approach using gas solubility*, PetroPhase 2011, 12th International Conference on Petroleum Phase Behaviour and Fouling, 10-14 July, London, UK.

LIST OF MAIN SYMBOLS

A_{I-S}	Interfacial tension-solubility constant
BST	Brine surface tension
IFT	Interfacial tension
J	Jacobian matrix of the first derivative of global error to weight
F_η	Corresponding state reducing factor
N	Number of feed inputs
OBM	Oil-base drilling mud
$O_{k,I}$	Output of the i neuron within the hidden k layer
P	Pressure (psia)
P_{ref}	Equivalent pressure
S_{g-w}	Solubility of gas in water (mole fraction)
$S_{k,I}$	Weighted sum
T	Temperature (°C)
T_r	Reduced temperature
T^*	Reduced temperature
T_{ref}	Equivalent temperature
VCF	Viscosity correction factor
V_c	Critical molar volume (ft^3/lb mol)
WST	Water surface tension
a_i	Correlation coefficients
b_i	Correlation coefficients
b	Bias term,
c_i	Correlation coefficients
d_i	Correlation coefficients
d'_i	Correlation coefficients
err^k	Residue vector
i_i	Correlation coefficients
I_i	Input vector
j_i	Correlation coefficients
k_i	Correlation coefficients
l_i	Correlation coefficients
m_i	Correlation coefficients
w	Weight parameter

ε/k	Energy scaling parameter (K)
μ	Step values of the Levenberg-Marquardt method
ζ	Viscosity reducing parameter
ρ_r	Reduced density
η_o	Dilute gas viscosity (cP)
η	Viscosity (cP)
η_{ref}	Viscosity of reference fluid (cP)
$\Delta\eta$	Excess viscosity (cP)
ψ_η^*	Effective cross section term

CHAPTER 1

INTRODUCTION

The knowledge of the physical properties of reservoir fluids plays a significant role in the upstream and downstream processes of the petroleum industry. The exploration and production of oil and gas is now facing the challenge of deeper hydrocarbon reservoirs with extreme pressure and temperature conditions. High pressure and high temperature (hereafter, HPHT) conditions in these reservoirs lead to higher exploitation costs in comparison with the development expenses of conventional reservoirs. Furthermore, reservoir fluids can be contaminated with oil-based mud filtrate in down-hole sampling, which can have a considerable influence on the hydrocarbon properties. Also, the presence of water and salts could have a significant effect on the behaviour of reservoir fluids.

Viscosity and interfacial tension are among the most influential parameters on fluid flow characteristics. All fluids in nature are known to offer some resistance to the applied shearing force. This resistance is quantified by viscosity, which reflects the internal molecular cohesion of the fluid and the rate of transfer of molecular momentum as a result of this shearing force. Moreover, when two fluids (e.g. liquid and gas) are in contact with each other, they are separated by a thin layer of uniform thickness called the interface, which results from the imbalance of molecular forces in this region caused by the physical attraction between molecules. At the interface, there exist more force-fields than in the bulk of phases and consequently those atoms at the interface have different internal pressure, intermolecular spacing and chemical potential (Danesh 1998). This physical behaviour of the interfaces is determined by the values of the contact phases' interfacial tension.

The two properties mentioned above have significant effects on fluid flow behaviour and consequently on many aspects of oil and gas exploitation and processes. Capillary number (a dimensionless group) for example, which has effect on fluid movement from multiphase flow behaviour in pipeline to relative permeability in porous media, is a ratio of viscous force over interfacial tension. The information about the fluids' viscosity is

essential to investigate the flow characteristics of hydrocarbon mixtures where transfer of momentum occurs. Accurate viscosity data for all flowing phases in multi-phase flow and hydraulic calculations over a wide range of operational conditions is vital for all sections of production evaluation and process design. Besides viscosity, reliable information on interfacial tension (IFT) is necessary in both petroleum and process engineering. In enhanced oil recovery (EOR) operations the relative permeability controls the flow behaviour of reservoir fluids in porous media. This parameter is strongly related to the interfacial tension at high pressure conditions (Bardon *et al.,* 1980). Reservoir processes such as water-oil contact movement, water alternating gas drive (WAG), trapping of hydrocarbons by water flood and depressurisation can be affected by the IFT of a hydrocarbon-water system (Bahramian *et al.,* 2007).

As is usually the case with many fluid properties, performing the measurements of *viscosity* and *interfacial tension* for various hydrocarbon systems under a wide range of pressures and temperatures would be a very expensive and protracted task. As a result, there is a growing need for developing *predictive techniques* for consistent estimation of viscosity and IFT values. Furthermore, generating some reliable *experimental data* can be a basis for evaluating the accuracy of the proposed models.

1.1 Literature Review

Petroleum and chemical industries employ several methods to predict the viscosity of fluids. The techniques described in the literature can be categorised as empirical, semi-theoretical, and theoretical models. Several reviews exist in the open sources that report viscosity prediction models for pure hydrocarbons and hydrocarbon mixtures (Boned *et al.,* 2003, Mehrotra *et al.,* 1996 and Yucel, 2005). Empirical and semi-theoretical approaches for viscosity calculation are more popular in the industry. Approaches like residual viscosity (Lohrenz *et al.,* 1964), corresponding states (Pedersen *et al.,* 1987) and in recent years, the artificial neural network (ANN) are of great interest to engineers for viscosity estimation.

Investigation of produced fluids from a reservoir can present important information on its phase behaviour and flow characteristics within its porous media. Oil-based muds (OBM) are frequently used drilling fluids that have the advantage of reducing drilling-induced damage to hydrocarbon bearing formation. However, miscibility of oil-based mud filtrate in reservoir fluids can lead to contamination of the obtained samples.

Subsequently, the original fluid properties and in particular the viscosity of samples can be affected and contaminated with OBM. In some cases, the presence of contamination may have a drastic impact on viscosity (this work), so retrieving the viscosity of original fluid from contaminated samples is of major importance to study fluid behaviour. In addition to the influence of mud on the fluid viscosity, the effect of dissolved water at high temperatures is of interest because it is almost always part of the reservoir fluid, and water will be more soluble in hydrocarbon phase at extreme conditions. It has been reported (Gozalpour *et al.,* 2005) that dissolved water may have an enormous impact on the physical properties of reservoir fluids, including viscosity.

There are various types of viscometers available for petroleum industry. Capillary tube, rolling ball, falling body and rotational viscometers are some of the well-known instruments in viscosity measurement. Capillary tube viscometers are the most commonly used equipment to perform fluid viscosity tests. They are not complex equipment (Tropea *et al.,* 2007). The concept of a capillary tube viscometer is based on the relation between the pressure difference (pressure drop) of the inlet and the outlet ends of the tube and the viscosity of the fluid. Knowing the pressure drop in laminar flow conditions, the Hagen-Poiseuille law (Bird *et al.,* 1960), which is a recognized theoretically based equation, can be employed to estimate the viscosity of the flowing fluid.

Several theories were employed in the prediction of interfacial tension between the hydrocarbon and aqueous phases. The Parachor method (Weinaug *et al.,* 1943) and the scaling law (Lee *et al.,* 1984) are the most commonly used methods of predicting the interfacial tension of liquid-vapour systems and have been evaluated and modified (Danesh *et al.,* 1991). However, these are not recommended for estimation of hydrocarbon and water IFT systems (Danesh, 1998). Some of the IFT predictive methods (Firoozabadi *et al.,* 1988 and Argaud, 1992) used the density difference of contacted phases and the reduced temperature of hydrocarbon mixtures as input data to make simple correlations. There are also some techniques that require mutual solubility values of adjacent phases to calculate the value of interfacial tension, which have been studied and reviewed in different sources (Bahramian *et al.,* 2004 and Ayirala *et al.,* 2006).

Several techniques for measurement of interfacial tension between two immiscible fluid phases have been proposed in scientific and technical texts. Methods such as the rising

bubble, pendant drop, sessile drop, du Nouy ring, Wilhelmy plate and spinning drop are discussed in different sources. The nature of the neighbouring fluids in IFT tests has the most important role in the selection of a method for interfacial tension measurement. Rusanov and Prokhorov (1996) presented a wide and complete investigation of various types of IFT measurement methods, along with a consideration of the theory behind each method. In addition, Drelich *et al.,* (2002) reviewed the accuracy and suitability of common methods used in performing interfacial tension tests. The pendant drop and rising bubble methods are among the standard techniques in IFT measurement. In the pendant drop method, a liquid droplet (heavier phase) requires to be suspended in the equilibrated vapour or liquid (lighter phase). By determining the droplet dimensions and analyzing the curved interface shape using the Young-Laplace equation, the IFT can be calculated. In case of using the rising bubble method, a bubble will be up-ward in the denser phase. The IFT calculation procedure for both methods is similar. As the mentioned techniques do not require advanced facilities, these are popular in the research area (Drelich *et al.,* 2002).

The reviews on literature are more extended in each chapter of this work.

1.2 Objectives and Brief Outline

The major objectives of the present work were to generate reliable experimental data on the viscosity and interfacial tension of reservoir fluids at high pressure and high temperature conditions. The data obtained were employed to evaluate, improve and propose predictive models to compute the mentioned physical properties. In addition, the effects of oil-based mud filtrate and dissolved water on the viscosity of various hydrocarbon mixtures were studied as part of this thesis. The impact of salt on interfacial tension of gas-brine systems was also investigated. A brief outline of each chapter's content is given below.

An explanation of the materials employed, experimental equipment and procedures for conducting viscosity and IFT measurements is provided in Chapter 2. Also, the methods of preparing the synthetic hydrocarbon mixtures and performing the density tests are detailed in this chapter.

Experimental viscosity data at high pressure and high temperature were measured and reported in Chapter 3 for three binary hydrocarbon systems: methane-heptane, methane-

decane and methane-toluene and three multi-component mixtures: a natural gas, a gas condensate and a synthetic volatile oil. The measurements were conducted in a HPHT rig equipped with a capillary tube at pressures ranging from 5,000 to 20,000 psia and temperature up to 200 °C. The experimental viscosity data generated for these mixtures were used to evaluate the performance of the proposed viscosity techniques as well as the models from the literature.

In Chapter 4, a new approach to retrieve the viscosity of the original fluid from contaminated samples is introduced. To evaluate this method, a series of viscosity experiments on three different dead oils originating from various geographical locations were performed. All the dead oils were intentionally contaminated with oil-based mud filtrate at different levels of contamination from 10 to 75 weight percent and the viscosity tests were also carried out on the contaminated samples. The experimental viscosity data were measured with a rolling ball viscometer. The temperature range for this series of tests was between 20 °C to 72 °C at atmospheric pressure.

The effect of dissolved water on the viscosity of hydrocarbon systems at high pressure and high temperature conditions was systematically investigated and presented in Chapter 5. The viscosity tests for three binary hydrocarbon systems and three multi-component mixtures with dissolved water were carried out and were compared with the viscosity value of the same hydrocarbon systems in water-free conditions. The HPHT facility, which is equipped with a capillary tube viscometer, was employed to perform the viscosity measurements.

A novel technique (named IFT-solubility) for predicting the gas-water (brine) interfacial tension is outlined in Chapter 6. This method is based on the observation that the IFT of gas-water systems at the water vapour pressure (zero solubility of gas in water) tends to the water surface tension. Methane, ethane, propane, nitrogen, carbon dioxide and hydrogen sulphide are the gases that were investigated in this work. This new approach was extended to binary and multi-component systems. The experimental data for mixtures were used to evaluate the performance of the proposed approach. A series of interfacial tension experimental data was generated on a methane-brine system. Different concentrations of salt were employed to investigate the effect of brine on IFT. These data were used to evaluate the capability of the IFT-solubility method in interfacial tension prediction of gas-brine systems.

Chapter 7 presents the conclusions of this study and recommendations for future work.

References

Ayirala, S.C. and Rao, D.N., 2006, *Solubility, miscibility and their relation to interfacial tension in ternary liquid systems*, Fluid Phase Equilibria, **249**, 82-91

Bahramian, A., Danesh, A., Gozalpour, F., Tohidi, B. and Todd, A.C., 2007, *Vapour–liquid interfacial tension of water and hydrocarbon mixture at high pressure and high temperature conditions*, Fluid Phase Equilibria, **252**, 66-73

Bahramian, A., Danesh, A., 2004, *Prediction of liquid–liquid interfacial tension in multi-component systems*, Fluid Phase Equilibria, **221**, 197–205

Bardon, C. and Longeron, D. G., 1980, *Influence of Very Low Interfacial Tension on Relative Permeability*, SPE **7609-PA**, 391-401

Bird, R. B., Stewart, W. E. and Lightfoot, E. N., 1960, *Transport Phenomena*, Wiley & Sons Inc., New York

Boned, C., Zéberg-Mikkelsen, C.K., Baylaucq, A. and Daugé, P., 2003, *High-pressure dynamic viscosity and density of two synthetic hydrocarbon mixtures representative of some heavy petroleum distillation cuts*, Fluid Phase Equilibria **212**, 143–164

Danesh, A., 1998, *PVT and Phase Behaviour of Petroleum Reservoir Fluids*, Elsevier Science B. V., The Netherlands

Danesh, A., Dandekar, A., Todd, A. C. and Sarkar, R., 1991, *A Modified Scaling Law and Parachor Method for Improved Prediction of Interfacial Tension of Gas Condensate Systems*, SPE **22710**, Proceeding of the 66th Annual Conference

Drelich, J., Fang, Ch., White, C.L., 2002, *Measurement of interfacial tension in fluid-fluid systems*, Encyclopaedia of Surface and Colloid Science by Marcel Dekker, Inc., 3152-3166

Gozalpour, F., Danesh, A., Fonseca, M., Todd, A.C., Tohidi, B. and Al-Syabi, Z., 2005, *Physical and Rheological Behaviour of High-Pressure/High-Temperature Fluids in Presence of Water*, SPE **94068**

Lee, S. T. and Chien, M. C. H., 1984, *A New Multicomponent Surface Tension Correlation Based on Scaling Theory*, SPE **12643** presented at the SPE/DOE Enhanced Oil Recovery Symposium, Tulsa, Oklahoma

Lohrenz, J., Bray, B. G. and Clark, C. R., 1964, *Calculating Viscosities of Reservoir Fluids from Their Compositions*, JPT, **Oct.**, 1171 - 1176

Mehrotra, A.K., Monnery, W.D., and Svrcek, W.Y., 1996, *A review of practical calculation methods for the viscosity of liquid hydrocarbons and their mixtures*, Fluid Phase Equilibria, **117**, 344-355

Pedersen, K. S., and Fredenslund, Aa., 1987, *An Improved Corresponding States Model for the Prediction of Oil and Gas Viscosities and Thermal Conductivities* Chem. Eng. Sci., **42**, 182-186

Rusanov, A.I and Prokhorov, V.A., 1996, *Interfacial Tensiometry*, Elsevier, Amsterdam

Tropea, C., Yarin, A. L. and Foss, J. F., 2007, Springer handbook of experimental fluid mechanics", **Vol. 1**

Weinaug, C. F. and Katz, D. L. 1943, *Surface Tension of Methane - Propane Mixtures*, I & EC, **35,** (2), 239 - 246

Yucel, H. G., 2005, *Empirical and Semi-theoretical Methods for Predicting the Viscosity of Binary n-Alkane Mixtures*, International Journal of Thermophysics, **26**, (6), 1759- 1768

CHAPTER 2

EXPERIMENTAL MATERIALS, EQUIPMENTS AND PROCEDURES

2.1 Introduction

The existing viscosity and interfacial tension experimental data of reservoir fluids are relatively scarce at high pressure and high temperature conditions and most of the available data are in the range of low to medium pressure and temperature. This is mostly due to technical limitations in conducting the measurements in extreme conditions. Since the number of deep reservoirs exploration is increasing, it is necessary to obtain experimental data at HPHT conditions. The potential HPHT reservoirs have increased with a factor 3 to 6 between 2001 and 2005 (www.hse.gov.uk). For example, Shearwater field with the depth of about 4,545 m has the pressure of 15,000 psia and temperature of about 180 °C and Elgin-Franklin field has the pressure of about 16,500 psia and temperatures of 190 °C. The mentioned reservoirs are located in the North Sea. Part of the present work is focused on performing viscosity and interfacial tension tests at high pressure and high temperature conditions. Furthermore, to study the effect of drilling fluids on the viscosity of crudes, a number of tests were also carried out.

The materials, compositions of the fluids and preparation of the study samples are presented in this chapter. The experimental facilities and methods for performing the viscosity and interfacial tension measurements are also detailed.

2.2 Materials and Fluid Preparation

Viscosities and interfacial tensions of various types of binaries, multi-components and real fluids of hydrocarbons were measured in this study. The following sections give more details on the materials and preparation of the mentioned mixtures:

2.2.1 *Materials*

To make the different synthetic mixtures which were needed in this work, the following compounds were used:

- Methane (Grade N4.5, Air Products Ltd.),
- *n*-Pentane (Aldrich, anhydrous, >=99%),
- *n*-Heptane (99+%, over Molecular Sieve, AcroSeal®, Acros Organics, New Jersey, USA),
- *n*-Decane (Aldrich, anhydrous, >=99%),
- *n*-Hexadecane (Aldrich, anhydrous, >=99%),
- *n*-C_{21} (Aldrich, 98%),
- Toluene (water < 30ppm, AcroSeal®, Acros Organics, New Jersey, USA),
- NaCl (Fisher BioReagents, >=99.5%, USA).

In order to perform viscosity tests with Ruska rolling ball viscometer and also to calibrate this set up, some standard fluids were employed. The viscosity data of the mentioned standard fluids are reported in Table 2.1. The calibration technique is outlined later in the current chapter. The standard fluids were selected in a way that the range of viscosities of interest can be covered:

- n-Tetradecane (Aldrich, anhydrous, >=99%),
- Standard fluids types N10, S20 and S2000 (Paragon Scientific Limited).

Table 2.1 Viscosity data of the standard fluids used for calibration of the Ruska rolling ball viscometer: Tetradecane (Ducoulombier et al. 1986) and standard fluids types N10, S20 and S2000 (Paragon Scientific Ltd.)

Temperature / °C	Viscosity *n*C_{14} / cP	Viscosity Type N10 / cP	Viscosity Type S20 / cP	Viscosity Type S2000 / cP
20	2.330	17.27	35.550	7117
40	1.600	8.229	14.930	1495
60	1.150	4.675	7.730	429.4
80	0.878	2.992	4.617	160.3

2.2.2 *Synthetic Fluids*

The synthetic mixtures were gravimetrically prepared with the desired compositions in a solvent cleaned and evacuated, 15 cc (316 stainless steel) HPHT pressure vessel. The binary and multi-component fluids for this work are:

- Methane / *n*-heptane,
- Methane / *n*-decane,
- Methane / toluene,
- Five-component synthetic volatile oil (methane / *n*-pentane / *n*-decane / *n*-hexadecane / *n*-C_{21}).

The nominal mole percentage of binary mixtures is 40 mole% for methane and 60 mole% for the other compounds. To make the dry samples, care was taken during the preparation of these fluids to minimise the anhydrous (water-free) hydrocarbons contact with air. Anhydrous chemicals were used to minimise the risk of water being present in the samples. Molecular weights, measured weights, mole percents of the added components and the uncertainties of the mole percent measurements (calculated by propagation of errors law that is detailed in Section 2.4.5) are available in Table 2.2 to Table 2.5.

Table 2.2 Composition of gravimetrically prepared methane/n-heptane binary mixture

Component	Molecular Weight (gm/gm-mole)	Mass (grams)	Composition mole%	±
n-Heptane	100.20	4.655	58.0	0.05
Methane	16.04	0.540	42.0	0.09

Table 2.3 Composition of gravimetrically prepared methane/n-decane binary mixture

Component	Molecular Weight (gm/gm-mole)	Mass (grams)	Composition mole%	±
n-Decane	142.29	5.198	61.0	0.07
Methane	16.04	0.375	39.0	0.11

Table 2.4 Composition of gravimetrically prepared methane/toluene binary mixture

Component	Molecular Weight (gm/gm-mole)	Mass (grams)	Composition mole%	±
Toluene	92.14	6.921	59.8	0.04
Methane	16.04	0.811	40.2	0.06

Table 2.5 Composition of gravimetrically prepared synthetic volatile oil

Component	Molecular Weight (gm/gm-mole)	Mass (grams)	Composition mole%	±
Methane	16.04	1.585	86.5	0.102
n-Pentane	72.15	0.136	1.7	0.012
n-Decane	142.28	0.295	1.8	0.006
n-Hexadecane	226.44	0.478	1.8	0.004
n-C_{21}	296.57	2.778	8.2	0.007

Different amounts of distilled water were added to the above anhydrous mixtures to prepare samples for testing effect of water as part of this investigation. The nominal levels of added water to the samples were 2 mole% and 5 mole%. The compositions of final fluids are shown in Tables 2.6 to 2.11 along with their dry compositions for comparison. It was verified that 2 mole% and 5 mole% of water would be fully dissolved in the mix of hydrocarbons (calculated with VPT EoS which is discussed in Chapters 3 and 6) in the temperatures and pressures ranges of interest, so there would be no free-water during the viscosity tests.

Table 2.6 Composition of gravimetrically prepared methane/n-heptane/water mixture (1)

Component	Molecular Weight (gm/gm-mole)	Mass (grams)	Composition mole%	Dry Composition mole%	±
Water	18.02	0.027	1.8	-	0.07
n-Heptane	100.20	4.607	55.9	56.9	0.06
Methane	16.04	0.559	42.3	43.1	0.09

Table 2.7 Composition of gravimetrically prepared methane/n-heptane/water mixture (2)

Component	Molecular Weight (gm/gm-mole)	Mass (grams)	Composition mole%	Dry Composition mole%	±
Water	18.02	0.078	4.95	-	0.06
n-Heptane	100.20	4.710	53.73	56.5	0.06
Methane	16.04	0.580	41.32	43.5	0.09

Table 2.8 Composition of gravimetrically prepared methane/n-decane/water mixture (1)

Component	Molecular Weight (gm/gm-mole)	Mass (grams)	Composition mole%	Dry Composition mole%	±
Water	18.02	0.019	2.0	-	0.11
n-Decane	142.29	4.421	59.8	61.1	0.06
Methane	16.04	0.318	38.2	38.9	0.14

Table 2.9 Composition of gravimetrically prepared methane/n-decane/water mixture (2)

Component	Molecular Weight (gm/gm-mole)	Mass (grams)	Composition mole%	Dry Composition mole%	±
Water	18.02	0.061	4.7	-	0.08
n-Decane	142.29	5.642	55.4	58.1	0.05
Methane	16.04	0.458	39.9	41.9	0.10

Table 2.10 Composition of gravimetrically prepared methane/toluene/water mixture (1)

Component	Molecular Weight (gm/gm-mole)	Mass (grams)	Composition mole%	Dry Composition mole%	±
Water	18.02	0.031	2.0	-	0.06
Toluene	92.14	4.641	58.7	59.9	0.06
Methane	16.04	0.542	39.3	40.1	0.09

Table 2.11 Composition of gravimetrically prepared methane/toluene/water mixture (2)

Component	Molecular Weight (gm/gm-mole)	Mass (grams)	Composition mole%	Dry Composition mole%	±
Water	18.02	0.076	4.6	-	0.06
Toluene	92.14	4.638	55.5	58.2	0.06
Methane	16.04	0.581	39.9	41.8	0.08

2.2.3 *Real Fluids*

In addition to the synthetic samples, a number of real hydrocarbon fluids were also used to conduct several experiments in the present work. A natural gas, a gas condensate, three dead oils and also a mineral oil-based drilling mud filtrate are among the fluids which were employed to perform the viscosity tests in this study. In this section, the specifications of these samples are given:

The molecular weight and the composition of natural gas, NG1, are reported in Table 2.12. Viscosity tests were performed on NG1 in the present work. The gas condensate, GCB00-1, was gravimetrically prepared by *livening* the fully characterised dead condensate, LTB98-1 (Reservoir Fluid Studies, Rep. No. PVT/03/1). The molecular weights and composition of GCB00-1 are available in Table 2.13.

Table 2.12 Compositions of natural gases used in the experiments of this study (supplied by British Oxygen Company-BOC)

Component	Molecular Weight (gm/gm-mole)	NG1 - Composition mole%
C_1	16.04	88.83
C_2	30.07	5.18
C_3	44.10	1.64
i-C_4	58.12	0.16
n-C_4	58.12	0.27
i-C_5	72.15	0.04
n-C_5	72.15	0.04
CO_2	44.01	2.24
N_2	28.01	1.6

Table 2.13 Semi-gravimetric composition of gas condensate (GCB00-1) used in the viscosity experiments of this study

Component	Measured MW	Specific Gravity	Semi-Gravimetric	
			weight%	mole%
N_2	28.01	-	0.00	0.00
C_1	16.04	0.300	40.55	69.62
CO_2	44.01	-	0.00	0.00
C_2	30.07	0.356	14.35	13.14
C_3	44.10	0.507	14.72	9.19
iC_4	58.12	0.563	1.42	0.67
nC_4	58.12	0.584	5.13	2.43
iC_5	72.15	0.625	1.15	0.44
nC_5	72.15	0.631	1.48	0.57
C_{6s}	88.5	0.678	1.80	0.56
C_{7s}	92	0.733	1.99	0.60
C_{8s}	103	0.757	2.36	0.63
C_{9s}	116	0.778	1.76	0.42
C_{10s}	131	0.790	1.32	0.28
C_{11s}	147	0.789	1.26	0.24
C_{12s}	161	0.809	0.95	0.16
C_{13s}	173	0.822	1.02	0.16
C_{14s}	186	0.839	1.04	0.15
C_{15s}	203	0.837	0.85	0.12
C_{16s}	215	0.843	0.73	0.09
C_{17s}	229	0.841	0.80	0.10
C_{18s}	246	0.843	0.60	0.07
C_{19s}	258	0.854	0.51	0.05
C_{20}^{+}	384	0.887	4.21	0.31

In order to investigate the effect of oil-based mud filtrate (OBM) on the viscosity of dead oil and also to propose a new method for prediction of original fluid viscosity, three different crudes were obtained from the UK North Sea, Norwegian North Sea and West of Africa and also a multi-component oil-based drilling mud filtrate named DMF-4 (which is a mineral oil) were chosen. The measured compositions of the mentioned crudes along with the composition of the oil-based mud filtrate (DMF-4) are presented in Table 2.14. The compositional analyses of the mentioned fluids were performed using gas chromatography (GC) method. So, the specific gravity and molecular weight of each

fraction were not reported in Table 2.14. In modelling part, the MW's of normal alkanes were employed for viscosity calculations. The measured densities (using an Anton Paar digital densitometer, DMA 45, which is detailed in Sections 2.3.3 and 2.4.4), the molecular weights and also the MWs of C_{20}^{+} fraction of the above mentioned fluids are reported in Table 2.15. In this table, the densities were reported at different temperatures since the tests were performed at lab temperature.

Table 2.14 Measured molar composition of the North Sea, Norwegian and West African crudes along with the oil-based mud filtrate (DMF-4) using GC method

Component	mole% North Sea Crude	mole% Norwegian Crude	mole% West African Crude	mole% (DMF-4) Oil-Based Mud
C_1	0.00	0.00	0.00	0.00
C_2	0.07	0.00	0.00	0.00
C_3	0.73	0.06	0.00	0.00
nC_4	2.47	0.28	0.00	0.00
nC_5	4.24	0.13	0.00	0.00
C_{6s}	5.44	0.53	0.05	0.00
C_{7s}	8.25	1.90	0.15	0.00
C_{8s}	9.17	2.96	0.67	0.02
C_{9s}	8.75	2.29	1.02	0.53
C_{10s}	7.60	2.95	2.35	4.29
C_{11s}	5.33	3.01	3.04	14.88
C_{12s}	4.64	3.86	3.92	26.06
C_{13s}	4.06	4.52	4.85	23.98
C_{14s}	3.85	4.92	5.99	18.03
C_{15s}	3.16	5.06	6.19	9.30
C_{16s}	2.82	4.78	5.29	2.43
C_{17s}	2.62	3.94	5.34	0.37
C_{18s}	2.41	4.09	4.24	0.095
C_{19s}	2.09	3.71	4.34	0.004
C_{20}^{+}	22.31	51.01	52.57	0.006

Table 2.15 Measured densities and molecular weights of the North Sea, Norwegian, West African crudes and the oil-based mud filtrate (DMF-4) along with the MWs of their C_{20}^{+} fraction

Fluids	Density / g.cm^{-3}	MW of the Fluid / (gm/gm-mole)	MW of the C_{20+} / (gm/gm-mole)
North Sea Crude	0.841 @ *19.30°C*	214	454
Norwegian Crude	0.933 @ *22.15°C*	325	460
West African Crude	0.946 @ *18.30°C*	372	529
DMF-4	0.801 @ *19.30°C*	170	384

In this study, it was decided to deliberately contaminate the above mentioned crudes with different levels of DMF-4. Preparation of the contaminated fluids was carried out by gravimetric addition of DMF-4 to the original fluids. Various amounts of the mentioned oil based mud (nominally 10, 25, 50 and 75 weight percent) were mixed with the dead oils to make the contaminated samples. The values of contamination levels added to the previously named crudes are detailed in Tables 2.16a to 2.18a. Also, the measured densities for the contaminated Norwegian and West African crudes are available in the mentioned tables. The molar compositions of these mixtures were determined by mass balance calculations and are reported in Tables 2.16b through 2.18b.

Table 2.16a Different levels of gravimetrically prepared contaminated North Sea dead oil with DMF-4 in weight percent and the predicted densities of the contaminated samples (using VPT EoS)

North Sea Dead Oil Weight / grams	DMF-4 Weight / grams	wt% DFM-4	Density / g.cm^{-3} @ 20°C
76.394	8.384	**9.89**	0.833
79.399	26.477	**25.01**	0.826
35.941	35.909	**49.98**	0.814
24.996	74.679	**74.92**	0.802

Table 2.16b Calculated molar composition (using mass balance) of the contaminated North Sea dead oil with different levels of DMF-4

Component	mole% DMF-4 9.89 wt%	mole% DMF-4 25.01 wt%	mole% DMF-4 49.98 wt%	mole% DMF-4 74.92 wt%
C_1	0.00	0.00	0.00	0.00
C_2	0.06	0.05	0.03	0.01
C_3	0.64	0.51	0.32	0.15
nC_4	2.17	1.74	1.09	0.52
nC_5	3.73	2.99	1.88	0.89
C_{6s}	4.78	3.83	2.41	1.14
C_{7s}	7.25	5.81	3.66	1.73
C_{8s}	8.06	6.46	4.07	1.94
C_{9s}	7.75	6.32	4.17	2.26
C_{10s}	7.20	6.62	5.76	4.99
C_{11s}	6.49	8.15	10.65	12.87
C_{12s}	7.24	10.97	16.56	21.55
C_{13s}	6.48	9.95	15.15	19.79
C_{14s}	5.57	8.04	11.75	15.05
C_{15s}	3.91	4.98	6.58	8.01
C_{16s}	2.77	2.70	2.60	2.51
C_{17s}	2.35	1.95	1.37	0.84
C_{18s}	2.13	1.72	1.12	0.58
C_{19s}	1.84	1.47	0.93	0.44
C_{20}^{+}	19.61	15.72	9.89	4.70

Table 2.17a Different levels of gravimetrically prepared contaminated Norwegian dead oil with DMF-4 in weight percent and the measured densities of the contaminated samples

Norwegian Dead Oil Weight / grams	DMF-4 Weight / grams	wt% DFM-4	Density / g.cm^{-3} @ 22.15°C
103.66	34.58	**25.01**	0.895
68.72	68.79	**50.03**	0.860
33.20	99.80	**75.04**	0.828

Table 2.17b Calculated molar composition (using mass balance) of the contaminated Norwegian dead oil with different levels of DMF-4

Component	mole% DMF-4 25.01 wt%	mole% DMF-4 50.03 wt%	mole% DMF-4 75.04 wt%
C_1	0.00	0.00	0.00
C_2	0.00	0.00	0.00
C_3	0.04	0.02	0.01
nC_4	0.07	0.04	0.02
nC_5	0.16	0.09	0.04
C_{6s}	0.31	0.17	0.07
C_{7s}	1.10	0.59	0.25
C_{8s}	1.72	0.94	0.41
C_{9s}	1.55	1.08	0.76
C_{10s}	3.52	3.87	4.11
C_{11s}	8.02	11.16	13.31
C_{12s}	13.23	19.11	23.13
C_{13s}	12.74	17.88	21.41
C_{14s}	10.46	13.92	16.30
C_{15s}	6.85	7.97	8.74
C_{16s}	3.79	3.17	2.74
C_{17s}	2.43	1.49	0.84
C_{18s}	2.40	1.35	0.62
C_{19s}	2.14	1.16	0.49
C_{20}^{+}	29.48	15.98	6.73

Table 2.18a Different levels of gravimetrically prepared contaminated West African dead oil with DMF-4 in weight percent and the measured densities of the contaminated samples

West African Dead Oil Weight / Grams	DMF-4 Weight / grams	wt% DFM-4	Density / g.cm^{-3} @ 18.30°C
111.02	37.02	**25.01**	0.904
56.83	56.83	**50.00**	0.870
25.30	75.90	**75.00**	0.836

Table 2.18b Calculated molar composition (using mass balance) of the contaminated West African dead oil with different levels of DMF-4

Component	mole% DMF-4 25.00 wt%	mole% DMF-4 50.00 wt%	mole% DMF-4 75.00 wt%
C_1	0.00	0.00	0.00
C_2	0.00	0.00	0.00
C_3	0.00	0.00	0.00
nC_4	0.00	0.00	0.00
nC_5	0.00	0.00	0.00
C_{6s}	0.03	0.01	0.01
C_{7s}	0.09	0.05	0.02
C_{8s}	0.39	0.22	0.11
C_{9s}	0.81	0.68	0.59
C_{10s}	3.17	3.68	4.03
C_{11s}	8.04	11.17	13.32
C_{12s}	13.27	19.12	23.14
C_{13s}	12.92	17.98	21.45
C_{14s}	11.07	14.26	16.44
C_{15s}	7.50	8.32	8.89
C_{16s}	4.08	3.33	2.81
C_{17s}	3.24	1.93	1.03
C_{18s}	2.49	1.39	0.64
C_{19s}	2.51	1.36	0.58
C_{20}^{+}	30.39	16.49	6.95

2.3 Experimental Equipments

Viscosity and interfacial tension experiments on various reservoir fluids were performed in the PVT laboratory with different equipments. The detailed descriptions of the facilities used in the laboratory are given below.

2.3.1 *High Pressure – High Temperature Set up*

This facility was manufactured within the Institute of Petroleum Engineering at Heriot-Watt University and has been designed to have a maximum working pressure of 29,000 psia and maximum working temperature of 250 °C. A schematic diagram of the HPHT experimental rig is shown in Figure 2.1. Due to the high temperature and pressure of the experiments performed on this set up, it was designed to operate with relatively small sample volumes of no more than 15 cm^3. The facility was centred on a specially manufactured high pressure, high temperature window cell and an opposed piston pump both of which were constructed by Sitec Engineering of Switzerland.

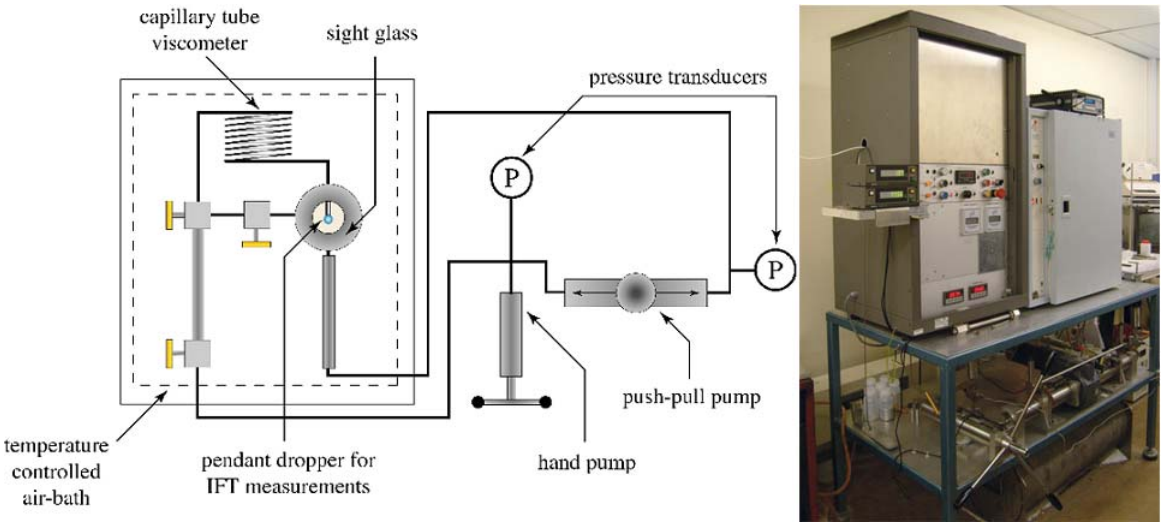

Figure 2.1 Schematic illustration of the high pressure - high temperature (HPHT) experimental facility

The HPHT facility is comprised of two small volume (15 cm^3) cells connected to each other at the top end. The low volume Sitec window cell is located at the top of one cell which is equipped with two opposing sapphire widows. This allows the study fluid to be viewed via a JVC TK-C1381 digital colour video camera and monitored from outside the oven on a monitor. Alternatively, the camera can be connected to a PC and by using Scenalyzer Live software the video can be captured. So the standard PVT measurements can be made on a study fluid. At the top of the opposite cell, there is a three-way valve, which is used to introduce fluids into the facility. The base of each of the two cells is

connected to opposite sides of a specially modified, motor driven, opposed piston mercury pump. This pump causes the sample to move backwards and forwards between the two cells. There is also a hand pump connected to the system, manufactured by Sitec Engineering of Switzerland that is used to control the pressure of the fluid by the injection or withdrawal of mercury. Both the opposed piston pump and the hand pump are fitted with Mitutoyo linear transducers readable to 0.005 mm on Mitutoyo SD-D1E readouts. As a 1 mm movement represents 0.151 cm^3 displacement in both pumps, the readability is 0.000755 cm^3. The opposed piston pump has a variable control with which the speed can be adjusted to a maximum of 5 $cm^3.sec^{-1}$. The rate can be set with a margin of error of ±0.00003 $cm^3.sec^{-1}$.

The 15 cm^3 cells and the window cell are sited within a Stuart Scientific oven (which controls the temperature) and the internal temperature is monitored by two high precision, PRT temperature probes. The temperature itself is displayed on two Druck DPI Series 280 readouts to a resolution of 0.1 °C.

Two Quartzdyne C30K pressure transducers (0 - 30,000 psia) measure the system pressure with a resolution of 0.01 psi, and with a reported maximum full-scale error of ±0.1%. The pressure transducers are monitored and recorded via a PC through RS 232 serial ports. These are located, external to the oven, on each of the two lines coming from the base of the cells (Figure 2.1).

All parts of the sample loop and pipe work are connected to the opposed piston pump and hand pump are rated to 29,000 psia. For safety purposes there is a pressure release valve set to 20,100 psia connected to a 20 litre tank for rapid release of pressure in case of emergency.

The HPHT facility is principally being employed for the investigation of interfacial tension and viscosity of hydrocarbon fluids under high temperature and pressure conditions. The descriptions of two HPHT set up configurations to conduct the viscosity and interfacial tension measurements are mentioned below:

For viscosity measurements a capillary tube is connected between the tops of the two cells in the oven (as illustrated in Figure 2.2). The capillary tube currently in use has a measured length of 14.781 metres and a calculated internal diameter of 0.29653 mm. To

calculate the internal diameter several pure compounds (methane, ethane, *n*-pentane and *n*-decane) were selected, with viscosities covering the range of viscosity that it might be expected to encounter during experimental studies. Using the experimentally measured differential pressures and the literature data the above internal diameter was calculated. The calibration process of the present capillary viscometer housed inside the HPHT set up is available in Reservoir Fluid Studies, Rep. No. PVT/03/1. A brief of the calibration process is outlined below:

The range of viscosity covered during the calibration was from approximately 0.015 to 2.90 cP, the temperatures ranged from 30 to 104°C over a pressure range of 1,000 to 20,000 psia. During the calibration procedures, Reynolds number (Re) did not raise above about 350 indicating that at all times laminar Newtonian flow was maintained. Differential pressure measurements were made at 104°C over a range of pressure from 1,011 to 7,498 psia at various flow rates with pure methane (supplied by Air Products, 99.995 mole% purity). The differential pressures in the calculation of the actual internal diameter of the capillary tube were obtained during this series of tests. The same procedures for ethane, *n*-pentane and *n*-decane were employed. All of the accumulated differential pressure data were then used to calculate an average internal diameter for the capillary tube, using Poiseuille's formulation (Equation 2.1). The range of internal diameters that were calculated ran from 0.029303 cm to 0.029830 cm so a mean internal diameter, 0.029653 cm, was considered for performing the viscosity tests in this work.

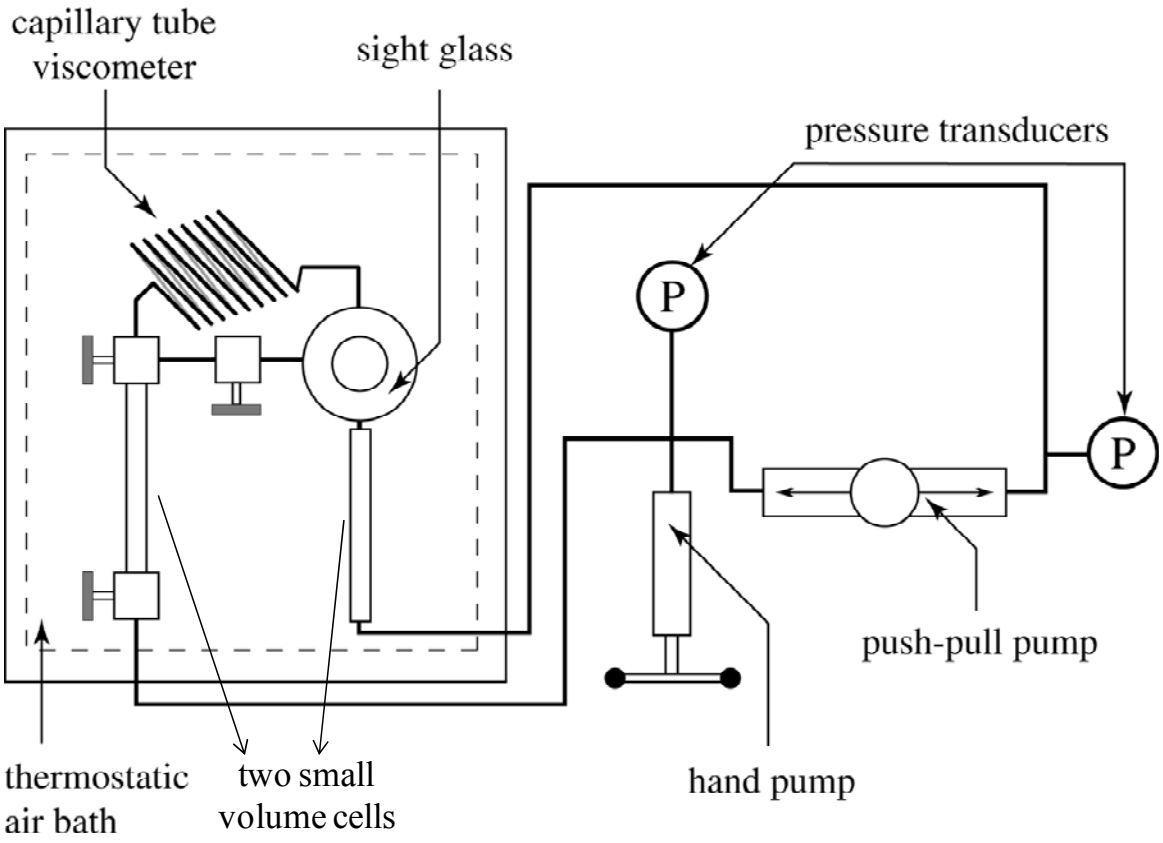

Figure 2.2 Schematic diagram depicting the high pressure - high temperature facility configured for viscosity measurement using the capillary tube method

In order to perform the interfacial tension, a needle (to inject water droplet for the pendant drop method or gas bubble in case of the rising bubble method) was mounted in the window cell of the HPHT setup. The outside diameter of the needle is 0.51 mm that was used as a reference for sizing the droplet or bubble. The Sitec HPHT window cell is a salt compatible cell and it is made of Hastelloy. The viewing system allows the pendant drop to be displayed on a monitor so that the captured video and images can be investigated and analysed by their dimensions using a Scenalyzer Live software. Using the mentioned viewing system, a magnification of approximately 400 times was obtained. Figure 2.3 shows the configuration of the HPHT facility for the measurement of interfacial tension. The diagram illustrates a droplet of fluid suspended from the tip of an oil wet stainless steel pendant dropper that was made before being fitted in the window cell.

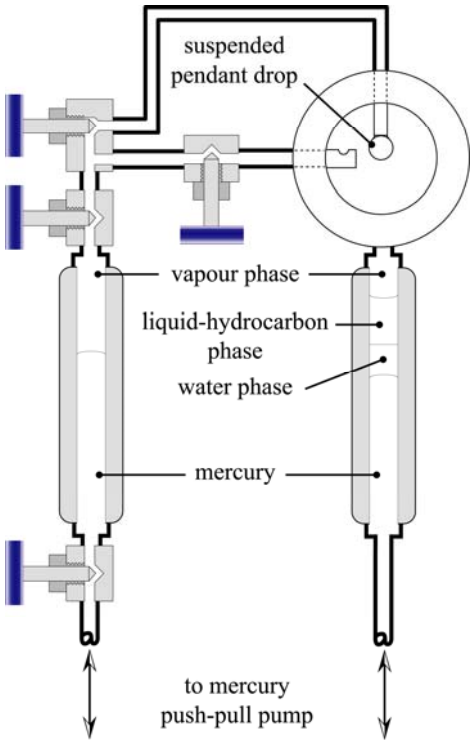

Figure 2.3 Schematic diagram illustrating the high pressure – high temperature facility fitted with the pendant dropper for interfacial tension measurement

A "rising bubble" configuration was also utilised. For this purpose, the needle was mounted from the bottom of the window cell and the gas bubble was rising through the needle (instead of liquid droplet).

2.3.2 *Rolling Ball Viscometer*

As part of this study, a Ruska high pressure rolling ball viscometer (Model No. 1602-818) was used to measure the viscosity of dead oils and its contaminated samples at atmospheric pressure and various temperatures (Figure 2.4). The calibration process is detailed in Section 2.4.2.

This equipment consists of the viscometer and a control box with clock. The main parts of the viscometer are a measuring barrel of 20 cm^3, a 5 mm diameter stainless steel ball, a solenoid at the top of the barrel, two high pressure valves at top and bottom of the set up, heating elements and thermocouple. The possible roll angles are 23°, 45° and 70°. The control box monitors and displays the temperature of the system and also the ball rolling time. This set up can measure the viscosity of 0.1 cP or higher, with a repeatability of 0.1%.

The Ruska rolling ball viscometer has the advantage of having an electric heating jacket for performing measurements at precisely controlled temperatures. The set up is also equipped with a solenoid to hold the ball at the top of the sample barrel so the ball will fall as the electric current through the solenoid is interrupted. The breaking of the solenoid current activates the time clock and when the ball reaches the end of its travel will stop the clock. This assembly makes it possible to measure the rolling time of the ball accurately.

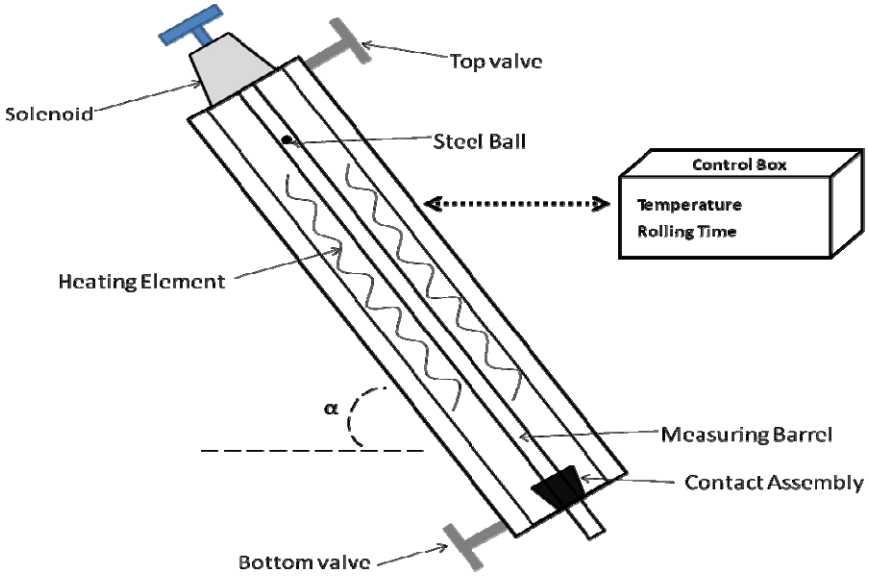

Figure 2.4 Schematic illustration depicting the Ruska high pressure rolling ball viscometer for viscosity measurements on various dead oils and their contaminated samples

2.3.3 *Densitometer*

The density measurements on the dead fluids and contaminated samples were performed using an Anton Paar Scientific densitometer, Model DMA 45, which the measurement accuracy is typically ± 0.001 g/cc. In this set up only small amount of sample is used to measure the density, so taking the representative sample would be very important in accuracy of the measurements.

The device is a vibration densitometer comprised of various parts (Figure 2.5). The U-shape sample tube (oscillator) is made of borosilicate glass and it is assembled at the centre of a double walled cylinder fused at both ends. The temperature of the system is controlled with a thermostatic by circulating a liquid around the cylinder. The oscillator is firmly attached to a metal block as the counter mass for oscillator. The provided window allows visual observation of the sample tube and its contents (i.e., fluid).

In order to remove the sample and clean the sample tube (oscillator) after completing the experiment, a built-in pump is installed. The sample tube is vibrating at constant amplitude. The oscillation period is measured every two seconds using a quartz crystal controlled timer and the data are available on the display.

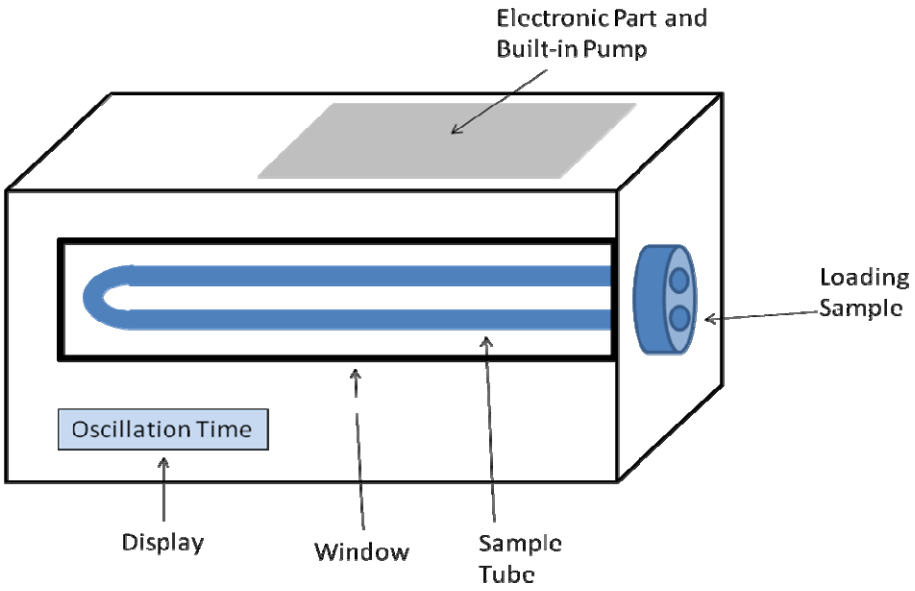

Figure 2.5 Schematic illustration depicting the vibration densitometer for density measurements on various dead oils and their contaminated samples

2.4 Experimental Procedures

A number of viscosity and interfacial tension experiments were performed on different hydrocarbon samples in this work. Tests were planned to simulate the behaviour of a fluid during the many processes which can occur, or which may be used, within the reservoir itself or on the surface. The following sections provide detailed descriptions of the procedures and methods used in the laboratory while carrying out these tests.

2.4.1 *Viscosity Measurements Procedure (In HPHT Set up)*

The measurements of viscosity at high pressure and high temperature conditions were performed using the capillary tube that is connected between the tops of the two cells in the HPHT facility (Figure 2.2). The method of viscosity determination involves passing the sample fluid (vapour or liquid) through the capillary tube at a number of different flow rates. The description of the technique is presented in the following paragraphs.

In order to establish equilibrium for making the viscosity measurements, the test fluid (that is loaded in one of the cells) can be pushed through the capillary tube into the other cell using the opposed piston pump. After travelling the entire sample through capillary tube, then mercury passes through and falls into the sample and this can agitate the fluid, thus providing a good mixing.

After achieving the desired temperature and pressure conditions, the sample was pumped through the capillary tube at a number of flow rates. To ensure the consistency of the measurements, at each pressure, viscosities were determined at three different flow rates and at each flow rate three readings were logged, so the reported viscosity data in this study are an average of at least nine separate readings.

Pumping the fluid through capillary tube by means of the opposed piston pump results in a dynamic differential pressure that was monitored and recorded until stable. Then the pump was stopped to record the static differential pressure. The difference between the dynamic and static differential pressure was calculated as the differential pressure across the tube (pressure drop). As mentioned above, several repetitions at each flow rate were performed and only the readings which provided less than 1% deviation from the average viscosity were selected. To ensure laminar flow conditions, Reynolds numbers were checked for the flow rates in which the measurements were performed. For example for natural gas, Reynolds number is ranging from 60 to 300 that are located in laminar zone.

Poiseuille equation, below, can relate the pressure drop across the capillary tube to the viscosity, tube characteristics and also flow rate for laminar flow:

$$\Delta P = \frac{128\, L\, Q \eta}{C\, \pi\, D^4} \tag{2.1}$$

Where, ΔP is differential pressure across the capillary tube viscometer in psi, Q represents flow rate in $cm^3.sec^{-1}$, L is length of the capillary tube in cm, D refer to internal diameter of the capillary tube in cm, η is viscosity of the flown fluid in cP and C is unit conversion factor equal to 6894757 if the above units are used.

The calibration process for capillary tube viscometer was reported earlier (Section 2.3.1). The other way in finding the internal diameter is employing the length and volume of the tube to estimate its radius. In this work, the calibrated ID with previously detailed method was used. The radius can only be taken as an average as the smoothness of the tube walls cannot be measured. Calculation of the effects of pressure and temperature showed that there was no major change in the tube radius at temperatures up to 200 °C and pressures to 20,000 psia. The tube length changes with temperature but this had no noticeable influence on the obtained viscosity. The set flow rate has no effect on the accuracy of the viscosity measurement. Only differential pressure as a variable in the above formulation can cause error in viscosity measurement. The usual variation in differential pressure measurement is 0.01 psi and this leads to ±1% of error in the calculated viscosity for those measured in this study.

2.4.2 *Viscosity Measurements Procedure (In Rolling Ball Set up)*

The measurement of viscosity with the rolling ball viscometer is based on the rolling time of a metal ball running through the test fluid. The theory of this technique is that the main force against the gravitational attraction on the ball is because of the viscosity of the sample.

In this thesis, the setup described earlier (Figure 2.4) was employed to measure the viscosity of different crudes and the intentionally contaminated crudes with oil based mud filtrate. With the aim of carrying out these series of tests, the reported standard fluids (Table 2.1) have been chosen to calibrate the viscometer. To perform the viscosity tests

by rolling ball viscometer, the relation between the ball rolling times through each standard fluid against the viscosity of these fluids should be specified. The relative viscosity of the study samples was then defined by using the graph of time vs. viscosity. The viscosity of standard fluids should cover the full range of viscosity of the test fluids. The obtained experimental data of time vs. viscosity with rolling ball viscometer for the mentioned standard fluids at angles of 70°, 45° and 23° were plotted in Figures 2.6 to 2.8. These graphs are only proper when the same ball (same size and weight) and the same rolling ball set up are employed. So, if the ball or the equipment were changed then the calibration should be performed again to regenerate the mentioned graphs. It is noticeable that the calibration of the rolling ball set up is temperature independent.

The experiments were performed at the above mentioned angles of tube inclination. The viscometer is equipped with a thermostatically controlled cylinder which controls the temperature. Each test was performed once the temperature was stabilised. At each temperature, the tests were repeated at least six times to make sure of the consistency of the measured results. The tests were performed at atmospheric pressure and temperature range of 20 to 72 °C.

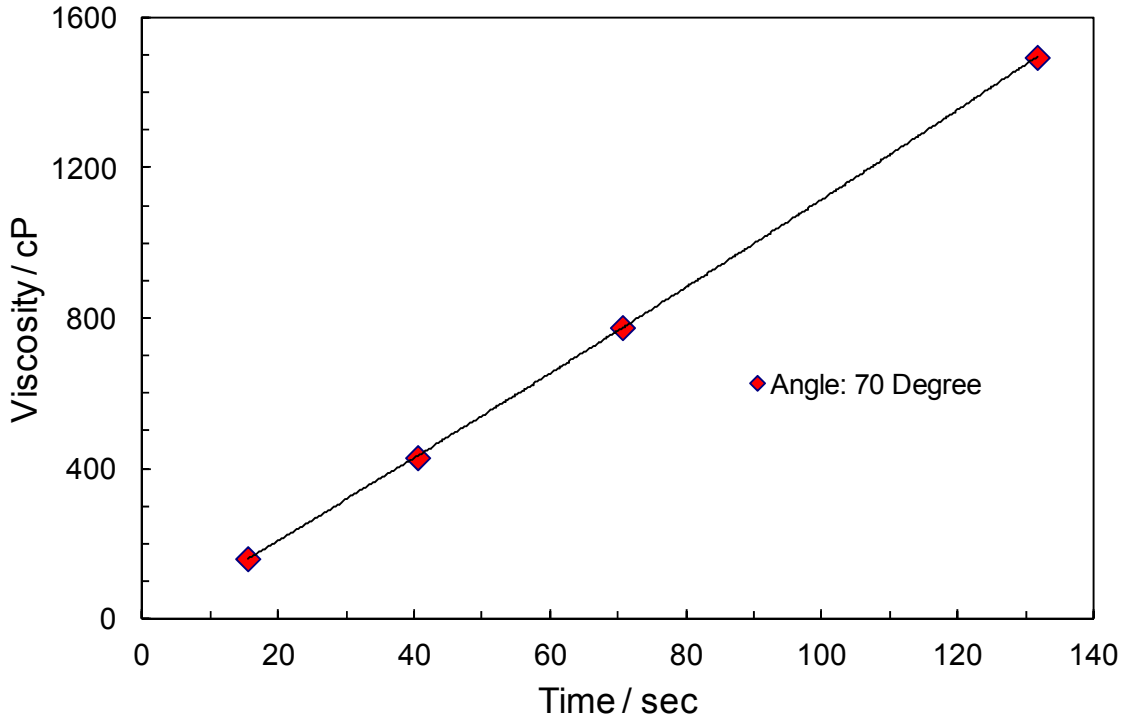

Figure 2.6 The relation between time taken for the ball to run through the standard fluids (Table 2.1) and their viscosity at slant of 70 degree (this work).
This graph was used to measure the viscosity of other study fluids reported in this thesis.

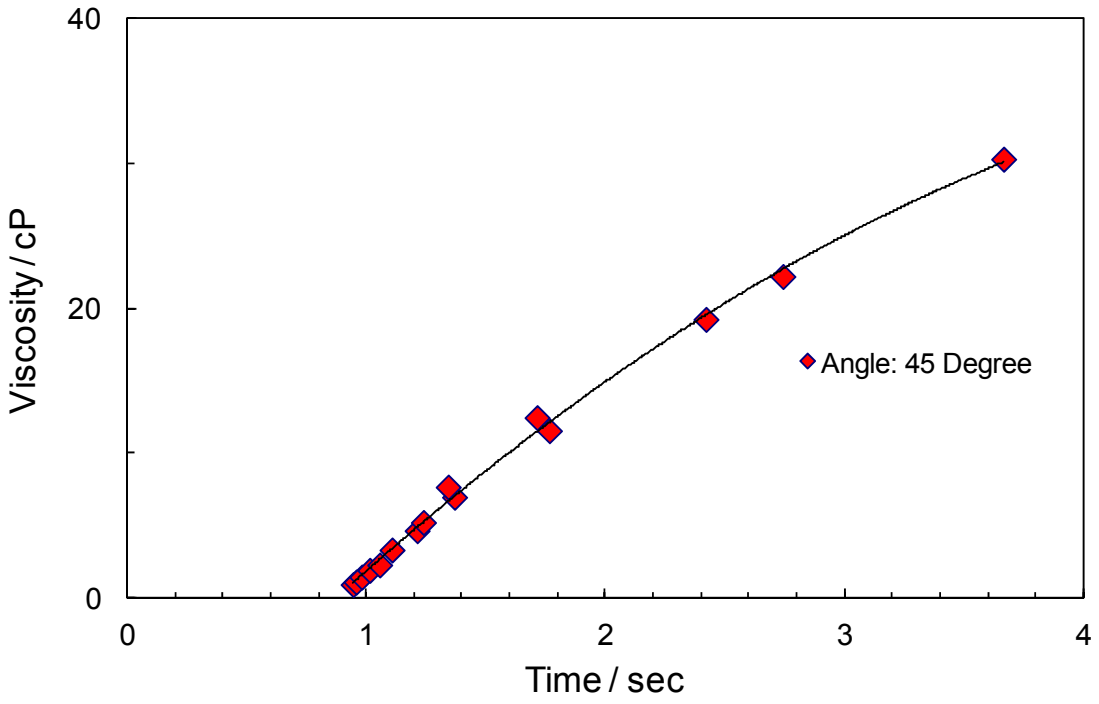

Figure 2.7 The relation between time taken for the ball to run through the standard fluids (Table 2.1) and their viscosity at slant of 45 degree (this work).
This graph was used to measure the viscosity of other study fluids reported in this thesis.

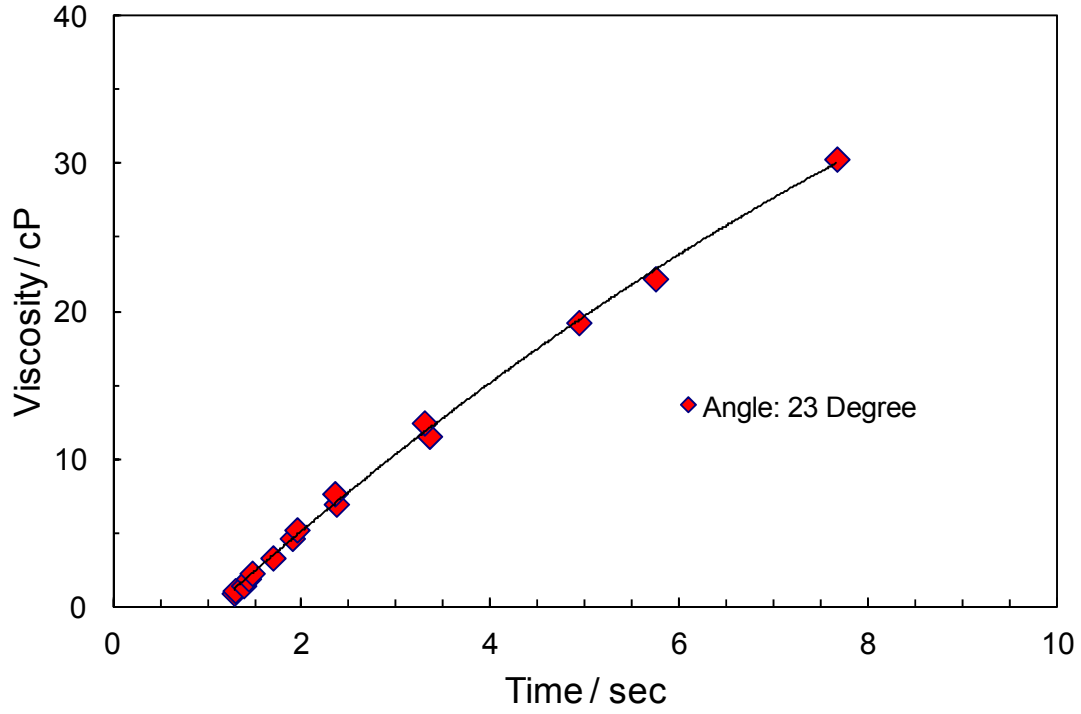

Figure 2.8 The relation between time taken for the ball to run through the standard fluids (Table 2.1) and their viscosity at slant of 23 degree (this work).
This graph was used to measure the viscosity of other study fluids reported in this thesis.

2.4.3 *Interfacial Tension Measurements Procedure*

The idea of the pendant drop method for measuring interfacial tension is based on suspending a droplet of heavier phase (e.g. liquid) surrounded by lighter phase (e.g. vapour) in the equilibrium condition as schematically shown in Figure 2.9. The shape of the droplet can define the interfacial tension value. This technique is known as a mere mathematical approach which is derived from a force balance between buoyancy and gravitational forces. Rushing *et al.,* 2008 reviewed the methodology of IFT calculation using this method. The dimensions of the droplet, d_e and d_s, and the density difference of the adjacent phases are used for interfacial tension measurement using the equation below.

$$\sigma = \frac{\Delta\rho g d_e^2}{H} \tag{2.2}$$

where σ is interfacial tension in $mN.m^{-1}$ ($dynes.cm^{-1}$), Δρ represents density difference between vapour and liquid phases in $g.cm^{-3}$, g refers to acceleration due to gravity in $cm.sec^{-2}$, d_e is equatorial diameter of liquid droplet in cm, H is liquid droplet shape factor and finally d_s is diameter of the liquid droplet measured at a distance of d_e from the bottom of the droplet in cm. The shape factor, H, can be found tabulated as a function of d_s/d_e ratio in Niederhauser *et al.,* 1947.

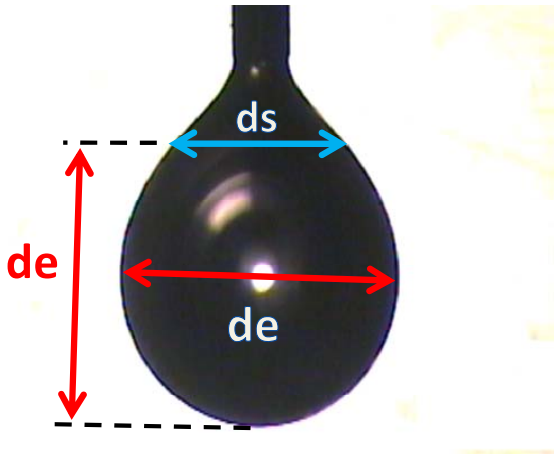

Figure 2.9 Droplet of heavier phase suspended in equilibrium lighter phase from the end of a pendant dropper in order to measure the interfacial tension

The drawn lines on the illustrated droplet (Figure 2.9) delineate the two required dimensions necessary for measurement of interfacial tension. The equatorial diameter, d_e, which is the largest diameter of the drop, is measured with the aid of a camera that was connected to a PC and by using Scenalyzer Live software the video and the images can be

captured. The other needed dimension, d_s, is measured by first moving up from the bottom of the drop a distance equal to the equatorial diameter and measuring the diameter of the droplet at this height. It has been tried to obtain at least six bubbles (or droplets) for each IFT data point. Among the bubbles (or droplets), the ones with no consistency with the rest of images were omitted. So, the measurements were based on the largest possible formed bubbles (or droplets) then using the average of their dimensions (d_e and d_s), IFT can be calculated.

In this work, "rising bubble" method was also employed to measure the IFT data. Changing the configuration of the set up from "pendant drop" to "rising bubble" was due to solve the problem related to the needle wettability. It was appeared that the needle got water wet and did not allow the droplet to form properly, so rising bubble method were chosen to omit the impact of water wet needle. The injecting needle was mounted upward from the bottom of the window cell. In this case the gas bubble (lighter phase) forms at the tip of the needle which is surrounded by liquid (heavier phase) in the equilibrium condition. The interfacial tension calculations and procedures are similar to the pendant drop technique that is outlined above. In Section 6.4.4 a comparison between these two methods are reported.

Figure 2.10 Gas bubble suspended upward in equilibrium liquid phase to measure the interfacial tension of gas-water system (using rising bubble method)

2.4.4 *Density Measurements Procedure*

The principle of the Anton Paar densitometer is based on the change of frequency produced in an oscillating hollow U-tube, when its mass is altered after filling with the test fluid. The period of oscillation is a function of the mass, volume and elasticity of the U-tube, as well as sample density. Before performing any measurements on dead oils, the Anton Paar densitometer is calibrated against two pure substances of known densities.

The used materials are air and distilled water. Firstly, air is injected into the density loop at the ambient temperature. Shortly after the set up starts to work, the time of oscillation 'T' of the densitometer tube is recorded by the mentioned facility at atmospheric pressures. The pressure which is needed for density value is taken from a barometer. The procedure is then repeated using distilled water. These values together with the literature values for density of air and water are then used to calculate two constants 'A' and 'B' at the pressure and temperature of the calibration (Paar Scientific Ltd). Since the mentioned two constants contain volume, spring constant and mass, they could be considered as "equipment constants". The density can be estimated by Equations 2.3 to 2.5.

$$A = \frac{T^2a - T^2b}{\rho_a - \rho_b} \tag{2.3}$$

$$B = T^2{}_b - A \cdot \rho_b \tag{2.4}$$

That T_a and T_b are oscillation times of densitometer for water and air, respectively, ρ_a and ρ_b refer to density of water and air, respectively at pressure and temperature of experiment and A and B represent the equipment constants which can be defined by performing calibration.

Following the injection of the fluid into the sample tube, it begins to oscillate automatically as the power is switched on. After a while, depending on the sample density, the display shows a number that refers to the period of oscillation. The measured value of T is continuously repeated on the display until the fluid is removed. The recorded value may fluctuate slightly until temperature equilibrium is reached. Knowing the above mentioned constants (A and B) and oscillation time of the study fluid, the density of the fluid can then be calculated:

$$\rho_f = \frac{T^2{}_f - B}{A} \tag{2.5}$$

Where ρ_f is density of the study sample and T_f is the oscillation time of densitometer for the test sample.

2.4.5 *Propagation of Errors*

In the experimental measurements, the uncertainties in mole percentage of each synthetic mixture were reported in this work. These calculations were performed using propagation of errors method for the synthetic hydrocarbon mixtures. Equations 2.6 and 2.7 are the formulations employed to calculate the uncertainty of mole fraction measurements:

$$\frac{dxi}{xi} = \sqrt{\left(\frac{dm_i}{mass_i}\right)^2 + \left(\frac{dMW_i}{MW_i}\right)^2 + SumTerm} \tag{2.6}$$

$$SumTerm = \sum_{j=1}^{n} x_j^2 \times \left[\left(\frac{dm_j}{mass_j}\right)^2 + \left(\frac{dMW_j}{MW_j}\right)^2\right] \tag{2.7}$$

Where, x_i is mole fraction, dx_i is the error value in mole measurement of mole fraction, dm_i is the error in weight measurements (equal to 0.001) and dMW is the uncertainty in molecular weight (equal to 0.01).

References

Ducoulombier, D., Zhou, H., Boned, C., Peyrelasse, J., Saint-Guirons, H., and Xans, P., 1986, *Pressure (1-1000 bars) and Temperature (20-100C) Dependence of the Viscosity of Liquid Hydrocarbons*, J. Phys. Chem., **90**, 1692-1700

Niedrehauser, D.O. and Bartell, F.E., 1947, *A Corrected Table for Calculation of Boundary Tensions by Pendant Drop Method*, Research on Occurrence and Recovery of Petroleum, A Contribution from API Research Project **27**, 114-146

Paar Scientific Ltd., Instruction Manual, *Calculating Digital Density Meter DMA 45*

Reservoir Fluid Studies, Final Report, 1999-2002, Institute of Petroleum Engineering, Heriot-Watt University, Report No.: PVT/03/1

Rushing, J.A., Newsham, K.E., Van Fraassen, K.C., Mehta, S.A. and Moore, G.R., 2008, *Laboratory Measurements of Gas-Water Interfacial Tension at HP/HT Reservoir Conditions*, SPE **114516**

www.hse.gov.uk, 2005, *High pressure, high temperature developments in the United Kingdom Continental Shelf*, Prepared by Highoose Limited for the Health and Safety Executive

CHAPTER 3

VISCOSITY: EXPERIMENTAL AND MODELLING

3.1 Introduction

Physical and rheological properties such as viscosity of reservoir fluids at HPHT conditions are required to determine the optimum number of wells and to design surface facilities. Therefore, experimental measurements of these properties are required to be made in laboratories. Experimental viscosity data for reservoir fluids especially at high pressure and high temperature conditions are scarce, despite increasing need for such data. It is, however, impossible to measure viscosity of hydrocarbon mixtures at all possible compositions in a wide range of temperatures and pressures. Even if it were possible, the cost of generating all the necessary experimental data would be prohibitive. For these reasons, there are growing demands for reliable and accurate analytical prediction methods for viscosity calculation, which are discussed in this chapter.

Viscosity estimation is essential for predicting flow regime and pressure drop of reservoir fluids when flowing through porous media, wellbore and surface facilities. Deep hydrocarbon reservoirs are increasingly being discovered world-wide. Due to their extreme conditions, high pressure and high temperature (HPHT), the costs of exploration and drilling are considerably higher than conventional reservoirs. In fact, drilling is one of the most expensive processes in the development of high pressure, high temperature reservoirs. Optimising the number of wells, therefore, plays an important role in minimising reservoir development expenditure.

As mentioned earlier, there are limited experimental viscosity data for hydrocarbon mixtures in the literature especially at HP and HT conditions. Different sources reported viscosity data for natural gas but almost none of them are at high pressure and high temperature conditions. Assael *et al.* (2001) reported natural gas viscosity data at 182 °C and atmospheric pressure and also in the temperature range up to 80 °C at pressures up to 2,200 psia. Vogel *et al.* (2004) covered viscosity data for up to 47 °C at pressures up to 2,900 psia for natural gases. There are some viscosity data on binary hydrocarbon systems such as methane-decane in the literature; however, the data are not at HP and HT

conditions. Knapstad *et al* (1990) performed viscosity tests on methane-decane in the temperature range up to 150 °C and pressure up to 5,800 psia, Audonnet *et al* (2004) covered viscosity range for temperature up to 120 °C and pressure up to 11,000 psia, Canet *et al* (2002) covered high pressure (up to 20,000 psia) and up to 100 °C. The existing viscosity data for hydrocarbon mixtures in open sources are limited at both high pressure and high temperature. So there is a need to fill the gap in experimental viscosity data for variety of hydrocarbon mixture systems at HPHT conditions.

This chapter is focused on two main objectives. First of all, new experimental viscosity measurements to cover both high pressure and high temperature conditions are reported for three binary hydrocarbon systems: methane-heptane, methane-decane and methane-toluene and three multi-component mixtures: a natural gas, a gas condensate and a synthetic volatile oil.

Secondly, the generated viscosity data on hydrocarbon mixtures (this work) were employed to investigate the reliability of various viscosity prediction models, including the Lohrenz–Bray–Clark (LBC) correlation (Lohrenz *et al*. 1964), the Pedersen correlation (Pedersen *et al.* 1984, 1987) and HW2 (a modified LBC correlation, Al-Syabi *et al.* 2001). Several new methods were also proposed as part of this work, which included a method based on artificial neural network, a simple correlation incorporating the effects of temperature, pressure, molecular weight and density, and finally an approach based on residual viscosity concept are among the evaluated viscosity prediction techniques in the present chapter.

3.2 Experimental Results

The HPHT facility is equipped with a capillary tube to conduct the viscosity tests on the mentioned hydrocarbon mixtures at pressures ranging from 5,000 to 20,000 psia and temperature up to 200 °C (reported in this chapter). The detailed descriptions of the facilities, procedures and methods used in the laboratory as well as the details on the materials, compositions and preparation of the mentioned fluids were presented in Chapter 2.

Viscosity data of binaries and the more complex fluids are tabulated in Tables 3.1 to 3.6. The errors in viscosity measurements which were reported in these tables were calculated using the propagation of errors law. Prior to making any viscosity measurements a very approximate bubble point measurement was made at each temperature, to ensure all measurements would be made above the system saturation pressure. This was done by transferring all of the sample fluid into the cell containing the window (Figure 2.1) and slowly reducing the pressure until bubbles could be seen rising in the inside the window.

3.2.1 *Methane/n-Heptane Binary*

The results of viscosity experiments performed on methane/*n*-heptane binary (58.0 mole% *n*-heptane) are reported in Table 3.1. At 50 °C a very approximate value of 2,850 psia for bubble point was observed but the bubbles formed were very small in size and proved very difficult to see. The bubble points at 100, 150 and 200 °C are 1872, 1835 and 1607 psia, respectively and the critical temperature and pressure of this system are 236 °C and 1146 psia (using PR EoS). The experiments were started from 5,000 psia for all temperatures which would be in the single phase. The sample was mixed again before starting the first viscosity measurement on this fluid at 5,013 psia and 50 °C (0.219±0.003 cP). The equilibrium pressure was raised in steps of about 2,500 psi to a maximum of about 19,005 psia at 50 °C (0.414±0.005 cP). The other experimentally measured data for the mentioned binary are at 100, 150 and 200 °C and at the pressure range of 5,000 to 20,000 psia. The reported data in Table 3.1 show the viscosity increases with increasing pressure and also increases with a decreasing temperature.

Table 3.1 Viscosity measurements (this work) of methane/n-heptane binary (58.0 mole% n-heptane). The mentioned binary composition is defined in Table 2.2

Temperature (°C)	Pressure (psia)	Viscosity (cp)	(±)	Temperature (°C)	Pressure (psia)	Viscosity (cp)	(±)
50	5013	0.219	0.003	**100**	5012	0.154	0.002
50	7515	0.254	0.003	**100**	7503	0.181	0.002
50	10003	0.286	0.004	**100**	10003	0.209	0.003
50	12497	0.323	0.004	**100**	12507	0.235	0.003
50	15001	0.356	0.005	**100**	15010	0.262	0.003
50	17505	0.393	0.005	**100**	17515	0.287	0.004
50	19005	0.414	0.005	**100**	20015	0.315	0.004
150	5013	0.115	0.002	**200**	5012	0.092	0.001
150	7504	0.142	0.002	**200**	7504	0.112	0.002
150	10011	0.162	0.002	**200**	10006	0.132	0.002
150	12505	0.184	0.002	**200**	12503	0.151	0.002
150	15013	0.204	0.003	**200**	15006	0.169	0.002
150	17506	0.227	0.003	**200**	17511	0.188	0.002
150	20007	0.246	0.003	**200**	20007	0.205	0.003

3.2.2 *Methane/n-Decane Binary*

Viscosity measurements were carried out on methane/*n*-decane binary (61.0 mole% *n*-decane) and are reported in Table 3.2. A very approximate bubble point test was made and value of 1,750 psia was seen at 50 °C. The sample was mixed again before starting measurements at about 1,847 psia (0.343±0.004 cP). The equilibrium pressure was raised in eight pressure steps to a maximum of 19,997 psia (0.902±0.011 cP). Approximate bubble point pressures of 1950, 2050 and 1950 psia were observed for 100, 150 and 200 °C, respectively, before the viscosity measurements were performed at each of these temperatures (simply to ensure the measurements were carried out in the single phase region). The bubble point calculations for the above mentioned temperatures were also performed with VPT EoS that are 1890, 2147, 2199 and 2082 psia for 50 to 200 °C. Also the calculated critical temperature and pressure for this binary are as 321 °C and 945 psia.

Table 3.2 Viscosity measurements (this work) of methane/n-decane binary (61.0 mole% n-decane). The mentioned binary composition is defined in Table 2.3

Temperature (°C)	Pressure (psia)	Viscosity (cp)	(±)	Temperature (°C)	Pressure (psia)	Viscosity (cp)	(±)
50	1847	0.343	0.004	**100**	2123	0.225	0.003
50	2501	0.361	0.005	**100**	2507	0.233	0.003
50	4997	0.430	0.005	**100**	5003	0.284	0.004
50	7501	0.502	0.006	**100**	7500	0.332	0.004
50	9999	0.574	0.007	**100**	10004	0.381	0.005
50	12494	0.648	0.008	**100**	12503	0.430	0.005
50	15000	0.728	0.009	**100**	15008	0.479	0.006
50	17503	0.812	0.010	**100**	17502	0.532	0.007
50	19997	0.902	0.011	**100**	20003	0.586	0.007
150	2231	0.155	0.002	**200**	2261	0.111	0.002
150	5002	0.202	0.003	**200**	5004	0.154	0.002
150	7504	0.241	0.003	**200**	7505	0.187	0.002
150	10005	0.278	0.004	**200**	10004	0.217	0.003
150	12507	0.316	0.004	**200**	12509	0.247	0.003
150	15007	0.353	0.004	**200**	15009	0.277	0.004
150	17504	0.391	0.005	**200**	17509	0.308	0.004
150	20002	0.427	0.005	**200**	20005	0.338	0.004

3.2.3 *Methane/Toluene Binary*

When the methane/toluene binary (59.8 mole% toluene) sample was loaded into the HPHT rig and equilibrated by mixing at 50 °C, an approximate bubble point pressure of 4,000 psia was measured with the appearance of bubbles in the windowed cell. The approximate measured bubble points for the mentioned binary at 100, 150 and 200 °C are about 3600, 3040 and 2785 psia, respectively. The bubble point calculations with VPT EoS resulted in 2811, 3040, 3020 and 2795 psia for 50 to 200 °C. Also the calculated critical temperature and pressure for this binary are as 281 °C and 1771 psia. The pressure range for this test was 5,000 to 20,000 psia with the step of 2,500 psi. As can be seen from the results in Table 3.3 the measured viscosity for this fluid ranges from 0.096±0.001 cP at 200 °C and 5,029 psia to 0.435±0.006 cP at 50 °C and 19,999 psia.

Table 3.3 Viscosity measurements (this work) of methane/toluene binary (59.8 mole% toluene). The mentioned binary composition is defined in Table 2.4

Temperature (°C)	Pressure (psia)	Viscosity (cp)	(±)	Temperature (°C)	Pressure (psia)	Viscosity (cp)	(±)
50	5009	0.238	0.003	**100**	5021	0.166	0.002
50	7512	0.270	0.003	**100**	7524	0.191	0.002
50	10014	0.303	0.004	**100**	10016	0.216	0.003
50	12519	0.334	0.004	**100**	12516	0.239	0.003
50	15006	0.367	0.005	**100**	15016	0.265	0.003
50	17496	0.401	0.005	**100**	17509	0.288	0.004
50	19999	0.435	0.006	**100**	20014	0.311	0.004
150	5013	0.123	0.002	**200**	5029	0.096	0.001
150	7518	0.145	0.002	**200**	7511	0.116	0.002
150	10007	0.165	0.002	**200**	10011	0.134	0.002
150	12509	0.185	0.002	**200**	12511	0.151	0.002
150	15009	0.203	0.003	**200**	15009	0.169	0.002
150	17507	0.223	0.003	**200**	17507	0.182	0.002
150	20019	0.241	0.003	**200**	20025	0.197	0.003

3.2.4 *Gas Condensate (GCB00-1)*

The gas condensate (GCB00-1) sample was mixed before starting the measurements to ensure the sample was at equilibrium. Measurements of viscosity were then preformed in pressure steps from about 6,000 to 20,000 psia and temperatures of 50, 100, 150 and 200 °C. The approximates critical temperature and pressure of this system were calculated using VPT EoS as -18 °C and 1400 psia, so at above mentioned temperatures the system would be in the gas phase. The data in Table 3.4 show the viscosity to increase with increasing pressure and also to increase as the temperature decreases. The measured viscosity for this fluid (which is described in Table 2.13) ranges from 0.034±0.001 cP at 200°C and 6,022 psia to 0.119±0.002 cP at 50 °C and 20,024 psia.

Table 3.4 Viscosity measurements (this work) of gas condensate (GCB00-1). The gas condensate composition is defined in Table 2.13

Temperature (°C)	Pressure (psia)	Viscosity (cp)	(±)	Temperature (°C)	Pressure (psia)	Viscosity (cp)	(±)
50	6012	0.057	0.001	**100**	6051	0.048	0.001
50	7524	0.065	0.001	**100**	7524	0.052	0.001
50	10021	0.076	0.001	**100**	10010	0.062	0.001
50	12507	0.087	0.001	**100**	12507	0.071	0.001
50	15038	0.099	0.001	**100**	15005	0.080	0.001
50	17560	0.108	0.002	**100**	17507	0.089	0.001
50	20024	0.119	0.002	**100**	20011	0.097	0.001
150	6035	0.038	0.001	**200**	6022	0.034	0.001
150	7527	0.044	0.001	**200**	7521	0.039	0.001
150	10007	0.054	0.001	**200**	10018	0.047	0.001
150	12504	0.062	0.001	**200**	12515	0.056	0.001
150	15012	0.070	0.001	**200**	15013	0.064	0.001
150	17503	0.078	0.001	**200**	17506	0.069	0.001
150	20008	0.085	0.001	**200**	20007	0.076	0.001

3.2.5 *Natural Gas (NG1)*

The viscosity tests performed on the natural gas (NG1) are reported in Table 3.5. Measurements of viscosity were conducted in pressure range from about 5,000 to 20,000 psia and temperatures of 50, 100, 150 and 200 °C. The critical temperature and pressure of the system are -62 °C and 906 psia and the cricondentherm and cricondenbar are -38 °C and 977 psia, respectively. This can prove that the experiments were performed in the single phase. The reported viscosity data of natural gas (Table 3.5) prove the viscosity has an increasing trend with increasing pressure and also with decreasing temperature, i.e., a typical gas hydrocarbon viscosity behaviour.

Table 3.5 Viscosity measurements (this work) of natural gas (NG1). The natural gas composition is defined in Table 2.12

Temperature (°C)	Pressure (psia)	Viscosity (cp)	(±)	Temperature (°C)	Pressure (psia)	Viscosity (cp)	(±)
50	5020	0.028	0.001	**100**	5019	0.026	0.001
50	7525	0.036	0.001	**100**	7527	0.032	0.001
50	10019	0.043	0.001	**100**	10008	0.038	0.001
50	12509	0.049	0.001	**100**	12506	0.042	0.001
50	15015	0.055	0.001	**100**	15020	0.048	0.001
50	17506	0.060	0.001	**100**	17517	0.053	0.001
50	19985	0.064	0.001	**100**	19985	0.057	0.001
150	5018	0.025	0.001	**200**	5023	0.024	0.001
150	7512	0.029	0.001	**200**	7518	0.028	0.001
150	10017	0.035	0.001	**200**	10015	0.033	0.001
150	12513	0.039	0.001	**200**	12513	0.037	0.001
150	15013	0.044	0.001	**200**	15012	0.041	0.001
150	17509	0.048	0.001	**200**	17514	0.045	0.001
150	19984	0.052	0.001	**200**	19979	0.049	0.001

3.2.6 *Synthetic Volatile Oil*

Before making any viscosity tests on the synthetic volatile oil (Table 2.5), an approximate bubble point observation was made. The examined bubble points for this fluid at 50, 100, 150 and 200 °C are about 10,050, 8,900, 8,100 and 7,250 psia, respectively. The bubble points were also calculated with VPT EoS at the mentioned temperatures and resulted in 10266, 9456, 8725, and 7888 psia which are in good agreement with the observed bubble points. The experimental viscosity data are reported for the range of mentioned temperatures and up to 20,000 psia in Table 3.6.

Table 3.6 Viscosity measurements of the synthetic volatile oil (this work). The composition of the synthetic volatile oil is defined in Table 2.5

Temperature (°C)	Pressure (psia)	Viscosity (cp)	(±)	Temperature (°C)	Pressure (psia)	Viscosity (cp)	(±)
50	11056	0.273	0.003	**100**	10043	0.180	0.002
50	12528	0.293	0.004	**100**	12522	0.206	0.003
50	15013	0.329	0.004	**100**	15013	0.233	0.003
50	17516	0.367	0.005	**100**	17512	0.259	0.003
50	20004	0.404	0.005	**100**	20008	0.286	0.004
150	9029	0.125	0.002	**200**	8041	0.090	0.001
150	10029	0.134	0.002	**200**	10018	0.106	0.001
150	12518	0.157	0.002	**200**	12508	0.125	0.002
150	15022	0.179	0.002	**200**	15011	0.144	0.002
150	17508	0.200	0.003	**200**	17507	0.163	0.002
150	20003	0.222	0.003	**200**	20006	0.182	0.002

3.2.7 *Evaluation of the Experimental Viscosity Data*

Due to lack of available experimental data at the same compositions in the literature, in particular at HPHT conditions, viscosity data of methane, ethane and propane were selected (NIST) for comparison purposes. Among the experiments performed in this work, natural gas (NG1) and gas condensate (GCB00-1) at 200 °C were chosen to compare with the viscosity values of the above mentioned pure compounds (Figure 3.1). The natural gas contains methane and ethane at 89 and 5 mole%, respectively and the gas condensate contains mainly methane, ethane and propane at 70, 13 and 9 mole%, respectively (the fluids compositions are presented in Tables 2.12 and 2.13). There is good agreement in trends and also in values between the experimental viscosity data reported in this work and those reported by NIST.

In addition to the above evaluation, the correctness of the viscosity results for the synthetic volatile oil generated in this study was considered and compared to the literature data in Chapter 5.

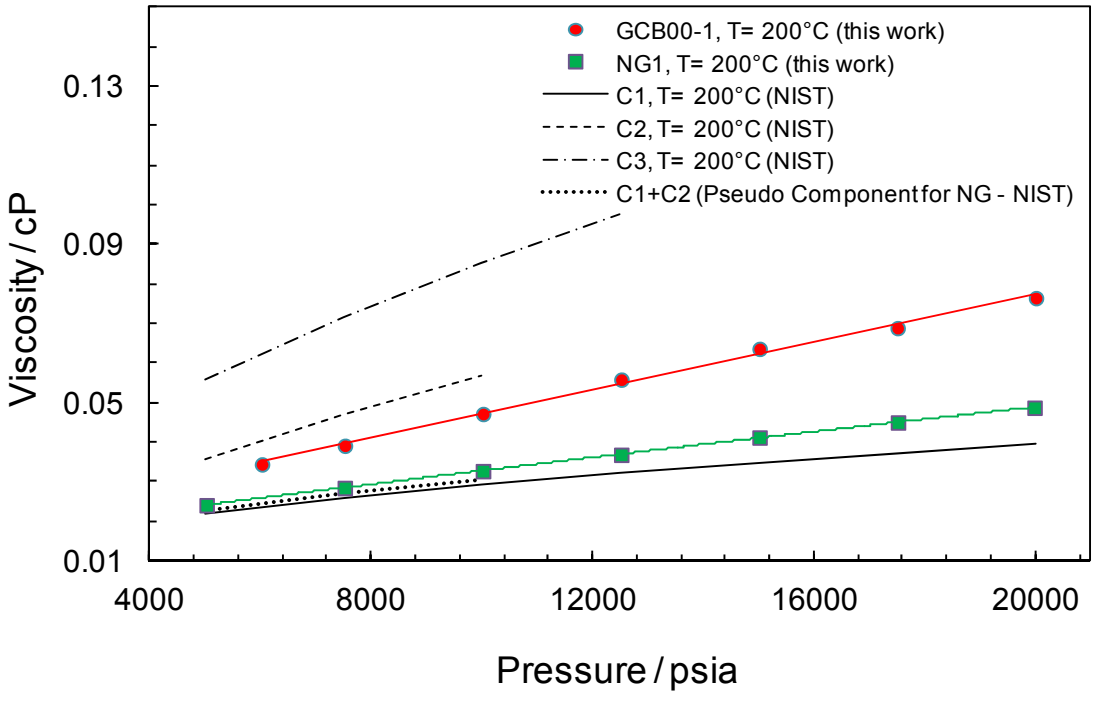

Figure 3.1 Measured viscosity data of gas condensate (GCB00-1) and natural gas (NG1) (this work) compared to the viscosities of methane, ethane, propane and a pseudo component for NG (NIST)

3.3 Viscosity Prediction Models

Some of the common viscosity prediction methods that are used by the petroleum industry have been reviewed in this section. Also a number of new viscosity models, developed as part of this work, are discussed.

3.3.1 *Pure Hydrocarbon Viscosity Data*

In order to optimize the coefficients of the existing predictive models or to develop new models, experimental viscosity data of pure hydrocarbons ranging from methane to octadecane (*n*-C_{18}) were employed. These data are reported in the open literature: (Agaev *et al.* 1963, Assael *et al.* 1991, Baylaucq *et al.* 1997, Brazier *et al.* 1969, Diller *et al.* 1980 and 1981, Chuang *et al.* 1976, Giddings *et al.* 1966, Lee 1965, Iwasaki *et al.* 1981, Diller 1982, Kiran *et al.* 1992, Iwasaki *et al.*1981, Oliveira *et al.* 1992, Isdale *et al.* 1979, Dymond *et al.* 1980 and 1981, Tanaka *et al.* 1991, Hogenboom *et al.* 1967). The experimental viscosity data gathered from the literature amount to 2,141 data points. The details of viscosity range, temperature and pressure of the experimental data are shown in Table 3.7.

Table 3.7 Range of experimental viscosity data of pure hydrocarbons used in tuning and developing of viscosity models in this work

Components	Temperature Range (°C)	Pressure Range (psia)	Viscosity Range (cP)	References
Methane	-173 to 27	4660 to 90	0.2185 to 0.0091	Diller 1980
	-75 to 0	60 to 7300	0.0499 to 0.0076	Chuang 1976
	38 to 171	200 to 8000	0.012 to 0.0355	Lee 1965
	10 to 138	15 to 8000	0.0107 to 0.0385	Giddings 1966
Ethane	-173 to 47	150 to 4500	0.009 to 1.1302	Diller 1981
	38 to 171	100 to 8000	0.0098 to 0.0933	Lee 1965
	50 to 75	145 to 1500	0.0109 to 0.0324	Iwasaki 1981
Propane	-183 to 27	250 to 4500	0.987 to 10.7	Diller 1982
	5 to 38	100 to 7800	0.0086 to 0.1865	Giddings 1966
	38 to 140	100 to 8000	0.0085 to 0.1605	Lee 1965

Butane	38 to 171	100 to 8000	0.0088 to 0.2371	Lee 1965
	50 to 170	2055 to 10150	0.0729 to 0.2386	Kiran 1992
Pentane	30 to 50	750 to 36400	0.1811 to 0.91	Oliveira 1992
	30	15 to 58800	0.216 to 1.5012	Brazier 1969
	38 to 171	200 to 3000	0.625 to 0.2303	Lee 1965
	45 to 170	1050 to 10150	0.0924 to 0.3325	Kiran 1992
Hexane	30 to 75	15 to 36252	0.0281 to 1.2882	Oliveira 1992
	0 to 60	15 to 58000	0.223 to 3.288	Brazier 1969
	25 to 100	15 to 60800	0.2357 to 2.1	Dymond 1980
	40 to 175	980 to 9548	0.114 to 0.4191	Kiran 1992
	25 to 75	15 to 72500	0.1908 to 1.411	Isdale 1979
Heptane	25 to 100	15 to 7346	0.1964 to 0.6295	Agaev 1963
	25 to 50	15 to 10046	0.6657 to 0.3041	Assael 1991
	50	15 to 14500	0.3030 to 0.6653	Baylaucq 1997
	30 to 75	15 to 36000	0.2429 to 1.8035	Oliveira 1992
Octane	30 to 75	15 to 36700	0.3875 to 2.7483	Oliveira 1992
	0 to 60	15 to 58800	0.359 to 5.6687	Brazier 1969
	25 to 75	15 to 21900	0.3031 to 1.680	Tanaka 1991
	50 to 100	15 to 7350	0.2440 to 0.5071	Agaev 1963
	25 to 100	15 to 73300	0.2457 to 8.67	Dymond 1981
	50 to 175	1865 to 9640	0.1868 to 0.7174	Kiran 1992
Nonane	30 to 50	15 to 10000	0.4869 to 1.1287	Assael 1991
Decane	30 to 75	15 to 38830	0.4628 to 5.3165	Oliveira 1992
	38 to 171	200 to 8000	0.2116 to 1.3020	Lee 1965
Undecane	30 to 50	15 to 9050	0.7472 to 1.8428	Assael 1991
Dodecane	38 to 135	15 to 52214	0.34 to 8.41	Hogenboom 1967
	25 to 75	15 to 21886	0.6654 to 3.567	Tanaka 1991
	25 to 100	15 to 72730	0.5080 to 10.44	Dymond 1981

Pentadecane	38 to 115	15 to 47040	0.54 to 11.160	Hogenboom 1967
Hexadecane	25 to 75	15 to 21820	1.231 to 7.92	Tanaka 1991
	25 to 100	15 to 61640	0.895 to 15.075	Dymond 1980
Octadecane	60 to 135	15 to 52920	0.750 to 12.820	Hogenboom 1967

3.3.2 *VPT Equation of State*

Since almost all of the viscosity prediction models require density value for viscosity estimation, a method to calculate fluid density is also necessary. For this reason, a thermodynamic approach, introduced by Valderrama, Patel and Teja, named hereafter VPT equation of state (Valderrama, 1990), with non-density-dependent (NDD) mixing rules (Avlonitis *et al*. 1994) was employed to model the phase equilibria and to predict fluid density. The authors (Valderrama, 1990 and Avlonitis *et al*. 1994) investigated the reliability of the proposed EoS for different hydrocarbon and non-hydrocarbon systems in their work. For instance, Figure 3.2 illustrates a comparison between the density data of n-decane taken from NIST against the VPT EoS prediction. As it can be seen in this graph the deviation between the density data reported by NIST and VPT equation of state prediction is about 2% (the error bars in the mentioned graph). Further discussion on the reliability of this equation of state is available in Chapter 6.

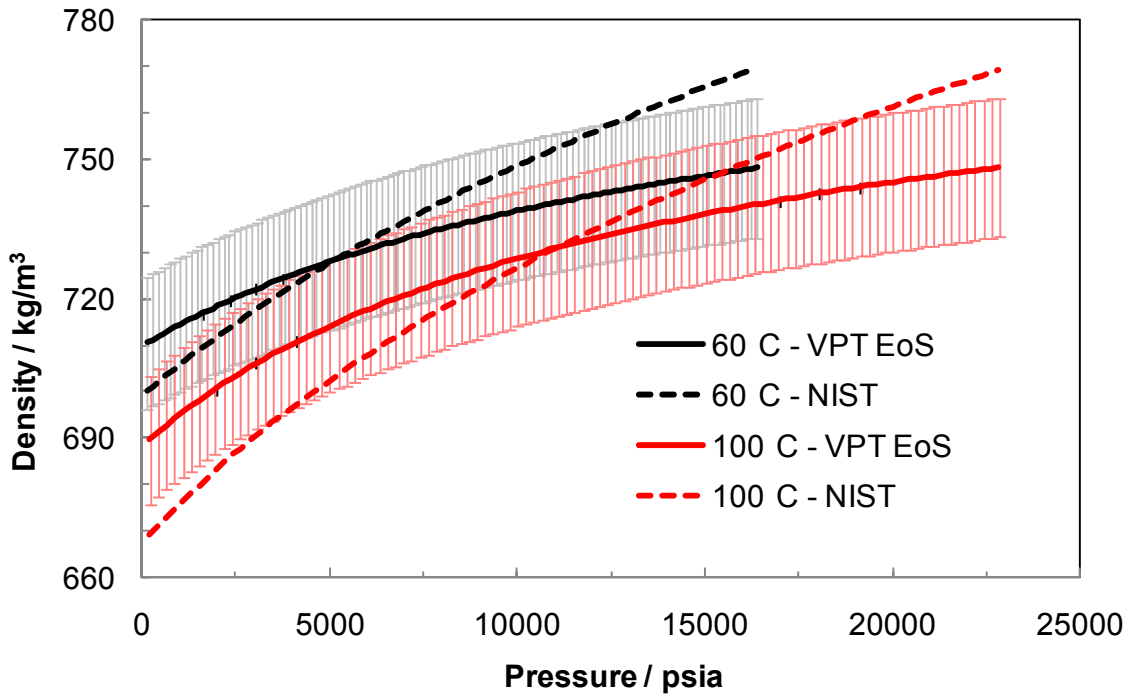

Figure 3.2 Density of decane: comparison between VPT-EoS prediction (solid lines) and density data from NIST (dash lines). The error bars show 2% of error.

3.3.3 *Viscosity Prediction Models (Literature)*

The Lohrenz-Bray-Clark (LBC) Method

Lohrenz *et al.* (1964) extended JST method (Jossi *et al.,* 1962) for calculating the viscosity of mixtures of naturally occurring hydrocarbons known as LBC method. A generalised relationship between viscosity and the fourth degree polynomial of the reduced density (ρ_r), of the form below (Equation 3.1), for non-polar gaseous and liquid substances, was formulated:

$$\left[(\eta-\eta_o)\zeta+10^{-4}\right]^{1/4}=a_0+a_1\rho_r+a_2\rho_r^{\,2}+a_3\rho_r^{\,3}+a_4\rho_r^{\,4} \tag{3.1}$$

Where ρ_r is reduced density, $a_{0\text{-}4}$ refer to correlation coefficients and ζ is viscosity reducing parameter which is the inverse of critical viscosity (Equation 3.2).

$$\eta_c=\frac{MW^{1/2}P_c^{2/3}}{T_c^{1/6}} \tag{3.2}$$

For monatomic compounds, the dilute gas viscosity, η_o, can be evaluated from the following empirical expression as a function of reduced temperature, T_r:

$$\eta_o\zeta_i = 0.00034T_r^{0.94} \qquad \text{for } T_r < 1.5 \qquad (3.3)$$

$$\eta_o\zeta_i = 0.0001778\left[4.58T_r - 1.67\right]^{5/8} \qquad \text{for } T_r > 1.5 \qquad (3.4)$$

The correlation coefficients, ($a_{0\text{-}4}$), are re-optimised with pure hydrocarbon experimental viscosity data (Table 3.7) and the density calculated by the VPT EoS. The calculated coefficients are shown in Table 3.8.

Table 3.8 The re-tuned coefficients for the LBC method using experimental viscosity data of pure hydrocarbons (Table 3.7) and the VPT EoS for the calculation of density

Coefficients	Value (using VPT EoS)	Value (original LBC)
a_0	0.113494	0.1023
a_1	-0.058862	0.023364
a_2	0.188612	0.058533
a_3	-0.108364	-0.40758
a_4	0.020258	0.0093324

A procedure for calculating the viscosities of hydrocarbon mixtures has been developed by authors (Lohrenz *et al.*, 1964) through the application of appropriate mixing rules. The mixture reducing parameter, ζ, can be calculated by molar averaging mixture critical properties and molecular weight, as shown below:

$$\zeta = \frac{\sum_{i=1}^{n}\left(x_i T_{ci}\right)^{1/6}}{\sum_{i=1}^{n}\left(x_i P_{ci}\right)^{2/3}\sum_{i=1}^{n}\left(x_i MW_i\right)^{1/2}} \qquad (3.5)$$

The low pressure mixture viscosity is calculated by the formulation of Herning *et al.* (1936) of the form:

$$\eta_{omix} = \frac{\sum_{i=1}^{n}\left(x_i\ \eta_{oi}\sqrt{MW_i}\right)}{\sum_{i=1}^{n}\left(x_i\ \sqrt{MW_i}\right)} \tag{3.6}$$

Where η_0, is defined above, x_i is the mole fraction of component *"i"* in the mixture, MW_i represents the molecular weight of component *"i"* in the mixture and the critical density can be calculated as below:

$$\rho_c = \frac{1}{V_c} = \frac{1}{\sum_{\substack{i=1 \\ i\neq C7+}}^{n}\left(x_i\ V_{ci}\right) + x_{C7+}\left(V_c\right)_{C7+}} \tag{3.7}$$

Where $(V_c)_{C7}^{+}$ is the critical molar volume of the C_7^{+} fraction calculated from the following expression;

$$V_{cC7+} = 21.573 + 0.015122\,MW_{C7+} - 27.656\,SG_{C7+} + 0.070615\,MW_{C7+}SG_{C7+} \tag{3.8}$$

That MW_{C7}^{+} is the molecular weight of the C_7^{+} fraction and SG_{C7}^{+} refers to the specific gravity of the C_7^{+} fraction. The unit of $(V_c)_{C7}^{+}$ is ft^3/lb mol.

The Modified LBC (HW2) (Al-Syabi et al., 2001):

Al-Syabi *et al.* (2001) modified the LBC method by applying the reduced temperature (T_r) and the molecular weight (MW) to the formulation to develop a new correlation. The authors presented two different formulations for methane (Equation 3.9) and heavier hydrocarbons (Equation 3.10).

$$\left(\Delta\eta_r + 10^{-4}\right)^{1/4} = \left(d_0' + d_1'\rho_r + d_2'\rho_r^2 + d_3'\rho_r^3 + d_4'T_r^{-3.2508}\rho_r^4\right) \tag{3.9}$$

$$\left(\Delta\eta_r + 10^{-4}\right)^{1/4} = \begin{pmatrix} d_0 + d_1\rho_r + d_2T_r^{-2.0183}MW^{0.44620}\rho_r^2 + \\ d_3T_r^{-2.47063}MW^{0.19188}\rho_r^3 + d_4 59T_r^{-1.1577}MW^{0.58683}\rho_r^4 \end{pmatrix} \tag{3.10}$$

The correlation coefficients, (d_{0-4} and d'_{0-4}), are re-tuned with pure hydrocarbon experimental viscosity data and using the density calculated by the VPT EoS. These coefficients are reported in Table 3.9.

Table 3.9 The re-tuned coefficients for the HW2 method by using experimental viscosity data of pure hydrocarbon (Table 3.7) and the VPT EoS for calculating density

Coefficients – Non Methane	Value	Coefficients - Methane	Value
d_0	0.095855	d'_0	0.102622
d_1	0.059779	d'_1	0.053888
d_2	-0.001282	d'_2	-0.006762
d_3	0.000516	d'_3	0.002354
d_4	9.48497E-05	d'_4	7.11483E-05

The employed procedure in calculating mixture viscosity using Equations 3.9 and 3.10 are similar to that employed by the LBC method.

The Pedersen Method (Pedersen et al. 1984, 1987):

The origin of this method is Tham *et al.* (1970) technique which was developed for predicting the viscosity of pure liquid hydrocarbons. Pedersen *et al.* (1984) generalised the above method for gas and liquid mixtures by employing Mo *et al.* (1974) mixing rules for calculating the mixture critical properties. Based on the above method, the viscosity of any substance can be determined from the below expression:

$$\eta(P,T) = \left(\frac{\eta_c}{\eta_{c,ref}}\right)\eta_{ref}\left(P_{ref},T_{ref}\right)F_\eta \qquad (3.11)$$

Where $\eta(P,T)$ represents viscosity of fluid of interest, $\eta_{ref}(P_{ref},T_{ref})$ is viscosity of reference fluid, P_{ref} , T_{ref} are equivalent pressure and temperature, respectively, proposed by the authors, η_c is critical viscosity (Equation 3.2), P_c and T_c refer to critical pressure (atm) and temperature (K) and F_η is corresponding state reducing factor, taken as the ratio of the rotational coupling factor of fluid of interest and the reference fluid.

3.3.4 *Developed Viscosity Prediction Models*

The above mentioned viscosity models were evaluated against the experimental viscosity data generated in present study. The results of these predictions are summarised in Table 3.14. Among the above discussed methods, Pedersen *et al.* (1984) showed better predictions for viscosity of most hydrocarbon systems. These methods were also compared with the newly introduced methods (in this section) and were evaluated in Section 3.4.

Three different methods, in an attempt to achieve better prediction results, were also developed in this work. These methods are discussed in this section:

The Modified Fenghour Correlation (this work):

Fenghour *et al.* (1997) developed a residual viscosity correlation for predicting the viscosity of CO_2. The method was reported to be valid in wide ranges of temperature and pressure from -73 to 1227 °C and up to 43,500 psia. The method is also employed by NIST website for viscosity prediction, so this proves the good accuracy of this technique in viscosity prediction of carbon dioxide. To make an effort, this method is extended in this work to predict the viscosity of hydrocarbon systems. For this reason the Fenghour correlation is modified by optimizing its constants for range of different hydrocarbons.

Fenghour *et al.* (1997) used the following equation to calculate the viscosity of the dilute gas phase (zero-density viscosity):

$$\eta_0(T) = \frac{1.00697 T^{1/2}}{\psi_\eta^*(T^*)} \tag{3.12}$$

The unit of $\eta_0(T)$, (the viscosity of dilute gas phase) is μ Pa s and T is in Kelvin. The reduced effective cross section term $\psi_\eta^*(T^*)$ is calculated by Equation 3.13 below:

$$\ln \psi_\eta^*(T^*) = \sum_{i=0}^{4} a_i (\ln T^*)^i \tag{3.13}$$

Where T^*, the reduced temperature, is given by:

$$T^* = kT/\varepsilon \tag{3.14}$$

The term, ε/k=251.196 is the energy scaling parameter. In this work, the mentioned parameter (ε/k) is considered as critical temperature (T_c) to cover all range of hydrocarbon data. The following series has been chosen by Fenghour *et al.* (1997) for the calculation of the residual viscosity term, Δη:

$$\Delta\eta(\rho,T)=\sum_{i=1}^{n} b_i(T)\rho^i \tag{3.15}$$

Where;

$$b_i=\sum_{j=1}^{m} d_{ij}/T^{*(j-1)} \tag{3.16}$$

Accordingly, Fenghour *et al.* (1997) used the above formulation and proposed Equation 3.17 for the residual viscosity term (excess viscosity), Δη.

$$\Delta\eta(\rho,T)=d_{11}\rho+d_{21}\rho^2+\frac{d_{64}\rho^6}{T^{*3}}+d_{81}\rho^8+\frac{d_{82}\rho^8}{T^*} \tag{3.17}$$

For obtaining a better fit for different hydrocarbons, in this study, the molecular weight, was introduced in Equation 3.17 as shown below:

$$\Delta\eta\,(\rho,T)=d_{11}\rho+d_{21}\rho^2+\frac{d_{64}\rho^6}{T^{*3}}+d_{81}\rho^8+\frac{d_{82}\rho^8}{T^*}+(c_1+c_2MW+c_3MW^2+c_4MW^3) \tag{3.18}$$

The correlation coefficients, *"a_i"*, *"d_{ij}"* and *"c_i"* of Equations 3.13 and 3.18 are optimised by utilising pure hydrocarbon experimental viscosity data (which are reported earlier in Table 3.7) and the calculated density. These coefficients are shown in Tables 3.10 to 3.12 for two different ranges of reduced density (less than 3 and greater than 3).

The coefficients were calculated for two different ranges of reduced density due to the fact that the coefficients couldn't be fit very well for all range of reduced densities. The mentioned coefficients resulted in a good match for the components with low reduced density (ρ_r< 3) with the absolute average deviation percentage (AAD%) of about 4%. But

these coefficients did not match very well for $\rho_r >= 3$ as the AAD% was about 18% for this set of data.

Table 3.10 Coefficients of viscosity of dilute gas formulation for various reduced density ranges (T in Kelvin and η_0 in μPa.s) employed in the modified Fenghour method (this work)

Reduced Density Ranges	a_0	a_1	a_2	a_3	a_4
< 3	0.6178185	-0.030298	-2.6300458	4.93050641	-2.7916887
>=3	-2.76774	-2.701	-17.3646	-30.46747605	-7.1134788

Table 3.11 Coefficients of the residual viscosity term for different reduced density ranges (T in Kelvin, η_0 in μPa.s and ρ in kg/m^3) employed in the modified Fenghour method (this work)

Reduced Density Ranges	d_{11}	d_{21}	d_{64}	d_{81}	d_{82}
< 3	0.0080155	0.000282	-6.729E-17	-5.384E-22	2.7566E-21
>=3	4.435858	-0.006	-7E-17	3.5846E-21	1.292E-20

Table 3.12 Coefficients of the residual viscosity term for different reduced density ranges (T in Kelvin, η_0 in μPa.s and ρ in kg/m^3) employed in the modified Fenghour method (this work)

Reduced Density Ranges	c_1	c_2	c_3	c_4
< 3	-2.7806357	0.278298	-0.0072819	4.5044E-05
>=3	1.737424	-27.89	0.16528	-0.000235619

The Temperature, Pressure, MW and Density Correlation (this work):

A generalized equation using non-critical properties of fluid as temperature, pressure molecular weight and density (TPMD method) in order to predict the viscosity of hydrocarbon is proposed in this work. For this reason a viscosity function is introduced as shown in Equations 3.19 and 3.20.

$$Viscosity\ Function = (i_0 + i_1\rho + i_2\rho^2 + i_3\rho^3 + i_4\rho^4 + i_5\rho^5) \times (j_0 + j_1 P) \times (k_0 + k_1 T) \times (l_0 + l_1 MW) \quad (3.19)$$

$$Viscosity = Exp[(Viscosity\ Function) + m_0 + m_1 P] \quad (3.20)$$

The adjusted coefficients are reported in Table 3.13. The units of the parameters are K, MPa, kg/m^3 for temperature, pressure and density, respectively. These coefficients are appropriate only if the VPT EoS was used for density calculation. The distribution of experimental viscosity data of pure hydrocarbons and the calculated one using the tuned coefficients against viscosity function (Equation 3.19) is shown in Figure 3.3. In this graph, there are three branches (in the experimental viscosity data) that do not follow the trend of the other viscosity data. It is noticeable that all of the mentioned data were obtained from the same source (Diller *et al.* 1981 and 1982). This method will also be used to predict the viscosity of some other mixtures: ranging from binary to real fluid, later in this chapter.

Table 3.13 Tuned coefficients for the TPMD method (this work) using experimental viscosity data of pure hydrocarbon (Table 3.7) and the VPT EoS for density calculation

Coefficients	Value	Coefficients	Value
i_0	-1.02E+01	j_0	0.007285
i_1	3.04E-02	j_1	5.857547
i_2	-9.46E-05	k_0	-0.00036
i_3	4.05E-07	k_1	0.320151
i_4	-7.01E-10	l_0	0.000909
i_5	4.23E-13	l_1	0.138143
m_0	-2.6626511	m_1	-0.00047996

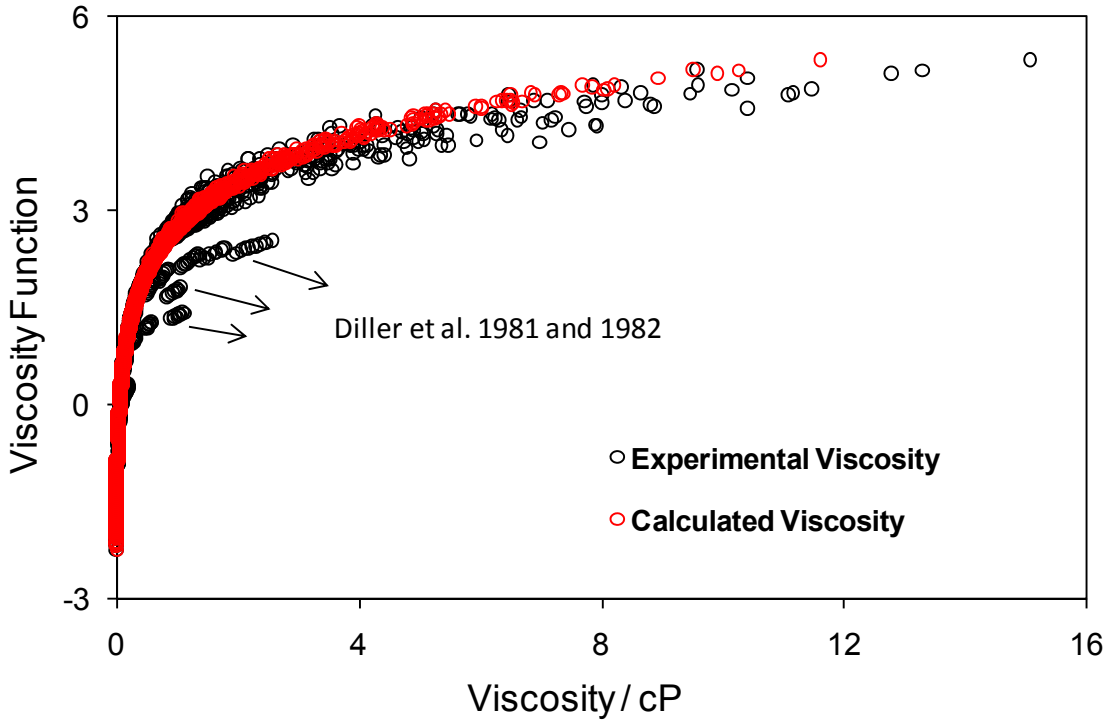

Figure 3.3 Experimental viscosity data of pure hydrocarbon (Table 3.7) versus the calculated viscosity using the TPMD method (this work) against the introduced viscosity function

The Artificial Neural Network (ANN) Method (this work):

Artificial neural network is a useful approach for correlating a limited quantity of experimental data with required variables.

Description; An artificial neural network consists of large numbers of computational units called neurons, connected to each other by means of directly weighted communication links as shown in Figure 3.4. The input layer of the network receives all the input data and introduces scaled data to the network. The data from the input neurons are propagated through the network via weighted interconnections. Every i neuron in a k layer is connected to every neuron in adjacent layers. The i neuron within the hidden k layer performs the following tasks: summation of the arriving weighted inputs (input vector $I_i = (I_{i,1},\ldots I_{i,Nk-1})$) and propagations of the resulting summation through a non-linear activation function f to the adjacent neurons of the next hidden layer or to the output neuron(s). In this work, the activation function is a sigmoid function:

$$f(x) = \tanh(x) = \frac{e^{x} - e^{-x}}{e^{x} + e^{-x}} \qquad x \in [0, 1] \tag{3.21}$$

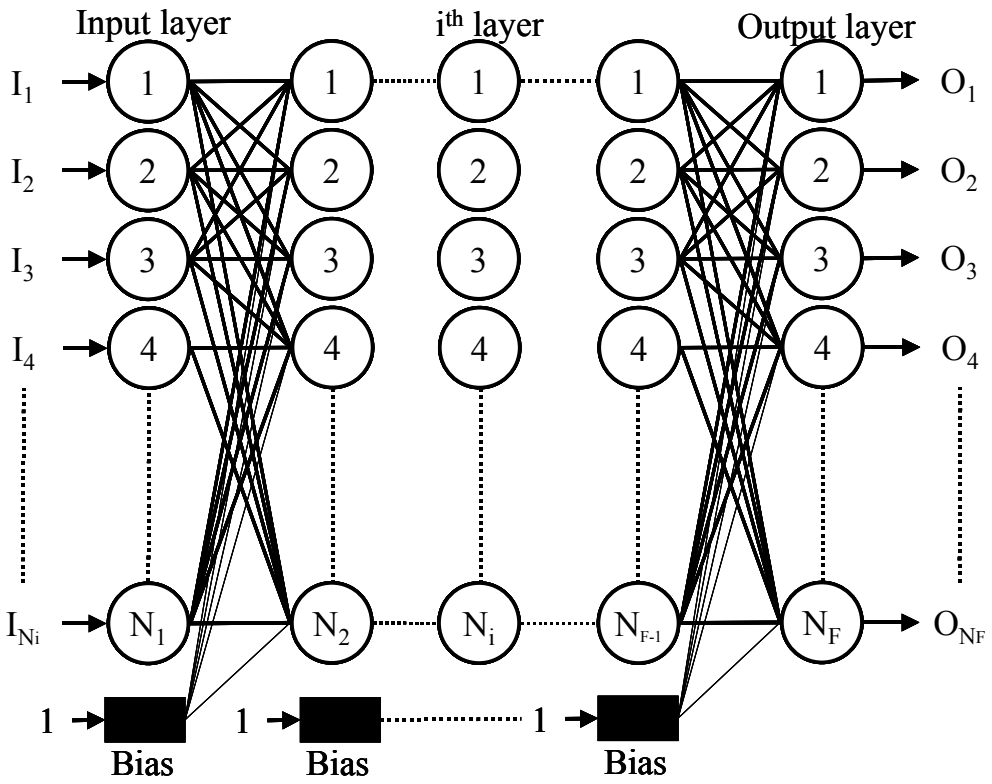

Figure 3.4 Architecture of a multi-layer feed forward artificial neural network

A bias term, b, is associated with each interconnection in order to introduce a supplementary degree of freedom. The expression of the weighted sum, S, to the i^{th} neuron in the k^{th} layer ($k \geq 2$) is:

$$S_{k,i} = \sum_{j=1}^{N_{k-1}} \left[(w_{k-1,j,i} I_{k-1,j}) + b_{k,i} \right] \tag{3.22}$$

Where w is the weight parameter between each neuron-neuron interconnection. Using this simple feed-forward networks with non-linear sigmoid activation functions, the output, $O_{k,i}$, of the i neuron within the hidden k layer is therefore:

$$O_{k,i} = \tanh\left(\sum_{j=1}^{N_{k-1}} \left[(w_{k-1,j,i} I_{k-1,j}) + b_{k,i} \right] \right) \tag{3.23}$$

To achieve a better stability and to have output of the same order of magnitude, the following scaling rule was applied to viscosity before normalisation:

$$Viscosity_{Network} = \ln(Viscosity_{\exp}) \tag{3.24}$$

During the training, input variables are fed to the network and the difference between the experimental outputs and the calculated outputs is used as a criterion for adjustment of network's synaptic weights. All synaptic weights and biases are first initialised randomly. The network is then trained and its synaptic weights are adjusted by an optimisation algorithm, until it correctly emulates the input/output mapping, by minimizing the average root mean square error. The optimisation method chosen in this work is the Levenberg-Marquardt algorithm (Levenberg 1944 and Marquardt 1963). The Levenberg-Marquardt optimisation algorithm consists of modifying the network's synaptic weight by the following formula:

$$w_j = w_{j-1} - [\overline{H}(w_{j-1}) + \mu_j \bar{I}_d]^{-1} \nabla J(w_{j-1}) \tag{3.25}$$

with

$$\overline{H}(w_j) = \sum_{k=1}^{N} \left(\frac{\partial err^k}{\partial w_j} \right) \left(\frac{\partial err^k}{\partial w_j} \right)^T + \sum_{k=1}^{N} \left(\frac{\partial^2 err^k}{\partial w_j \partial w_j^T} err^k \right) \tag{3.26}$$

Where err^k, μ, J, N are the residue vector, the step values of the Levenberg-Marquardt method, the Jacobian matrix of the first derivative of global error to weight and the number of feed inputs , respectively. err^k is defined by:

$$err^l = Y^l_{\exp.} - Y_{cal}{}^l \tag{3.27}$$

Finally, viscosity data are then transformed back to their original scale.

Data; The data set was subdivided into 3 classes: training (approximately, 50%), validation (approximately, 25%) and test set (approximately 25%), having the same repartition of data (same range of temperature, pressure, MW, density and viscosity). After partitioning of the data set, the training-set was used to tune the parameters, i.e. determination of the optimum values of synaptic weights and biases. The validation-set is used during the adjustment of the network's synaptic weights to evaluate the algorithms performance on independent data and stop the tuning if the error on the validation set increases. The validation-set is not an independent data set but does not have any influence in the parameter fitting procedure. Finally, the test-set measures the generalization ability of the model after the fitting process. The range of temperatures and compositional data used in input is given in Table 3.7.

Architecture; To find the optimal network architecture, a trial and error procedure is applied, in which the structure of the network is changed and the resulting network is trained, validated and tested using the previously describe algorithm and procedures.

If the number of neurons is too small, the network may fail to train correctly and the overall accuracy of the network would suffer. However, a network with too many nodes can fail to capture the underlying relationship between input and output variables, it cannot learn to generalize, the network only memorize the training example, "over-fitting". The overall tuning and validation test accuracy of the network and the test-set accuracy are used to compare the performance of the various network trial architectures.

3.4 Evaluation of the Viscosity Prediction Models

The experimental viscosity data generated in present work (Tables 3.1 to 3.6) were employed to evaluate the above mentioned viscosity models. It is worth mentioning that these experimental viscosity data could be considered as independent data since they were not used in any of the proposed correlations or optimising any of the models' coefficients.

Methane - Heptane (Binary No. 1) Figures 3.5a – 3.5d illustrate a comparison between the measured and predicted viscosity for this binary. The ANN method gave better prediction of viscosity trends and values than the other methods. Also, the HW2 and Pedersen methods predict viscosity of this binary system reasonably well. In general, the discussed models can calculate viscosity of this mixture more accurately at high

temperature and low pressure conditions. This could be due to the reliability of the mentioned methods at lower density of the tested fluid.

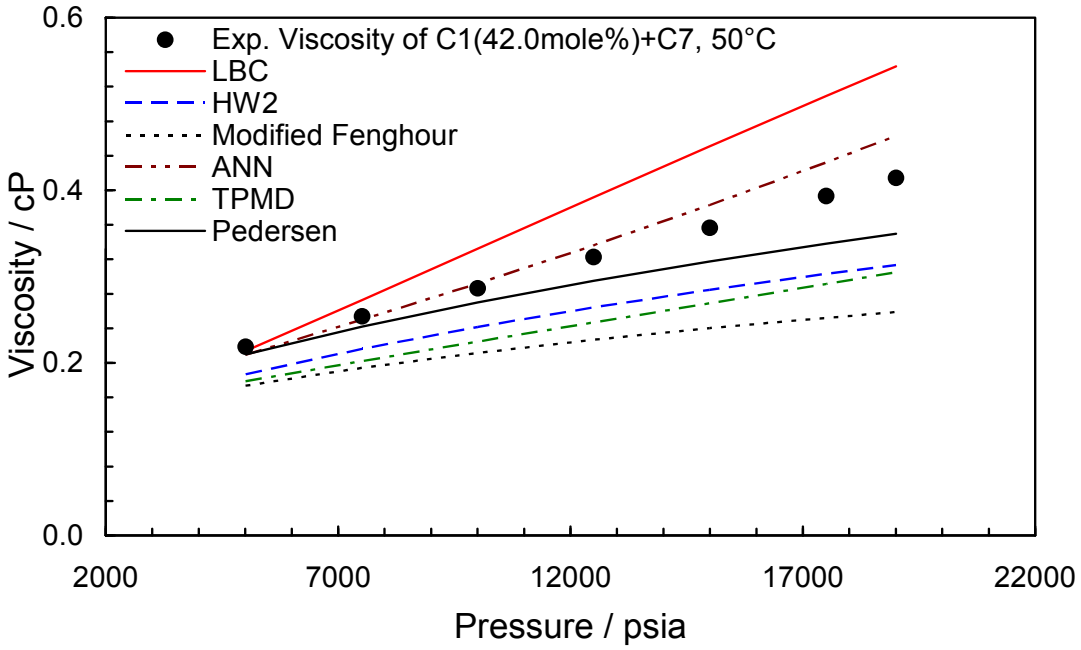

Figure 3.5a Experimental (this work) and predicted viscosities versus pressure for methane/heptane binary at 50 °C

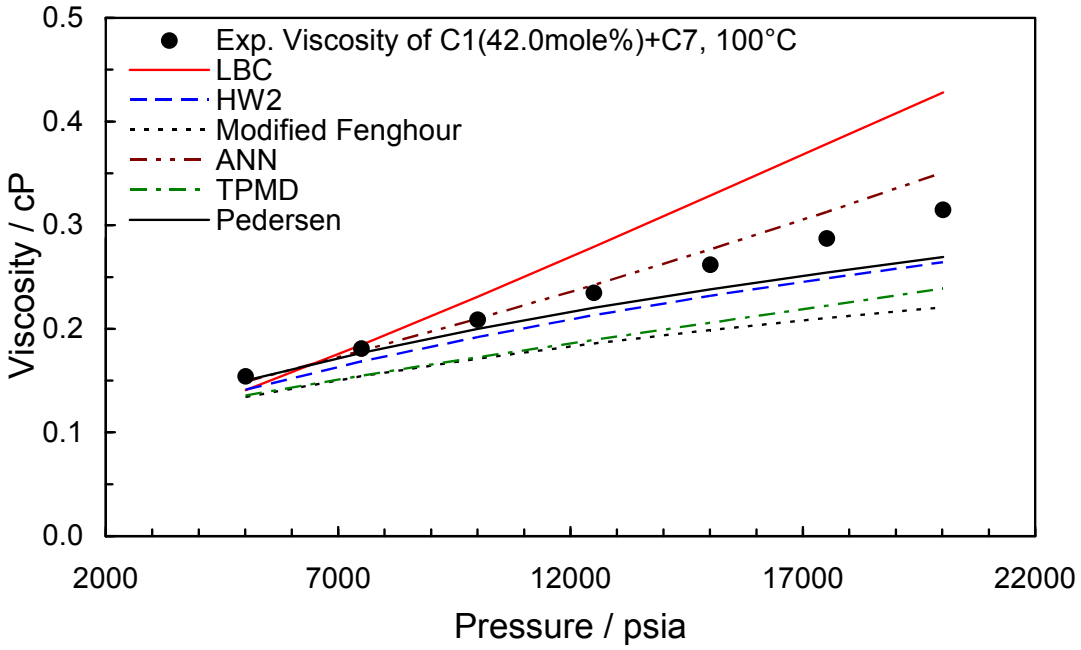

Figure 3.5b Experimental (this work) and predicted viscosities versus pressure for methane/heptane binary at 100 °C

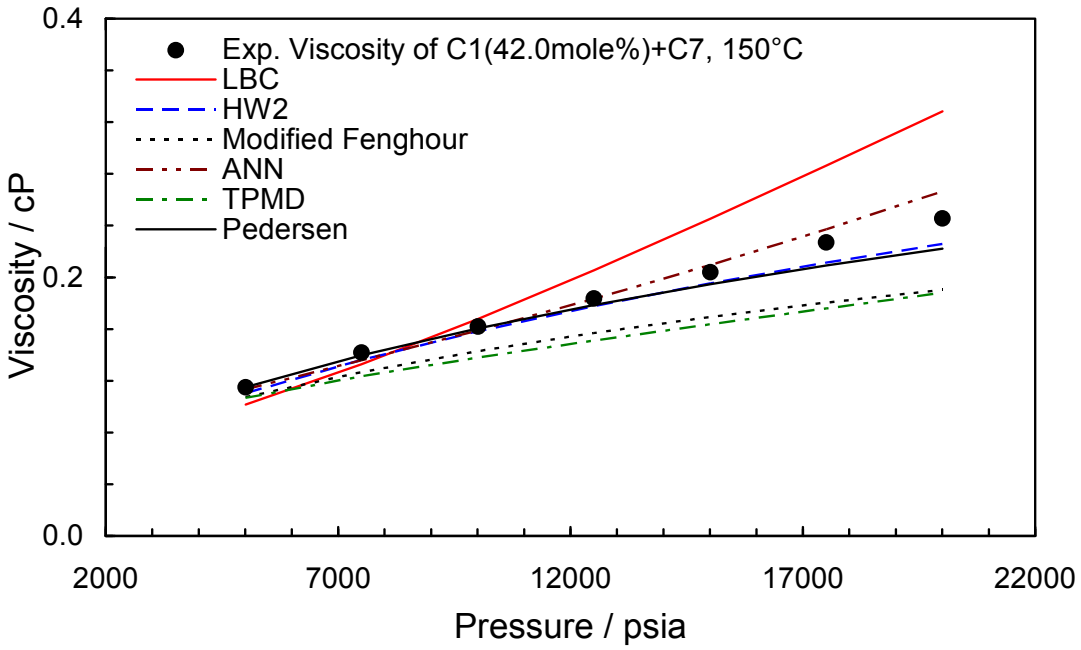

Figure 3.5c Experimental (this work) and predicted viscosities versus pressure for methane/heptane binary at 150 °C

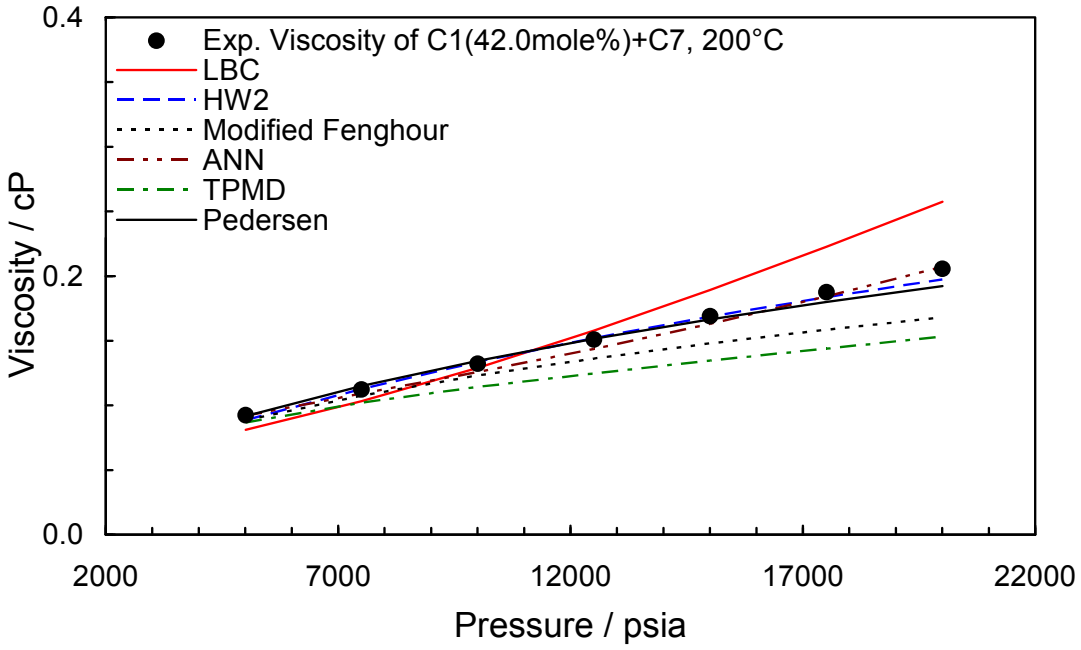

Figure 3.5d Experimental (this work) and predicted viscosities versus pressure for methane/heptane binary at 200 °C

Methane – Decane (Binary No. 2) Figures 3.6a – 3.6d present a comparison between experimental data and predicted viscosity for this binary. The ANN, LBC and Pedersen predict the viscosity of this binary better than other models presented here. The mentioned models can predict the trends of viscosity very well in the range of pressure and temperature.

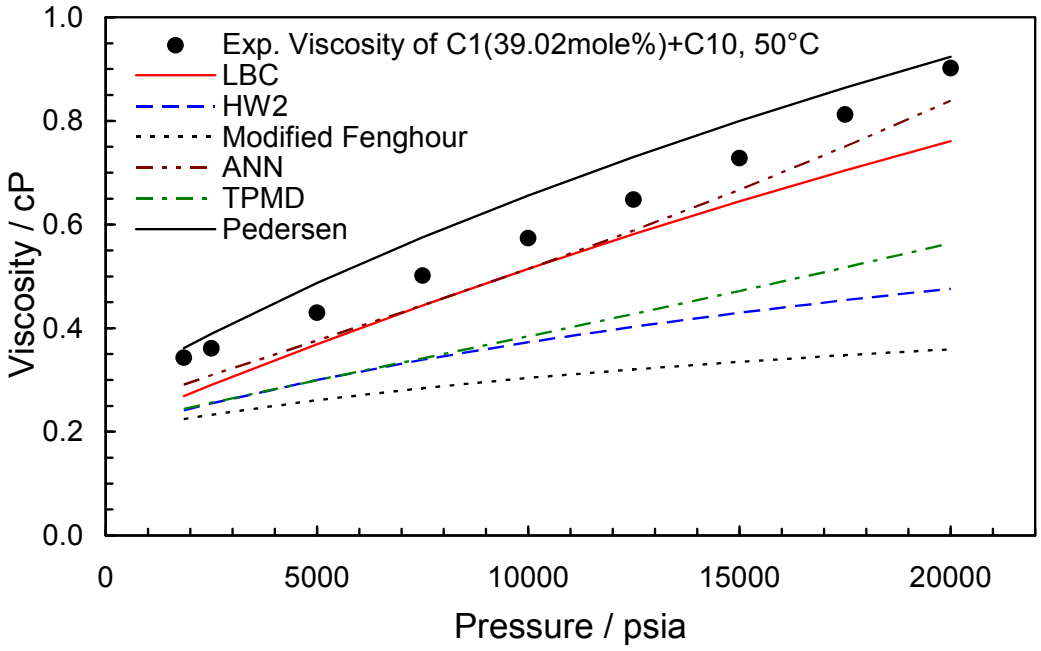

Figure 3.6a Experimental (this work) and predicted viscosities versus pressure for methane/decane binary at 50 °C

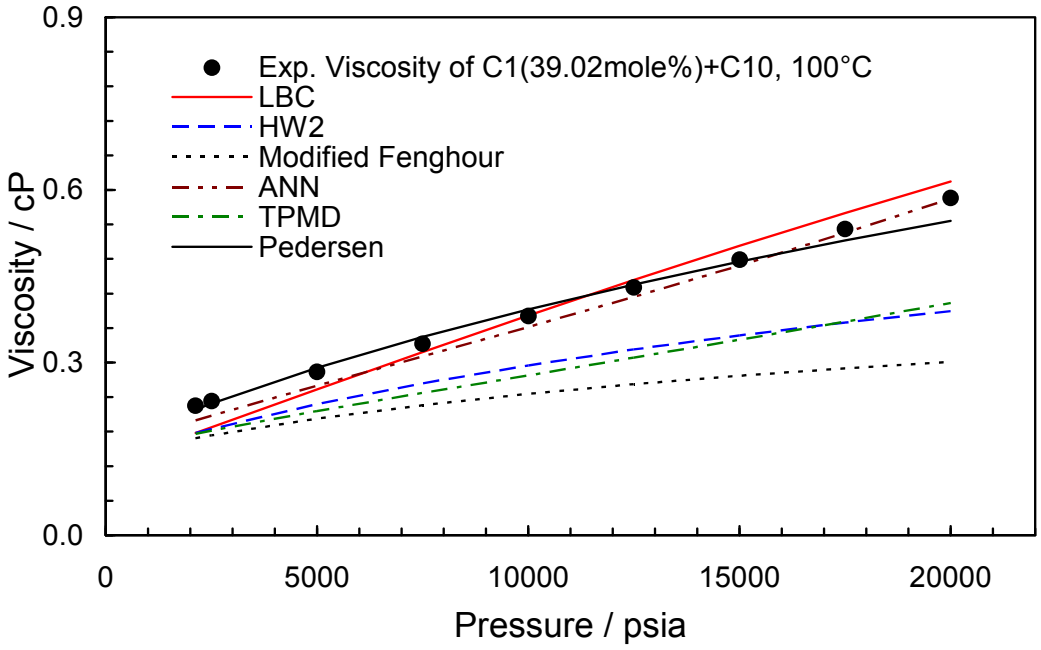

Figure 3.6b Experimental (this work) and predicted viscosities versus pressure for methane/decane binary at 100 °C

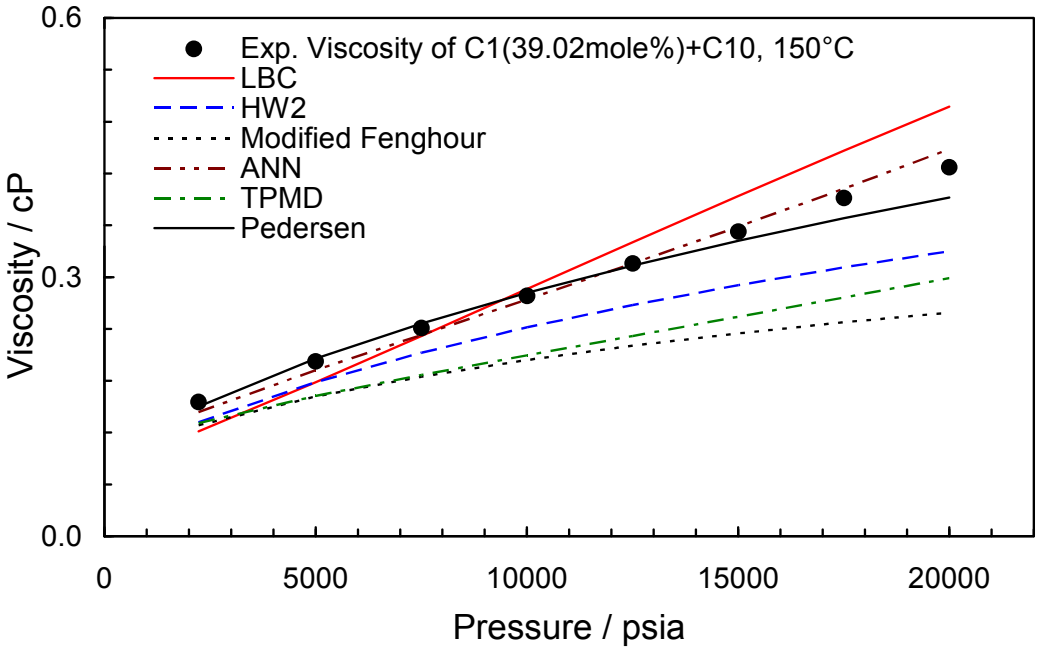

Figure 3.6c Experimental (this work) and predicted viscosities versus pressure for methane/decane binary at 150 °C

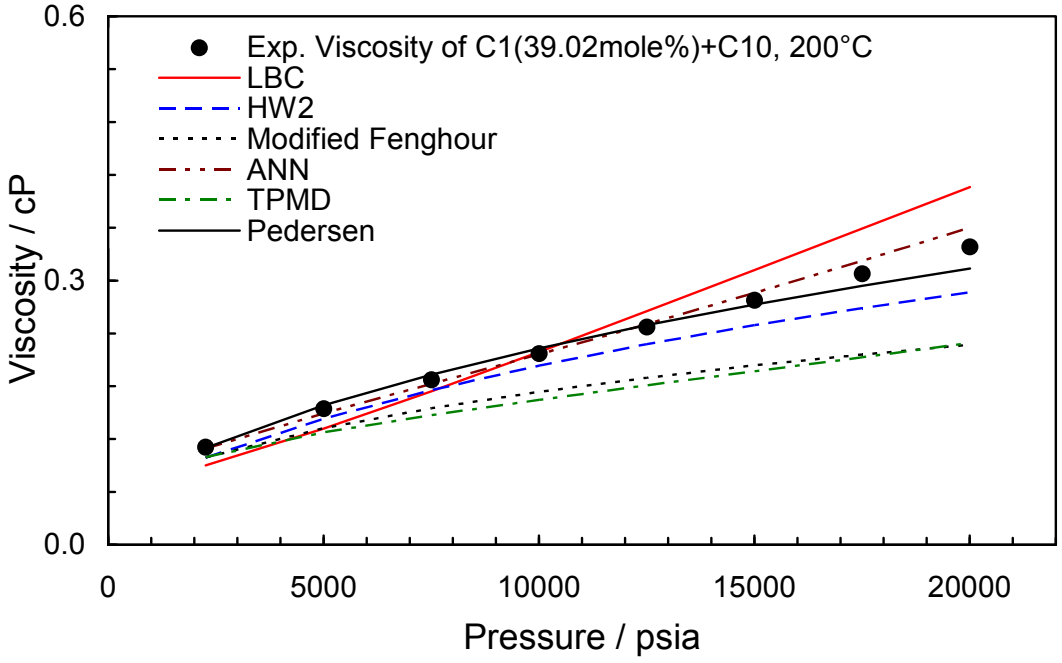

Figure 3.6d Experimental (this work) and predicted viscosities versus pressure for methane/decane binary at 200 °C

Methane – Toluene (Binary No. 3) Figures 3.7a – 3.7d compare the measured and predicted viscosity for this binary. For this system, predictions using Pedersen, HW2 and LBC are superior to other methods. The TPMD method is not presented in these graphs as no cyclic compounds viscosity data were used in tuning the model (the same is applicable to the ANN method).

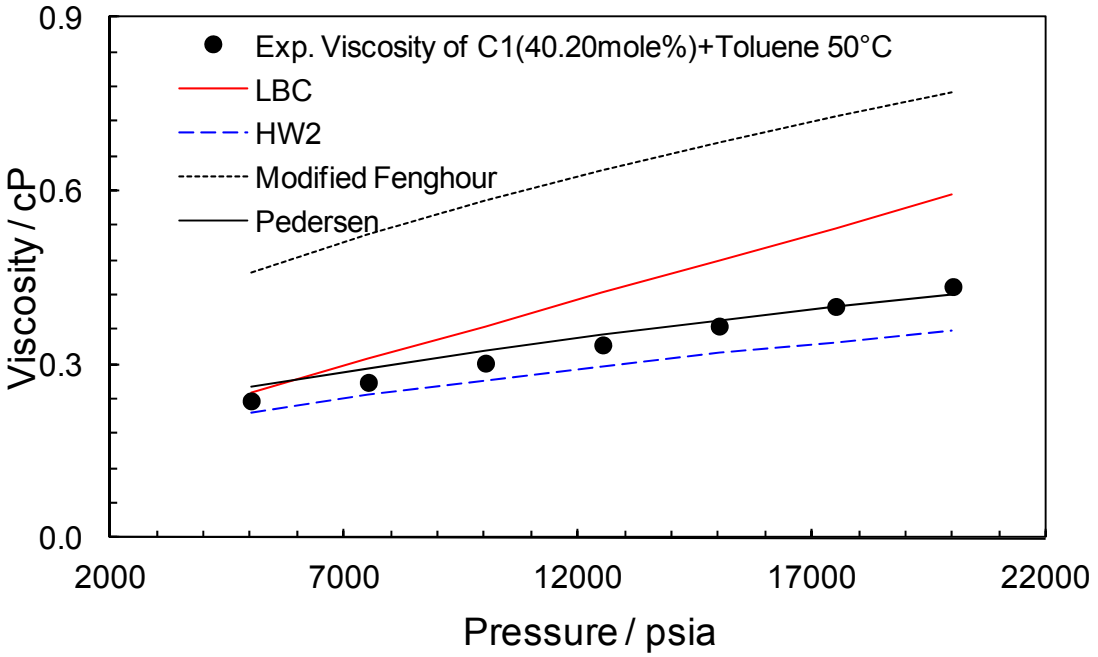

Figure 3.7a Experimental (this work) and predicted viscosities versus pressure for methane/toluene binary at 50 °C

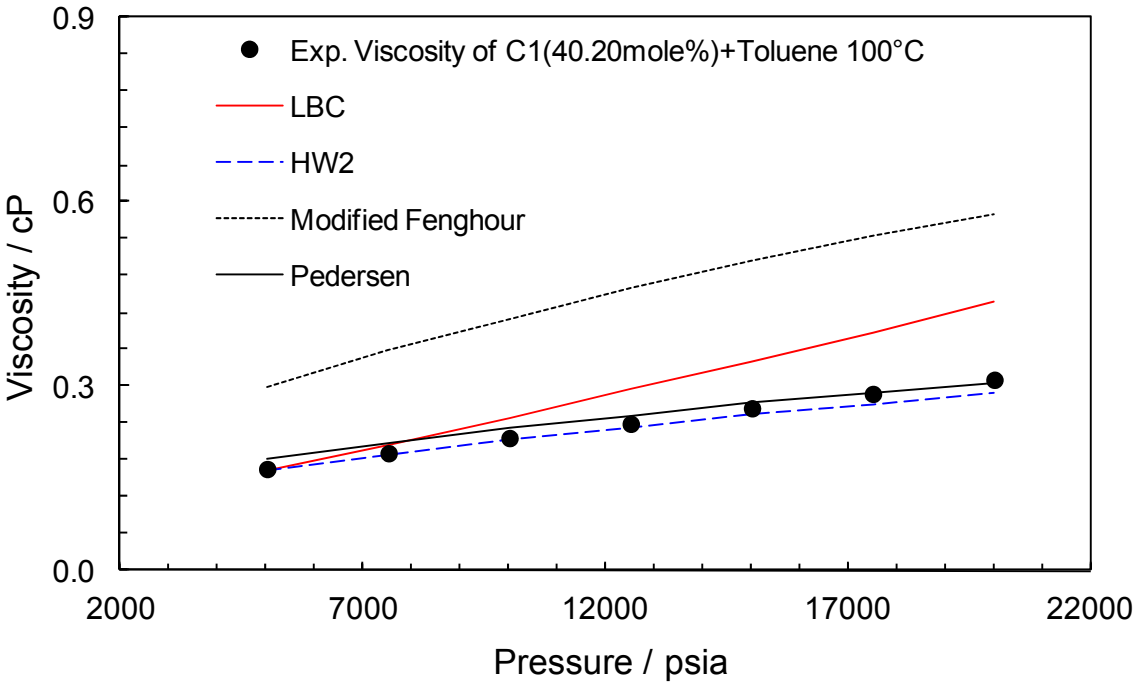

Figure 3.7b Experimental (this work) and predicted viscosities versus pressure for methane/toluene binary at 100 °C

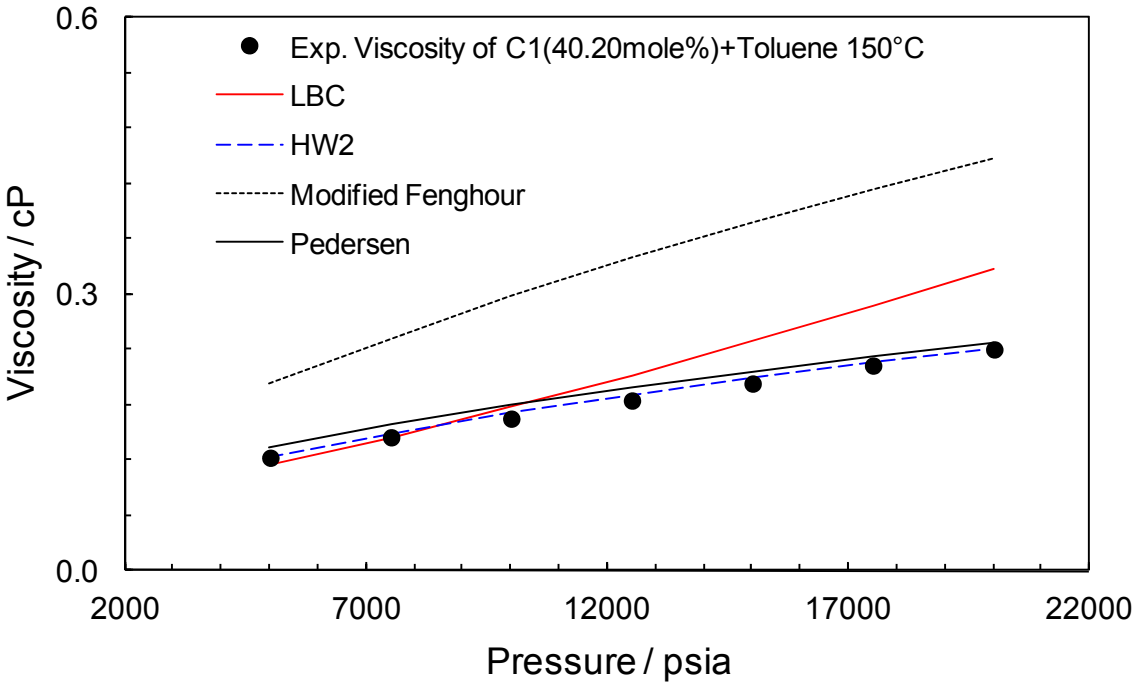

Figure 3.7c Experimental (this work) and predicted viscosities versus pressure for methane/toluene binary at 150 °C

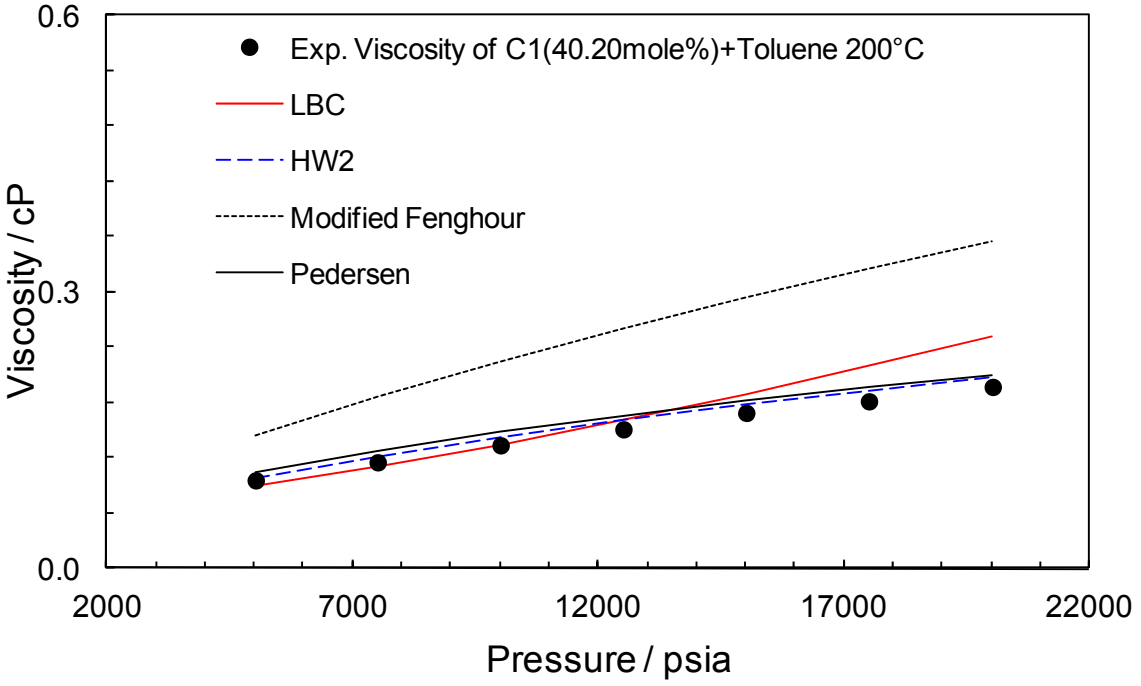

Figure 3.7d Experimental (this work) and predicted viscosities versus pressure for methane/toluene binary at 200 °C

Gas Condensate (GCB00-1) Figures 3.8a – 3.8d show the comparison between experimental data and predicted viscosity for gas condensate (GCB00-1). Generally, for this real reservoir fluid, the predictions of almost all models are in good agreement with the experimental data. Only LBC could not predict the trend of viscosity especially at lower temperatures.

The critical properties are needed to predict viscosity. For SCN fractions, T_c, P_c and V_c of normal alkane were employed. The critical properties of the plus fraction were also calculated (with knowing the MW).

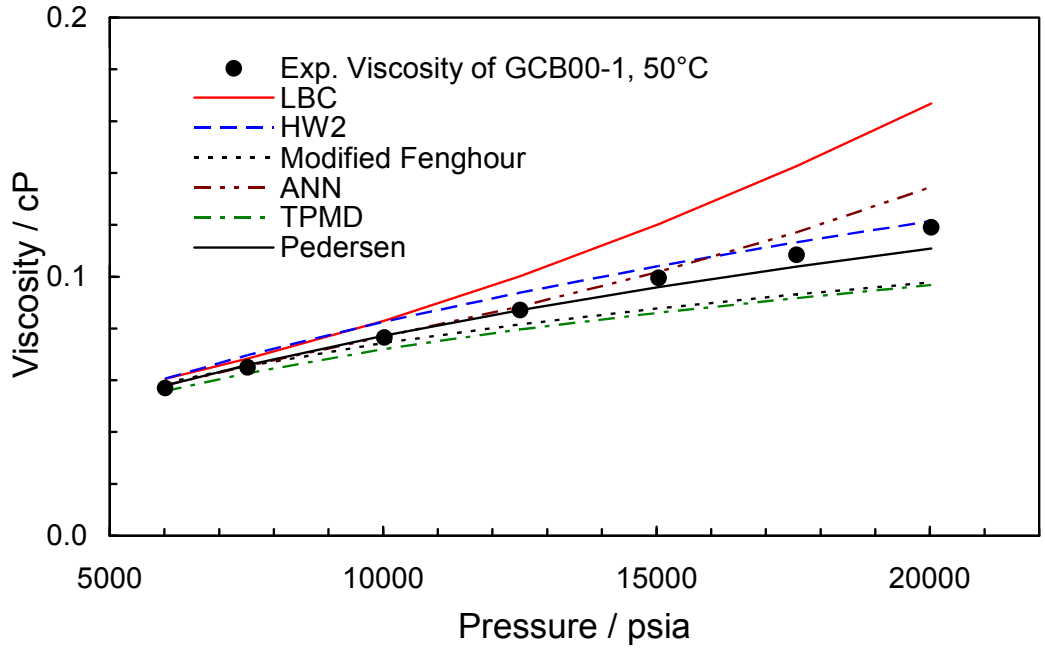

Figure 3.8a Experimental (this work) and predicted viscosities versus pressure for gas condensate (GCB00-1) at 50 °C

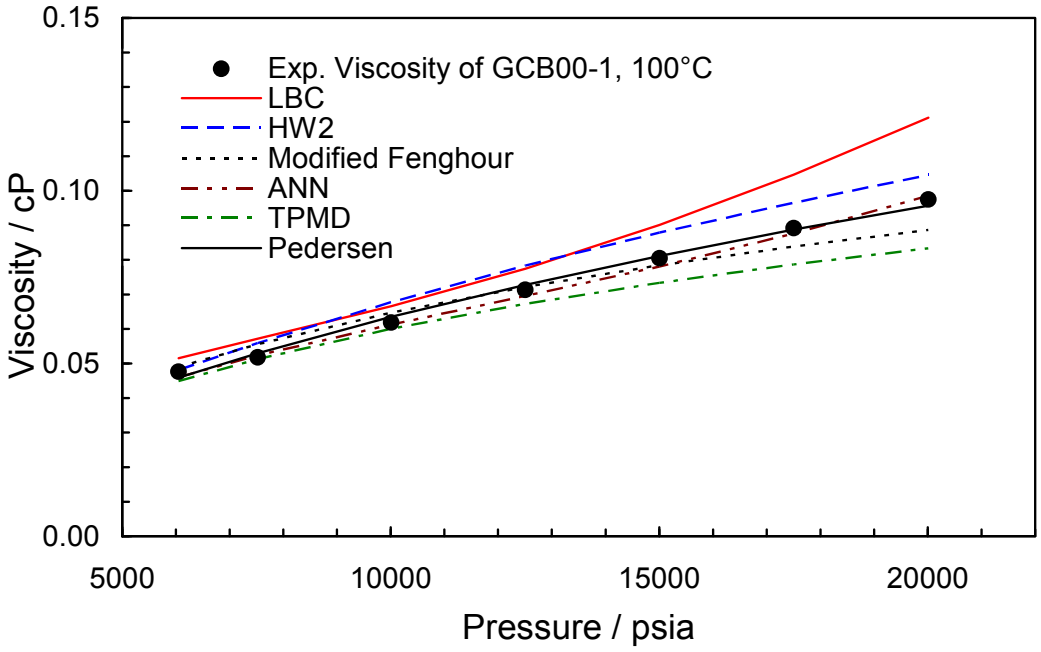

Figure 3.8b Experimental (this work) and predicted viscosities versus pressure for gas condensate (GCB00-1) at 100 °C

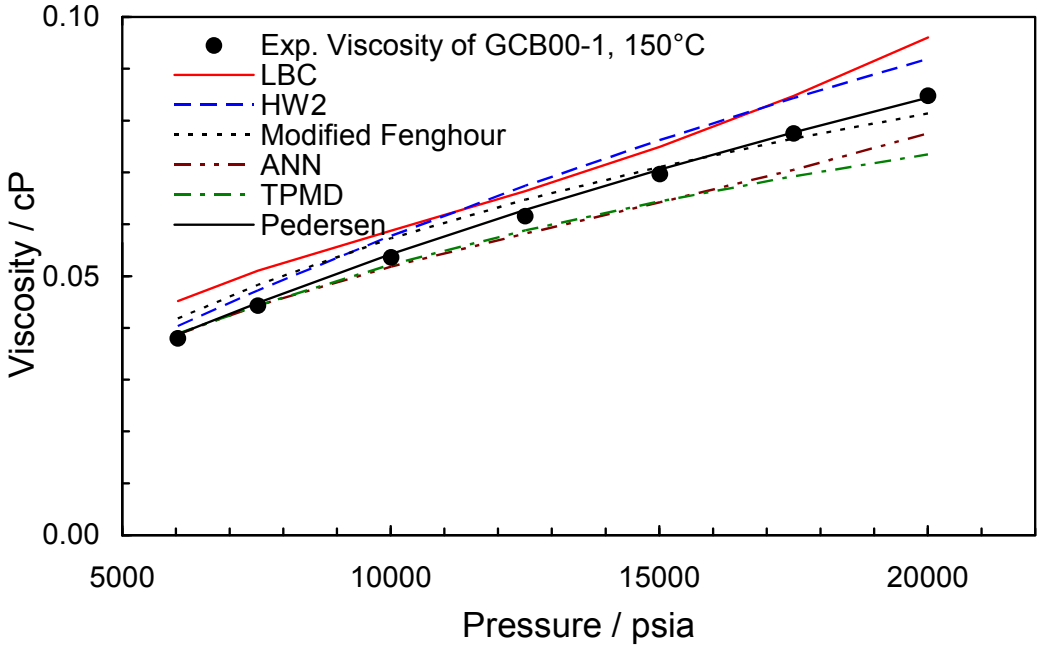

Figure 3.8c Experimental (this work) and predicted viscosities versus pressure for gas condensate (GCB00-1) at 150 °C

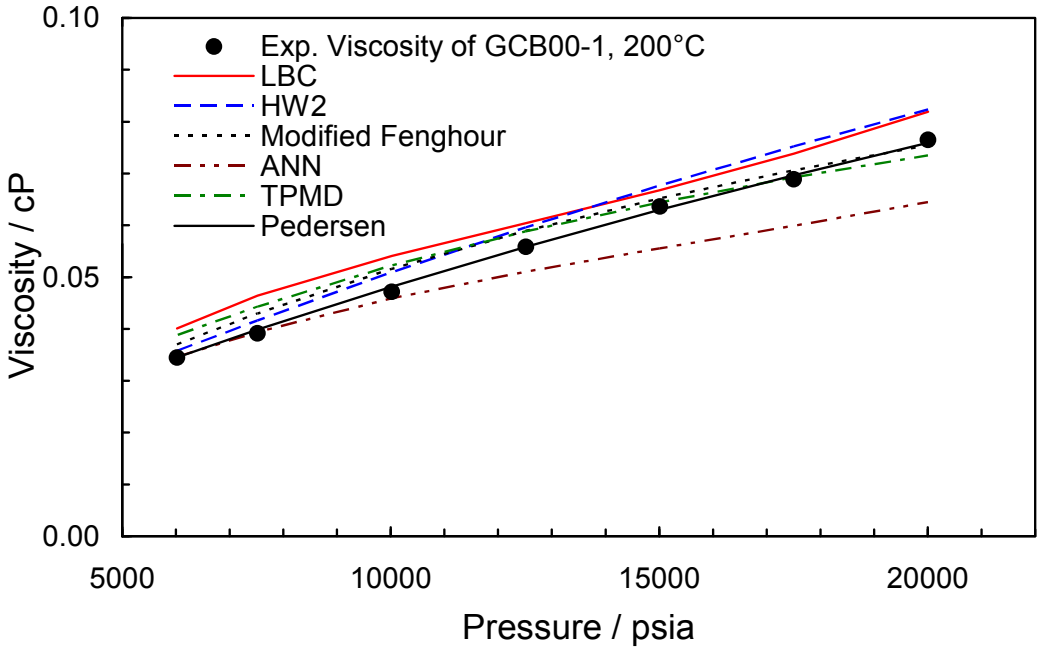

Figure 3.8d Experimental (this work) and predicted viscosities versus pressure for gas condensate (GCB00-1) at 200 °C

Natural Gas (NG1) Figures 3.9a – 3.9d evaluate the predicted viscosity values for natural gas (NG1) by comparing them with the experimental data. Except the Pedersen and LBC methods, the other studied techniques can predict the experimental data of NG1 viscosity reasonably well.

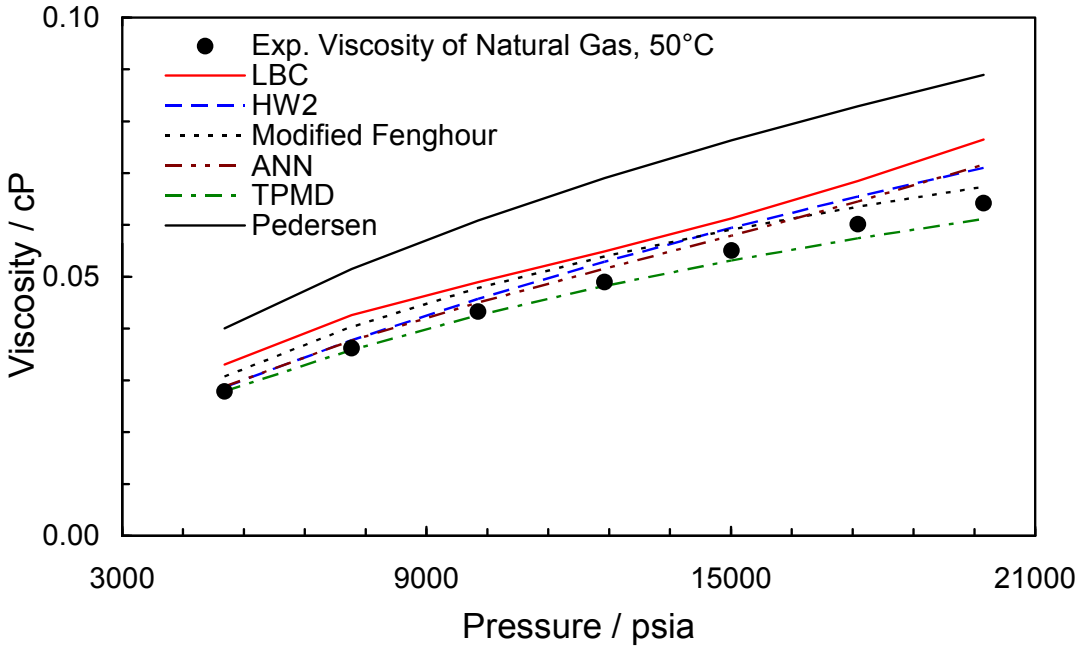

Figure 3.9a Experimental (this work) and predicted viscosities versus pressure for natural gas (NG1) at 50 °C

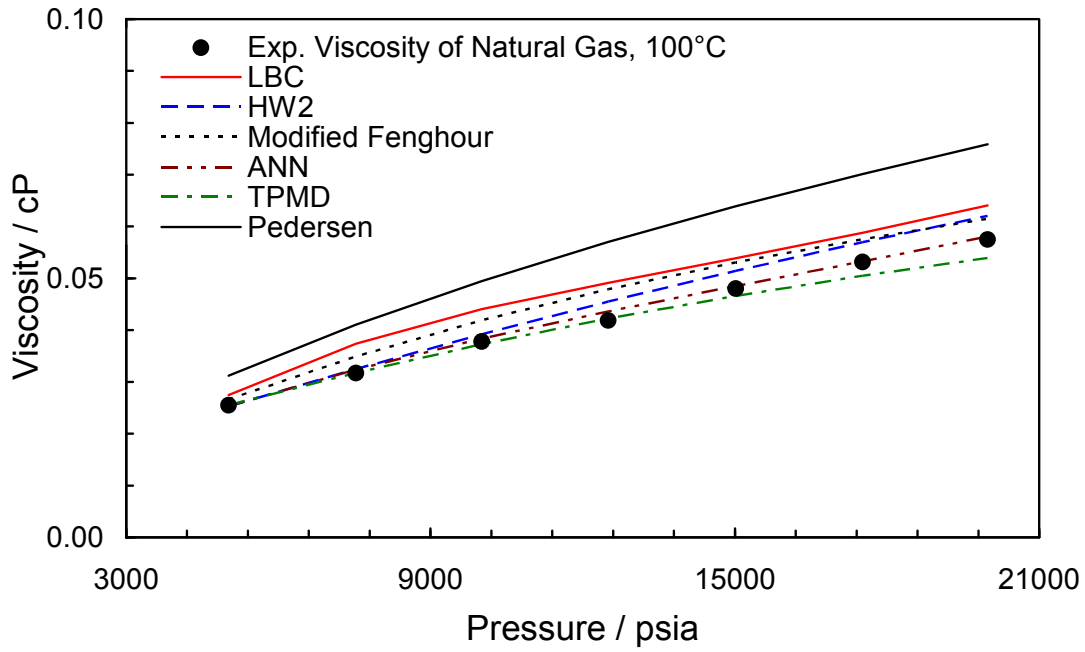

Figure 3.9b Experimental (this work) and predicted viscosities versus pressure for natural gas (NG1) at 100 °C

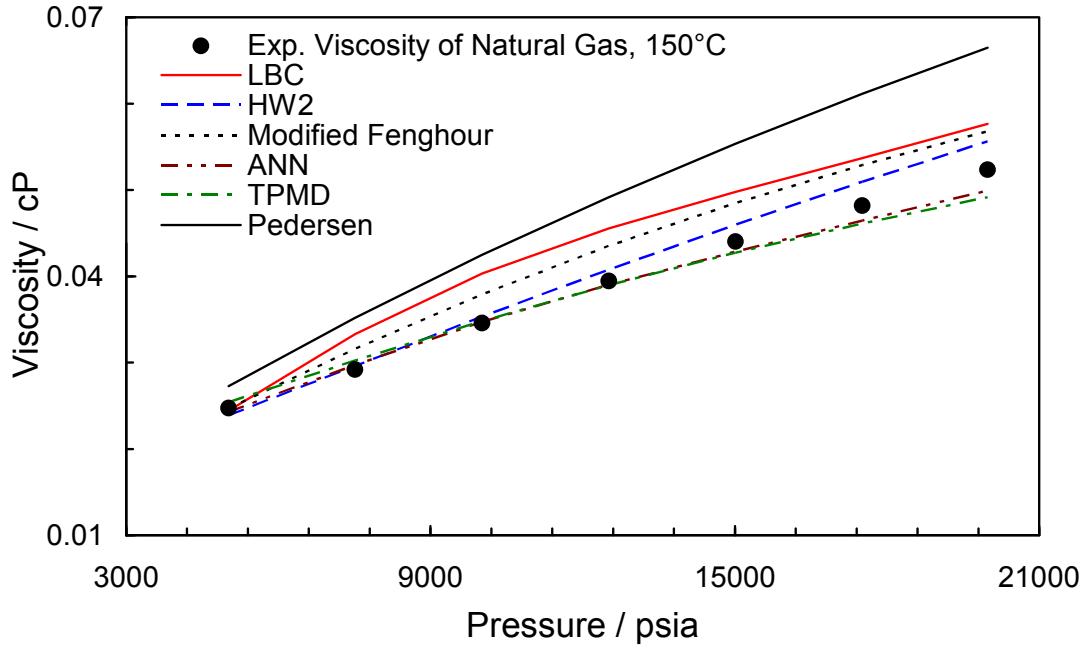

Figure 3.9c Experimental (this work) and predicted viscosities versus pressure for natural gas (NG1) at 150 °C

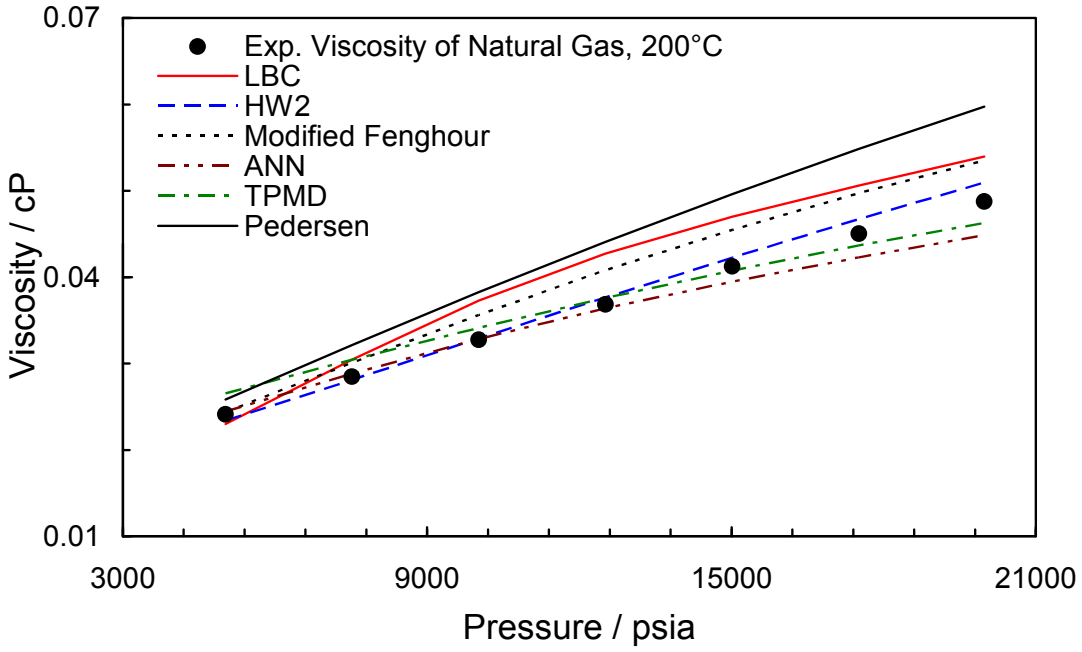

Figure 3.9d Experimental (this work) and predicted viscosities versus pressure for natural gas (NG1) at 200 °C

Synthetic Volatile Oil Figures 3.10a – 3.10d show a comparison between experimental data and predicted viscosity for synthetic volatile oil. Very good viscosity predictions for this fluid were obtained with the Pedersen, LBC and ANN methods.

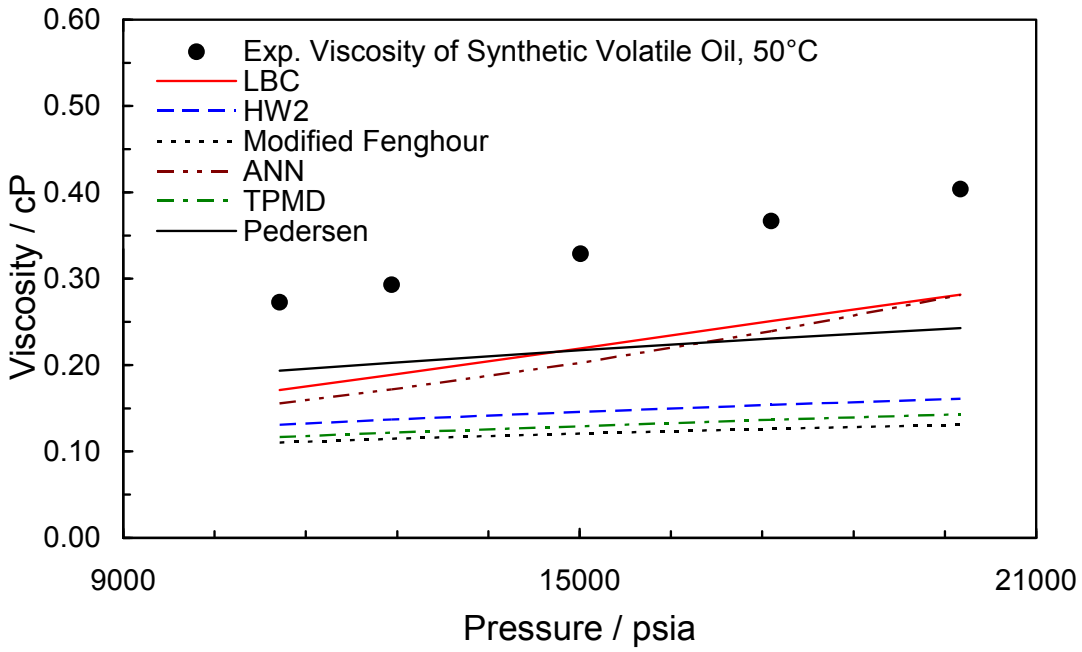

Figure 3.10a Experimental (this work) and predicted viscosities versus pressure for synthetic volatile oil at 50 °C

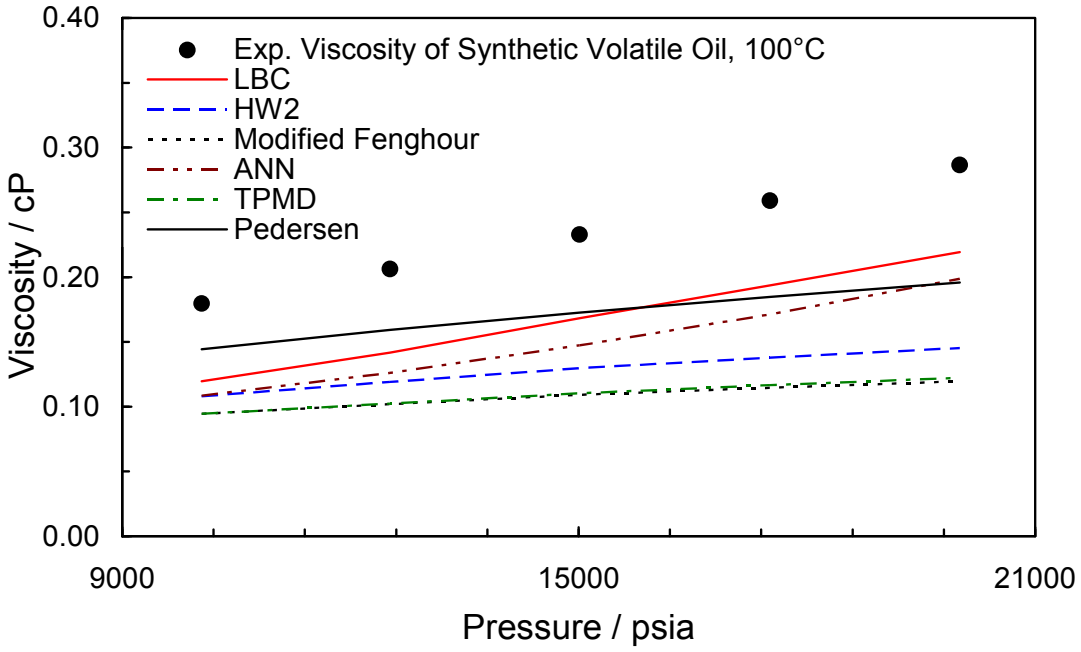

Figure 3.10b Experimental (this work) and predicted viscosities versus pressure for synthetic volatile oil at 100 °C

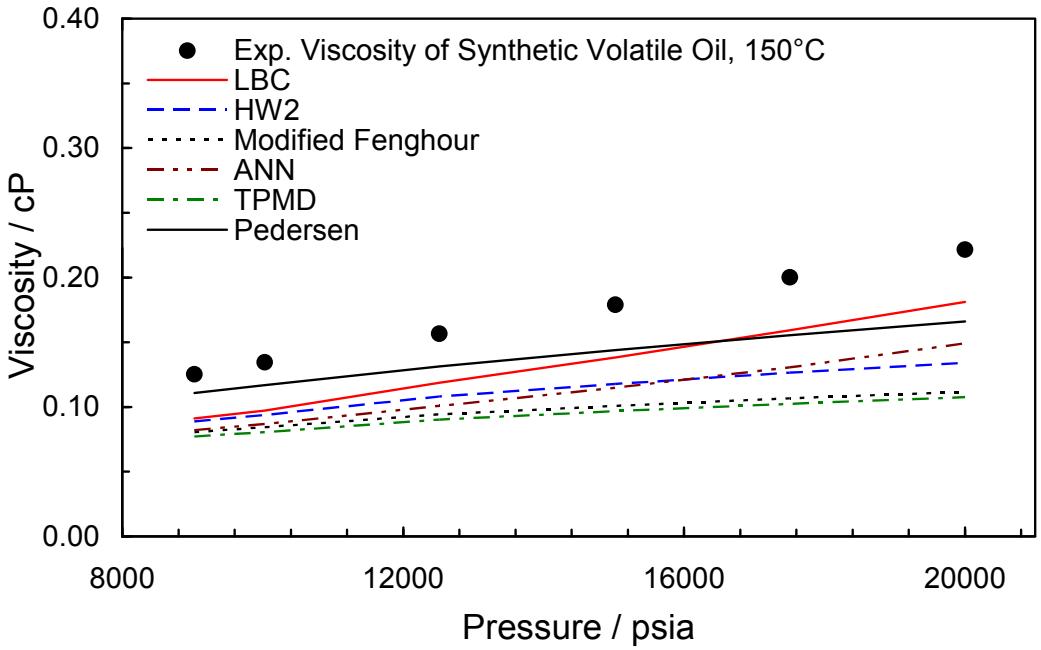

Figure 3.10c Experimental (this work) and predicted viscosities versus pressure for synthetic volatile oil at 150 °C

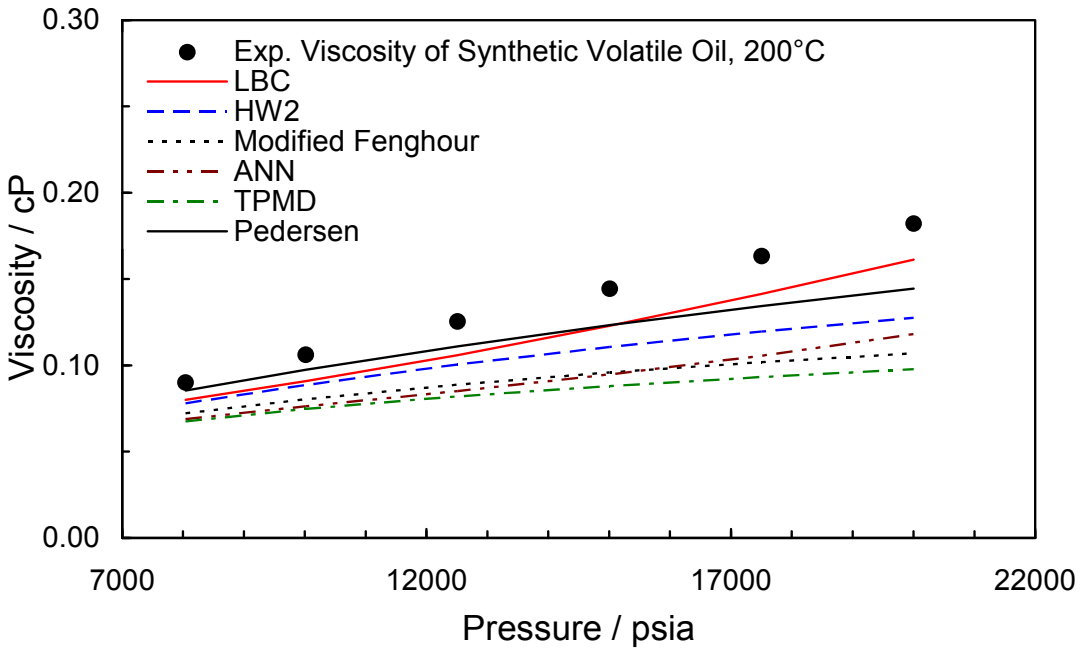

Figure 3.10d Experimental (this work) and predicted viscosities versus pressure for synthetic volatile oil at 200 °C

The average absolute deviation percentages of the investigated viscosity prediction techniques in estimating various fluid viscosities are reported in Table 3.14. The ANN and TPMD methods could predict the viscosity of different fluids reasonably well only if these methods have been tuned in the range of fluids parameters (like density and MW). Consequently it is recommended to use these techniques only in the accepted range of temperature and pressure. Since these two methods (ANN and TPMD) were not tuned for toluene (cyclic compounds), their prediction results were not reported in the table below.

As it can be seen in Table 3.14, the viscosity prediction results of the newly developed methods (ANN and TPMD) are not superior to the other techniques. However these methods have the advantage of being very simple to use because no critical properties of the fluid were employed in viscosity calculation. So by optimising the coefficients of TPMD (or ANN method) for the range of interest, this method is expected to show promising results in viscosity prediction.

Table 3.14 The summary of average absolute deviation percentage (AAD%) of predicted viscosities using different techniques

Models / Fluids	LBC	HW2	Pedersen	Modified Fenghour (this work)	TPMD (this work)	ANN (this work)
Binary No.1 (C_1/nC_7)	17	9	6	19	19	4
Binary No.2 (C_1/nC_{10})	11	22	5	34	27	6
Binary No.3 (C_1/ Toluene)	18	6	7	81	not used	not used
Gas Condensate (GCB00-1)	13	7	2	6	7	5
Natural Gas	13	5	28	9	3	3
Synthetic Volatile Oil	24	38	22	46	48	35

3.5 Conclusions and Perspective

A high-pressure and high-temperature apparatus has been used for measuring viscosity of hydrocarbon systems. Due to limited number of experimental viscosity data on hydrocarbon mixtures at HPHT conditions in open sources, a series of viscosity measurements have been performed on three binary hydrocarbon systems: methane/heptane, methane/decane and methane/toluene and also on three multi-component mixtures: a natural gas, a gas condensate and a synthetic volatile oil. Viscosity data has been generated in a temperature range from 50 °C to 200 °C and up to 20,000 psia. The results can provide valuable information to evaluate and develop viscosity prediction techniques appropriate for extreme conditions.

The reported experimental data were used to assess several viscosity models and compare their performance. Viscosity prediction models like: the Lohrenz–Bray–Clark (LBC), the Pedersen correlations and HW2 (a modified LBC correlation) and some proposed methods (as part of this research) such as an ANN method, a simple correlation incorporating the effects of temperature, pressure, molecular weight and density (TPMD) and a residual viscosity correlation method (modified Fenghour) were the selected and developed viscosity prediction techniques in this study for evaluation. Among the evaluated models, the Pedersen, LBC and HW2 methods show better predictions. The ANN and TPMD can be reliable in viscosity estimation if they have been used in the correct range of temperature and pressure. However, the modified Fenghour method showed prediction with acceptable accuracy for the complex fluids examined in this chapter.

Some of the discussed models in present chapter were employed to propose a new technique for viscosity prediction of various dead oils from the viscosity of contaminated samples that is detailed in Chapter 4.

References

Al-Syabi, Z., Danesh A., Tohidi, B., Todd, A.C. and Tehrani, A.D., 2001, *A residual viscosity correlation for predicting the viscosity of petroleum reservoir fluids over wide ranges of pressure and temperature*, Chemical Engineering Science, **56**, 6997–7006

Agaev, N. A. and Golubev, I. F., 1963, *The Viscosity of n-Hexane in the Liquid and Gaseous State at High Pressures and Different Temperatures*, Dokl. Akad. Nauk USSR, **151**, (3), 635-640

Assael, M. J., Dalaouti, N. K. and Vesovic, V., 2001, *Viscosity of Natural-Gas Mixtures: Measurements and Prediction,* International Journal of Thermophysics, **22**, 1

Assael, M. J. and Papadaki, M., 1991, *Measurements of the Viscosity of n-Heptane, n-Nonane, and n-Undecane at Pressures up to 70 MPa*, Int. J. Thermophys., **12,** (5), 801-810

Audonnet, F. and Pádua, A.H., 2004, *Viscosity and density of mixtures of methane and n-decane from 298 to 393 K and up to 75 MPa*, Fluid Phase Equilibria, **216**, 235–244

Avlonitis, D., Danesh, A. and Todd, A. C., 1994, *Prediction of VL and VLL equilibria of mixtures containing petroleum reservoir fluids and methanol with a cubic EoS*, Fluid Phase Equilib., **94**, 181-216

Baylaucq, A., Boned, C., Dauge, P., and Lagourette, B., 1997, *Measurements of the Viscosity and Density of Three Hydrocarbons and the Three Associated Binary Mixtures Versus Pressure and Temperature*, Int. J. Thermophys., **18**, (1), 3-23

Brazier, D. W. and Freeman, G. R., 1969, *The effects of pressure on the density, dielectric constant, and viscosity of several hydrocarbons and other organic liquids*, Canadian J. Chemistry, **47**, 893-899

Canet, X., Baylaucq, A. and Boned, C., 2002, *High-Pressure (up to 140 MPa) Dynamic Viscosity of the Methane+Decane System*, International Journal of Thermophysics, **23**, 6

Chuang, S., Chappelear, P.S and Kobyashi, R., 1976, *Viscosity of methane, Hydrogen and Four Mixtures of Methane and Hydrogen from -100°C to 0°C at High Pressure*, J. Chem. Eng. Data, **21**, (4), 403-410

Diller, D. E, 1980, *Measurements of the Viscosity of Compressed Gaseous and Liquid Methane*, Physica, **104 A**, 417-426

Diller, D. E and Saber, J. M., 1981, *Measurements of the Viscosity of Compressed Gaseous and Liquid Ethane*, Physica, **108 A**, 143-152

Diller, D. E, 1982, *Measurements of the Viscosity of Saturated and Compressed Liquid Propane*, J. Chem. Eng. Data. **27**, 240-243

Dymond, J. H., Young, K. J. and Isadale, J. D., 1980, *Transport Properties of Nonelectrolyte Liquid Mixtures-II. Viscosity Coefficients for n-Hexane + n-Hexadecane System at Temperature from 25 to 100 °C at Pressures Up to the Freezing Pressure or 500 MPa*, Int. J. Thermophys., **1** (4), 345-373

Dymond, J. H., Robertson, J, and Isadale, J. D., 1981, *Transport Properties of Nonelectrolyte Liquid Mixtures-III. Viscosity Coefficients for n-Octane, n-Dodecane, and Equimolar Mixtures of n-Octane + n-Dodecane and n-Hexane + n-Dodecane from 25 to 100 °C at Pressures Up to the Freezing Pressure or 500 MPa*, Int. J. Thermophys., **2** (2), 133-154

Fenghour, A., Wakeham, W.A. and Vesovic, V., 1997, *The Viscosity of Carbon Dioxide*, Journal of Physical and Chemical Reference Data, **27**, 31-44

Giddings J. G., Kao J. T. F. and Kobayashi R., 1966, *Development of a high pressure Capillary Tube Viscometer and its Application to Methane, Propane, and their Mixtures in the Gaseous and Liquid Regions*, J. Chem. Phys., **45,** (2)

Herning, F. and Zipprer, L., 1936, *Calculation of the Viscosity of Technical Gases Mixtures from the Viscosity of Individual Gases*, Gas u. Wasserfach, **79,** (49), 69

Hogenboom, D. L, Webb, W. and Dixon, J. A., 1967, *Viscosity of Several Liquid Hydrocarbons as a Function of Temperature, Pressure and Free Volume*", J. Chem. phys., **46,** (7), 2586 - 2598

Isdale, J.D., Dymond, J.H. and Brawn, T.A., 1979, *Viscosity and Density of n-Hexane - Cyclohexane Mixtures Between 25 and 100 °C up to 500 MPa*, High Temperatures - High Pressures, **11**, 571-580

Iwasaki, H. and Takahashi, M., 1981, *Viscosity of Carbon Dioxide and Ethane*, J. Chemical Physics, **74,** (3), 1930-1943

Kiran, E. and Sen, Y. L., 1992, *High-Pressure Viscosity and Density of n-Alkanes*, Int. J. Thermophys., **13,** (3), 411-442

Knapstad, B., Skjølsvik, P. A. and Øye, H. A., 1990, *Viscosity of the n-Decane-Methane System in the Liquid Phase*, Berichte der Bunsengesellschaft für physikalische Chemie, **94**, 10, 1156–1165

Lohrenz, J., Bray, B.G. and Clark, C.R., 1964, *Calculating Viscosities of Reservoir Fluids from Their Compositions*, J. Pet. Tech. (JPT), 1171-1176

Lee, A. L, 1965, *Viscosity of Light Hydrocarbons*, Monograph on API Research Project 65, American Petroleum Institute, New York

Levenberg K., 1944, *A method for the solution of certain non-linear problems in least squares*, Quarterly Journal of Applied Mathematics, **2**,164-168

Marquardt D.W., 1963, *An algorithm for least squares estimation of non-linear parameters*, Journal of the Society of Industrial and Applied Mathematics, **11**, 431-441

Mo, K. C. and Gubbins, K. E., 1974, *A Modified Benedict-Webb-Rubin Equation of States for Methane Using Recent Experimental Data*, Cryog., **14**, 276

NIST Chemistry Web Book

Oliveira, C. M. B. P. and Wakeham, W. A., 1992, *The Viscosity of Five Liquid Hydrocarbons at Pressures Up to 250 MPa*, International Journal of Thermophysics, **13,** (5), 773-790

Pedersen, K. S., Fredensland, Aa., Christensen, P. L. and Thomassen, P., 1984, *Viscosity of Crude Oils*, Chem. Eng. Sci., **39**, 1011-1016

Pedersen, K. S., and Fredenslund, Aa., 1987, *An Improved Corresponding States Model for the Prediction of Oil and Gas Viscosities and Thermal Conductivities,* Chem. Eng. Sci., **42**, 182-186

Valderrama JO. 1990, *A Generalized Patel-Teja Equation of State for Polar and Non-Polar Fluids and their Mixtures*, J. Chem. Eng. Jpn. **23**, 87-91

Vogel, E., Kuchenmeister, C., and Jaeschke, M., 2004, *Experience of Measurements with a Vibrating-Wire Viscometer on Natural Gases*, International Journal of Thermophysics, **25**, 6

Tham, M. J. and Gubbins, K. E., 1970, *Correspondence Principle for Transport Properties of Dense Fluids*, Ind. Eng. Chem. (I & CE) Fund., **9**, 63-70

CHAPTER 4

VISCOSITY OF ORIGINAL FLUID: EXPERIMENTAL AND PREDICTION

4.1 Introduction

Down hole sampling is frequently used to collect reservoir fluids for analysis. However, the reservoir fluid samples obtained are often contaminated with mud filtrates, particularly oil based mud filtrate which is miscible with reservoir fluid and subsequently affects its properties. It is also reported that even the presence of small amount of oil-based mud filtrate (in the obtained reservoir fluid sample), could drastically change the physical properties of the fluid (Gozalpour *et al.,* 1999). Since the drilling operation is normally performed by applying over-balance pressure in mud column, the drilling fluid invades the formation, so when a wireline process to take the sample is conducted, the filtrate is still in the well bore (Austad *et al.*, 2001)

Obtaining a mud-free (contamination-free) reservoir fluid sample is often a challenging and time consuming operation, so it is essential to be able to retrieve the properties of the original, un-contaminated fluid from contaminated samples using predictive models.

Several attempts were reported in the literature to calculate the original dead oil properties and particularly viscosity. Most of the methods are based on the viscosity of blends. The blend viscosity methods are empirical correlations that need the viscosity and other properties of each sample in the mixture. Sutton and Bergman (2008) performed a comprehensive review on this type of the viscosity predictive methods. In addition, some techniques are derived from the compositional analysis of the samples to retrieve the clean oil composition (Austad *et al.,* 2001 and Gozalpour *et al.,* 1999).

The objective of the present chapter is to investigate the influence of mud filtrate on the viscosity of hydrocarbon system. A Ruska high pressure rolling ball viscometer was used to perform the viscosity measurements. Experimental viscosity data are presented for three different dead oils in their original states and at several levels of contamination with a multi-component mineral oil based drilling fluid over a range of temperatures.

In this chapter, a new technique in predicting the viscosity of original fluid from the viscosity of contaminated sample is introduced as an application of the reviewed viscosity predictive methods presented in Chapter 3. The new approach to retrieve the viscosity of original fluid from the viscosity of contaminated sample is evaluated using experimental viscosity data.

4.2 Experimental Results

The Ruska high pressure rolling ball viscometer (Model No. 1602-818) was employed to measure viscosity of dead oils and their contaminated samples at atmospheric pressure and various temperatures. The rolling ball viscometer was calibrated with standard fluids. The standard fluids were chosen with viscosity values, which would cover the values generated by the test fluids over the temperature range investigated. The rolling ball viscometer set up and the measurement procedures are detailed in Chapter 2.

Different levels of contaminated samples were prepared gravimetrically at various weight percent of mud filtrate in the crudes. UK North Sea (hereafter called the North Sea), Norwegian North Sea (hereafter called the Norwegian) and West African dead oils and DMF-4 which is a mineral oil based mud filtrate are the investigated fluids in this study. The contamination levels of filtrate in dead oils are nominally as 10, 25, 50 and 75 weight percent. The viscosity tests were also performed on the dead oils and the mud filtrate. The temperature range for this series is between 20 °C to 72 °C at atmospheric pressure. The density of dead oils, mud filtrate and contaminated samples were also measured by an Anton Paar digital densitometer (DMA 45). The measured densities, compositions, molecular weights and the MWs of C_{20}^{+} fraction of the experimented crude oils and the intentionally contaminated samples (Tables 2.14 to 2.18) along with the fluid preparation technique are reported in Chapter 2.

4.2.1 *Viscosity Measurements*

The viscosity tests were performed on the above crudes and different levels of contaminated samples with the oil-based mud filtrate (DMF-4). The temperatures for these series of viscosity tests were 20, 30, 45, 60 and 72 °C at atmospheric pressure. These series of generated experimental viscosity data covering a viscosity range of about 1 to 1100 cP.

Bergman and Sutton (2007) proposed a method to check the consistency of viscosity data. The authors indicated that there is a linear relationship between *Ln(T+310)* and *Ln(Ln(Viscosity+1)* where T is in Fahrenheit and the viscosity is in cP. This relationship for viscosity of pure hydrocarbons (for different types of hydrocarbons) is plotted in Figure 4.1. This method was employed to evaluate the consistency of the generated viscosity data in this study.

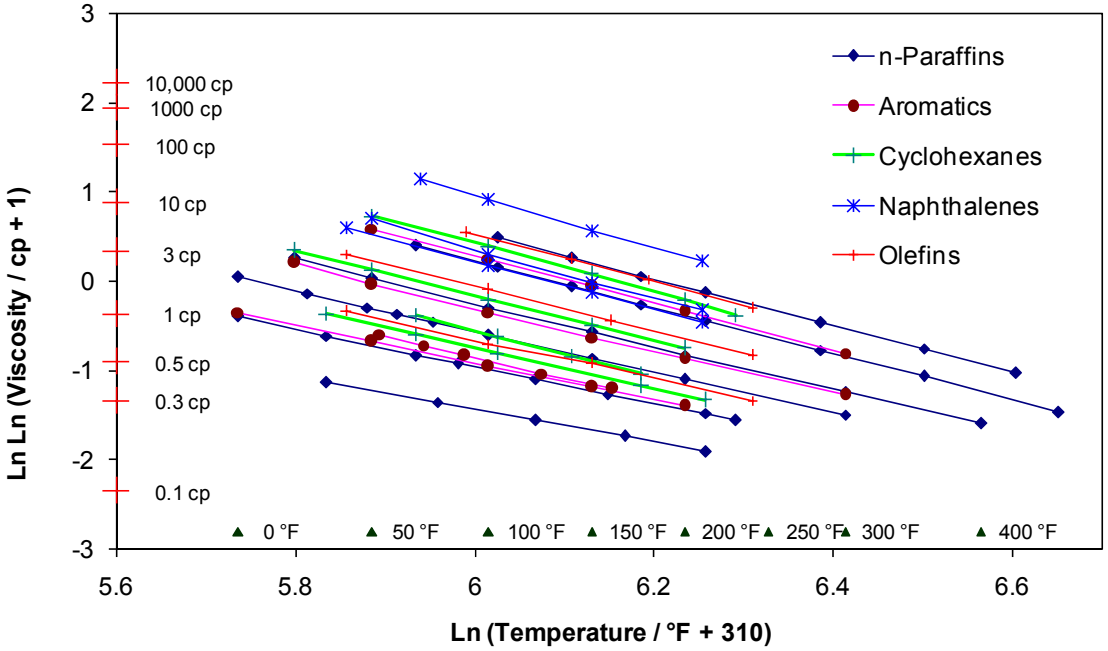

Figure 4.1 Viscosity and temperature relationship for pure hydrocarbons by family (Bergman and Sutton, 2007), this method was employed to investigate consistency of viscosity data generated in this work.

The experimental viscosity values of the North Sea dead oil along with the contaminated samples are reported in Table 4.1 and plotted in Figure 4.2. These data were also plotted as suggested by Bergman and Sutton in Figure 4.3 to investigate the consistency of the viscosity data. Almost all the plotted data show good agreement with the linear relationship. Only the viscosity data related to mud filtrate (DMF-4) has some discrepancy which could be due to the limitation of the viscometer in measuring viscosity for low viscosity fluids. Also at the range of high temperature for 10 and 25 wt% of filtrate the viscosity results showed some minor discrepancy.

Table 4.1 Experimental viscosity data (this work) of the North Sea Dead Oil and different levels of contaminated samples with mud filtrate (DMF-4) at atmospheric pressure

	Viscosity / cP					
T / C	North Sea Dead Oil	9.98 wt% DMF-4	25.01 wt% DMF-4	49.98 wt% DMF-4	74.92 wt% DMF-4	DMF-4
20	12.87	10.76	9.07	5.11	2.99	1.88
30	9.77	8.37	6.90	3.99	2.51	1.53
45	6.32	5.72	4.78	3.12	1.87	1.48
60	4.70	3.95	3.84	2.48	1.35	1.11
72	3.68	2.84	2.70	1.82	1.02	0.88

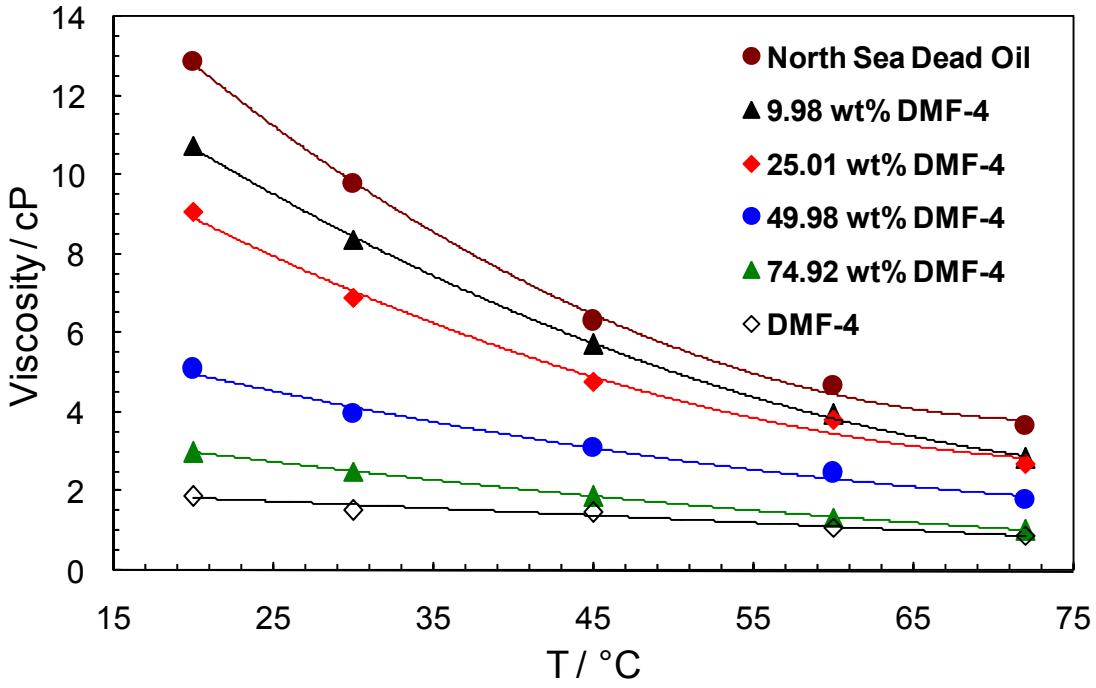

Figure 4.2 Experimental viscosity data of the North Sea Dead Oil and different levels of contaminated samples with mud filtrate (DMF-4) at atmospheric pressure (this work)

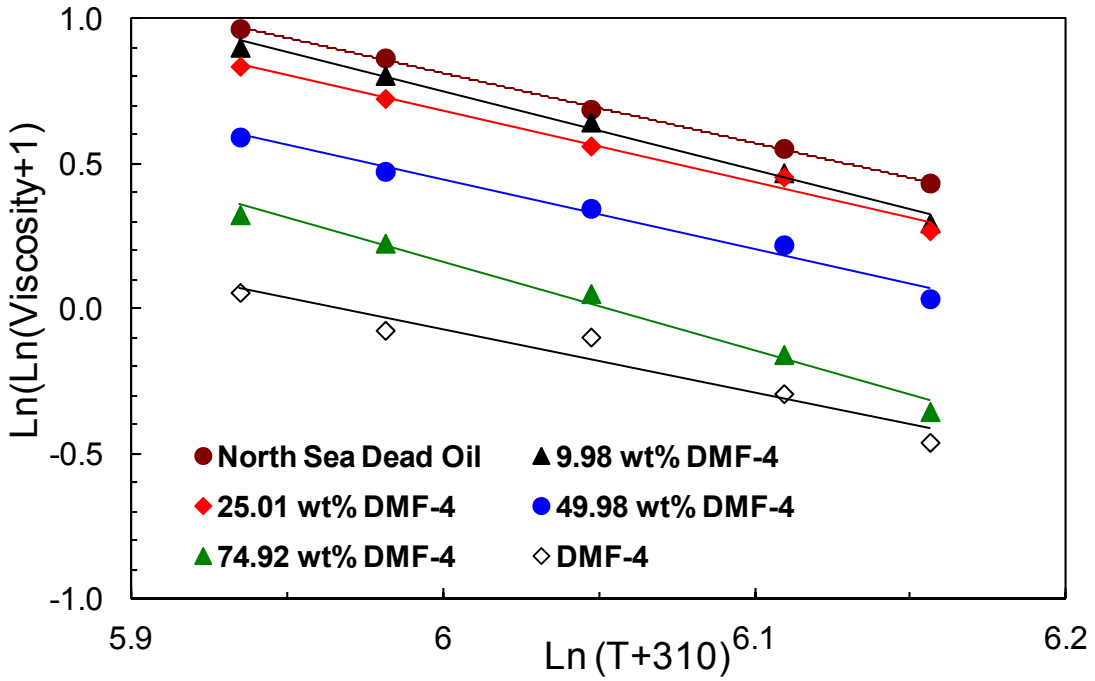

Figure 4.3 Relationship between viscosity and temperature for experimental viscosity data of the North Sea Crude and contaminated samples using a Bergman-Sutton Plot in order to investigate the consistency of the generated viscosity data in this work.

The experimental viscosity data of the Norwegian dead oil along with the contaminated samples are reported in Table 4.2 and Figure 4.4 and in Figure 4.5 for contaminated samples only. Also the Bergman-Sutton graph is plotted in Figure 4.6 to investigate the consistency of the data. All the generated viscosity data demonstrate the expected linear behaviour.

Table 4.2 Experimental viscosity data (this work) of the Norwegian Dead Oil and different levels of contaminated samples with mud filtrate (DMF-4) at atmospheric pressure

	Viscosity / cP			
T / °C	Norwegian Dead Oil	25.01 wt% DMF-4	50.03 wt% DMF-4	75.04 wt% DMF-4
	304.91 @ 18.5 °C	47.10 @ 18.5 °C	11.73 @ 19.5 °C	4.04 @ 20 °C
30	144.82	28.25	8.27	3.19
45	62.14	16.05	5.48	2.68
60	35.01	10.50	3.87	2.13
72	24.38	8.24	3.39	1.75

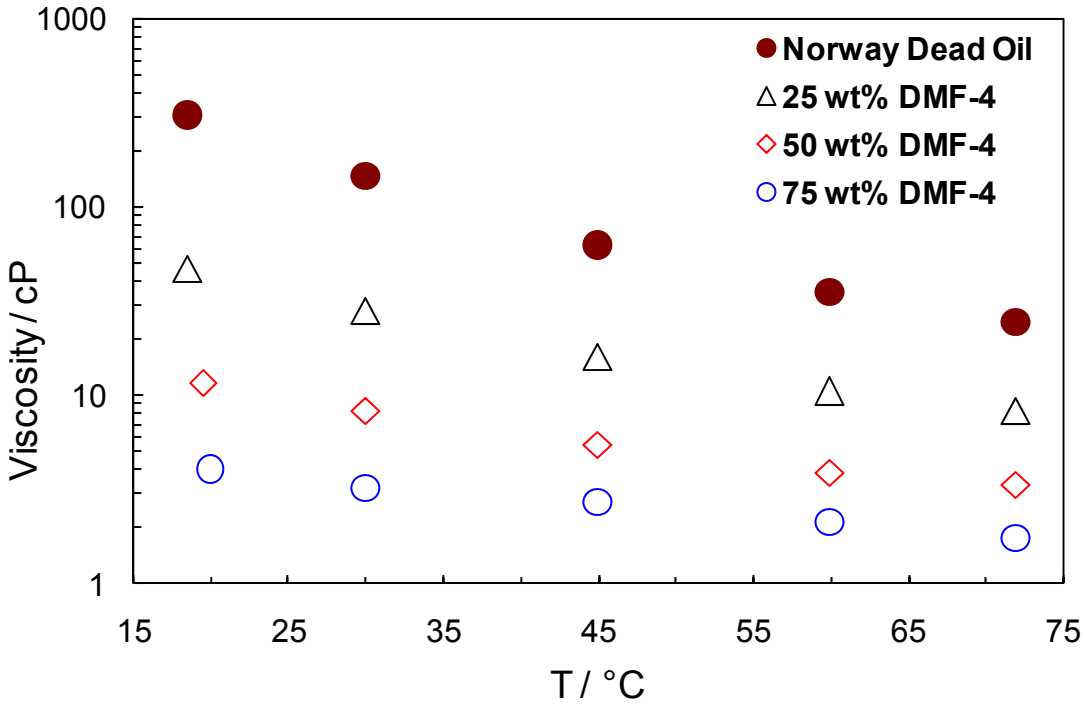

Figure 4.4 Experimental viscosity data of the Norwegian Dead Oil and different levels of contaminated samples with mud filtrate (DMF-4) at atmospheric pressure (this work)

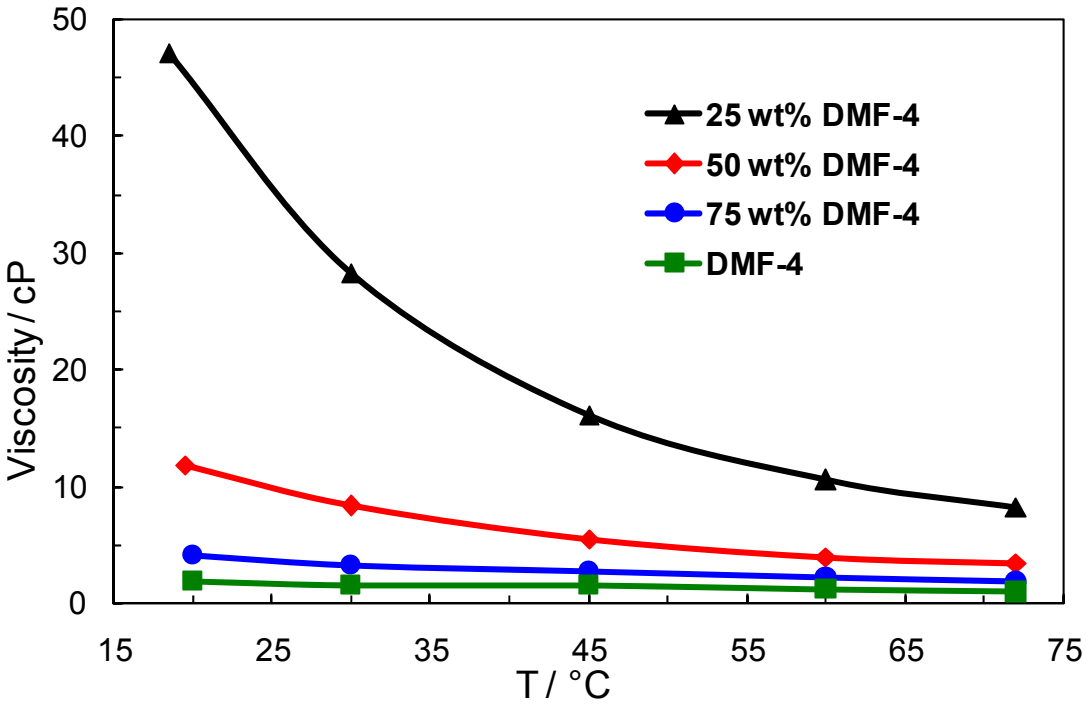

Figure 4.5 Experimental viscosity data of different levels of contaminated Norwegian Dead Oil with mud filtrate (DMF-4) at atmospheric pressure (this work)

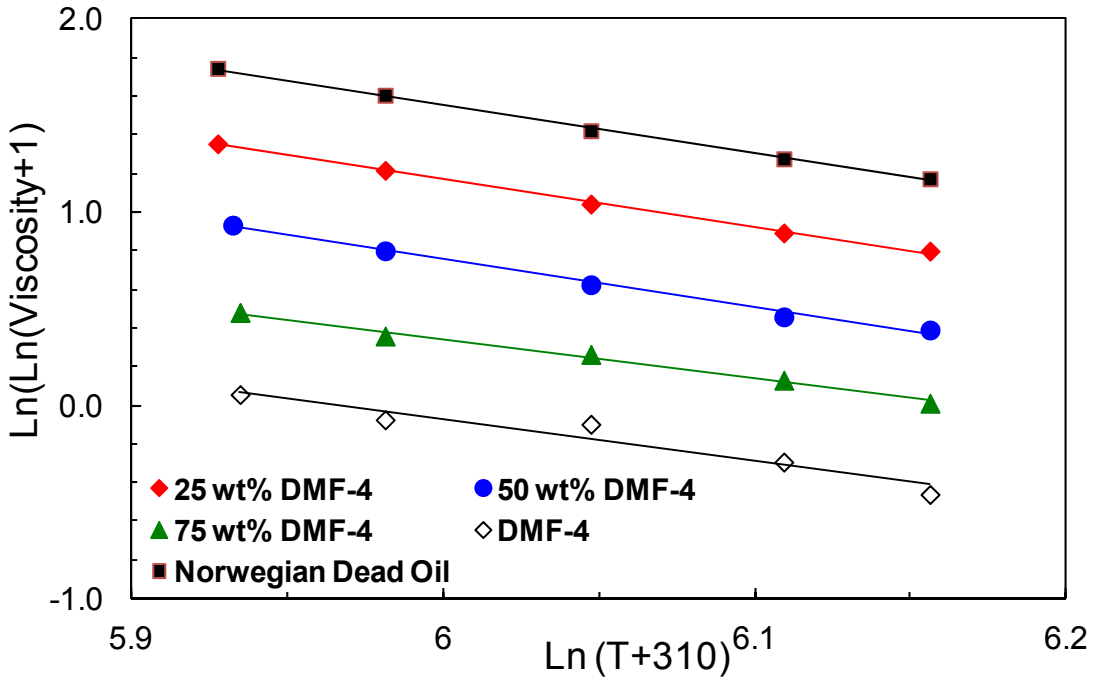

Figure 4.6 Relationship between viscosity and temperature for experimental viscosity data of the Norwegian Crude and contaminated samples using a Bergman-Sutton plot in order to investigate the consistency of the generated viscosity data in this work.

The West African dead oil experimental viscosity data along with the contaminated crudes are presented in Table 4.3 and Figure 4.7 and Figure 4.8 (contaminated samples only). As it can be seen in the mentioned table and graphs, addition of the mud filtrate has a considerable effect on the viscosity of this sample. For instance, addition of 25 wt% mud filtrate to the crude reduced the viscosity of the sample from 1,095 cP to 63.5 cP at about 18 °C that is equal to 17.2 times reduction in viscosity. The Bergman-Sutton graph is plotted in Figure 4.9 to examine the consistency of the data which all data show a linear relation.

Table 4.3 Experimental viscosity data (this work) of the West African Dead Oil and different levels of contaminated samples with mud filtrate (DMF-4) at atmospheric pressure

	Viscosity / cP			
T / °C	West African Dead Oil	25 wt% DMF-4	50 wt% DMF-4	75 wt% DMF-4
	1095.83 @ 18.1 °C	63.50 @ 17.3 °C	12.99 @ 22.7 °C	4.79 @ 16.7 °C
30	431.77	35.93	10.29	3.72
45	149.86	20.01	6.49	2.96
60	66.04	13.40	4.59	2.37
72	37.19	11.14	3.46	2.02

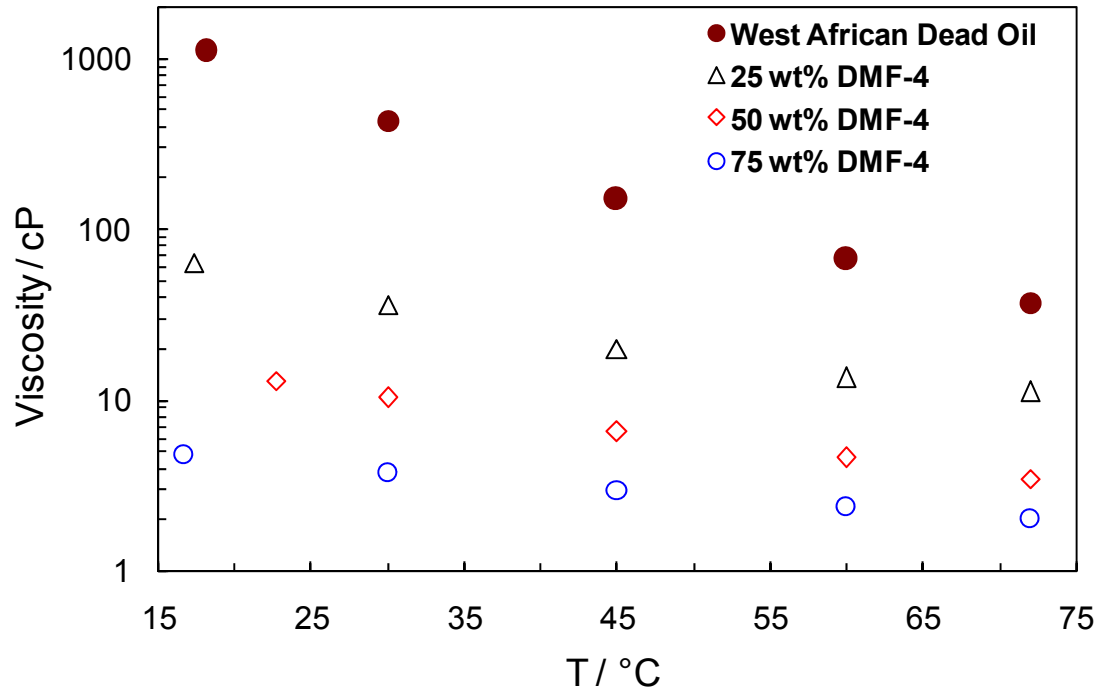

Figure 4.7 Experimental viscosity data of the West African Dead Oil and different levels of contaminated samples with mud filtrate (DMF-4) at atmospheric pressure (this work)

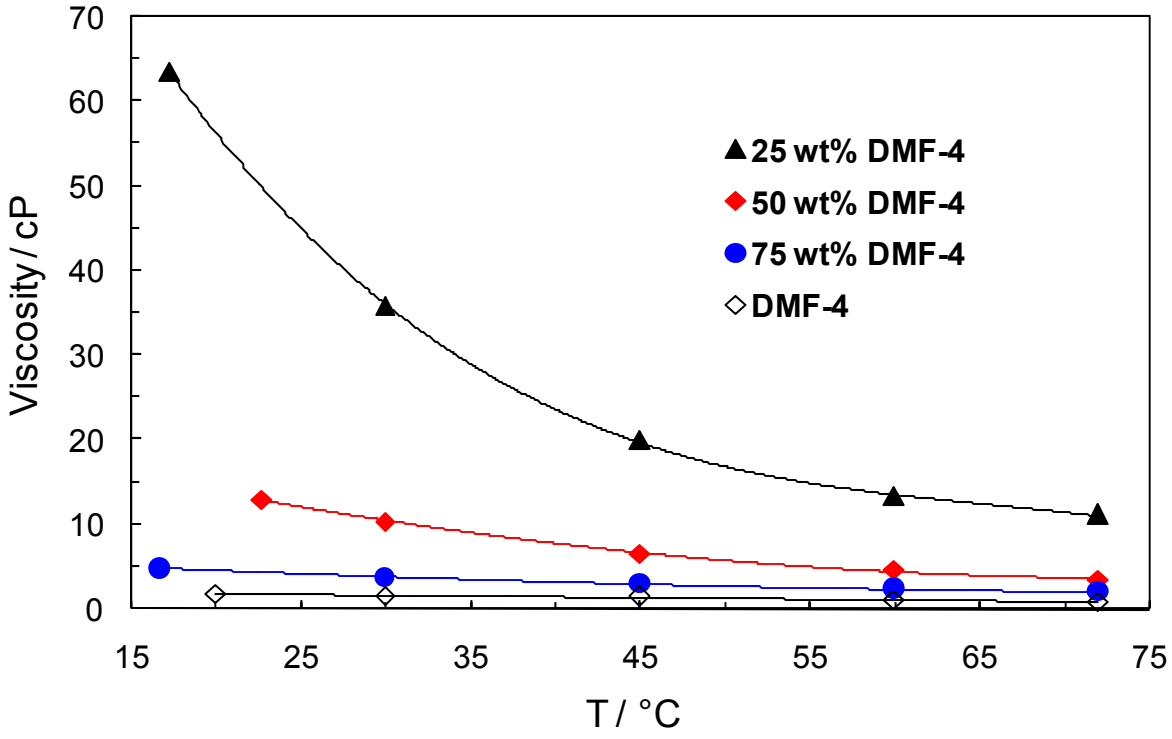

Figure 4.8 Experimental viscosity data of different levels of contaminated West African Dead Oil with mud filtrate (DMF-4) at atmospheric pressure (this work)

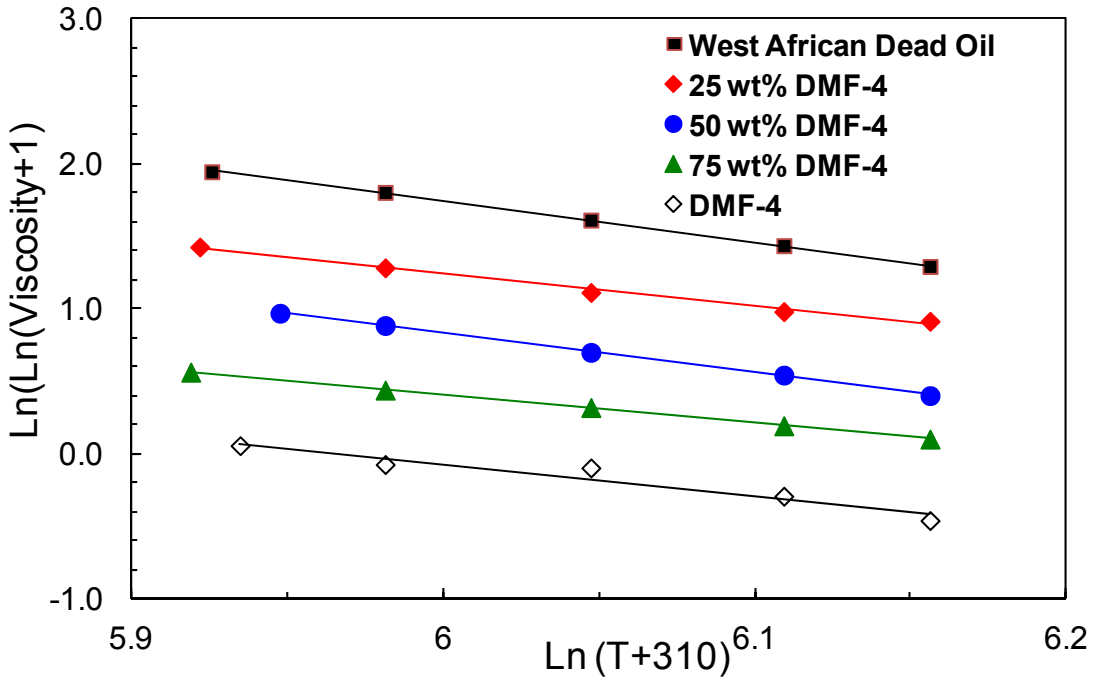

Figure 4.9 Relationship between viscosity and temperature for experimental viscosity data of the West African Crude and contaminated samples using Bergman-Sutton plot in order to investigate the consistency of the generated viscosity data in this work.

4.3 Viscosity Prediction of Original Dead Oil

A new approach for predicting the viscosity of the original (clean) fluid from the viscosity of contaminated samples was proposed as part of present thesis. The predictive method is described below.

4.3.1 *Methodology*

In predicting the viscosity of the original uncontaminated fluid, parameters including viscosity and the composition of the contaminated fluid and also the composition of the original fluid are required. The composition of the original fluid and the level of contamination can be defined using such techniques as the skimming and subtraction methods (Gozalpour *et al.,* 1999) which are explained later in this section. In this work, the viscosity of the original fluid is predicted using the composition and the measured viscosity data of the contaminated sample and also the composition of the original dead oil as it is outlined below:

For this reason some of the viscosity predictive models discussed in Chapter 3 are considered to evaluate the applicability of this approach. The method is based on the assumption that the deviation of each model from experimental data for nearly identical fluid is relatively close to each other. By knowing the deviation of each predicted

viscosity value from the measured value of contaminated sample, the viscosity of the original fluid can be predicted using predictive models and the application of a viscosity correction factor (VCF). The VCF can be defined as below:

$$VCF = (Viscosity_{experimental}) / (Viscosity_{predicted}) \quad (4.1)$$

In order to calculate the $VCF_{original\ fluid}$ (which is the VCF at zero contamination), the relation between levels of contamination and VCF at each temperature is considered. This has been performed by plotting VCF against contamination levels and reading the viscosity correction factor at zero level of contamination by using extrapolation. This concept is illustrated schematically in Figure 4.10. It worth to mention that the trend of VCF vs. contamination level could be increasing, decreasing or even remains the same, depends on the viscosity model and the fluid. So by multiplying these correction coefficients to the calculated viscosity by any of the predictive models, a more accurate prediction could be obtained. It is also possible to plot VCF vs. temperature at each contamination level in order to calculate VCF at zero contamination which is not preferred due to the difficulties in calculation and also the predicted results were not superior to the other method. Since the deviation of the predicted viscosity from experimental data can vary by changing pressure (or temperature) and level of contaminations, the correction factors could be introduced as a function of P (or T) and contamination levels for each viscosity predictive technique.

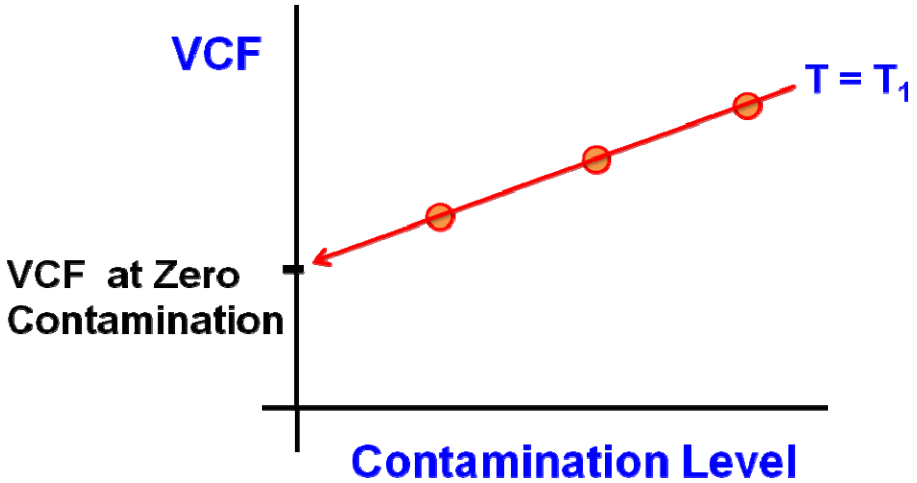

Figure 4.10 Calculation of viscosity correction factor at zero contamination using extrapolation of VCF at different levels of contaminations

If there is only one contaminated sample available, the calculated viscosity correction factor of contaminated sample could be used for predicting the viscosity of original fluid (in particular at low contamination levels). Alternatively, the level of contamination could be deliberately increased to calculate VCF at higher contamination levels. Again, VCF for uncontaminated sample could be calculated from plotting VCF vs. contamination level.

As it was explained above, a linear relation between VCF and contamination level was considered to calculate the VCF $_{\text{original fluid}}$ in this work. Polynomial relation was also examined for this reason and finally it was determined to perform the viscosity predictions using linear relation since in all cases the acceptable results were obtained.

4.3.2 *Dead Oil Composition Retrieval*

The skimming and subtraction techniques can be used in the retrieval of the uncontaminated oil composition, as it is required in the prediction of the fluid viscosity. It has been reported (Gozalpour et al. 1999) that there is an exponential relationship between the molecular weights of the compounds present in the C_{8+} fraction of real reservoir fluids and the corresponding concentration of compounds. So, if the molar concentration of single carbon number groups is plotted against their molecular weights, it will give a straight line on a semi-logarithmic scale. Based on this observation, in a contaminated fluid the graph of the composition of C_{8+} fraction versus molecular weight on a semi-logarithmic scale will show a deviation from the straight line over the region of contamination. This hump can be seen in any addition of filtrate and also in any type of filtrate. The only limitation could be the bio-degradable dead oils that do not follow the mentioned linear trend in their compositions. This effect can be seen in Figures 4.11 to 4.13 for the three investigated dead oils and different levels of contamination with mud filtrate. The details of these fluids are described in Tables 2.14 to 2.18. It is noticeable that in Figure 4.11 the data were extended up to C_{36+}, however in Table 2.14 the compositional data are only reported up to C_{20+}.

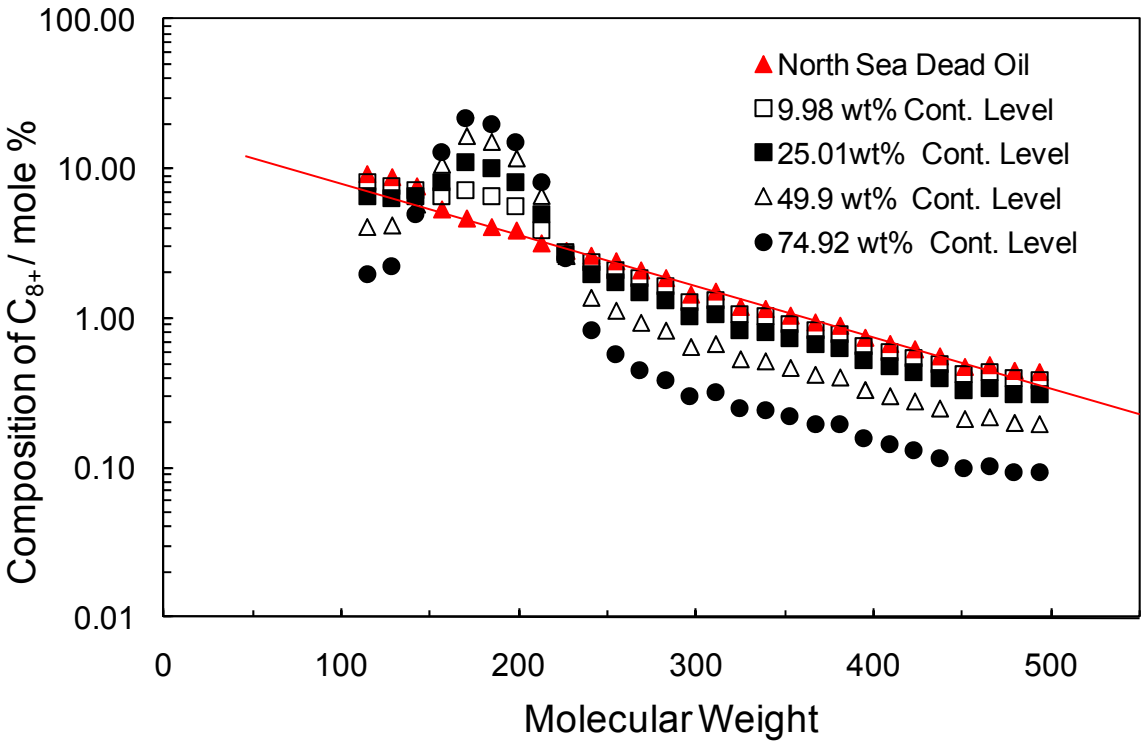

Figure 4.11 Molar composition of C_{8+} cut against molecular weight of the North Sea Dead Oil and different levels of contaminated sample with OBM. This technique can be employed to calculate the composition of clean dead oil.

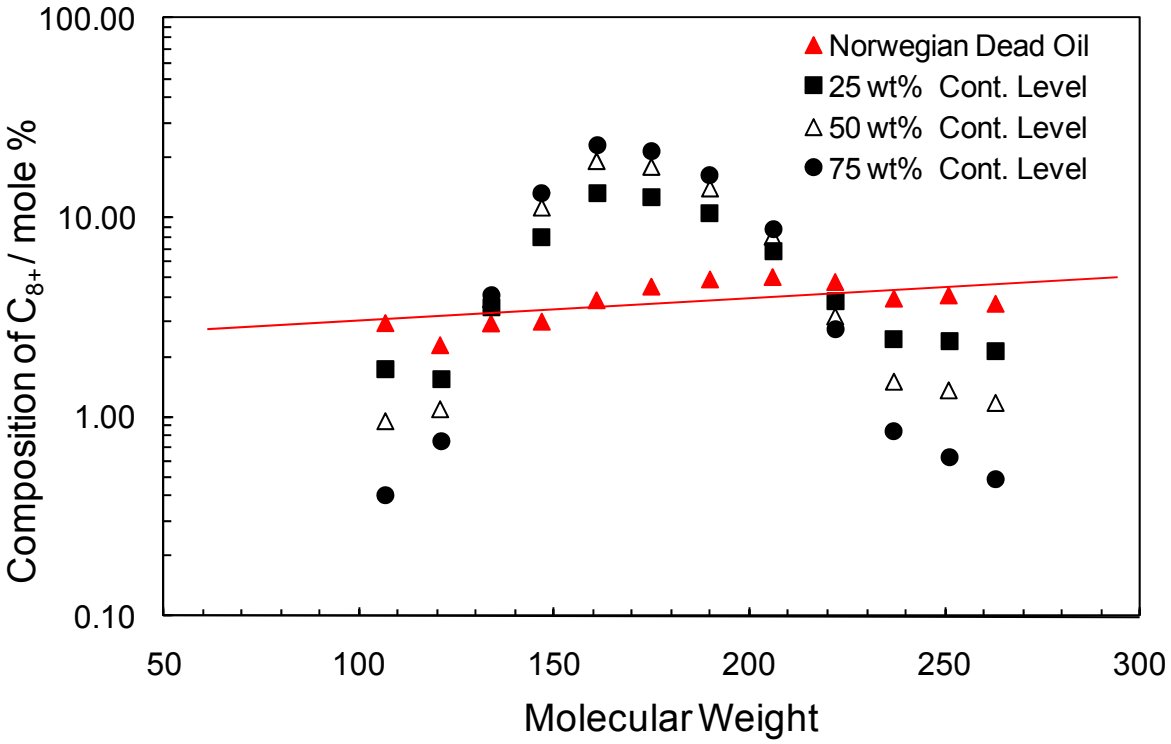

Figure 4.12 Molar composition of C_{8+} cut against molecular weight of the Norwegian Dead Oil and different levels of contaminated sample with OBM. This technique can be employed to calculate the composition of clean dead oil.

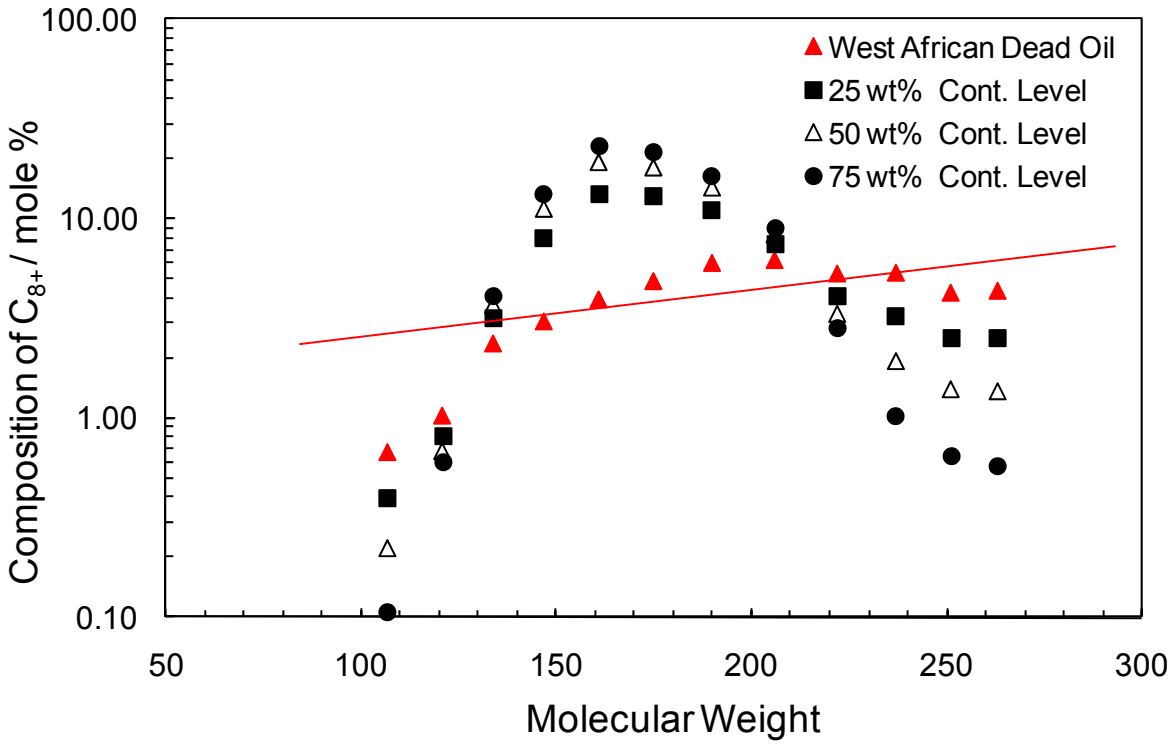

Figure 4.13 Molar composition of C_{8+} cut against molecular weight of the West African Dead Oil and different levels of contaminated sample with OBM. This technique can be employed to calculate the composition of clean dead oil.

4.4 Viscosity Modelling

The literature contains many methods for viscosity prediction, ranging from mathematically rigorous to completely empirical. In Chapter 3 the LBC (Lohrenz *et al.*, 1964) and HW2 (Al-Syabi *et al.*, 2001) viscosity models were reviewed. As well as the LBC and HW2 methods, some correlations were also proposed and reported in Chapter 3 as part of this research, including a modification of the Fenghour *et al.* (1997) method. In this chapter, the reliability of the new approach (using VCF) for predicting the original fluid viscosity is discussed. In all mentioned viscosity models the VPT EoS was employed for density calculations.

To investigate the capability of this method (using VCF), the above viscosity predictive methods along with a correlation introduced by Bergman and Sutton (2007) were employed to predict the viscosity of dead oils contaminated with various concentrations of mud filtrate. Unlike the above named models, the BS method (Bergman and Sutton, 2007) is not a composition based correlation. As it is mentioned below (Equation 4.2) this correlation is a function of the API gravity, boiling point and temperature of the fluid at which the viscosity measured.

$$\nu = f(\gamma_{API}, T_b, T) \quad (4.2)$$

Where ν is the kinematic viscosity, so to convert this parameter to absolute viscosity, knowledge of density at temperature is required. Authors employed a large data base of dead oil viscosities to develop the correlation.

4.5 Evaluation of the Proposed Method

In this section the reliability of the newly introduced approach to retrieve the viscosity of original fluid from contaminated samples is evaluated. To perform this evaluation the experimental viscosity data of crudes originated from the North Sea, Norway and West of Africa and various contaminated samples with a mineral oil base mud filtrate (DMF-4) were chosen. As explained above, viscosity correction factor for each investigated model and fluid should be determined.

The viscosities of the contaminated fluids were predicted using the previously mentioned models. Comparing the experimental and predicted viscosity data of the contaminated samples, the correction factors (VCF) could be calculated as a function of temperature and concentration of filtrate in the dead oils. Having known the viscosity correction factors at different levels of contamination, the VCF at zero contamination (clean fluid) then can be estimated with extrapolation.

4.5.1 *The North Sea Dead Oil*

This crude was contaminated intentionally with 9.98, 25.01, 49.9, 74.92 weight percent of mud filtrate (DMF-4) for viscosity tests. The compositions (Tables 2.14 and 2.16) and the sample preparation method are detailed in Chapter 2. The calculated VCF of different investigated viscosity models vs. mud filtrate concentrations over the range of experimented temperature are depicted in Figures 4.14 to 4.17. The values of the viscosity correction factor for prediction of the uncontaminated sample ($VCF_{original\ fluid}$) for each model is taken from the value at zero weight percent contamination which can be obtained from the above figures.

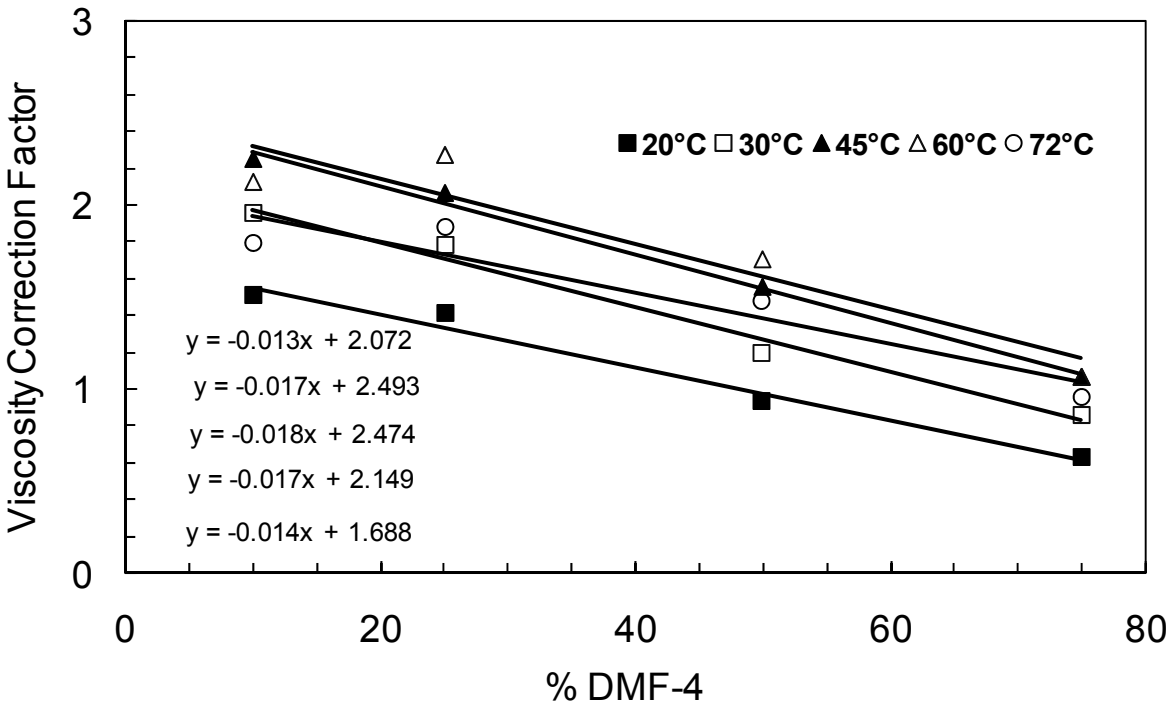

Figure 4.14 Viscosity correction factor (Equation 4.1) of Modified Fenghour Method for prediction of the contaminated North Sea Dead Oil vs. mud filtrate (DMF-4) wt. Percent. The regression values (R^2) are between 0.88 and 0.99.

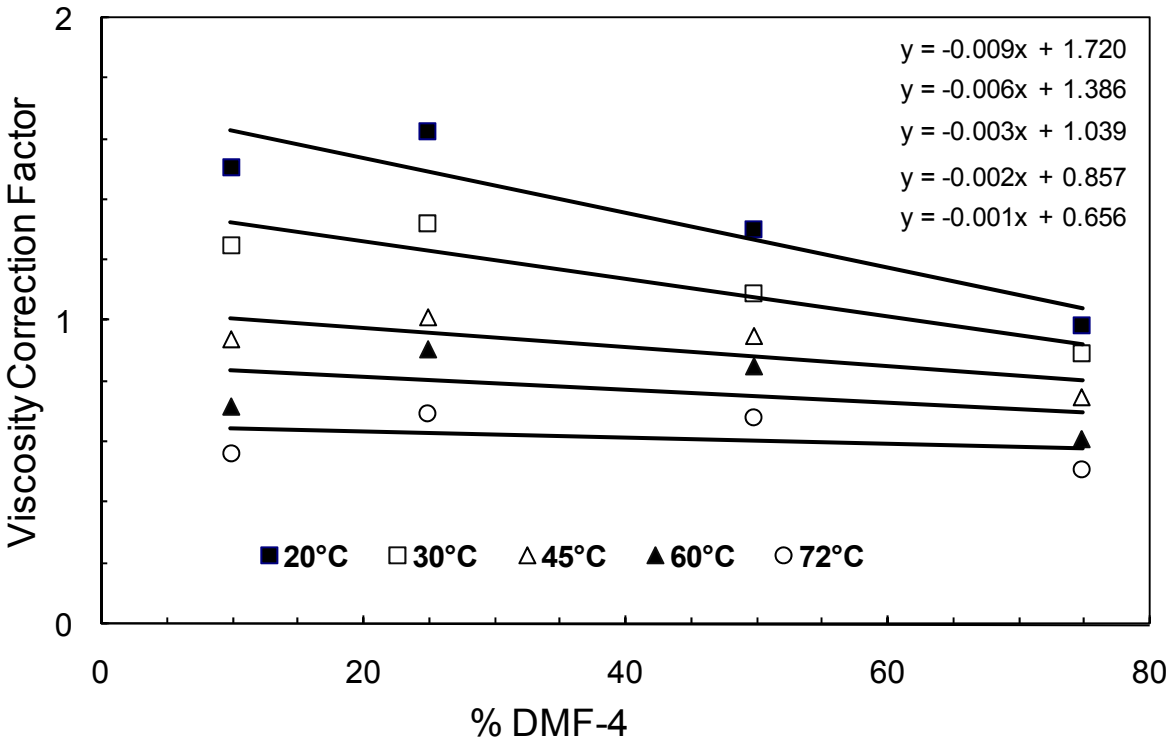

Figure 4.15 Viscosity correction factor (Equation 4.1) of LBC for prediction of the contaminated North Sea Dead Oil vs. mud filtrate (DMF-4) wt. percent. The regression values (R^2) are between 0.11 and 0.86.

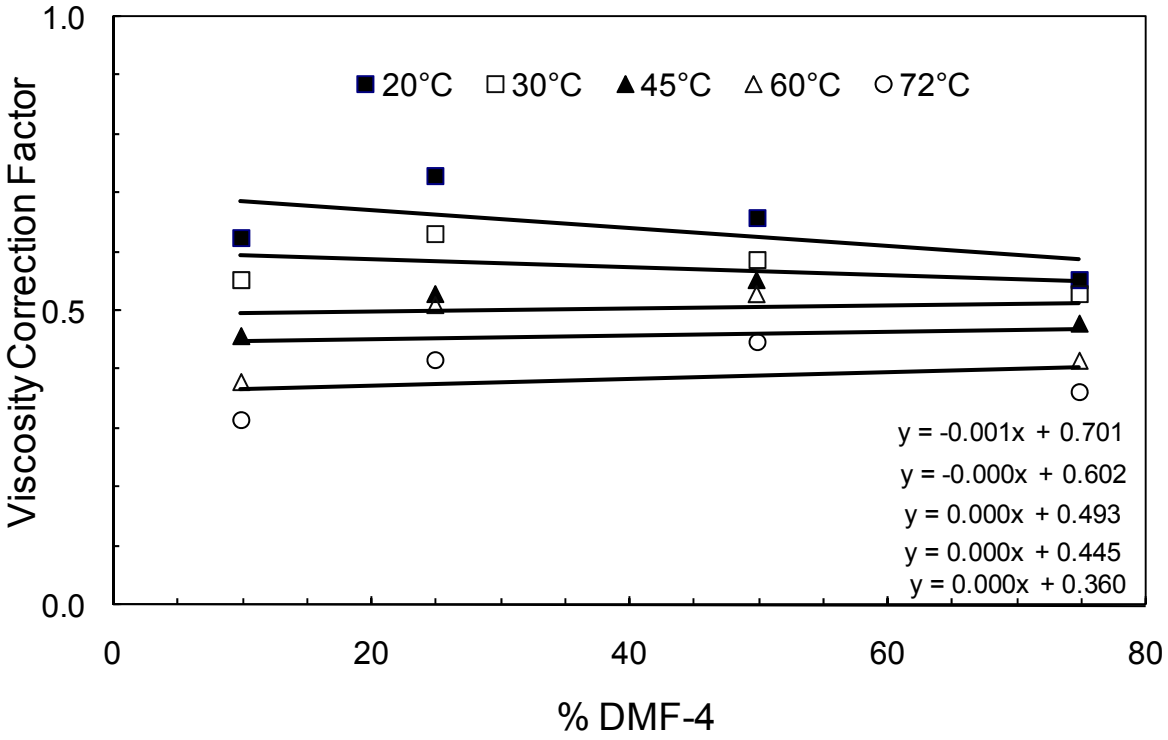

Figure 4.16 Viscosity correction factor (Equation 4.1) of HW2 for prediction of the contaminated North Sea Dead Oil vs. mud filtrate (DMF-4) wt. Percent. The regression values (R^2) are between 0.35 and 0.88.

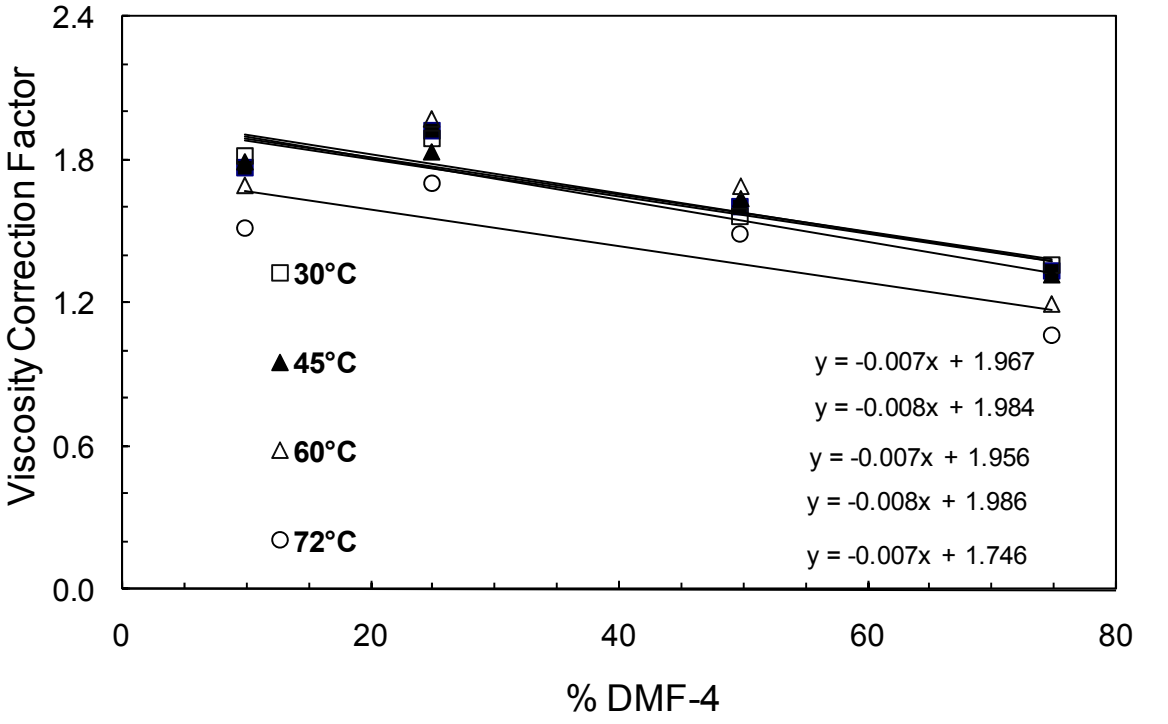

Figure 4.17 Viscosity correction factor (Equation 4.1) of Bergman-Sutton for prediction of the contaminated North Sea Dead Oil vs. mud filtrate (DMF-4) wt. percent. The regression values (R^2) are between 0.61 and 0.78.

As mentioned before, the VCF $_{original\ fluid}$ was reported in Figures 4.14 to 4.17 which are the values of the VCF at 0 wt% mud filtrate (it can be read from y-intercept by extrapolation). For example, in Figures 4.14 the VCF $_{original\ fluid}$ values are 2.072, 2.493, 2.474, 2.149 and 1.688 at 20 to 72 °C, respectively. The predicted viscosity of the North Sea dead oil corrected with the VCF$_{original\ fluid}$ along with the average absolute deviation percentage of each model are reported in Figure 4.18 and Table 4.4.

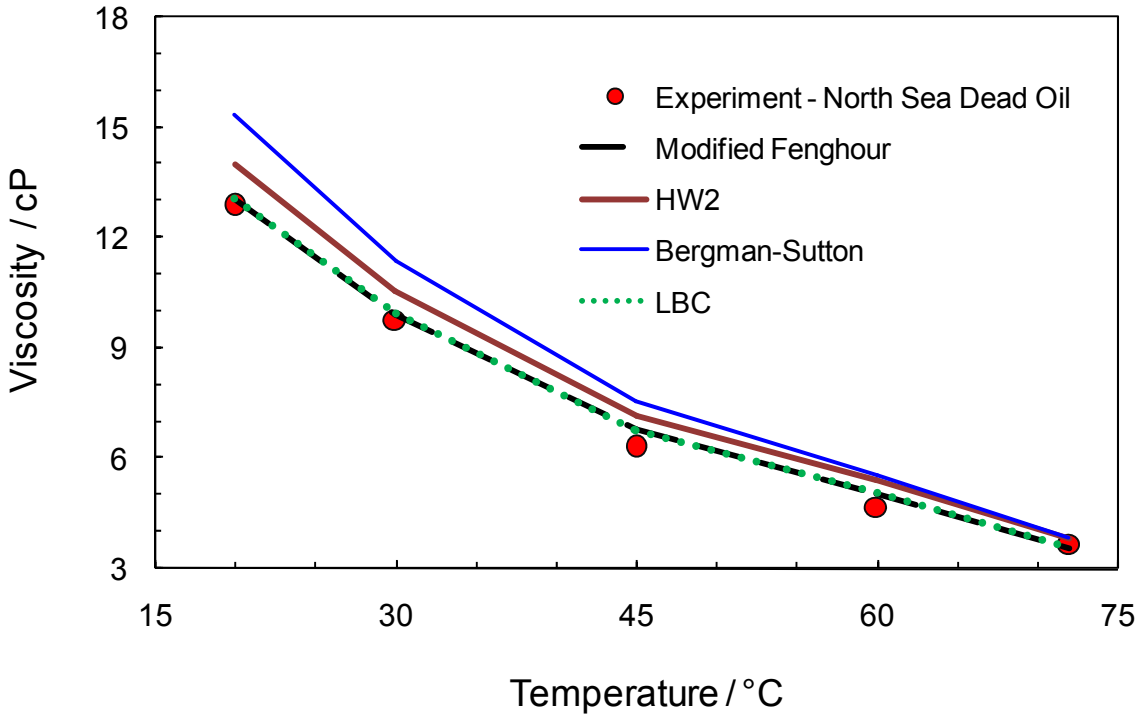

Figure 4.18 Prediction of the North Sea Dead Oil viscosity by different methods using the contaminated viscosity data and new approach (using VCF)

Table 4.4 AAD% between experimental and predicted viscosities of the Original North Sea Dead Oil using contaminated viscosity data and the new approach (using VCF)

	Modified Fenghour	LBC	HW2	Bergman-Sutton
with VCF	4	4	10	15
without VCF	52	29	122	40

As reported in Table 4.4, using the VCF approach could improve the prediction of the North Sea dead oil viscosity. The best predictions resulted by using the LBC and modified Fenghour which returned deviations of 4%. It is noticeable that LBC method

predicts the viscosity of this crude with a relatively good accuracy even without using the viscosity correction factor.

4.5.2 *The Norwegian Dead Oil*

This fluid was contaminated with 25.01, 50.03 and 75.04 weight percent of mud filtrate (DMF-4) for performing the viscosity experiments. The compositions of the fluid and contaminated samples are presented in Tables 2.14 and 2.17. The calculated VCF of different investigated viscosity models vs. mud filtrate concentrations over the range of experimented temperature are depicted in Figures 4.19 to 4.22. The value of the viscosity correction factor for prediction of the uncontaminated sample for each model was taken from the value at zero weight percent contamination which can be calculated from the above figures ($VCF_{original\ fluid}$).

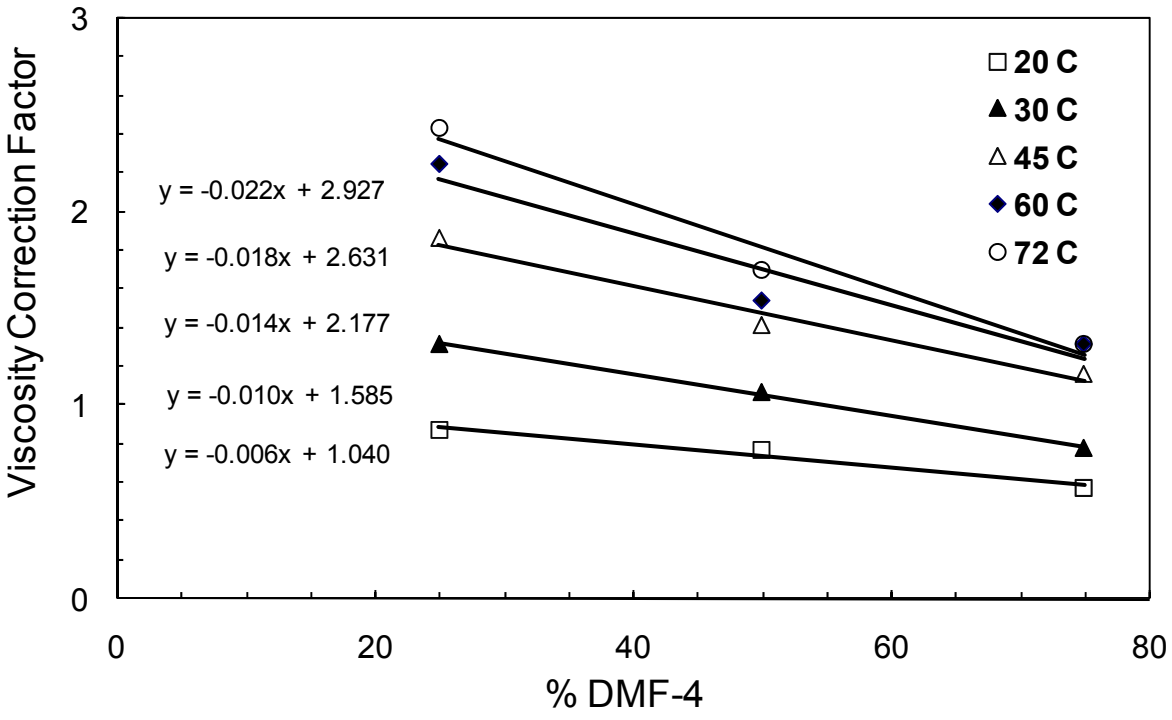

Figure 4.19 Viscosity correction factor (Equation 4.1) of Modified Fenghour Method for prediction of contaminated Norwegian Dead Oil vs. mud filtrate (DMF-4) wt. Percent. The regression values (R^2) are between 0.92 and 0.98.

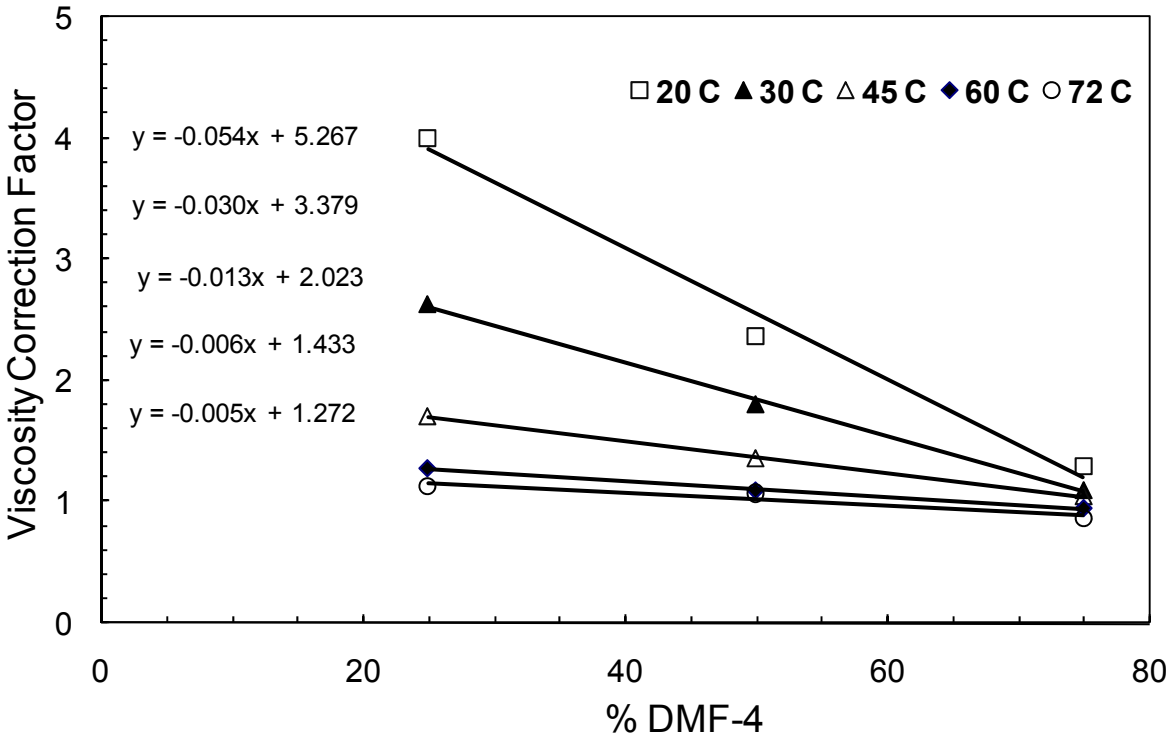

Figure 4.20 Viscosity correction factor (Equation 4.1) of LBC for prediction of contaminated Norwegian Dead Oil vs. mud filtrate (DMF-4) wt. Percent. The regression values (R^2) are between 0.98 and 0.99.

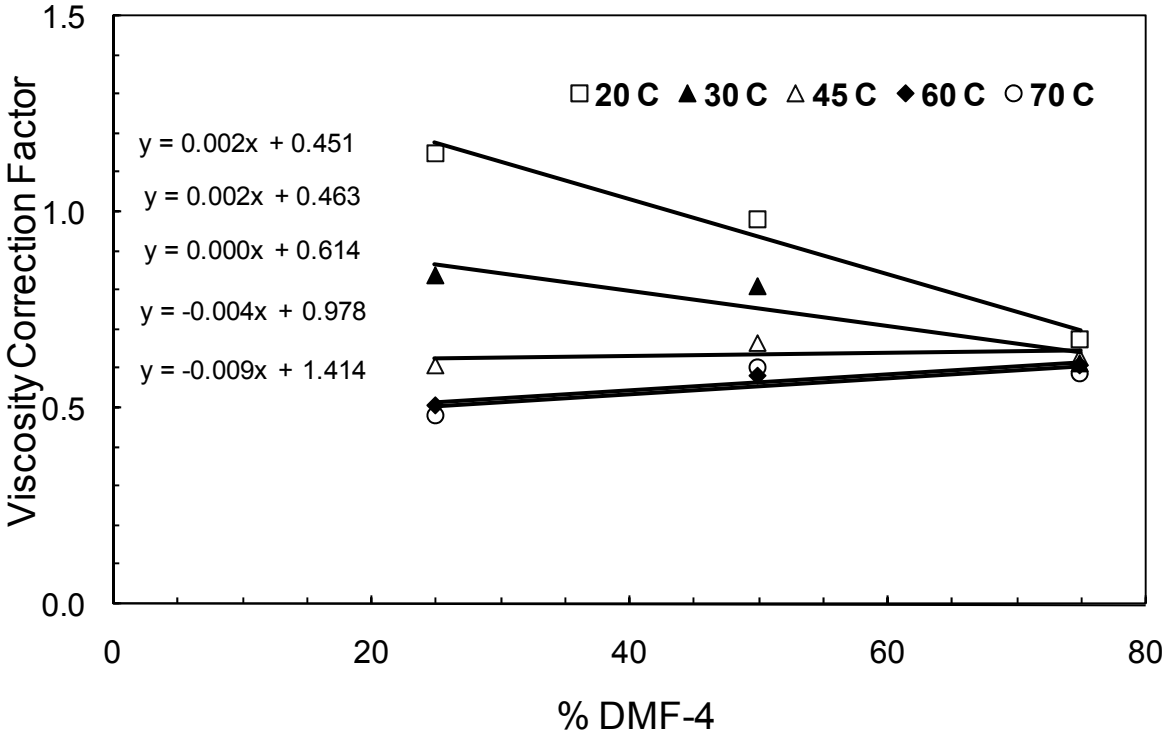

Figure 4.21 Viscosity correction factor (Equation 4.1) of HW2 for prediction of contaminated Norwegian Dead Oil vs. mud filtrate (DMF-4) wt. percent. The regression values (R^2) are between 0.84 and 0.97.

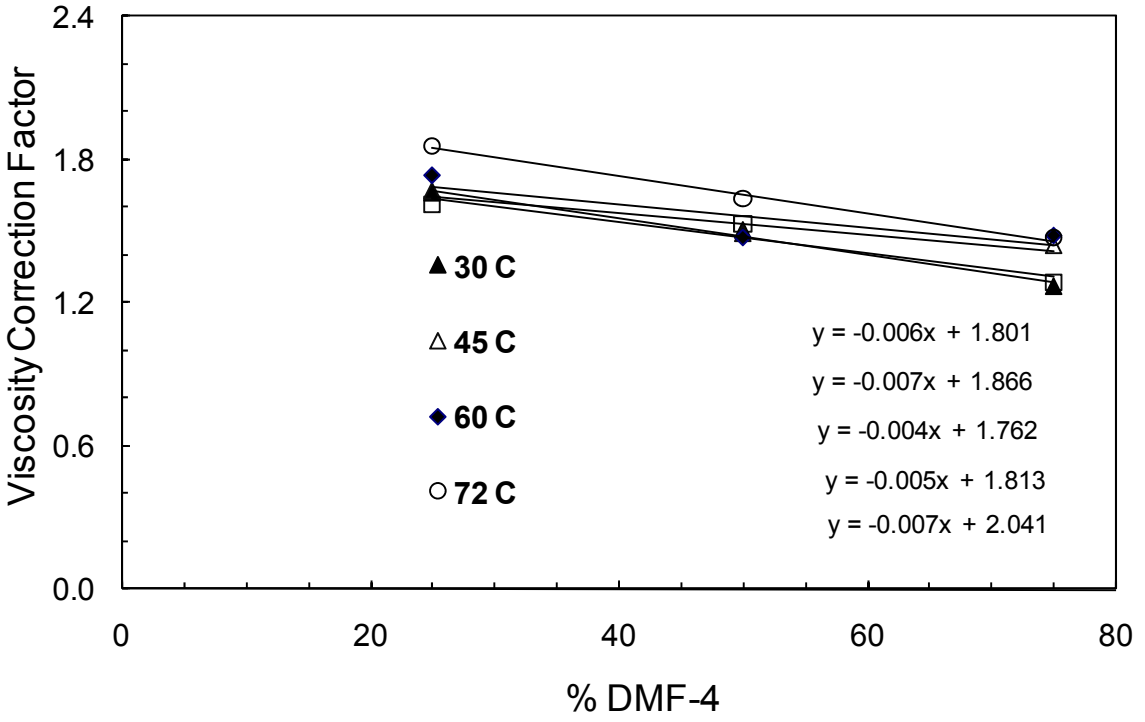

Figure 4.22 Viscosity correction factor (Equation 4.1) of Bergman-Sutton for prediction of contaminated Norwegian Dead Oil vs. mud filtrate (DMF-4) wt. percent. The regression values (R^2) are between 0.73 and 0.99.

The $VCF_{original\ fluid}$ values that should be employed in viscosity prediction of the Norwegian dead oil are reported in Figures 4.19 to 4.22 which are extrapolated from y-intercept. For example, in Figures 4.19 the $VCF_{original\ fluid}$ values are 2.927, 2.631, 2.177, 1.585 and 1.040 at 20 to 72 °C, respectively. As detailed above, the $VCF_{original\ fluid}$ values are the viscosity correction factor at 0 wt.% of mud filtrate. The predicted viscosity of the Norwegian dead oil corrected with the $VCF_{original\ fluid}$ along with the average absolute deviation percentage of each model are reported in Figure 4.23 and Table 4.2.

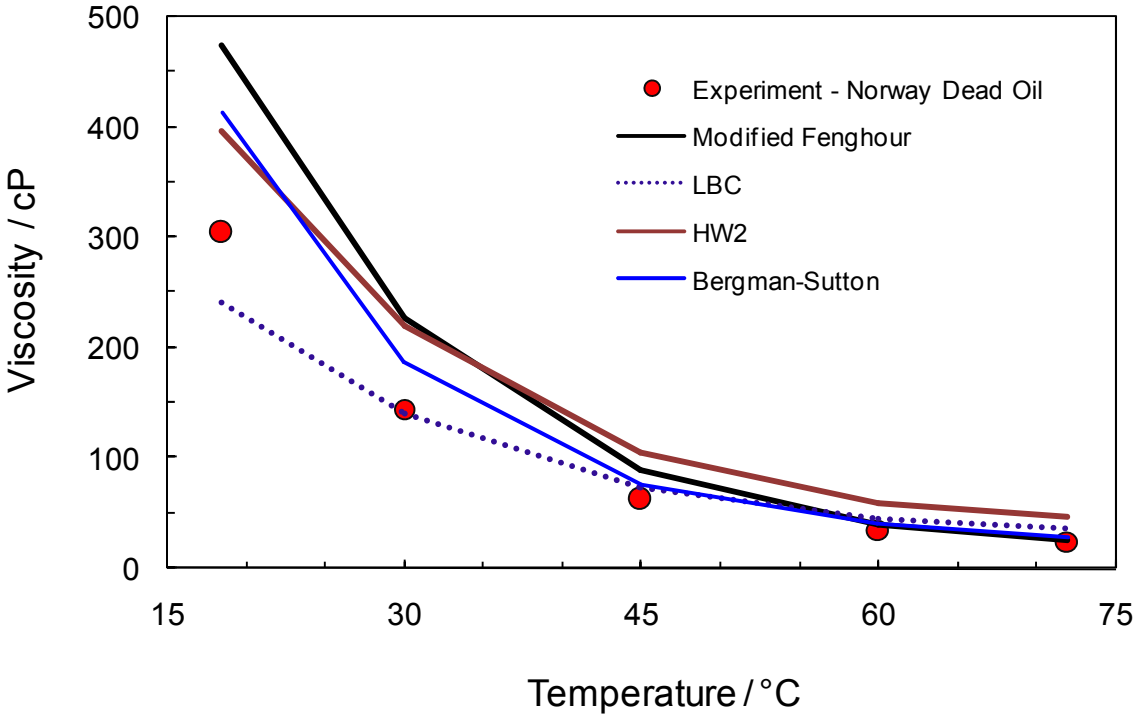

Figure 4.23 Prediction of the Norwegian Dead Oil viscosity by different methods using the contaminated viscosity data and new approach (using VCF)

Table 4.5 AAD% between experimental and predicted viscosities of the Original Norwegian Dead Oil using contaminated viscosity data and new approach (using VCF)

	Modified Fenghour	LBC	HW2	Bergman-Sutton
with VCF	35	24	63	24
without VCF	41	44	166	33

As reported in Table 4.5, using the VCF method could improve the prediction of the Norwegian dead oil viscosity. The best predictions were obtained by using the LBC and Bergman-Sutton methods, which returned AAD of 24% for both of the methods. The BS method presents good prediction even without using VCF.

4.5.3 *The West African Dead Oil*

This dead oil was contaminated with 25, 50 and 75 weight percent of mud filtrate (DMF-4). The compositions of the test fluid and the intentionally contaminated samples along with the properties of these samples were reported in Tables 2.14 and 2.18. The evaluated viscosity correction factor of the investigated viscosity methods against mud filtrate concentrations over the range of experimented temperature are plotted in Figures 4.24 to 4.27. The value of the $VCF_{original\ fluid}$ for prediction of the uncontaminated sample for each model is extrapolated from the value at zero weight percent contamination (y-intercept) which can be found from the mentioned graphs. For instance, in Figures 4.24 the $VCF_{original\ fluid}$ values are 3.813, 3.531, 3.113, 2.491 and 1.767 at 20 to 72 °C, respectively.

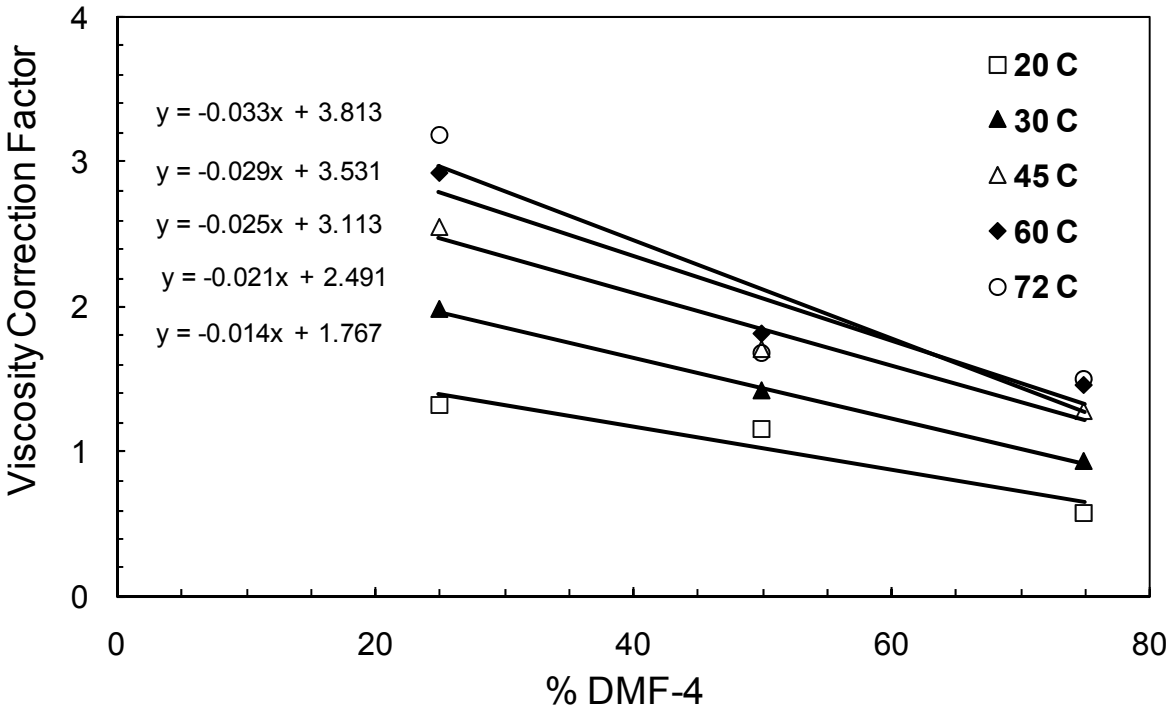

Figure 4.24 Viscosity correction factor (Equation 4.1) of Modified Fenghour for prediction of contaminated West African Dead Oil vs. mud filtrate (DMF-4) wt. percent. The regression values (R^2) are between 0.83 and 0.97.

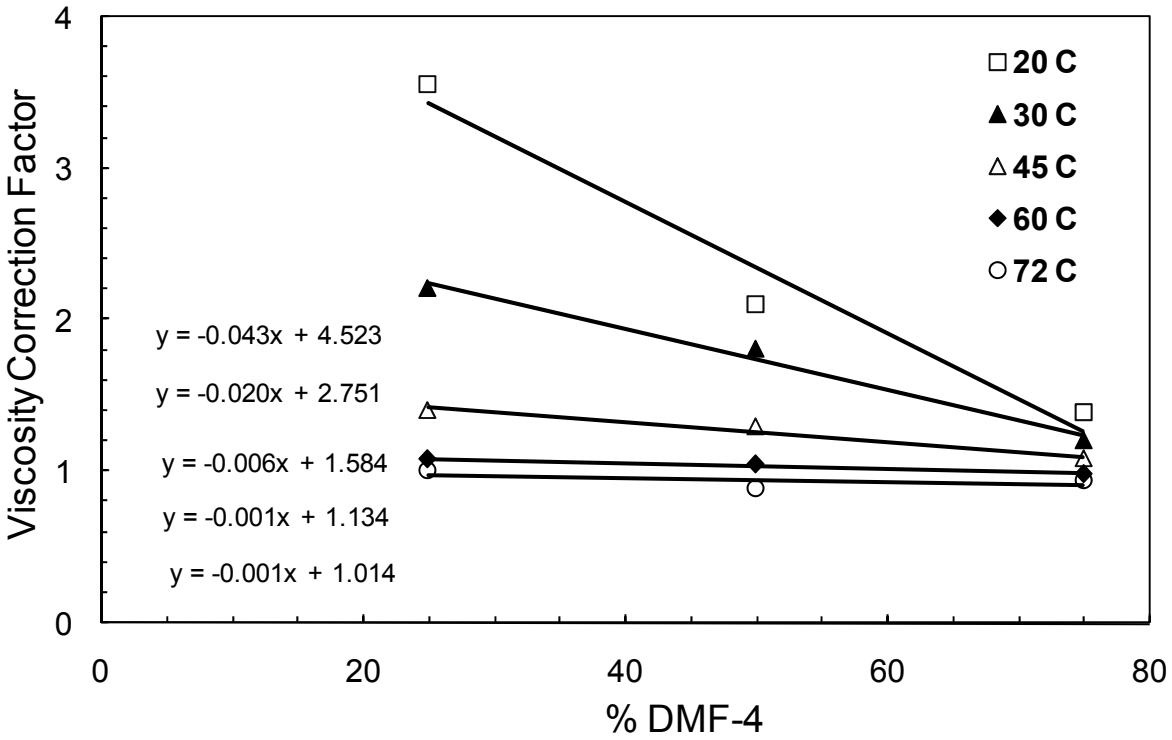

Figure 4.25 Viscosity correction factor (Equation 4.1) of LBC for prediction of contaminated West African Dead Oil vs. mud filtrate (DMF-4) wt. percent. The regression values (R^2) are between 0.96 and 0.99.

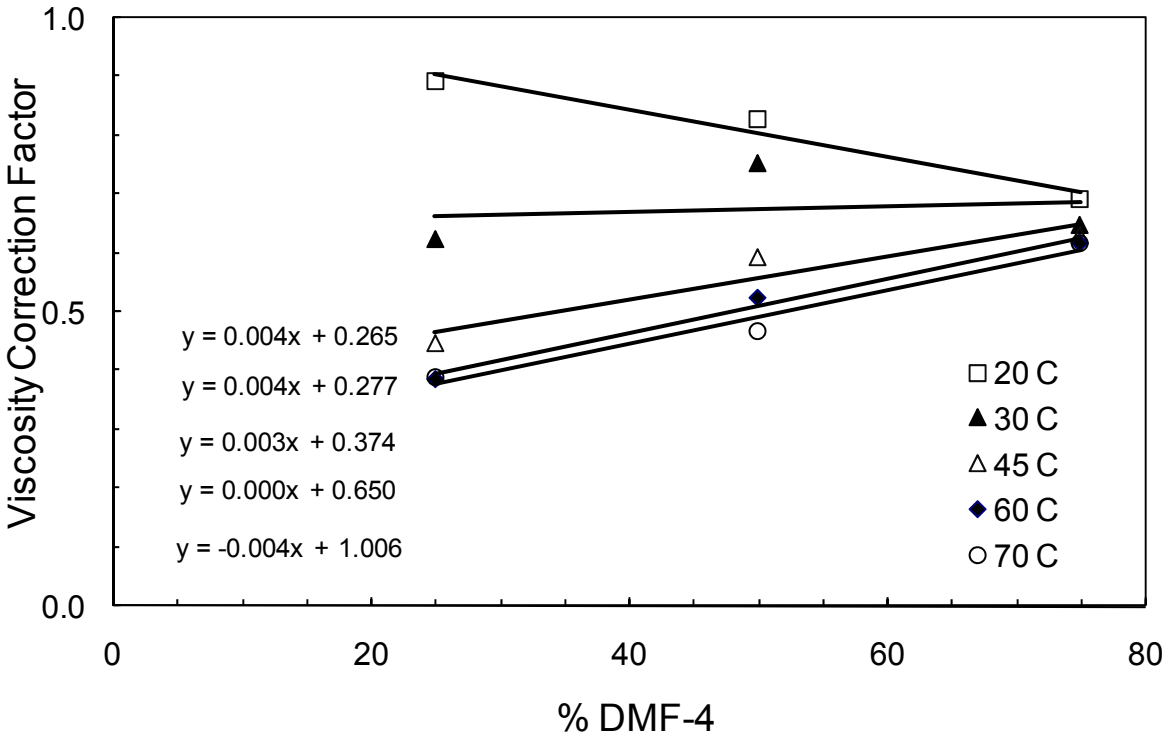

Figure 4.26 Viscosity correction factor (Equation 4.1) of HW2 for prediction of contaminated West African Dead Oil vs. mud filtrate (DMF-4) wt. percent. The regression values (R^2) are between 0.90 and 0.96.

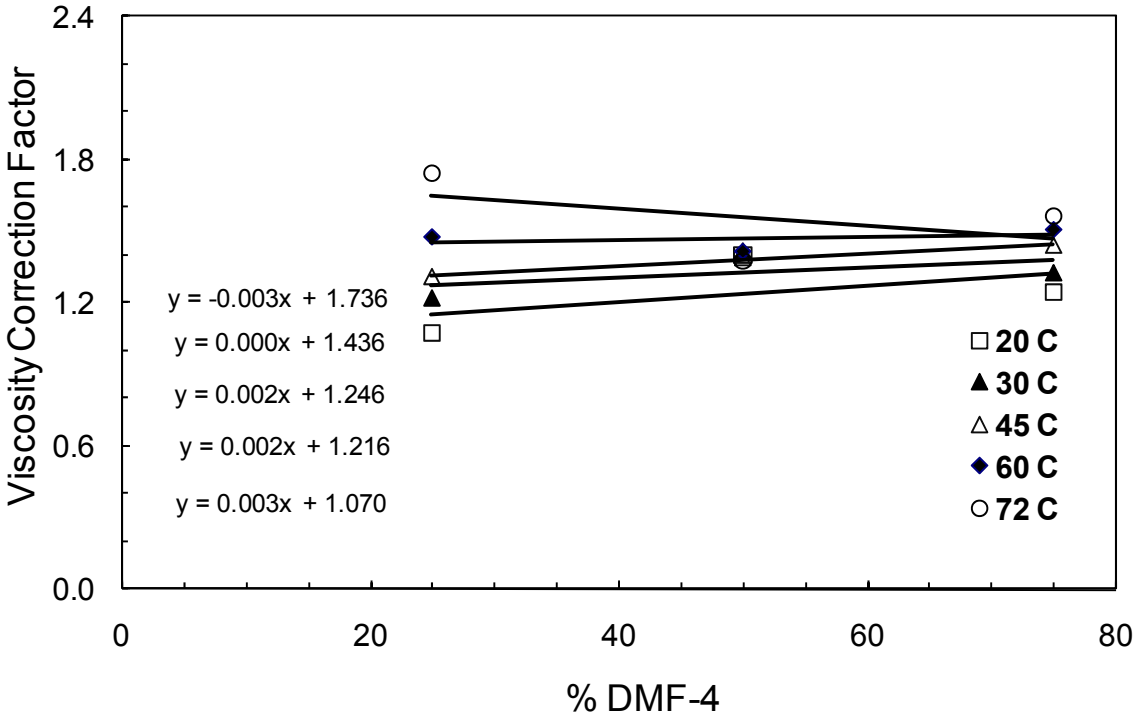

Figure 4.27 Viscosity correction factor (Equation 4.1) of Bergman-Sutton for prediction of contaminated West African Dead Oil vs. mud filtrate (DMF-4) wt. percent. The regression values (R^2) are between 0.23 and 0.99.

In order to predict the viscosity of uncontaminated West African crude the $VCF_{original\ fluid}$ has to be determined. These values are reported in Figures 4.24 to 4.27. As detailed above, the $VCF_{original\ fluid}$ values are the viscosity correction factor at zero weight percent of the mud filtrate (DMF-4). The predicted viscosities of the West African dead oil corrected with the $VCF_{original\ fluid}$ are shown in Figure 4.28. Also the average absolute deviation percentage of each predictive method is tabulated in Table 4.6.

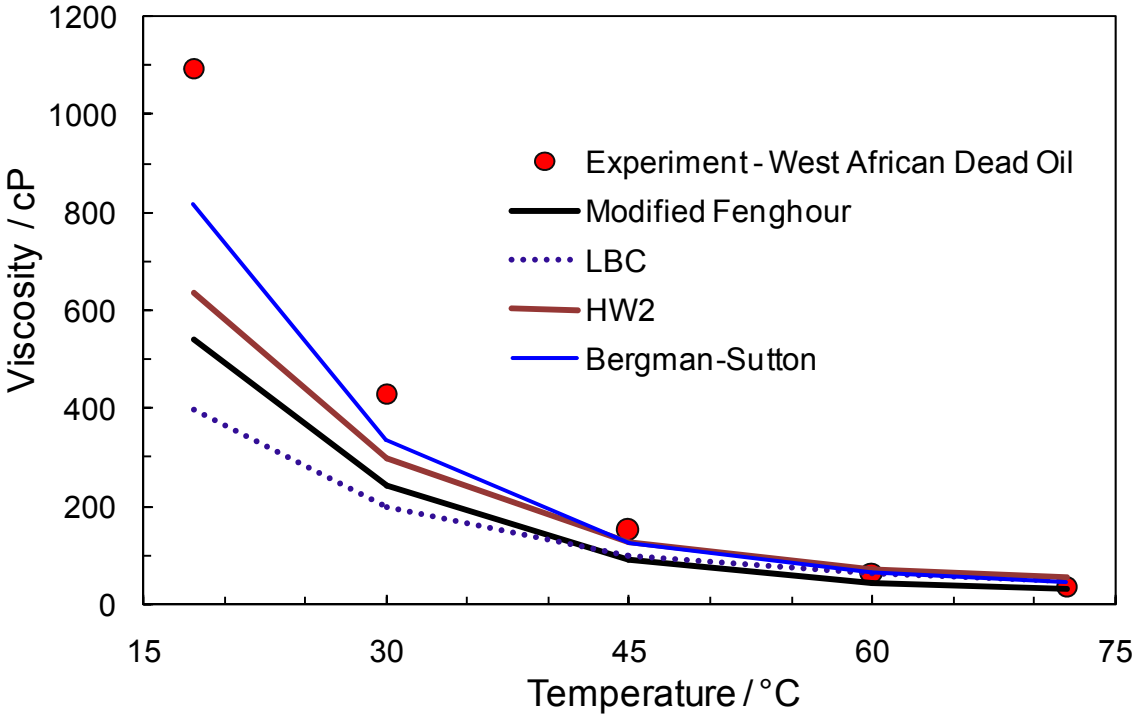

Figure 4.28 Prediction of West African Dead Oil viscosity by different methods using the contaminated viscosity data and new approach (using VCF)

Table 4.6 AAD% between experimental and predicted viscosities of the Original West African Dead Oil using contaminated viscosity and new approach (using VCF)

	Modified Fenghour	LBC	HW2	Bergman-Sutton
with VCF	36	38	29	18
without VCF	78	56	186	31

The predictive viscosity models show promising results at higher temperatures (Figure 4.28). As reported in Table 4.6, using the VCF could improve the prediction of the West African dead oil viscosity. LBC has a real challenge when it comes to predict "heavy oil" or dense fluid phase viscosities. BS method shows good accuracy even without using viscosity correction factor (AAD% of 31) however the prediction result using VCF improved the estimated viscosity of the clean oil to the deviation of 18%.

4.6 Conclusions

Viscosity measurements have been performed on three different dead oils. The fluids originated from different geographical locations such as the North Sea, Norway and West of Africa. These crudes were intentionally contaminated with various levels of a mineral oil-based mud (DMF-4) to measure the viscosity of contaminated samples as well as the original fluids. Wide ranges of viscosity from about 1 to 1,095 cP were covered using the mentioned fluids. Also, the effect of adding mud filtrate on the viscosity of dead oils was investigated by comparing the viscosity of original (clean) dead oil with the contaminated samples. It was shown that contamination of small amount of oil based mud filtrate with dead oil could change the viscosity of clean sample drastically. The pattern of changing the viscosity of study crudes with mixing filtrate (DMF-4) was different. For example, at 20 °C, addition of 25 wt% mud filtrate to the North Sea dead oil reduced the viscosity of the crude from 12.87 to 9.07 cP i.e., a viscosity ratio of 1.4 (viscosity of original crude/ viscosity of contaminated sample), while the ratios of decrease were much larger at 6.5 (i.e., from 305 to 47 cP) and 17.2 (from 1096 to 63.5 cP) for Norwegian and West African crudes, respectively.

These experimental data were used to study the reliability of a new approach to retrieve viscosities of uncontaminated oils from contaminated samples. This new technique (to correct the viscosity prediction for each model) is derived from the idea that the deviation of each viscosity model from experimental data for nearly identical fluid is relatively close to each other. To evaluate the reliability of this method, experimental viscosity data of the above mentioned dead oils in the original and contaminated states (with DMF-4) were compared against different viscosity models. The proposed method can improve the calculated viscosity using various predictive models (which are described in Chapter 3). The corrected viscosity values (using contaminated fluids) had an acceptable accuracy, i.e., a good agreement between the experimental viscosity data (this work) and the predicted results were achieved, however, at low temperatures large deviations were seen despite using the VCF approach.

References

Austad, T. and Timothy P.I., 2001, *Compositional and PVT properties of reservoir fluids contaminated by drilling fluid filtrate*, Journal of Petroleum Science and Engineering, **30**, 213–244

Al-Syabi, Z., Danesh A., Tohidi, B., Todd, A.C. and Tehrani, A.D., 2001, *A residual viscosity correlation for predicting the viscosity of petroleum reservoir fluids over wide ranges of pressure and temperature*, Chemical Engineering Science, **56**, 6997–7006

Bergman, D.F. and Sutton, R.P., 2007, *A Consistent and Accurate Dead Oil Viscosity Method,* SPE **110194,** presented at the SPE Annual Technical Conference, Anaheim, CA

Gozalpour, F., Danesh, A., Tehrani, D.-H., Todd, A.C., and Tohidi, B., 1999, *Predicting Reservoir Fluid Phase and Volumetric Behaviour from Samples Contaminated with Oil-Based Mud*, SPE **56747**

Fenghour, A., Wakeham, W.A. and Vesovic, V., 1997, *The Viscosity of Carbon Dioxide*, Journal of Physical and Chemical Reference Data, **27**, 31-44

Lohrenz, J., Bray, B.G. and Clark, C.R., 1964, *Calculating Viscosities of Reservoir Fluids from Their Compositions*, J. Pet. Tech. (JPT), 1171-1176

Sutton, R.P. and Bergman, D.F., 2008, *Application of the Bergman-Sutton Method for Determining Blend Viscosity*, SPE **117711**

CHAPTER 5

VISCOSITY: EFFECT OF DISSOLVED WATER

5.1 Introduction

As discussed in Chapter 3, newly explored reservoirs often encountered extreme conditions that can be up to 200 °C and 18,000 psia. Some examples of the reservoirs at HPHT conditions were cited in Section 2.1. For these reservoirs, the costs of subsurface operations are considerably higher than conventional reservoirs. Knowing the fluid properties especially at HPHT conditions are essential for field development and consequently a cost effective reservoir management. Moreover, gaining knowledge on the effect of other compounds like water on the hydrocarbon properties would be of great benefit in this respect.

Water is present in almost all hydrocarbon reservoirs. Dissolved water in the hydrocarbon phase is one of the forms that this compound can be found in the reservoir fluids. The influence of the dissolved water on physical and rheological properties of hydrocarbons would be of interest in particular at high temperatures (and high pressures in case of liquid hydrocarbons), as the solubility of water increases at these conditions. Hence, experimental measurements of these properties are necessary to be made in the laboratory.

Information on the effect of dissolved water on the hydrocarbon viscosity at high pressure and high temperature conditions is very scarce in the open literature (Glandt *et al.* 1995 and Gozalpour *et al.* 2005). Also, the reported viscosity measurements do not cover a wide range of hydrocarbons, and/or temperature and pressure conditions.

The viscosity measurement of hydrocarbon mixtures with water at HPHT conditions have been systematically pursued in this work and reported in this chapter. These tests have been performed in an attempt to quantify the effect of water on hydrocarbon systems at high pressure and temperature conditions. This systematic generation of viscosity data initiated from an observation that the addition of around 5 mole% water to a synthetic volatile oil, consisting of mainly n-alkanes, increased the viscosity of the hydrocarbon

mixture as much as 20% at 200 °C. Also the viscosity of a synthetic gas condensate was increased by 2-4% due to addition of about 5 mole% of water at 175 °C (Gozalpour et al 2005).

Six hydrocarbon systems with various amounts of dissolved water were studied in this work to investigate the impact of dissolved water. Experimental viscosity data of the dry systems were detailed in Tables 3.1 to 3.6. The HPHT facility, which is equipped with a capillary tube viscometer, was used to carry out the viscosity measurements. A schematic of the HPHT facility (configured for viscosity measurement) and the procedure for viscosity measurements are outlined in Chapter 2.

5.2 Experimental Results

n-Heptane, *n*-decane and toluene were the hydrocarbon liquids selected for the investigation. The liquid hydrocarbons were prepared gravimetrically as binary mixtures, combined with methane, to a nominal composition of 60 mole% hydrocarbon liquid / 40 mole% methane. Two concentrations of water, (nominally 2 and 5 mole%) were then added to these systems. These concentrations of water were selected after predicting the solubility of water in each composition, to ensure that the water would be fully dissolved over the experimental temperature and pressure ranges. To calculate the solubility of water in hydrocarbon phase, VPT EoS (Valderrama 1990) which was discussed in Chapters 3 and 6 was employed. More details on the materials and compositions of the mentioned samples are presented in Chapter 2.

To investigate the effect of dissolved water on viscosity of hydrocarbon mixtures, three multi-component systems with and without dissolved water were selected: Gas condensate (GCB00-1), natural gas (NG1) and a synthetic volatile oil, which are described in Chapter 2. Excess water (about three times more than the amount of water that is needed to obtain saturated hydrocarbon) was added to obtain water saturated hydrocarbons for the viscosity measurement with water. Water droplets were also visible during the tests to prove the presence of excess water. In one instance, for the viscosity test on the natural gas, instead of using saturated hydrocarbon with water, about 1% water was added to the system. The concentration of water in this case was selected after predicting the solubility of water to ensure that the water would be fully dissolved over the temperature and pressure ranges of the experiments. The results generated in this chapter were compared with the viscosity of the dry hydrocarbons reported in Chapter 3

to study the effect of dissolved water on viscosity. Since the viscosity of the hydrocarbon systems over the small range of pressure do not change drastically, no interpolation was performed to match the viscosity data points of the two dry and wet hydrocarbon systems at different pressures.

One of the small volume cell (Figure 2.1) in the HPHT facility was loaded with the test sample and was installed in the thermostatically controlled air-bath. The rest of the high pressure equipment was evacuated then filled with clean mercury. Heating was then applied, the pressure increased and the fluid pumped back and forth through the capillary tube viscometer, so that it could attain single-phase and thermal equilibrium. This mixing process was repeated before starting viscosity measurements for each of the remaining temperatures studied, so the hydrocarbon saturated with water would be made. Following sections present the experimental results of these series of viscosity tests:

5.2.1 *Methane / n-Heptane / Water*

The methane/*n*-heptane binary were employed to prepare two different mixtures with water. The concentrations of added water were nominally 2 and 5 mole percent. Viscosity tests were performed on these samples to study the influence of dissolved water on hydrocarbon system.

The first mixture contains 1.8±0.07 mole% of distilled water (the mixture). The details of this fluid are shown in Table 2.6 along with the dry composition, for comparison with the original mixture. Predictions for the solubility of water in the prepared mixture indicated that measurements could be made at both; 150 and 200 °C and there won't be any free water at these temperatures.

The results of the viscosity experiment are presented in Table 5.1 and shown in Figure 5.1. Table 5.1 includes the percentage difference between these measurements and those made without any dissolved water, the average deviation is -1.1%, which is below the experimental error (an accuracy of ±2% estimated using propagation of errors). Water viscosity from the literature (NIST web book) has also been added to Figure 5.1 to show the influence that water has on the hydrocarbon/water mixture.

Table 5.1 Viscosity measurements (this work) of methane / n-heptane (55.9 mole%) / water (1.8 mole%) mixture at 150 °C. The table also presents a comparison between viscosity data of the investigated hydrocarbon system with and without dissolved water.

Pressure (psia)	Viscosity (cp)	(±)	Viscosity Difference from Dry System (Table 3.1) (%)
5014	0.113	0.002	-1.8
7510	0.137	0.002	-3.1
10005	0.161	0.002	-0.7
12506	0.184	0.002	-0.1
15006	0.204	0.003	0.0
17509	0.224	0.003	-1.4
19996	0.244	0.003	-0.5

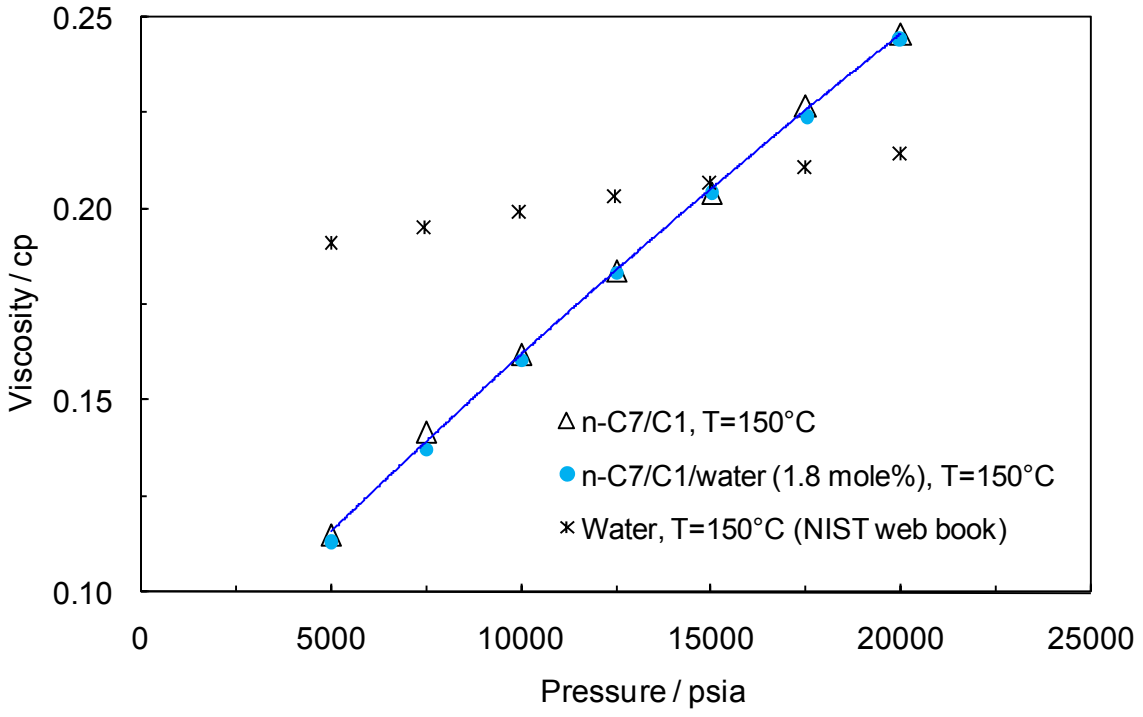

Figure 5.1 Pressure versus viscosity measurements (this work) for methane / n-heptane (55.9 mole%) / water (1.8 mole%) and also dry system at 150 °C. Water viscosity from NIST web book is also plotted for comparison reason.

The air-bath/fluid temperature was raised to obtain a fluid equilibrium temperature of 200 °C and after allowing time for the fluid to equilibrate the viscosity over the range 5,013 to 20,002 psia (0.088±0.001 cp to 0.202±0.003 cP) was measured. Table 5.2 lists the full results and also the percentage change from the measurements made where no dissolved water was present in the mixture. Here, the average difference between these data and those measured under the same conditions for the water-free system is -2.7% which equated to only a small reduction in measured viscosity. All of the gathered data from these experiments are available in Figure 5.2, including the literature values for water for comparison.

Table 5.2 Viscosity measurements (this work) of methane / n-heptane (55.9 mole%) / water (1.8 mole%) mixture at 200 °C. The table also presents a comparison between viscosity data of the investigated hydrocarbon system with and without dissolved water.

Pressure (psia)	Viscosity (cp)	(±)	Viscosity Difference from Dry System (Table 3.1) (%)
5013	0.088	0.001	-5.1
7513	0.110	0.002	-2.4
10005	0.129	0.002	-2.3
12507	0.147	0.002	-2.3
15007	0.165	0.002	-2.3
17506	0.183	0.002	-2.5
20002	0.202	0.003	-1.9

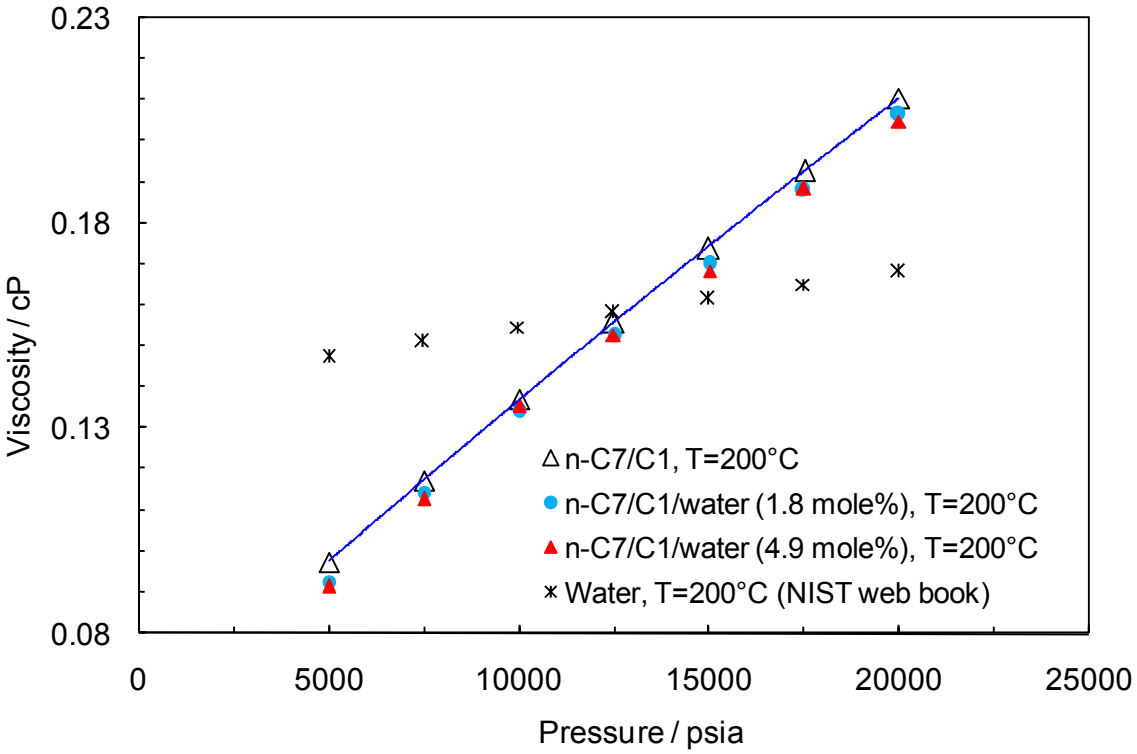

Figure 5.2 Pressure versus viscosity measurements (this work) for methane / n-heptane (55.9 mole%) / water (1.8 mole%), methane / n-heptane (53.7 mole%) / water (4.9 mole%) and also dry system at 200°C. Water viscosity from NIST web book is also plotted for comparison reason.

After thorough solvent cleaning of all equipment a second mixture was prepared but this time including a higher concentration of distilled water (the mixture contains 4.9±0.06 mole% water). The preparation details of this fluid are shown in Table 2.7. It was predicted that this concentration of water would only be soluble at 200 °C over the pressure range of interest. Table 5.3 contains the results of these measurements at 200 °C (the plot is available in Figure 5.2). An average reduction in viscosity of -3.1% can be seen when compared to the water-free hydrocarbon fluid, which is a statistically significant reduction.

Table 5.3 Viscosity measurements (this work) of methane / n-heptane (53.7 mole%) / water (4.9 mole%) mixture at 200 °C. The table also presents a comparison between viscosity data of the investigated hydrocarbon system with and without dissolved water.

Pressure (psia)	Viscosity (cp)	(±)	Viscosity Difference from Dry System (Table 3.1) (%)
5014	0.087	0.001	-6.3
7506	0.108	0.002	-4.0
10008	0.130	0.002	-1.2
12503	0.148	0.002	-2.1
15010	0.163	0.002	-3.3
17504	0.183	0.002	-2.2
20002	0.200	0.003	-2.8

5.2.2 *Methane / n-Decane / Water*

The methane/*n*-decane binary were mixed with about 2 and 5 mole percent of water to investigate the effect of dissolved water on the viscosity of the hydrocarbon binary. Predictions for the solubility of water in the prepared mixture indicated measurements could be made at both; 150 and 200 °C.

The results of the experiment carried out at 150 °C are available in Table 5.4 and are shown in Figure 5.3. Table 5.4 includes the percentage difference between these measurements and those conducted with no dissolved water, the average of these values is 2.4% of a difference, which is just above the detectable difference measurable by this technique (an accuracy of ±2% for the employed measurement technique).

Table 5.4 Viscosity measurements (this work) of methane / n-decane (59.8 mole%) / water (2.0 mole%) mixture at 150 °C. The table also presents a comparison between viscosity data of the investigated hydrocarbon system with and without dissolved water.

Pressure (psia)	Viscosity (cp)	(±)	Viscosity Difference from Dry System (Table 3.2) (%)
2239	0.160	0.003	2.8
5005	0.207	0.003	2.5
7500	0.247	0.004	2.5
10003	0.285	0.004	2.3
12508	0.322	0.005	2.1
15002	0.360	0.005	2.0
17513	0.401	0.005	2.5
20006	0.439	0.005	2.8

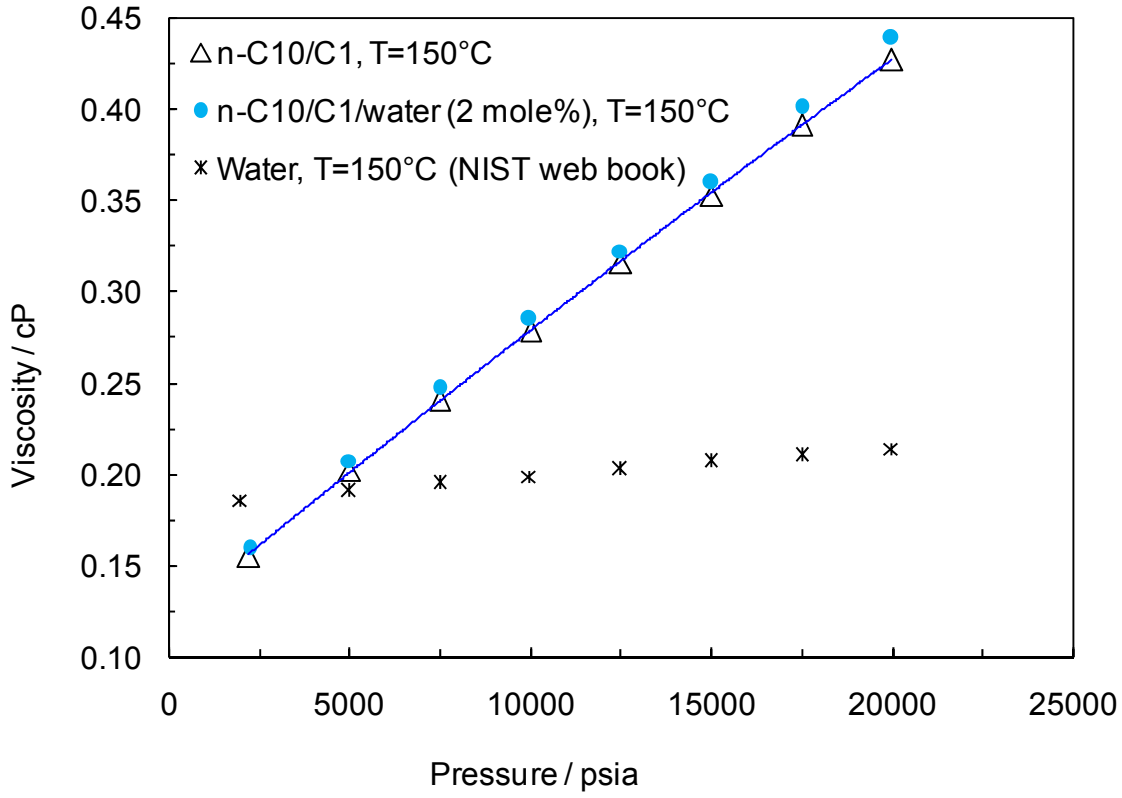

Figure 5.3 Pressure versus viscosity measurements (this work) for methane / n-decane (59.8 mole%) / water (2.0 mole%) and also dry system at 150 °C. Water viscosity from NIST web book is also plotted for comparison reason.

The temperature at the next step was adjusted to 200 °C and the viscosity over the range of 2,220 to 20,028 psia (0.114±0.002 cp to 0.345±0.004 cP) was measured. Table 5.5 lists the full results and also the percentage change from the viscosity measurements made on dry sample. Here, the average difference between these data and those measured under the same conditions for the water-free system was 2.7% which equated to only a small increase in the measured viscosity, similar to the change at 150 °C. The generated data from these experiments are available in Figure 5.4, including the literature values for water for comparison.

Table 5.5 Viscosity measurements (this work) of methane / n-decane (59.8 mole%) / water (2.0 mole%) mixture at 200 °C. The table also presents a comparison between viscosity data of the investigated hydrocarbon system with and without dissolved water.

Pressure (psia)	Viscosity (cp)	(±)	Viscosity Difference from Dry System (Table 3.2) (%)
2220	0.114	0.002	2.7
5003	0.159	0.002	3.0
9994	0.224	0.003	3.3
15010	0.284	0.004	2.3
20028	0.345	0.004	2.0

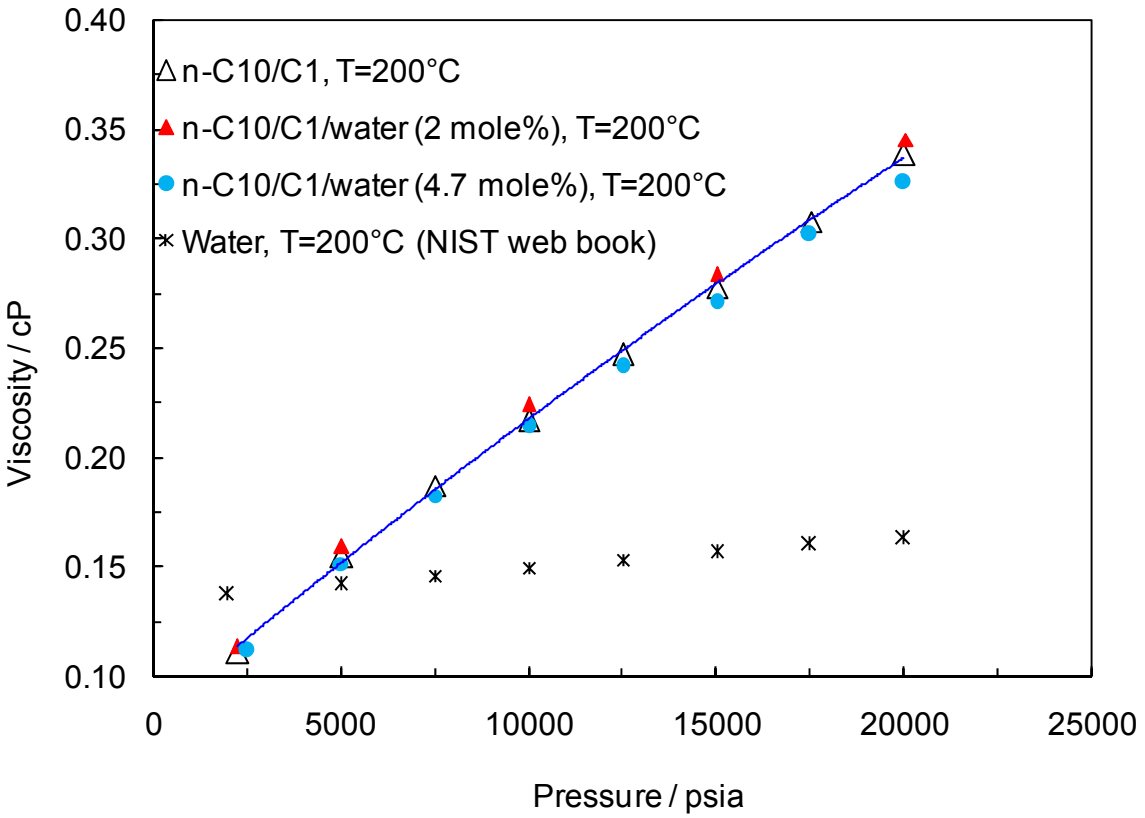

Figure 5.4 Pressure versus viscosity measurements (this work) for methane / n-decane (59.8 mole%) / water (2.0 mole%), methane / n-decane (55.4 mole%) / water (4.7 mole%) and also dry system at 200 °C. Water viscosity from NIST web book is also plotted for comparison reason.

The second mixture was prepared by adding 4.7±0.08 mole% distilled water. The composition of this fluid is shown in Table 2.9. It was predicted that this concentration of water would not be soluble in the methane / *n*-decane mixture at 100 and 150 °C but would however be soluble at 200 °C over the pressure range of our measurements. Table 5.6 contains the results of these measurements at 200 °C (the plot is available in Figure 5.4, above). An average reduction in viscosity of -1.9% can be seen when compared to the water-free hydrocarbon fluid, this is within the statistical deviation of the measurement technique, so there is no statistically significant difference between the samples with and without the dissolved water.

Table 5.6 Viscosity measurements (this work) of methane / n-decane (55.4 mole%) / water (4.7 mole%) mixture at 200 °C. The table also presents a comparison between viscosity data of the investigated hydrocarbon system with and without dissolved water.

Pressure (psia)	Viscosity (cp)	(±)	Viscosity Difference from Dry System (Table 3.2) (%)
2504	0.112	0.002	1.0
5004	0.151	0.002	-1.9
7502	0.182	0.002	-2.5
10008	0.214	0.003	-1.3
12501	0.242	0.003	-2.2
15006	0.271	0.003	-2.5
17496	0.302	0.004	-1.9
20005	0.326	0.004	-3.7

5.2.3 *Methane / Toluene / Water*

It was calculated that a mix of methane and toluene with 2 mole% water would remain in single phase in the temperature range of interest (100 to 200 °C). .

Table 5.7 shows the trend of increasing viscosity with increasing pressure from 0.170±0.002 cP at 5,014 psia to 0.316±0.004 cP at 20,002 psia. The data are plotted in Figure 5.5, which also include the literature data for water. The average difference between the viscosity measurements made with and without fully dissolved water was an increase of 1.9% which is within the measurement accuracy of this technique.

Table 5.7 Viscosity measurements (this work) of methane / toluene (58.7 mole%) / water (2.0 mole%) mixture at 100 °C. The table also presents a comparison between viscosity data of the investigated hydrocarbon system with and without dissolved water.

Pressure (psia)	Viscosity (cp)	(±)	Viscosity Difference from Dry System (Table 3.3) (%)
5014	0.170	0.002	2.5
7509	0.198	0.003	3.3
10017	0.220	0.003	1.6
12526	0.243	0.003	1.7
15010	0.266	0.003	0.7
17508	0.292	0.004	1.5
20002	0.316	0.004	1.6

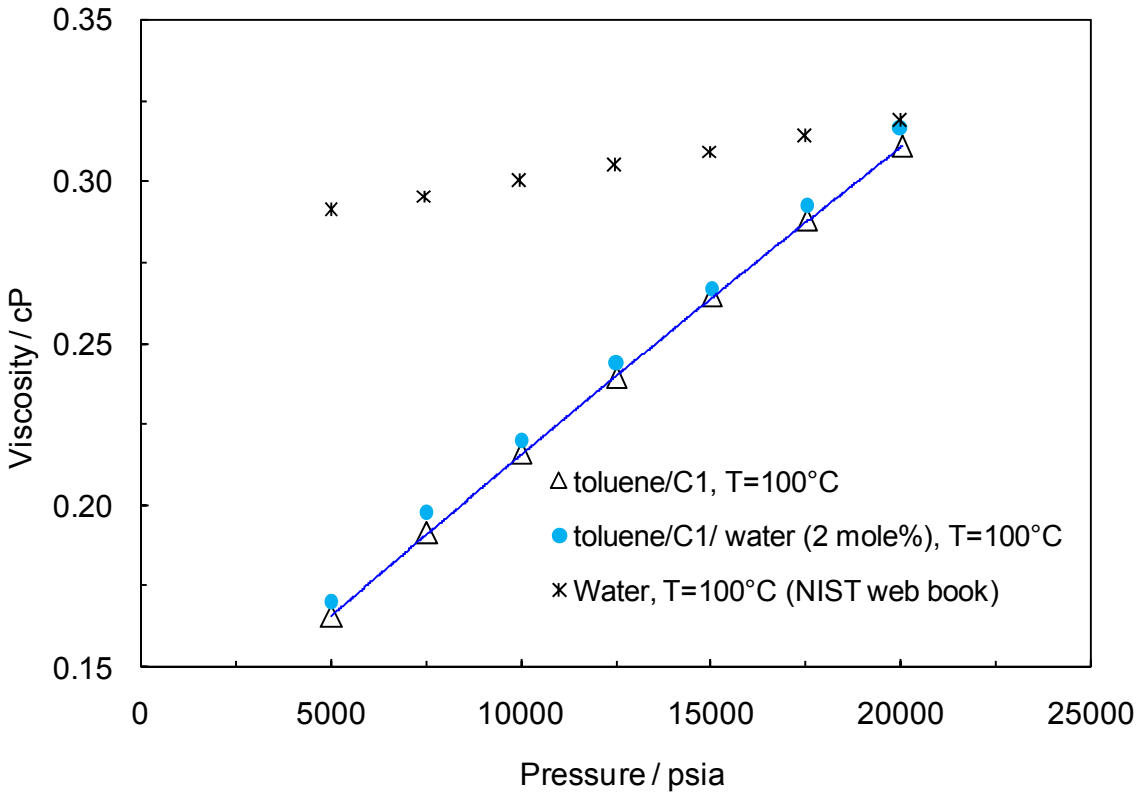

Figure 5.5 Pressure versus viscosity measurements (this work) for methane / toluene (58.7 mole%) / water (2.0 mole%) and also dry system at 100 °C. Water viscosity from NIST web book is also plotted for comparison reason.

An average increase in viscosity of 1.8% was seen when the study was performed at 150 °C, again this indicates that there is no major effect on the system viscosity with the addition of 2.0 mole% of water into the methane / toluene mixture, at this temperature. These data can been seen in Table 5.8 and plotted in Figure 5.6.

Table 5.8 Viscosity measurements (this work) of methane / toluene (58.7 mole%) / water (2.0 mole%) mixture at 150 °C. The table also presents a comparison between viscosity data of the investigated hydrocarbon system with and without dissolved water.

Pressure (psia)	Viscosity (cp)	(±)	Viscosity Difference from Dry System (Table 3.3) (%)
5024	0.125	0.002	1.9
7504	0.149	0.002	2.7
10003	0.167	0.002	0.9
12508	0.188	0.002	1.4
15004	0.208	0.003	2.0
17519	0.227	0.003	1.7
20008	0.245	0.003	1.9

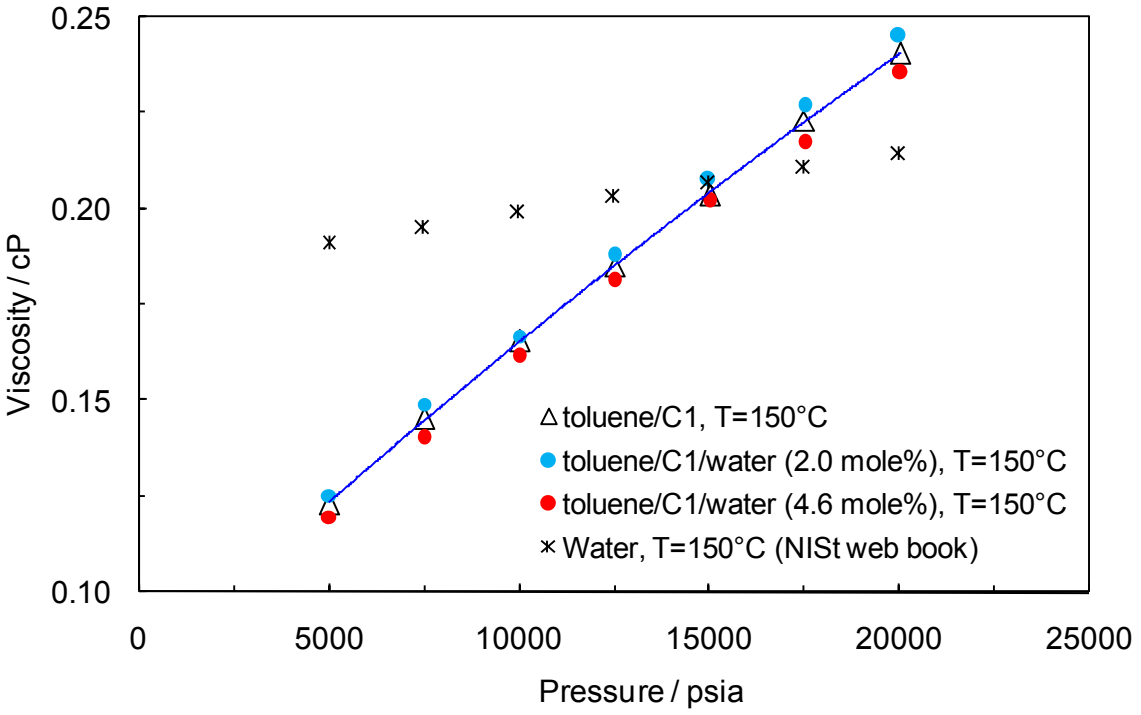

Figure 5.6 Pressure versus viscosity measurements (this work) for methane / toluene (58.7 mole%) / water (2.0 mole%), methane / toluene (55.5 mole%) / water (4.6 mole%) and also dry system at 150 °C. Water viscosity from NIST web book is also plotted for comparison reason.

It was estimated that a mix of methane and toluene with 5 mole% water would remain in single-phase in the experiment's temperature range (from 150 to 200 °C). The composition of the gravimetrically prepared methane / toluene / water (4.6±0.06 mole%) mixture were reported in Table 2.11. At temperature of 150 °C, a decrease in viscosity was measured at 2.3%. This is about the accuracy of the measurement technique accuracy which is 2%. Table 5.9 contains the results of these measurements and Figure 5.6 (above) contains the comparative plot.

Table 5.9 Viscosity measurements (this work) of methane / toluene (55.5 mole%) / water (4.6 mole%) mixture at 150 °C. The table also presents a comparison between viscosity data of the investigated hydrocarbon system with and without dissolved water.

Pressure (psia)	Viscosity (cp)	(±)	Viscosity Difference from Dry System (Table 3.3) (%)
5017	0.120	0.002	-2.7
7508	0.140	0.002	-3.4
10010	0.161	0.002	-2.4
12506	0.181	0.002	-2.0
15015	0.202	0.003	-0.8
17508	0.217	0.003	-2.6
20027	0.236	0.003	-2.1

Tables 5.10 and 5.11 list the results of the measurements performed at 200 °C for the samples containing 2.0 and 4.6 mole% water, respectively. With 2.0 mole% water dissolved in the sample an increase in viscosity below the accuracy of the system was measured (1.4%). However, increasing the concentration of dissolved water to 4.6 mole% did amount to a slight decrease in viscosity of -3.5%. Figure 5.7 shows the data.

Table 5.10 Viscosity measurements (this work) of methane / toluene (58.7 mole%) / water (2.0 mole%) mixture at 200 °C. The table also presents a comparison between viscosity data of the hydrocarbon system with and without dissolved water.

Pressure (psia)	Viscosity (cp)	(±)	Viscosity Difference from Dry System (Table 3.3) (%)
5015	0.097	0.001	0.9
7507	0.118	0.002	1.9
10017	0.135	0.002	1.1
12505	0.154	0.002	1.8
15015	0.170	0.002	0.4
17505	0.185	0.002	1.9
20005	0.201	0.003	2.0

Table 5.11 Viscosity measurements (this work) of methane / toluene (55.5 mole%) / water (4.6 mole%) mixture at 200 °C. The table also presents a comparison between viscosity data of the hydrocarbon system with and without dissolved water.

Pressure (psia)	Viscosity (cp)	(±)	Viscosity Difference from Dry System (Table 3.3) (%)
5020	0.091	0.001	-4.8
7507	0.112	0.002	-3.3
10005	0.129	0.002	-3.9
12508	0.147	0.002	-3.1
15009	0.162	0.002	-4.3
17510	0.177	0.002	-2.8
20000	0.192	0.003	-2.5

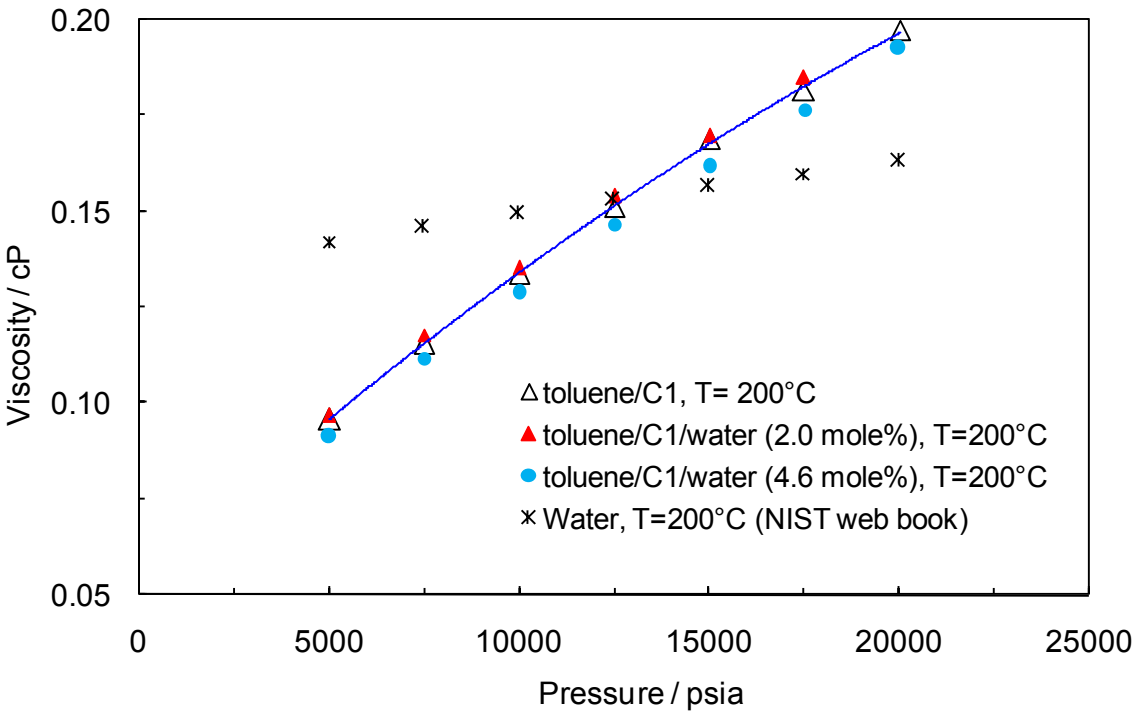

Figure 5.7 Pressure versus viscosity measurements (this work) for methane / toluene (58.7 mole%) / water (2.0 mole%), methane / toluene (55.5 mole%) / water (4.6 mole%) and also dry system at 200 °C. Water viscosity from NIST web book is also plotted for comparison.

5.2.4 *Gas Condensate (GCB00-1) / Water*

To investigate the effect of dissolved water on the viscosity of gas condensate (named GCB00-1 and detailed in Table 2.13), a number of tests were performed on this mixture in the presence of excess distilled water (to make the GCB00-1 saturated with water). During the tests, the fluid was moved backward and forward in an attempt to push any possible water droplet out of the capillary tube. The flushing process was run for about one hour for each pressure. Then the viscosity tests on saturated gas condensate GCB00-1 were carrying out. This mixing process was repeated before starting viscosity measurements for each of the temperatures studied (50, 100, 150 and 200 °C).

The measurements were started at about 6,036 psia (0.060±0.001 cP) and the equilibrium pressure was raised in steps of about 2500 psi to a maximum of 20,007 psia (0.121±0.002 cP). The complete table of viscosity measurements for 50 °C are available in Table 5.12 and are shown in Figure 5.8. Table 5.12 includes the percentage difference between these measurements and those made where no dissolved water was present in the

mixture, the average of these values was +3.7%. It is noticeable that water viscosity at 50 °C ranges from 0.554 cP at 5,000 psia to 0.582 cP at 20,000 psia (NIST web book).

Table 5.12 Viscosity measurements (this work) of gas condensate (GCB00-1) saturated with water at 50 °C. The table also presents a comparison between viscosity data of the investigated hydrocarbon system with and without dissolved water.

Pressure (psia)	Viscosity (cp)	(±)	Viscosity Difference from Dry System (Table 3.4) (%)
6036	0.060	0.001	5.3
7521	0.068	0.001	4.7
10009	0.079	0.001	2.9
12513	0.091	0.001	4.7
15040	0.103	0.001	3.3
17510	0.112	0.001	2.9
20007	0.121	0.002	1.8

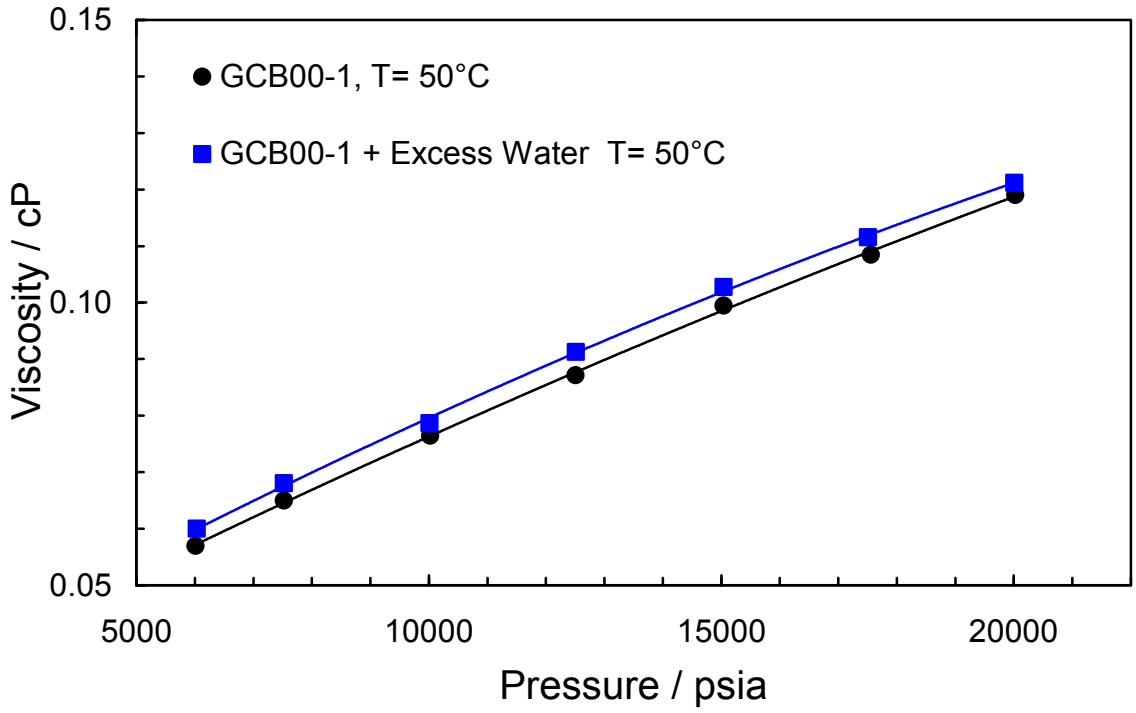

Figure 5.8 Pressure versus viscosity measurements (this work) for gas condensate (GCB00-1) saturated with water at 50°C.
Water viscosity at 50 °C ranges from 0.554 cP at 5,000 psia to 0.582 cP at 20,000 psia (NIST web book).

The temperature was increased to 100 °C and after allowing time for the fluid to equilibrate, viscosity over 6,016 to 20,009 psia was measured. Table 5.13 lists the full results and also percentage change from the measurements made where no dissolved water was present in the mixture. Here, the average difference between these data and those measured under the same conditions for the water-free system is +3.4% which equated to only a small increase in the measured viscosity. Water viscosity at 100 °C from the literature (NIST web book) ranges from 0.291 cP at 5,000 psia to 0.318 cP at 20,000 psia. All of the gathered data from these experiments are available in Figure 5.9.

Table 5.13 Viscosity measurements (this work) of gas condensate (GCB00-1) saturated with water at 100 °C. The table also presents a comparison between viscosity data of the investigated hydrocarbon system with and without dissolved water.

Pressure (psia)	Viscosity (cp)	(±)	Viscosity Difference from Dry System (Table 3.4) (%)
6016	0.049	0.001	2.7
7520	0.054	0.001	3.8
10020	0.065	0.001	4.7
12505	0.073	0.001	2.7
15015	0.083	0.001	3.5
17508	0.091	0.001	2.5
20009	0.101	0.001	3.4

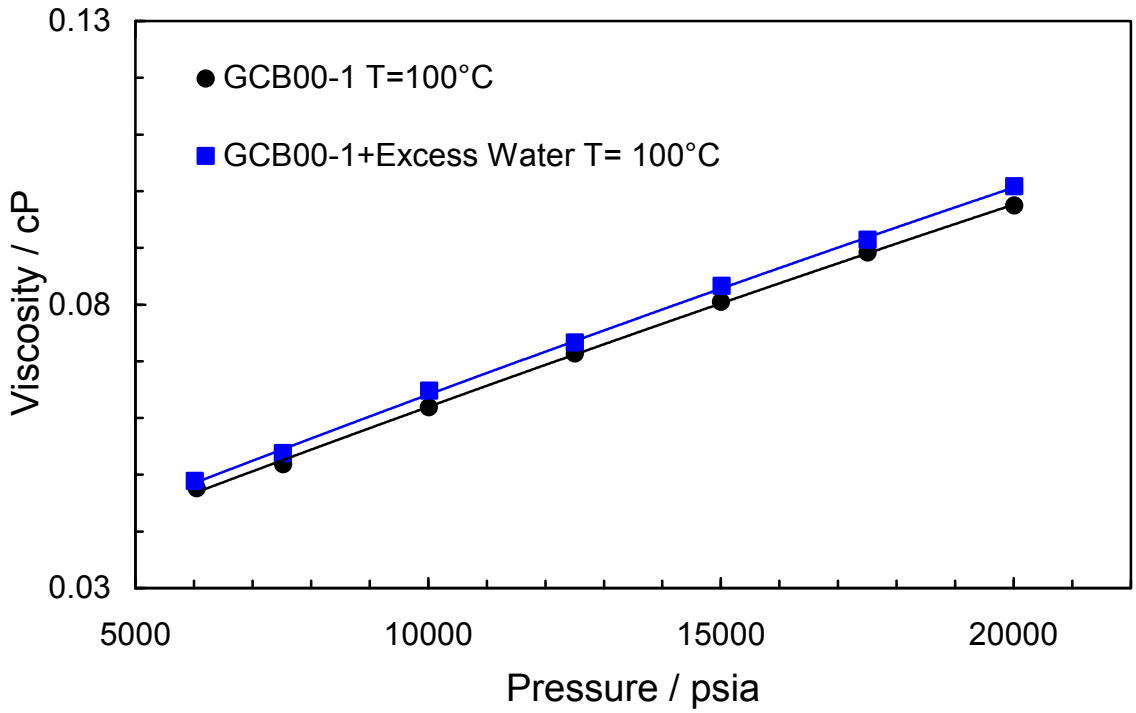

Figure 5.9 Pressure versus viscosity measurements (this work) for gas condensate (GCB00-1) saturated with water at 100 °C.
Water viscosity at 100 °C ranges from 0.291 cP at 5000 psia to 0.318 cP at 20,000 psia (NIST web book).

The same procedure was followed to conduct viscosity measurements for GCB00-1 saturated with water over the range of about 6,000 to 20,000 psia at 150 °C and 200 °C. Tables 5.14 and 5.15 list the full results and also the percentage change from the measurements made where no dissolved water was present in the mixture. Here, the average differences between these data and those measured under the same conditions for the water-free system are +7.3% and +8.7% for 150 °C and 200 °C, respectively. The water viscosity at 150 °C ranges from 0.191 cP at 5,000 psia to 0.214 cP at 20,000 psia and at 200 °C ranges from 0.142 cP at 5,000 psia to 0.163 cP at 20,000 psia (NIST web book). All of the gathered data from these experiments are available in Figures 5.10 and 5.11.

Table 5.14 Viscosity measurements (this work) of gas condensate (GCB00-1) saturated with water at 150 °C. The table also presents a comparison between viscosity data of the hydrocarbon system with and without dissolved water.

Pressure (psia)	Viscosity (cp)	(±)	Viscosity Difference from Dry System (Table 3.4) (%)
6012	0.0426	0.001	12.3
7520	0.0480	0.001	8.5
10021	0.0588	0.001	9.8
12511	0.0662	0.001	7.5
15009	0.0743	0.001	6.6
17510	0.0803	0.001	3.6
20008	0.0870	0.001	2.6

Table 5.15 Viscosity measurements (this work) of gas condensate (GCB00-1) saturated with water at 200 °C. The table also presents a comparison between viscosity data of the hydrocarbon system with and without dissolved water.

Pressure (psia)	Viscosity (cp)	(±)	Viscosity Difference from Dry System (Table 3.4) (%)
6021	0.040	0.001	16.3
7529	0.043	0.001	9.9
10019	0.052	0.001	10.9
12511	0.060	0.001	7.5
15024	0.068	0.001	6.8
17523	0.073	0.001	5.9
20003	0.079	0.001	4.0

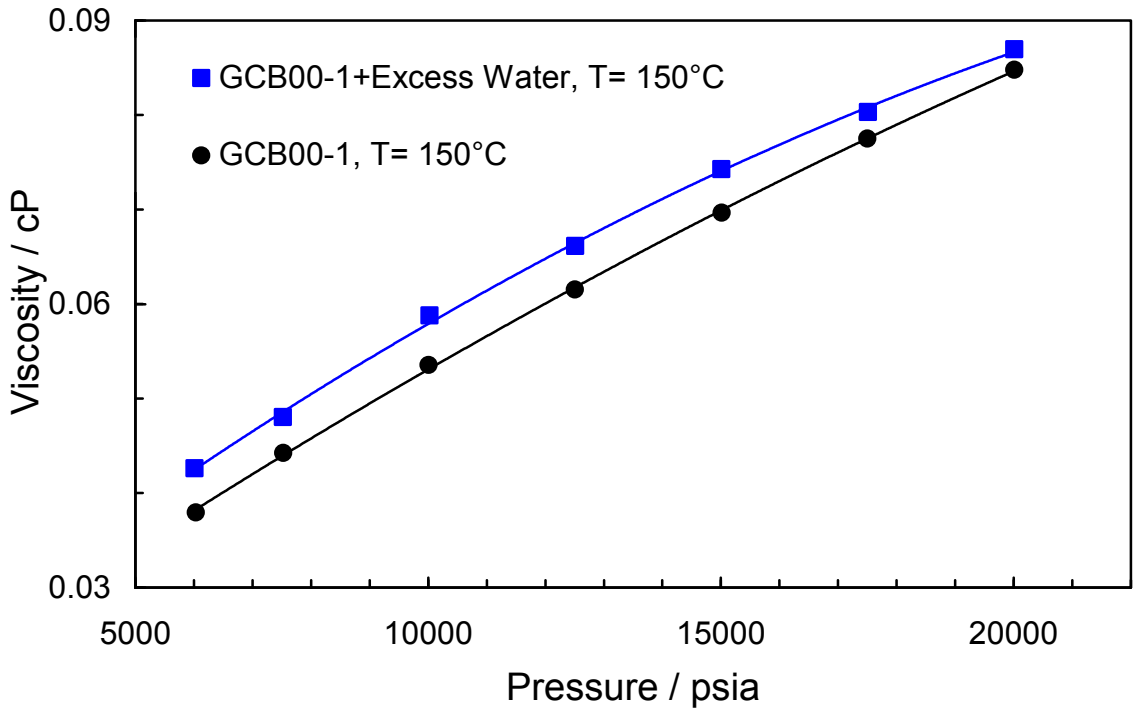

Figure 5.10 Pressure versus viscosity measurements (this work) for gas condensate (GCB00-1) saturated with water at 150°C.
Water viscosity at 150 °C ranges from 0.191 cP at 5000 psia to 0.214 cP at 20,000 psia (NIST web book).

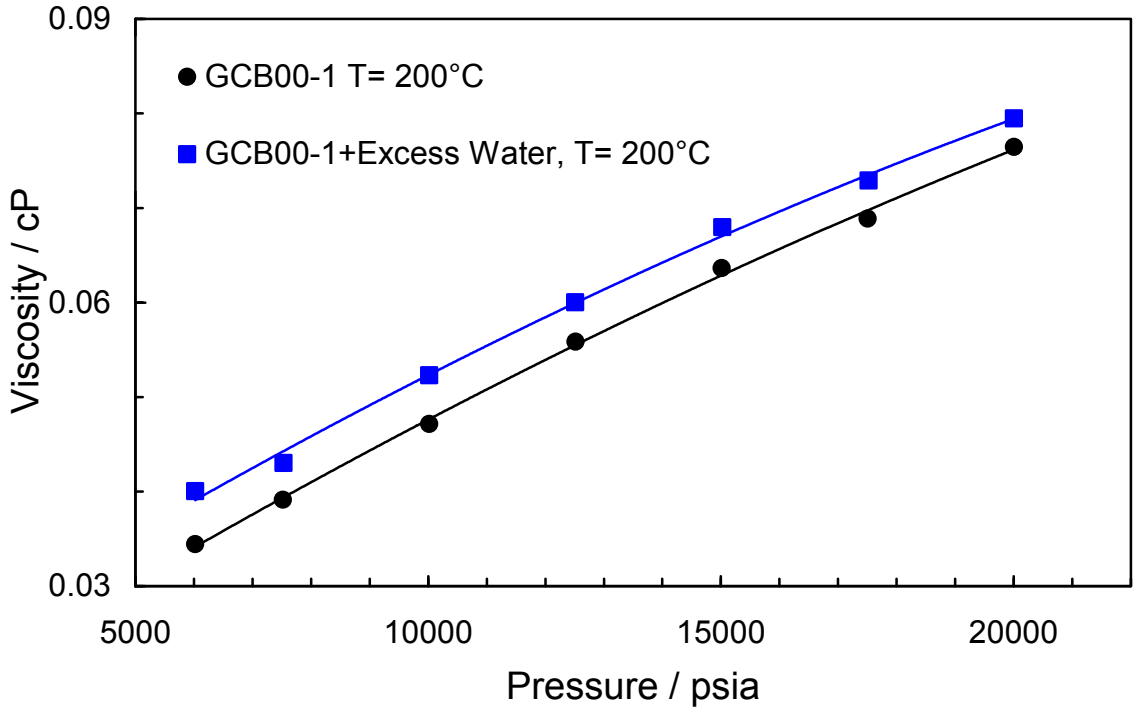

Figure 5.11 Pressure versus viscosity measurements (this work) for gas condensate (GCB00-1) saturated with water at 200 °C.
Water viscosity at 200 °C ranges from 0.142 cP at 5000 psia to 0.163 cP at 20,000 psia (NIST web book).

5.2.5 *Natural Gas (NG1) / Water*

The viscosity test on natural gas (NG1) was performed with an excess of distilled water to make the natural gas saturated with water. During the tests in order to make sure of the absence of any water droplet in the capillary tube, the fluid was pumped backward and forward to push any possible water droplet out of the capillary tube. The backward and forward process was repeated for about one hour for each pressure. Then the viscosity tests on saturated natural gas were carrying out. This mixing process was repeated before starting viscosity measurements for each of the temperatures studied (50, 100, 150 and 200 °C).

The measurements were conducted at 5,020 psia (0.030±0.001 cP) and then the equilibrium pressure was raised in steps of about 2,500 psi to a maximum of 20,023 psia (0.067±0.001cP). The complete set of viscosity measurements for 50 °C is available in Table 5.16 and is shown in Figure 5.12. The percentage differences between these measurements and those made where no dissolved water are listed in Table 5.16, the average of these values is +4.8%. The water viscosity from the literature (NIST web book) at 50 °C ranges from 0.554 cP at 5,000 psia to 0.582 cP at 20,000 psia.

Table 5.16 Viscosity measurements (this work) of natural gas (NG1) saturated with water at 50 °C. The table also presents a comparison between viscosity data of the hydrocarbon system with and without dissolved water.

Pressure (psia)	Viscosity (cp)	(±)	Viscosity Difference from Dry System (Table 3.5) (%)
5020	0.030	0.001	6.3
7516	0.038	0.001	5.6
10023	0.045	0.001	4.1
12520	0.051	0.001	4.8
15034	0.058	0.001	4.7
17537	0.063	0.001	4.4
20023	0.067	0.001	3.8

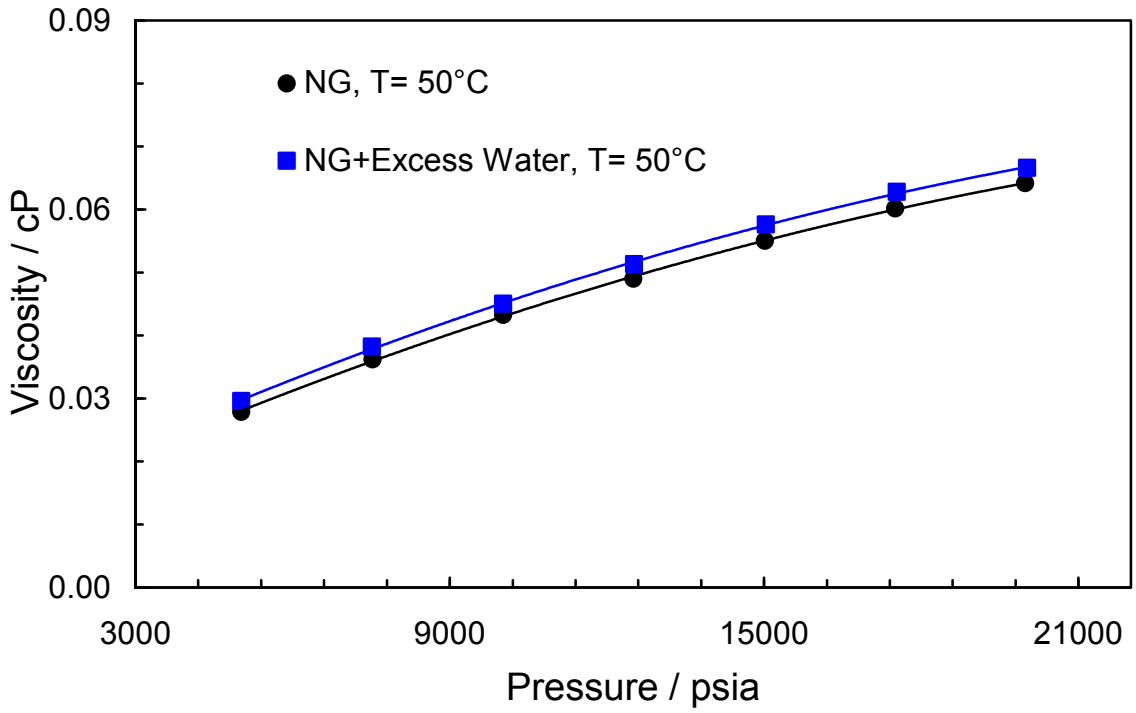

Figure 5.12 Pressure versus viscosity measurements (this work) for natural gas (NG1) saturated with water at 50 °C.
Water viscosity at 50 °C ranges from 0.554 cP at 5,000 psia to 0.582 cP at 20,000 psia (NIST web book).

Table 5.17 shows the full results and also the percentage change for the measurements made at 100 °C. Here, the average difference between these data and those measured under the same conditions for the water-free system is +13.2% which is a significant change. Water viscosity at 100 °C from the literature (NIST web book) ranges from 0.291 cP at 5,000 psia to 0.318 cP at 20,000 psia. The measured data from these experiments are presented in Figure 5.13.

Table 5.17 Viscosity measurements (this work) of natural gas (NG1) saturated with water at 100 °C. The table also presents a comparison between viscosity data of the hydrocarbon system with and without dissolved water.

Pressure (psia)	Viscosity (cp)	(±)	Viscosity Difference from Dry System (Table 3.5) (%)
5052	0.031	0.001	21.1
7515	0.036	0.001	12.1
10034	0.045	0.001	18.2
12521	0.050	0.001	19.5
15025	0.050	0.001	4.9
17512	0.059	0.001	10.5
20051	0.061	0.001	6.2

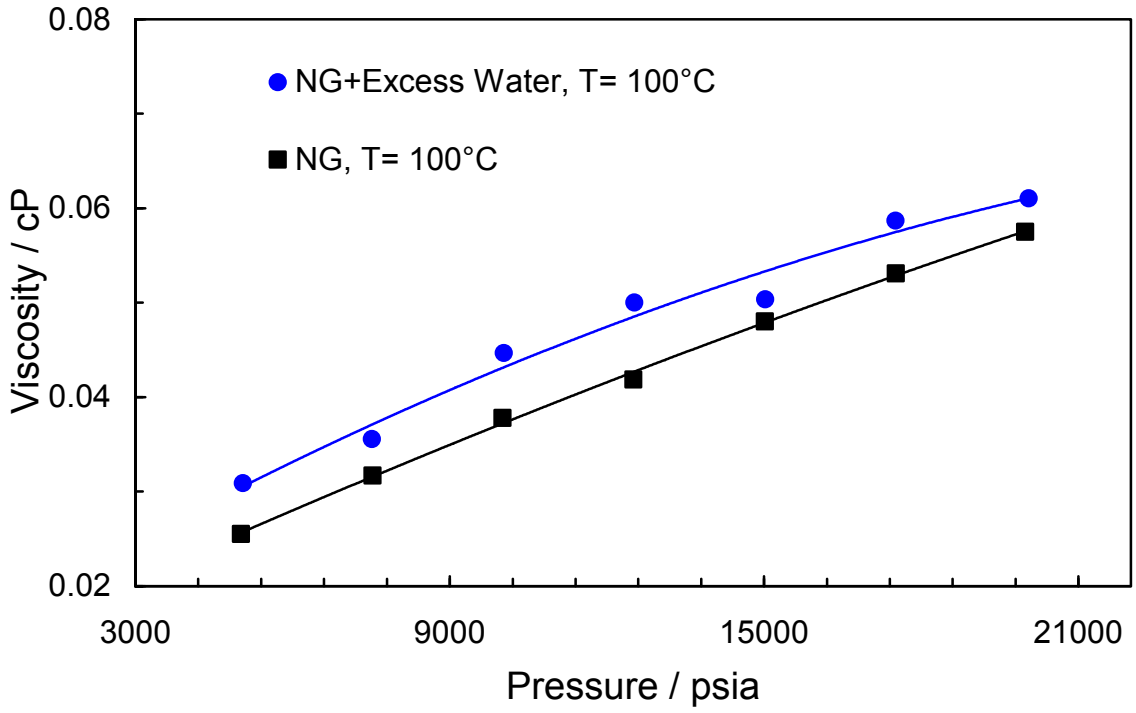

Figure 5.13 Pressure versus viscosity measurements (this work) for natural gas (NG1) saturated with water at 100 °C.
Water viscosity at 100 °C ranges from 0.291 cP at 5,000 psia to 0.318 cP at 20,000 psia (NIST web book).

As depicted in Figure 5.13, measurement of viscosity at 100 °C proved to be scattered. The problem at higher temperatures were more severe that at 150 °C the measurement and generating consistent data despite great care in performing the experiments is difficult. So for performing the measurements at 150 °C and 200 °C a sample containing 0.89% mole percent water in natural gas was prepared. It was calculated that natural gas with 1 mole% water would remain in single-phase over the temperature range of interest, (from 150 to 200 °C).

The same procedure was followed to perform the viscosity measurements at 150 °C for the natural gas with 0.89 mole% water over the range of about 7,707 (as the volume of fluid in the cell higher at this temperature the starting pressure was higher than normal) to 20,009 psia. Tables 5.18 reports the complete results and percentage change from the measurements made where no dissolved water was present. The average difference between these data and those measured under the same conditions for the water-free system is +7.8% at 150 °C. The measurement for 20,009 psia is not considered as some water droplets were seen on the inside surface of the pressure vessel window. Water viscosity at 150 °C from the literature (NIST web book) ranges from 0.191 cP at 5,000 psia to 0.214 cP at 20,000 psia. All of the gathered data from these experiments were plotted in Figure 5.14.

Table 5.18 Viscosity measurements (this work) of natural gas (NG1) with 0.89 mole % water at 150 °C. The table also presents a comparison between viscosity data of the hydrocarbon system with and without dissolved water.

Pressure (psia)	Viscosity (cp)	(±)	Viscosity Difference from Dry System (Table 3.5) (%)
7707	0.032	0.001	
10007	0.037	0.001	6.1
12513	0.042	0.001	7.2
15016	0.048	0.001	9.9
17504	0.052	0.001	8.1
20009	0.058	0.001	11.8

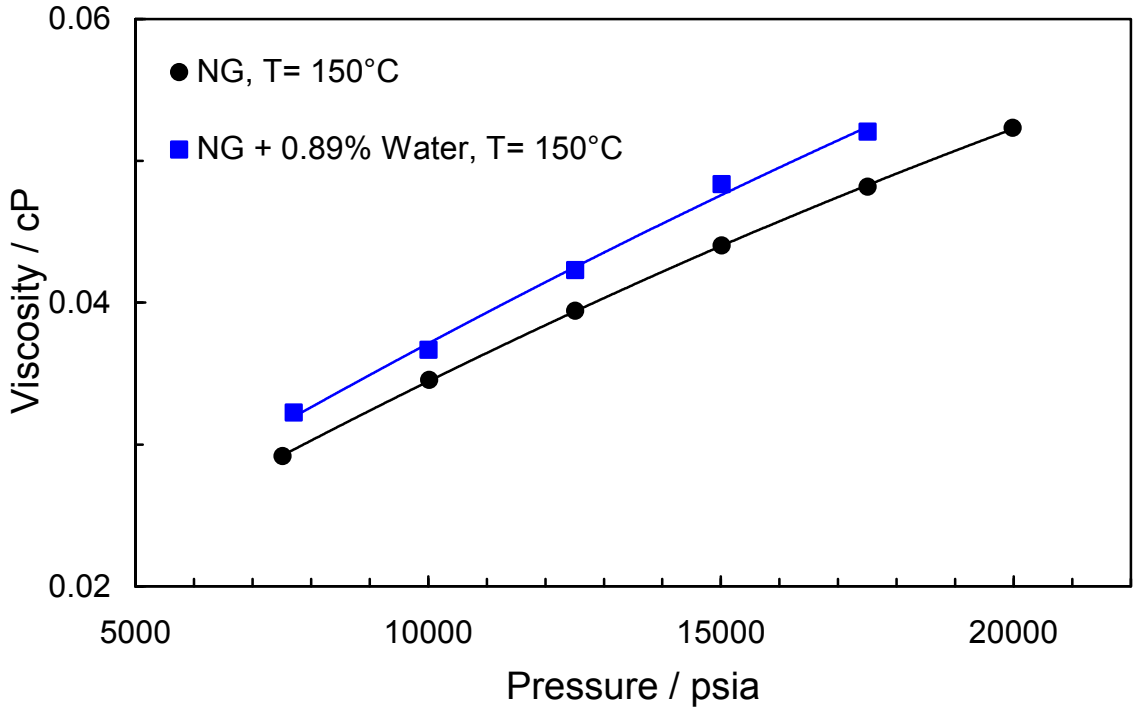

Figure 5.14 Pressure versus viscosity measurements (this work) for natural gas (NG1) with 0.89 mole% water at 150 °C.
Water viscosity at 150 °C ranges from 0.191 cP at 5000 psia to 0.214 cP at 20000 psia (NIST web book).

The same procedure was followed to perform viscosity measurements for natural gas with 0.89 mole% water at 200 °C over the range of about 8,863 (due to increase in the volume of the fluid in the cell in this temperature the starting pressure is higher than usual) to 20,003 psia. Table 5.19 lists the results and also the percentage change from the measurements made where no dissolved water was present in the mixture. The average differences between these data and those measured under the same conditions for the water-free system is +0.8% at 200 °C. Water viscosity at 200 °C from the literature (NIST web book) ranges from 0.142 cP at 5,000 psia to 0.163 cP at 20,000 psia. All of the gathered data from these experiments are available in Figure 5.15.

Table 5.19 Viscosity measurements (this work) of natural gas (NG1) with 0.89 mole % water at 200 °C. The table also presents a comparison between viscosity data of the hydrocarbon system with and without dissolved water.

Pressure (psia)	Viscosity (cp)	(±)	Viscosity Difference from Dry System (Table 3.5) (%)
8863	0.032	0.001	2.3
10005	0.033	0.001	0.9
12510	0.037	0.000	1.1
15012	0.041	0.001	0.0
17501	0.045	0.001	0.1
20003	0.049	0.001	0.2

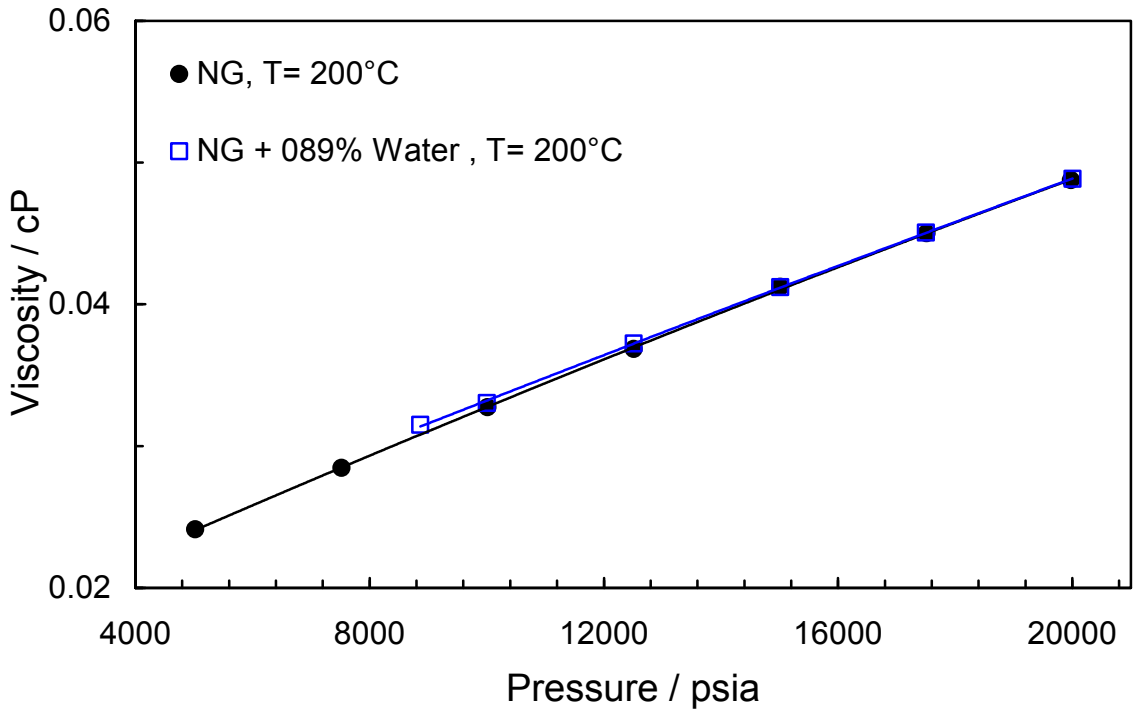

Figure 5.15 Pressure versus viscosity measurements (this work) for natural gas (NG1) with 0.89 mole% water at 200 °C.
Water viscosity at 200 °C ranges from 0.142 cP at 5000 psia to 0.163 cP at 20000 psia (NIST web book).

5.2.6 *Synthetic Volatile Oil / Water*

A five component synthetic volatile oil (composition reported in Table 2.5) was prepared gravimetrically and by adding excess amount of water, a mixture saturated with water was obtained to investigate the effect of dissolved water on viscosity of the sample at various conditions.

The sample was mixed before starting the measurements at about 11,025 psia (0.271±0.003 cP) the equilibrium pressure was raised in steps of about 2,500 psi to a maximum of 20,011 psia (0.403±0.005 cP). The complete set of viscosity measurements for 50 °C are available in Table 5.20 and are shown in Figure 5.16, including the literature values for water for comparison (NIST web book). Table 5.20 includes the percentage difference between these measurements and those made where no dissolved water was present in the mixture, the average of these values is -0.42% which is below experimental error margin (an accuracy of ±2% estimated for the employed measurement technique).

Table 5.20 Viscosity measurements (this work) of synthetic volatile oil saturated water at 50 °C. The table also presents a comparison between viscosity data of the hydrocarbon system with and without dissolved water.

Pressure (psia)	Viscosity (cp)	(±)	Viscosity Difference from Dry System (Table 3.6) (%)
11025	0.271	0.003	-0.67
12528	0.292	0.004	-0.45
15027	0.328	0.004	-0.25
17521	0.364	0.005	-0.69
20011	0.403	0.005	-0.06

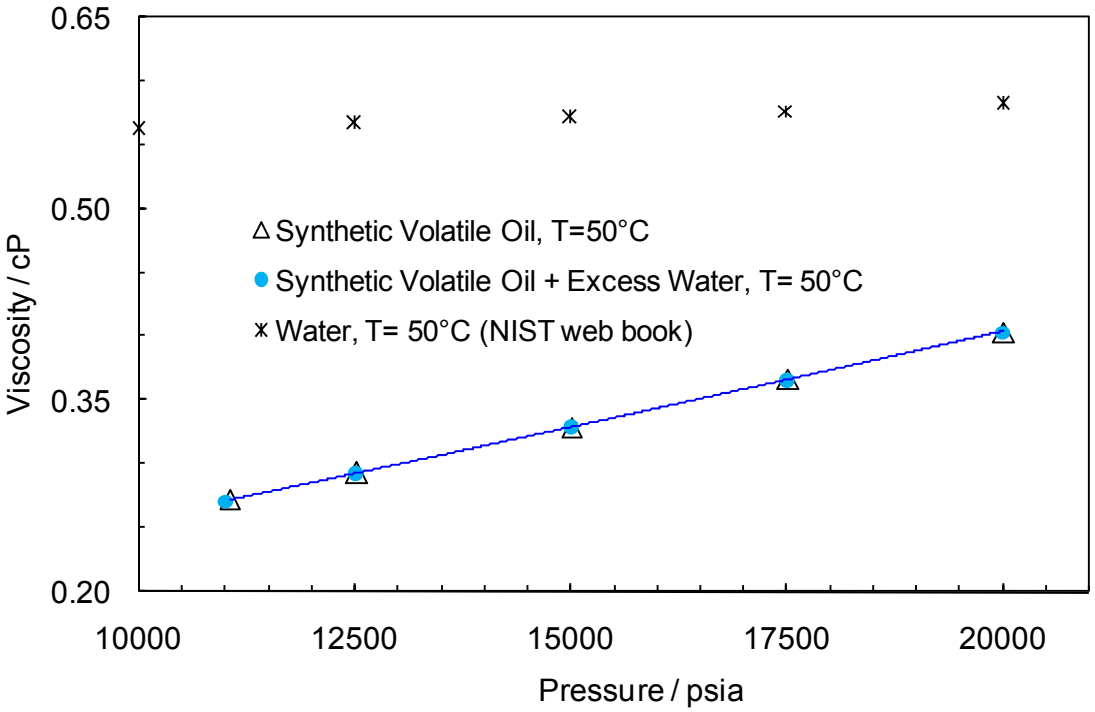

Figure 5.16 Pressure versus viscosity measurements (this work) for synthetic volatile oil saturated with water and also dry system at 50 °C. Water viscosity from NIST web book is also plotted for comparison.

The same procedure was followed for viscosity measurements of synthetic volatile oil saturated with water at 100, 150 and 200 °C. Table 5.21 lists the viscosity data and also the percentage change from the measurements made where no dissolved water was present in the mixture which in all cases are less than ±1%. All of the gathered data from these experiments are available in Figures 5.17 to 5.19 including the literature values for water for comparison (NIST web book).

Table 5.21 Viscosity measurements (this work) of synthetic volatile oil saturated water at 100, 150 and 200 °C. The table also presents a comparison between viscosity data of the hydrocarbon system with and without dissolved water.

Temperature (°C)	Pressure (psia)	Viscosity (cp)	(±)	Viscosity Difference from Dry System (Table 3.6) (%)
100	10026	0.180	0.002	0.41
100	12527	0.206	0.003	0.16
100	15042	0.234	0.003	0.54
100	17521	0.259	0.003	0.03
100	20012	0.287	0.004	0.20
150	9031	0.126	0.002	0.69
150	10033	0.134	0.002	-0.13
150	12529	0.157	0.002	0.46
150	15028	0.179	0.002	-0.18
150	17520	0.200	0.003	-0.30
150	20012	0.222	0.003	0.33
200	8036	0.091	0.001	0.63
200	10035	0.106	0.001	0.85
200	12522	0.126	0.002	0.35
200	15037	0.144	0.002	0.13
200	17521	0.163	0.002	-0.02
200	20019	0.181	0.002	-0.32

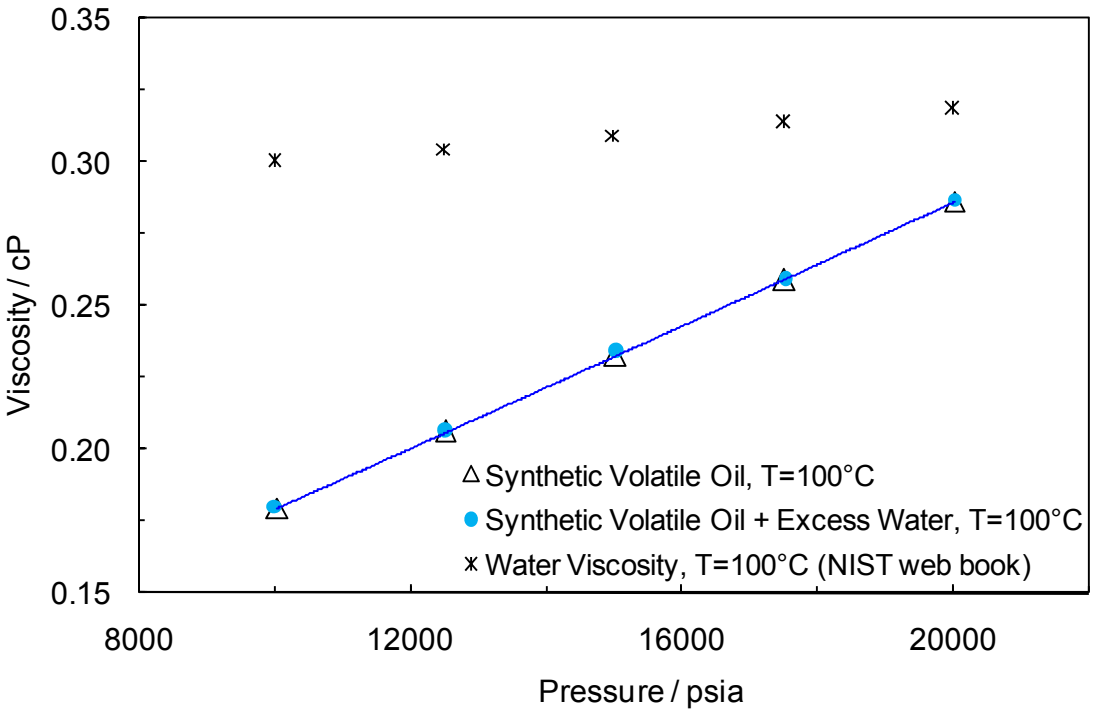

Figure 5.17 Pressure versus viscosity measurements (this work) for synthetic volatile oil saturated with water and also dry system at 100 °C. Water viscosity from NIST web book is also plotted for comparison reason.

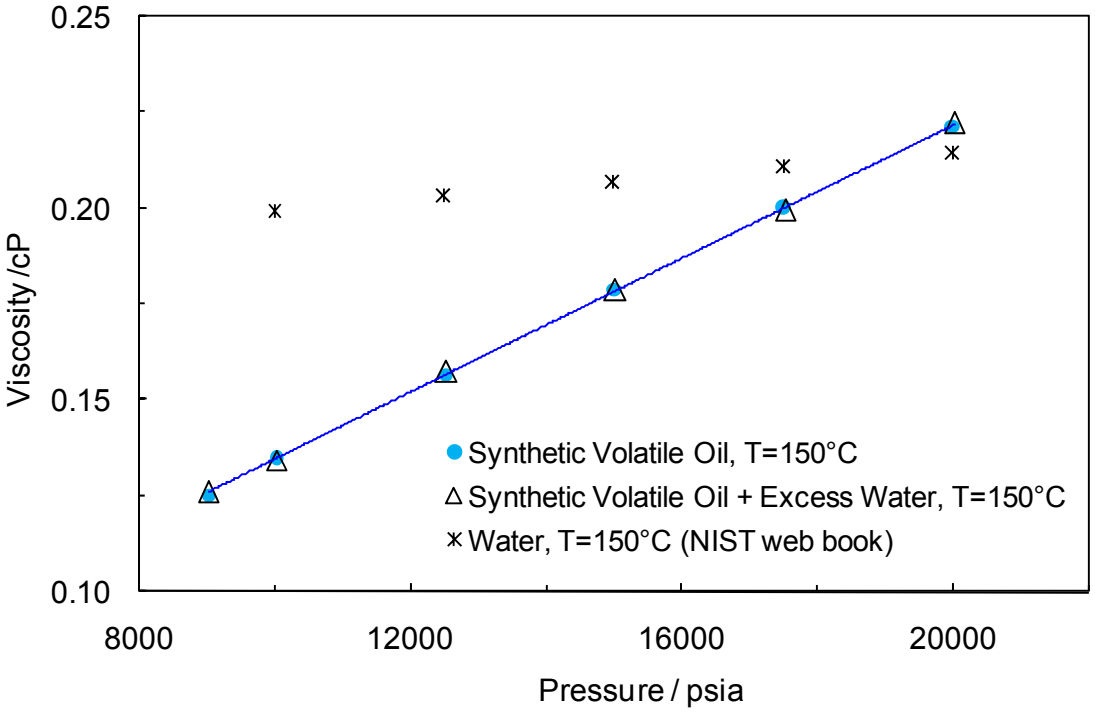

Figure 5.18 Pressure versus viscosity measurements (this work) for synthetic volatile oil saturated with water and also dry system at 150 °C. Water viscosity from NIST web book is also plotted for comparison.

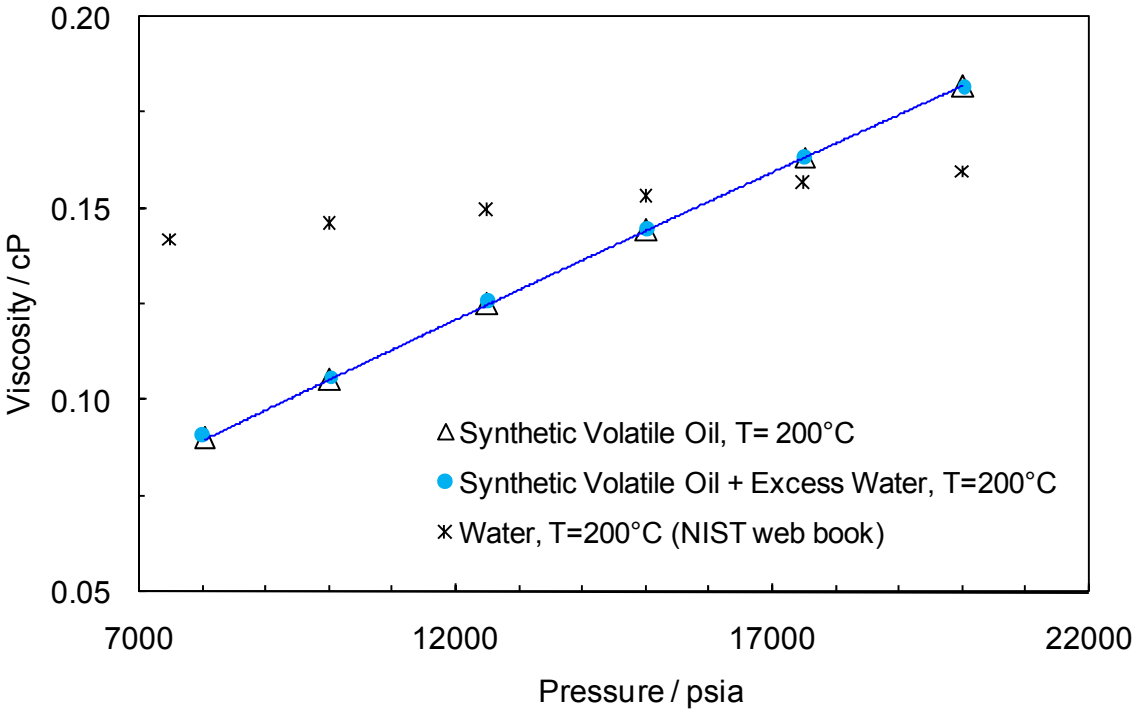

Figure 5.19 Pressure versus viscosity measurements (this work) for synthetic volatile oil saturated with water and also dry system at 200 °C. Water viscosity from NIST web book is also plotted for comparison.

5.3 Discussion

In this section the reliability of the experimental viscosity results generated in this work is discussed. For this reason, a similar fluid reported in literature (Gozalpour *et al.* 2005) was employed to investigate the reliability of viscosity data.

Since the viscosity data for synthetic volatile oil with dissolved water system generated in this work are not in agreement with the viscosity data of volatile oil *with water* reported by Gozalpour *et al.* (2005), an investigation was conducted to ensure the reliability of the viscosity experimental results generated in this work.

As reported in Table 5.22 the compositions of the prepared synthetic volatile oil in this work is similar to the one used in *Reservoir Fluid Studies, Final Report, 1996-99* and Gozalpour *et al.* 2005 (HWU2). The viscosity data for the synthetic volatile oil generated at 200 °C as part of this study and the one reported by the above mentioned authors are depicted in Figure 5.20. It can clearly be seen that these two sets of experimental viscosity data (without water) are in good agreement.

Table 5.22 Comparison between the compositions of the prepared synthetic volatile oil in this work (Table 2.5) and the synthetic volatile oil reported in Reservoir Fluid Studies, Final Report, 1996-99 which is named by Gozalpour *et al.* 2005 the HWU2

Component	This work Composition mole%	HWU2 Composition mole%
Methane	86.5	86.49
n-pentane	1.7	1.65
n-decane	1.8	1.81
n-hexadecane	1.8	1.85
n-C_{21}	8.2	8.20

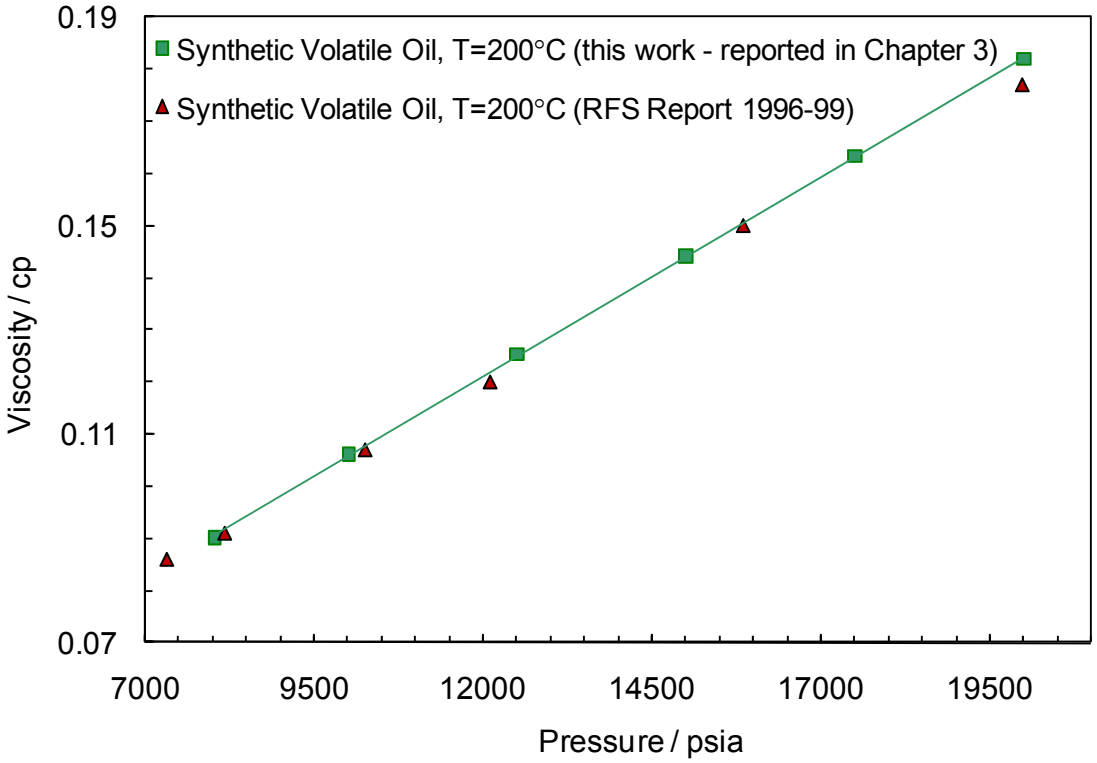

Figure 5.20 Comparison between the viscosity experimental data of synthetic volatile oil (this work) and viscosity of synthetic volatile oil reported in Reservoir Fluid Studies, Final Report, 1996-99 and published by Gozalpour *et al.* 2005 the HWU2

Despite the good agreement between the experimental viscosity data of the dry synthetic volatile oil systems reported in this study and the above mentioned source, the data generated on the volatile oil with water systems do not agree with each other (Figure 5.21). Gozalpour *et al.* 2005 reported an increase of 20% by addition of 5.4 mole% water to volatile oil at 200 °C. But in this work, no significant increase was observed even when the system was fully saturated with water. Moreover, as shown in Figure 5.19, the

viscosity of pure water and dry synthetic volatile oil are very close to each other, therefore, addition of water cannot increase the viscosity of volatile oil significantly.

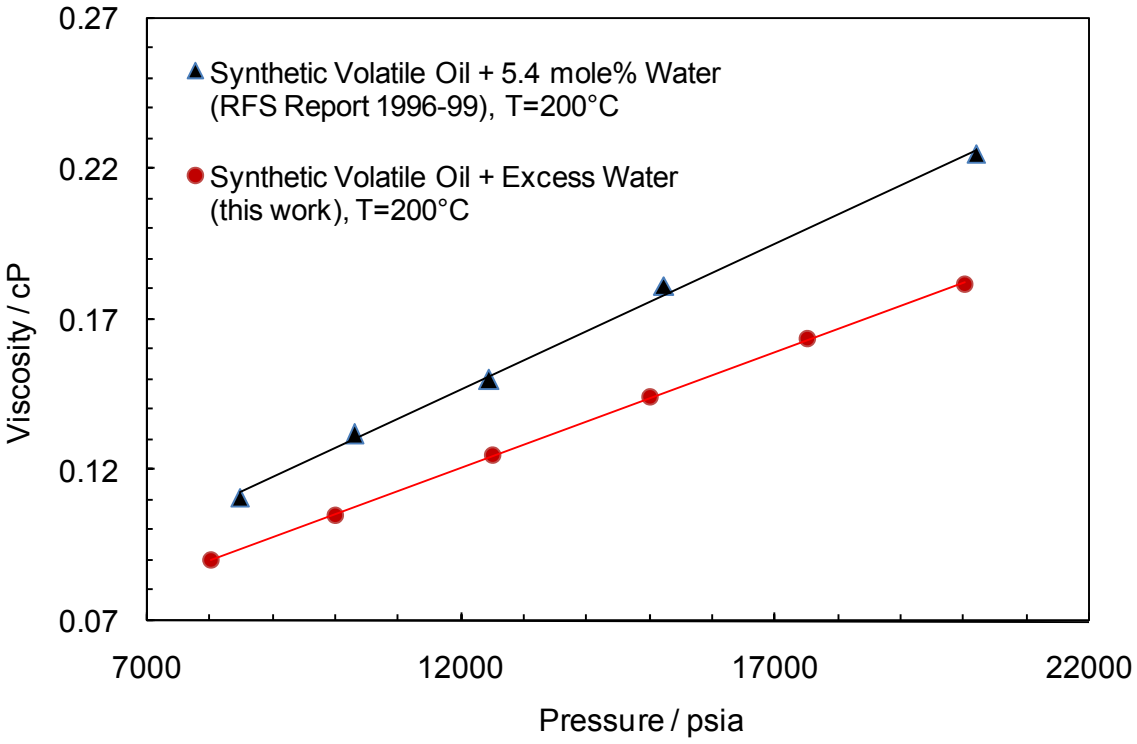

Figure 5.21 Comparison between the viscosity experimental data of synthetic volatile oil saturated with water (this work) and viscosity of synthetic volatile oil with 5.4 mole% dissolved water reported in Reservoir Fluid Studies, Final Report, 1996-99 and published by Gozalpour *et al.* 2005 *the HWU2*

5.4 Conclusions

The primary aim of this chapter was to investigate the influence of dissolved water on the viscosity of hydrocarbon mixtures at HPHT conditions. Experiments were performed systematically with various amounts of water. Binary mixtures of methane with *n*-heptane, *n*-decane and toluene were prepared and mixed with about 2 and 5 mole% of water and also three more complex systems, i.e., gas condensate, natural gas and a synthetic volatile oil.

This series of experiments were planned following a study (Gozalpour *et al.* 2005) which reported a drastic change in the viscosity of a synthetic volatile oil at HPHT due to addition of water (around 5 mole%).

These experimental measurements showed that the presence of water has only a small effect on the viscosity of the three binaries studied. Two concentrations of water were studied for each binary system – over a temperature range of 100 to 200 °C and pressures above saturation pressure to 20,000 psia. The tests continued with investigating the effect of dissolved water on the viscosity of complex systems like gas condensate, natural gas and synthetic volatile oil which were saturated with water at HPHT conditions. This effect is more significant in gas phase rather than liquid which could be due to the presence of more water in gas phase than liquid phase and also could be due to the fact that liquid viscosity is closer to water viscosity. Despite the results reported in the literature (Gozalpour *et al.* 2005), almost no significant increase in the viscosity of the saturated synthetic volatile oil with water was observed.

References

Glandt, C.A., and Chapman, W.G, 1995, *Effect of water dissolution of oil viscosity*, SPE Reservoir Engineering, **24631**

Gozalpour, F., Danesh, A., Fonseca, M., Todd, A.C., Tohidi, B. and Al-Syabi, Z., 2005, *Physical and Rheological Behaviour of High-Pressure/High-Temperature Fluids in Presence of Water*, SPE Europec/EAGE Annual Conference, **94068-MS**

Reservoir Fluid Studies, Final Report, 1996-1999, Institute of Petroleum Engineering, Heriot-Watt University, Report No.: PVT/99/1

Valderrama JO., 1990, *A Generalized Patel-Teja Equation of State for Polar and Non-Polar Fluids and their Mixtures*, J. Chem. Eng. Jpn., **23**, 87-91

CHAPTER 6

INTERFACIAL TENSION: EXPERIMENTAL AND MODELLING

6.1 Introduction

The interfacial tension (IFT) data of gas-water (brine) systems is one of the most important parameter of petroleum industry. The IFT can affect water-gas contact movement and distribution of hydrocarbons in a reservoir, water alternating gas drive, gas-injected enhanced oil recovery processes and multiphase flow calculations (Danesh 1998 and Abdullah *et al.*, 2009). This property also has influence on the process of injecting and storing acid gases like carbon dioxide and hydrogen sulphide separated from sour natural gas into reservoir which is of growing interest (Shah *et al.* 2008).

The thermodynamic based methods of IFT prediction may show reliable results but, due to their complexity, mostly are not popular for engineering purposes (Schmidt *et al.* 2007). Despite the fact that the Parachor method (MacLeod 1923 and Weinaug *et al.* 1943) and the scaling law (Lee *et al.,* 1984) have gained more attention in the oil and gas industry than other predictive methods for the IFT of vapour-liquid (hydrocarbon systems), they are however not recommended for the predictions of hydrocarbon-water interfacial tension (Danesh 1998). It was shown by Firoozabadi and Ramey (1988) that their proposed IFT function against the density difference of hydrocarbon-water shows a single curve for IFT data in the majority of correlated pure hydrocarbon-water systems. Argaud (1992) and Sutton (2009) modified the correlation of Firoozabadi and Ramey (1988). Argaud (1992) incorporated the ratio of Parachor to molar mass of each compound as a corrective factor in the correlation. Sutton (2009) also used more constants in the formulation and more IFT data to retune the correlation parameters. He also replaced the critical temperatures for gas systems with an empirical constant.

The interfacial tension and its relation to the mutual solubility in different liquid-liquid and liquid-gas IFT systems have been reported in open sources (Bahramian *et al.,* 2004 and 2005). Ayirala *et al*. (2006) investigated the IFT of benzene against aqueous ethanol solutions at several concentrations. The authors found a strong relationship between the

solubility and IFT in benzene and aqueous ethanol solution systems. Bennion *et al.* (2008) related the solubility of carbon dioxide in water (and two different brine solutions) with the IFT of this system. They proposed three cubic regressed equations for predicting the IFT between carbon dioxide and water and two different aqueous brine solutions. A further correlation based on exponential equations for calculating the carbon dioxide and water and aqueous brine solution IFT systems were developed (Bachu *et al*., 2009). The above correlations include numerous constants to cover different ranges of temperature and salinity.

Hydrocarbon reservoirs contain not only hydrocarbon fluids but contaminants like water and brine. Presence of salts can affect the physical properties of the fluid and in particular the interfacial tension between water (brine) and hydrocarbon phases. Addition of salt(s) to water causes an increase in interfacial tension of water-hydrocarbon system. This effect has been reported in open sources for different brine and liquid hydrocarbon IFT systems. Cai *et al.* (1996) reported IFT data on brine and pure liquid hydrocarbons such as *n*-C_6, *n*-C_8, *n*-C_{10}, *n*-C_{12}, *n*-C_{14} and *n*-C_{16} and also some mixtures of these compounds. Badakhshan and Bake (1990) presented data on the IFT of *n*-C_6, Cyclo *n*-C_6 and toluene with brine. IFT data on hexane and brine system was reported by Ikeda *et al.* (1992). Several data sets on IFT of gas-water can be found in different sources (it has been reviewed by Rushing *et al.,* 2008). However, IFT experimental data on *gas-brine* hydrocarbon systems are scarce in the literature. The only work on this system has been reported by Rushing *et al.,* (2008), where they performed a series of interfacial tension experiments on natural gas-brine systems, but only at one salt concentration.

In this chapter a new technique using the relationship between interfacial tension and solubility is presented in an attempt to predict the interfacial tension between gas-water systems. This method (IFT-solubility correlation) was investigated using hydrocarbon gases such as methane, ethane and propane, inert gas (nitrogen) and also acid gases like carbon dioxide and hydrogen sulphide. The technique was evaluated against predictive models employing various gas mixtures-water IFT data taken from different open sources.

In addition to the newly introduced method for IFT prediction, interfacial tension data were measured in a salt compatible HPHT cell. The experiments were performed to determine the effect of salt concentration on the IFT of gas-brine system, and in particular

methane-brine. Also the IFT-solubility correlation was extended to predict the gas-brine interfacial tension. The generated methane-brine IFT data were employed to evaluate the performance of this method in estimating IFT of brine systems.

6.2 Experimental Results

New sets of IFT tests were conducted on methane with water and brine systems. Various amounts of sodium chloride (5 and 10 wt%) were gravimetrically added to distilled water to make the brine solutions for IFT measurements. The experiments were performed over a wide range of temperatures (37.8 to 200 °C) and pressures (up to about 15,000 psia). The generated results for brine were then compared with the IFT of distilled water-methane system to investigate the effect of salinity on interfacial tension.

Density difference of the two phases is required for interfacial tension measurements (as explained in Chapter 2). For this purpose, density of methane and distilled water were obtained from NIST web book. The densities of brine solutions at atmospheric pressure were taken from literature (Dittman 1977) and then corrected for higher pressure.

The HPHT facility was equipped with a salt compatible cell to conduct the IFT tests using pendant drop and rising bubble methods. The equipment specification, test procedure, materials, compositions and preparation of the brine solutions are presented in Chapter 2.

6.2.1 *Methane-Water*

The interfacial tension of methane-water system was measured for comparison with methane-brine systems to investigate the effect of salt on IFT. Figure 6.1 shows the interfacial tension data generated in this work together with the data reported in open sources. The IFT data (at 37.8, 100 and 200 °C) generated in this work show good agreement with the literature data.

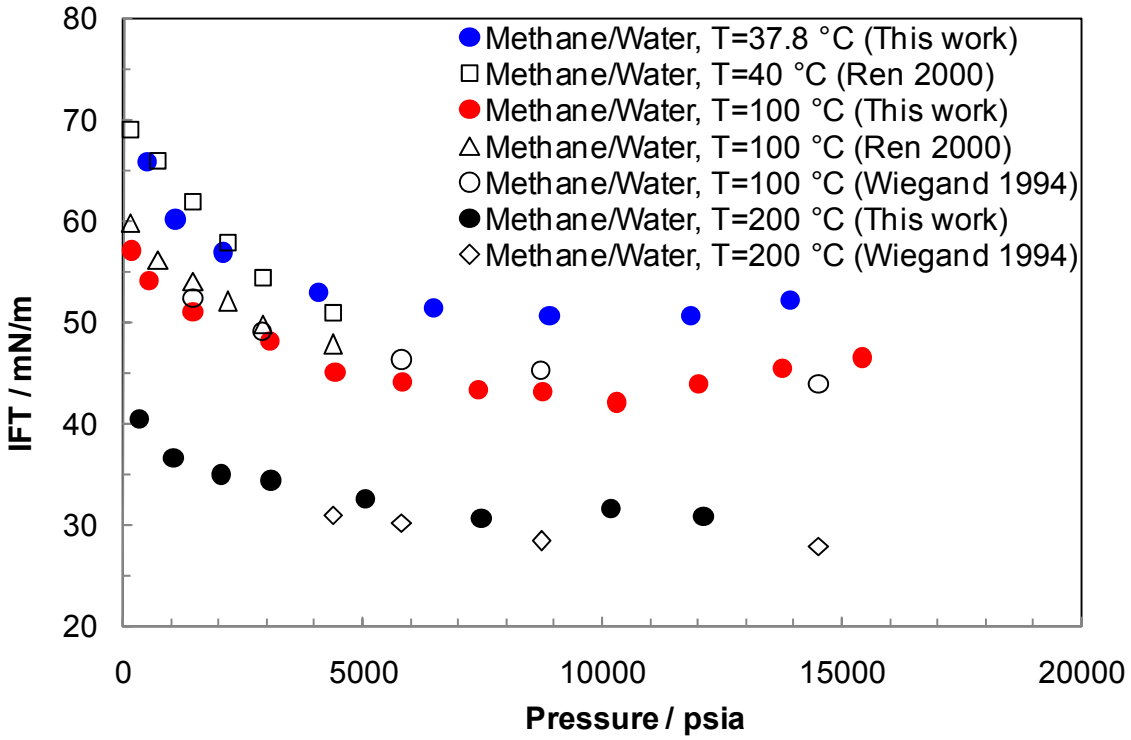

Figure 6.1 Comparison between experimental IFT data for methane-water system generated in this work and data gathered from open sources.

The experiments were performed at temperatures of 37.8 to 200 °C. In these series of tests, the pendant drop method was employed to measure IFT at 100, 150 and 200 °C and the rising bubble technique was used to perform the tests at 37.8 °C. The measurements were performed at pressures up to about 15,000 psia.

The experimental results are plotted in Figure 6.2. The interfacial tension of this system, at each temperature, has a sharp decreasing trend with increasing pressure up to about 4000 psia. But for higher pressures, the IFT values do not change drastically with pressure and also the IFT values go up again after crossing a certain pressure. The reason could be due to changing (or becoming more similar) the behaviour of methane from gas to liquid at high pressure range. This behaviour is also reported by Schmidt *et al.* 2007. The measured interfacial tension for this system ranges from about 30 mN/m (at 200 °C and 12,102 psia) to 65.8 mN/m (at 37.8 °C and 492 psia). The results are tabulated in Table 6.1.

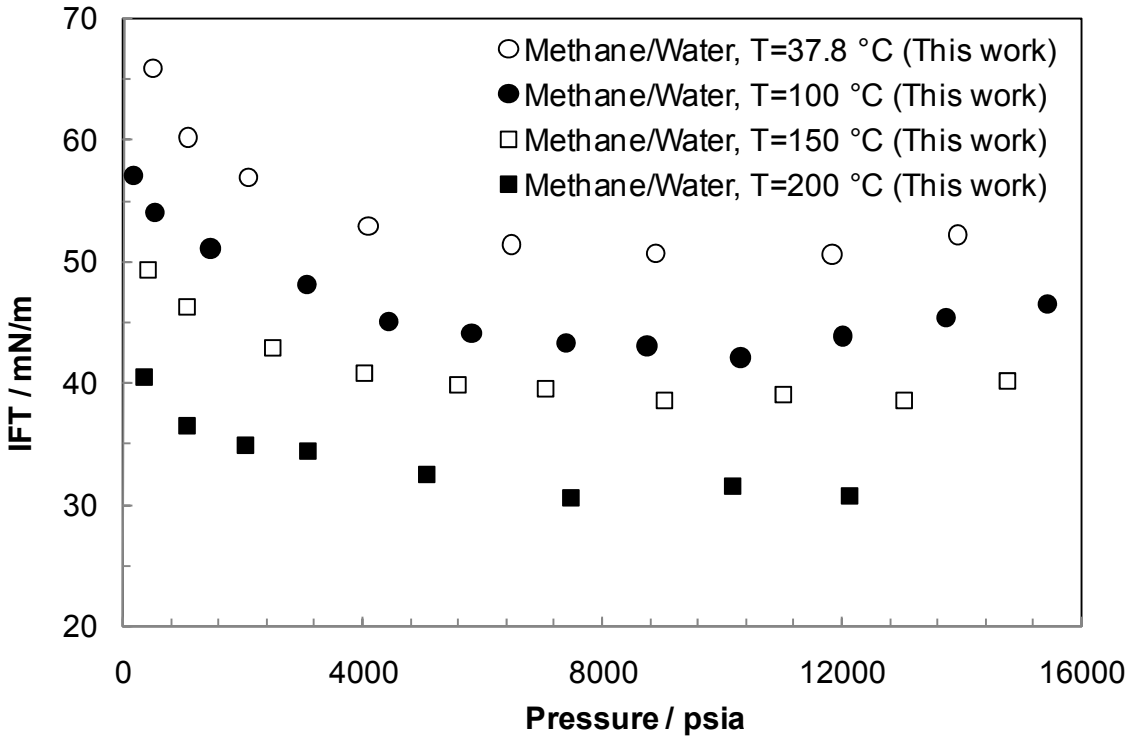

Figure 6.2 Experimental IFT data of methane-water system over a wide range of temperatures from 37.8 to 200 °C generated in this work.
The data were used to evaluate the reliability of the measurement technique (Figure 6.1) and also to compare with the methane-brine systems for investigating the effect of salt on IFT.

Table 6.1 Experimental methane-water IFT from 37.8 to 200 °C.

Temperature (°C)	Pressure (psia)	Interfacial Tension (mN/m)	Temperature (°C)	Pressure (psia)	Interfacial Tension (mN/m)
37.8	492	65.8	**150**	397	49.3
37.8	1093	60.1	**150**	1057	46.3
37.8	2085	56.8	**150**	2490	42.8
37.8	4092	52.8	**150**	4031	40.8
37.8	6488	51.3	**150**	5580	39.9
37.8	8890	50.6	**150**	7025	39.5
37.8	11834	50.5	**150**	9033	38.5
37.8	13920	52.1	**150**	11010	39.1
100	175	57	**150**	13020	38.6
100	530	54	**150**	14760	40.2
100	1460	51	**200**	350	40.4
100	3066	48	**200**	1055	36.5
100	4430	45	**200**	2043	34.9
100	5815	44	**200**	3078	34.3
100	7400	43.2	**200**	5046	32.5
100	8747	43	**200**	7475	30.6
100	10305	42.0	**200**	10170	31.5
100	12003	43.8	**200**	12102	30.7
100	13740	45.3			
100	15430	46.4			

6.2.2 *Methane-Brine (5 wt% NaCl)*

IFT tests were carried out at temperatures of 37.8 to 200 °C on methane-brine (5 wt% NaCl solution) system. In these series of tests, the rising bubble technique was used to perform all the experiments. Measurements were made at pressure up to about 13,000 psia.

The measured data are plotted in Figure 6.3. Similar to methane-water system, the interfacial tension of this system has a decreasing trend with increasing temperature and pressure. The measured interfacial tension for this system ranges from about 33.4 mN/m (at 200 °C and 11,800 psia) to 68.8 mN/m (at 37.8 °C and 480 psia). The results are reported in Table 6.2.

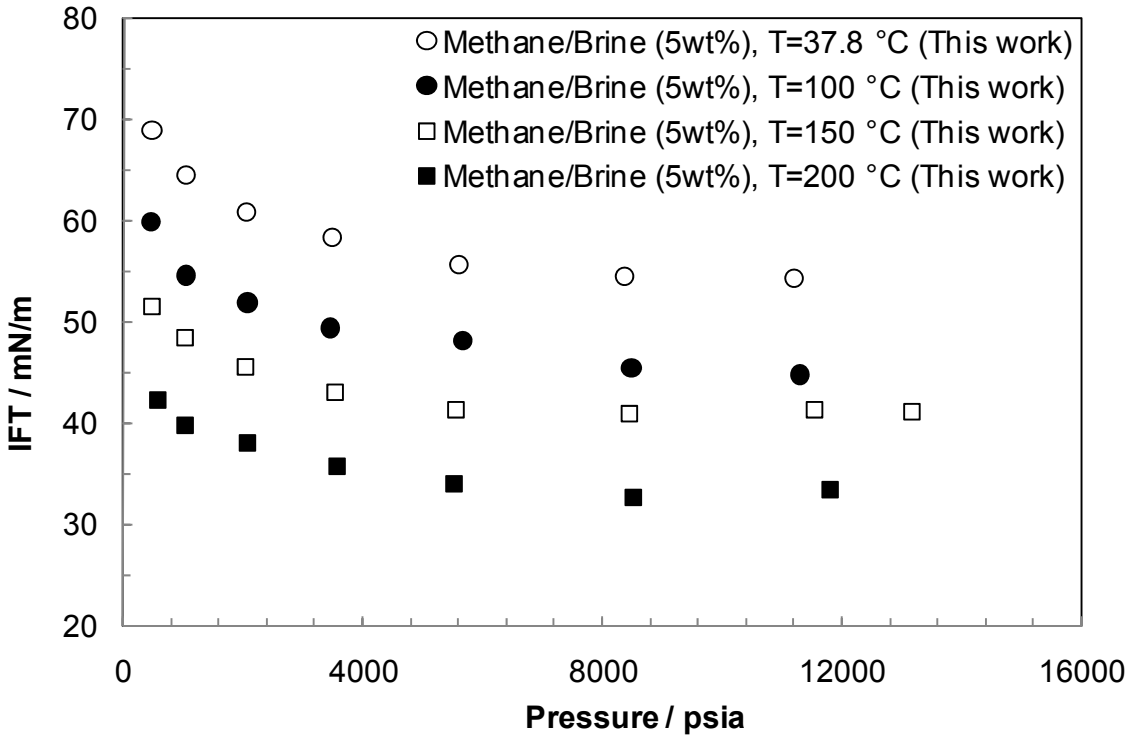

Figure 6.3 Experimental IFT data of methane-brine (5wt% NaCl) system over a wide range of temperatures from 37.8 to 200 °C generated in this work.

Table 6.2 Experimental methane-brine (5wt% NaCl) IFT from 37.8 to 200 °C

Temperature (°C)	Pressure (psia)	Interfacial Tension (mN/m)	Temperature (°C)	Pressure (psia)	Interfacial Tension (mN/m)
37.8	480	68.8	**150**	482	51.4
37.8	1046	64.4	**150**	1031	48.5
37.8	2058	60.7	**150**	2030	45.5
37.8	3490	58.2	**150**	3525	43.0
37.8	5612	55.6	**150**	5545	41.3
37.8	8360	54.4	**150**	8450	41.0
37.8	11200	54.2	**150**	11540	41.2
100	476	59.8	**150**	13160	41.1
100	1047	54.5	**200**	568	42.3
100	2073	51.8	**200**	1030	39.7
100	3457	49.3	**200**	2054	38.0
100	5680	48.1	**200**	3564	35.7
100	8480	45.3	**200**	5520	33.9
100	11300	44.7	**200**	8497	32.7
			200	11800	33.4

6.2.3 *Methane-Brine (10 wt% NaCl)*

Interfacial tension was measured for methane-brine (10 wt% NaCl) at temperatures of 37.8 to 200 °C and pressures up to about 13,400 psia. In these series of tests, the rising bubble technique was employed to perform the experiments.

The measured data are plotted in Figure 6.4. The interfacial tension of this system has a decreasing trend with increasing temperature and pressure. The measured interfacial tension for this system ranges from about 34 mN/m (at 200 °C and 13,150 psia) to 78.2 mN/m (at 37.8 °C and 412 psia). The results show that IFT in presence of 10 wt% sodium chloride solution are higher than the data for pure water and the one for 5 wt% NaCl solution. The results are tabulated in Table 6.3.

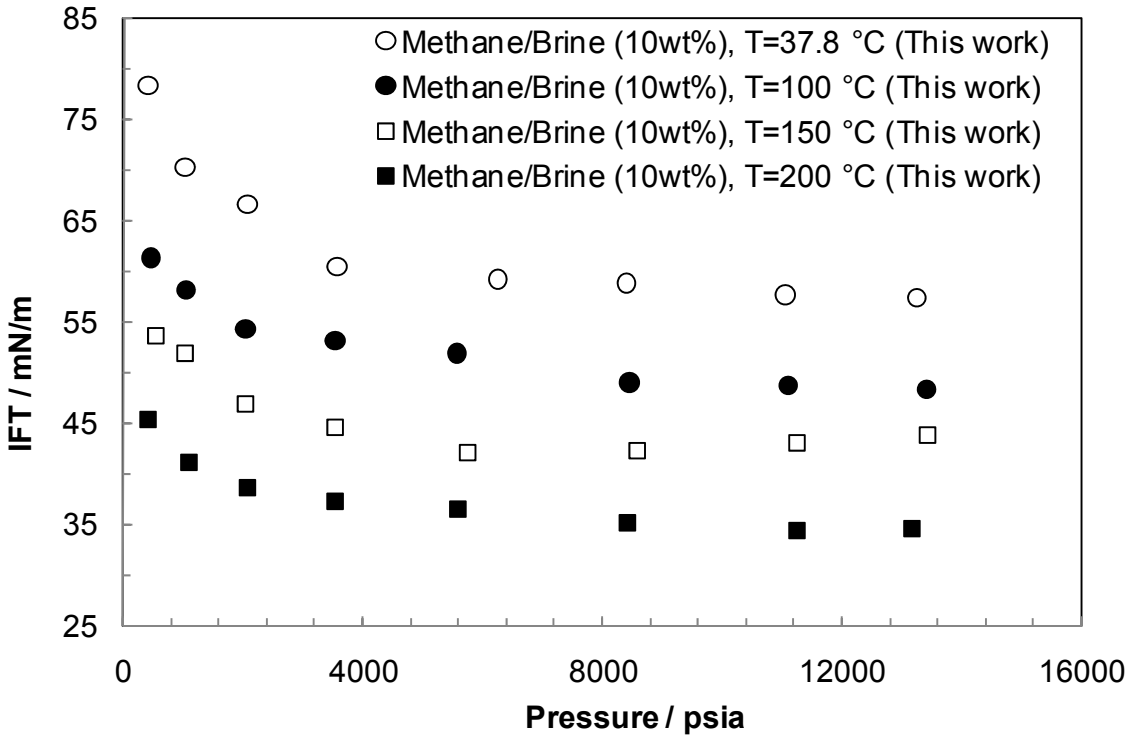

Figure 6.4 Experimental IFT data for methane-brine (10 wt% NaCl) system in wide range of temperatures from 37.8 to 200 °C generated in this work

Table 6.3 Experimental methane-brine (10 wt% NaCl)IFT from 37.8 to 200 °C

Temperature (°C)	Pressure (psia)	Interfacial Tension (mN/m)	Temperature (°C)	Pressure (psia)	Interfacial Tension (mN/m)
37.8	412	78.2	**150**	550	53.6
37.8	1037	70.2	**150**	1035	51.8
37.8	2081	66.5	**150**	2038	46.9
37.8	3571	60.4	**150**	3535	44.5
37.8	6250	59.1	**150**	5730	42.1
37.8	8410	58.7	**150**	8580	42.2
37.8	11050	57.6	**150**	11226	43.1
37.8	13240	57.3	**150**	13400	43.8
100	463	61.2	**200**	409	45.4
100	1050	58.1	**200**	1089	41.1
100	2040	54.2	**200**	2078	38.6
100	3541	53.1	**200**	3543	37.2
100	5580	51.8	**200**	5570	36.4
100	8450	48.9	**200**	8410	35.2
100	11100	48.6	**200**	11250	34.4
100	13410	48.2	**200**	13150	34.6

6.3 Interfacial Tension Prediction

To introduce a new IFT predictive method, the changes of IFT in gas-water (brine) systems versus solubility of gases in aqueous solutions have been studied. The correlations are based on the observed behaviour of the interface at zero solubility. It was shown that for various gases, the interfacial tension of gas-water systems should tend to the water surface tension at zero solubility of gas in water, i.e. at the water vapor pressure. In other words, it was seen that the plot of gas-water IFT against gas solubility in water, crosses the value of water surface tension by extrapolating the data to zero gas solubility (depicted in Figure 6.5).

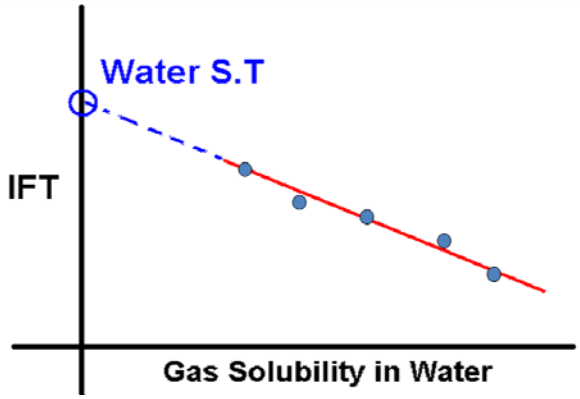

Figure 6.5 The graph is showing the concept behind the newly introduced interfacial tension correlation. It is observed that the IFT of gas-water system at zero solubility of gas in water approaches water surface tension value.

According to the above concept, a method is proposed for predicting gas-water IFT from water surface tension (WST) and the solubility of gas in water (named IFT-solubility correlation). In addition, each gas shows a specific slope in the (IFT/WST) vs. solubility plot which were estimated for various gases. The relation is formulated as below:

$$IFT/WST = A_{I-S} \times S_{g-w} + 1 \tag{6.1}$$

Where, $A_{I\text{-}S}$ is the slope of the (IFT/WST) vs. solubility plot that is considered as a constant value for each pure gas-water system (which is discussed in this chapter) and $S_{g\text{-}w}$ is the solubility of gas in water (mole fraction).

6.3.1 *Pure Gas-Water IFT*

To develop this correlation, IFT data of pure gas-water systems from literature were gathered. Table 6.4 presents the sources of data, pressure and temperature ranges and the number of IFT data. It should be noted that only the IFT data in the vapour region of the mentioned references were used.

Table 6.4 References, ranges and number of experimental data points on pure gas-water IFT

Compound	Reference	Temperature Range / °C	Pressure Range / psia	No. of Data
Methane	Hough *et al.* 1951	2 - 176	14.5 - 8800	93
	Jennings *et al.* 1971			
	Jho *et al.* 1978			
	Ren *et al.* 2000			
	Sachs *et al.* 1995			
	Sun *et al.* 2004			
Ethane	Jho *et al.* 1978	8 – 48	72.5 - 590	10
Propane	Wiegand *et al.* 1994	25	14.5 - 130.5	6
Nitrogen	Yan *et al.* 2001	25 - 100	145 - 4350	40
Carbon Dioxide	Bennion *et al.* 2008	11 - 125	14.5 - 6525	160
	Hebach *et al.* 2002			
	Jho *et al.* 1978			
	Kvamme *et al.* 2007			
	Chiquet *et al.* 2007			
Hydrogen Sulphide	Herrick *et al.* 1973	25 - 120	43.5 - 2100	58
	Shah *et al.* 2008			

IFT data in Table 6.4 were used to investigate the proposed theory and also to calculate the $A_{I\text{-}S}$ values for each pure gas-water system. For this reason the IFT/WST values were plotted against solubility of each gas (Figures 6.6 to 6.11). Water surface tension data were obtained from the work performed by Vargaftik *et al.* (1983) and the VPT equation of state (Valderrama 1990) was used for predicting gas solubility in aqueous phase.

By passing lines through the experimental data points, as demonstrated in Figures 6.6 to 6.11, and setting the y-intercept to 1, the slopes of the mentioned lines ($A_{I\text{-}S}$) for each of the pure gas-water system were calculated using a least square method. The $A_{I\text{-}S}$ and regression values are presented in Table 6.5.

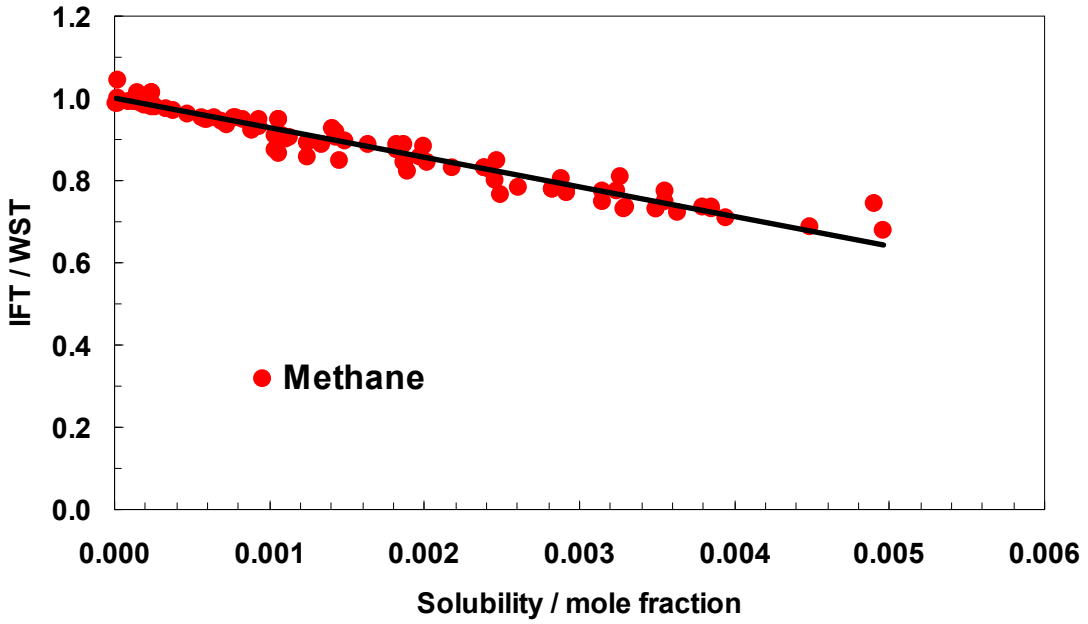

Figure 6.6 Values of IFT/WST vs. solubility of methane in water. Sources of the IFT data are presented in Table 6.4.

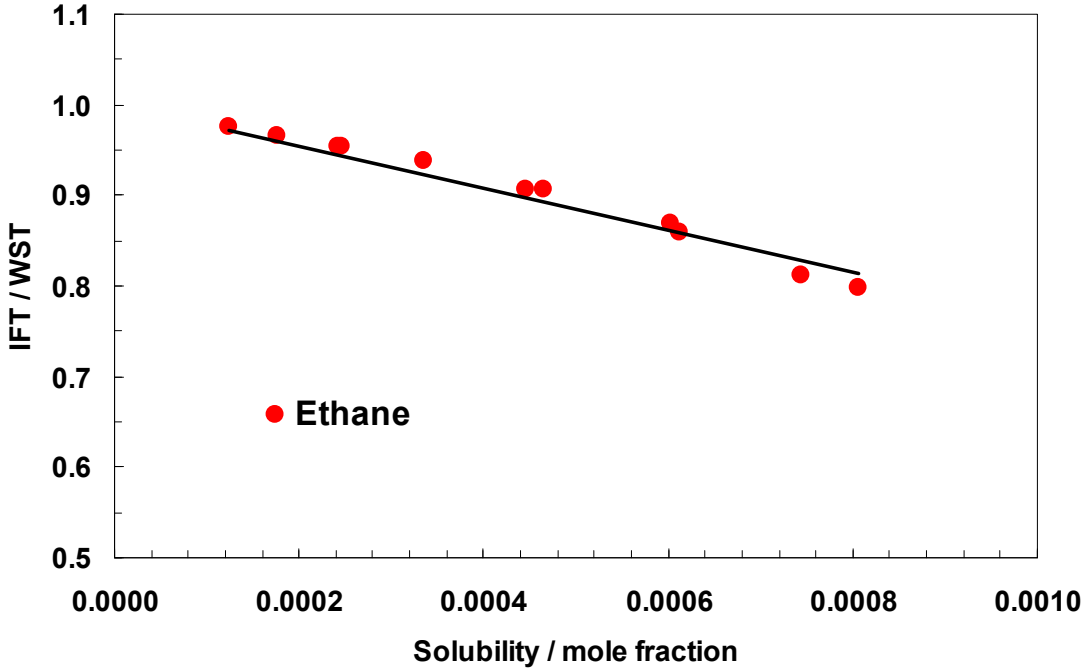

Figure 6.7 Values of IFT/WST vs. solubility of ethane in water. Sources of the IFT data are presented in Table 6.4.

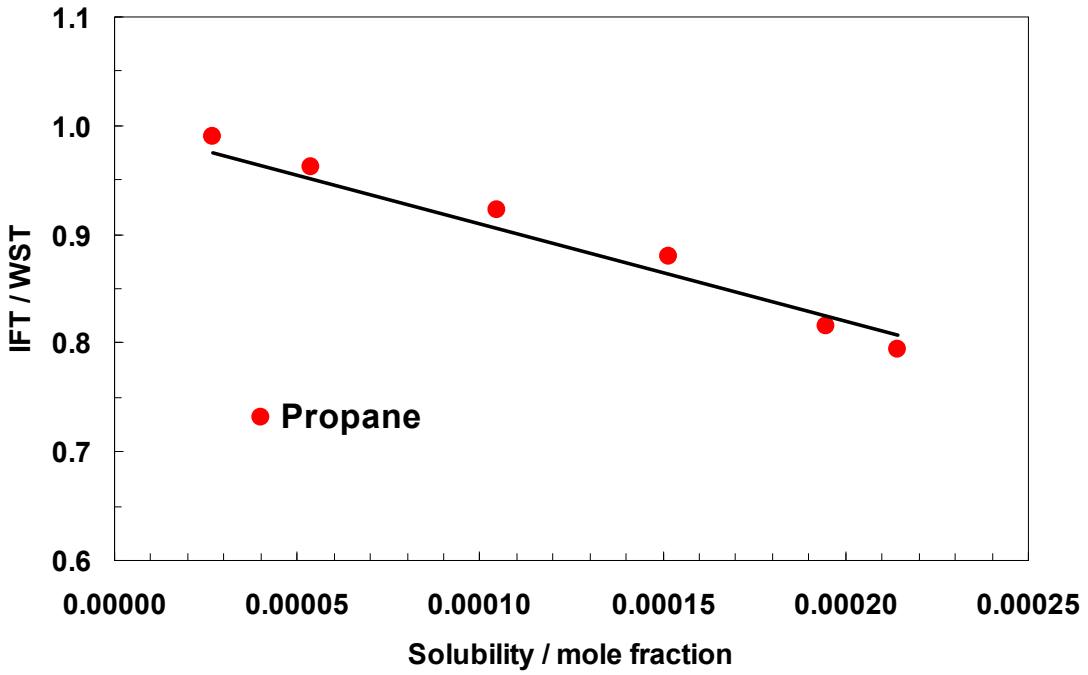

Figure 6.8 Values of IFT/WST vs. solubility of propane in water. Sources of the IFT data are presented in Table 6.4.

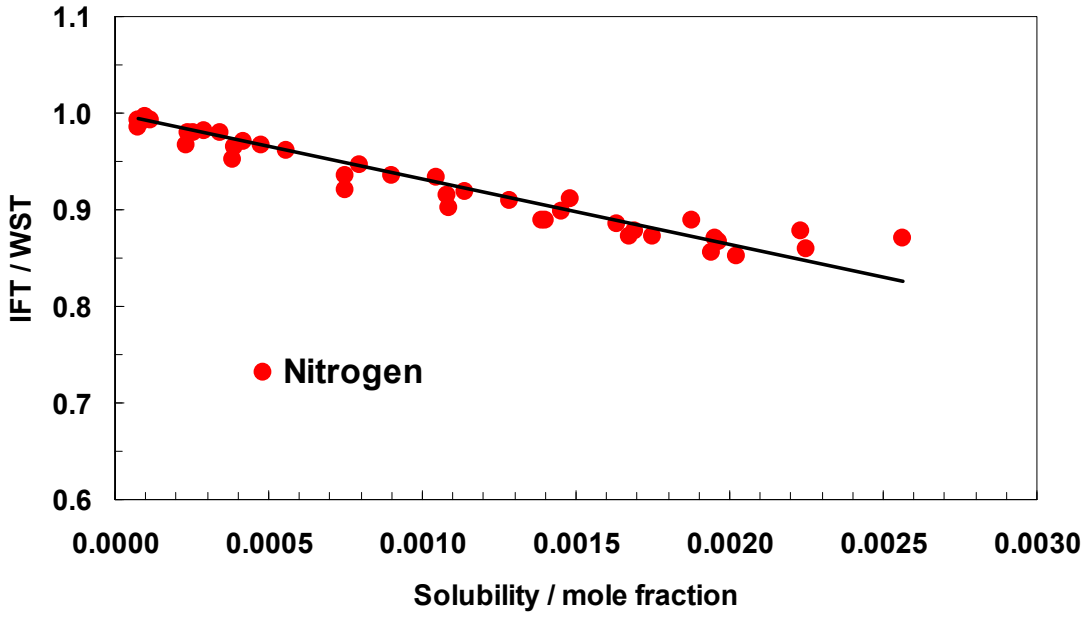

Figure 6.9 Values of IFT/WST vs. solubility of nitrogen in water. Sources of the IFT data are presented in Table 6.4.

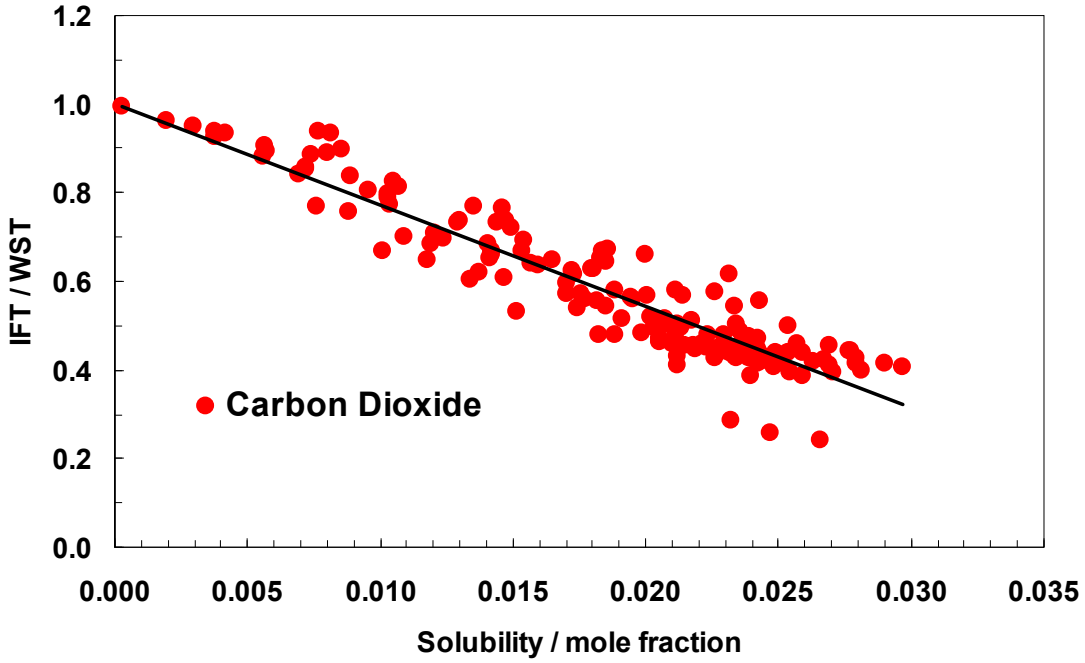

Figure 6.10 Values of IFT/WST vs. solubility of carbon dioxide in water. Sources of the IFT data are presented in Table 6.4.

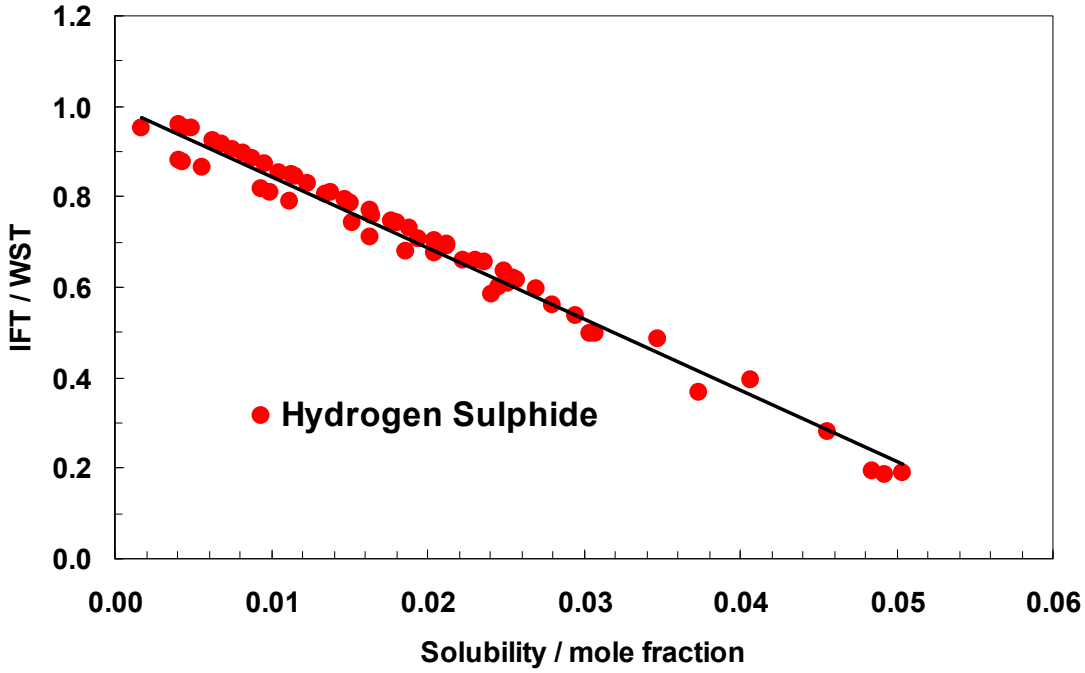

Figure 6.11 Values of IFT/WST vs. solubility of hydrogen sulphide in water. Sources of the IFT data are presented in Table 6.4.

Table 6.5 The $A_{I\text{-}S}$ and regression values for various pure gas-water systems calculated for IFT-solubility method

Compounds	$A_{I\text{-}S}$	Regression Value
Methane	-73.37	0.94
Ethane	-229.76	0.97
Propane	-897.03	0.97
Nitrogen	-67.74	0.91
Carbon Dioxide	-22.79	0.89
Hydrogen Sulphide	-15.67	0.98

6.3.2 *Gas Mixture-Water IFT*

With the aim of extending the capability of the proposed method (Equation 6.1) to predict IFT in gas mixture-water systems, $S_{g\text{-}w}$, is considered as the summation of the total gas solubility in water (mole fraction) and $A_{I\text{-}S}$ of the gas mixture is defined as below:

$$\left(A_{I-S}\right)_{mix}^{1/m} = \sum_{i=1}^{n} \left(A_{I-S}\right)_{i}^{1/m} \times x_i \tag{6.2}$$

Where, x_i is the solubility (mole fraction) of each gas in water in dry basis. The accuracy of this technique in predicting IFT of gas mixture-water will be discussed in this chapter. After examining different gas mixtures, m was set to 1 in the above formulation to calculate the $A_{I\text{-}S}$ values for mixture.

6.3.3 *VPT Equation of State*

The Valderrama (1990) modification of the Patel-Teja equation of state (VPT-EoS) with the non-density-dependent (NDD) mixing rules (Avlonitis *et al*., 1994) was used to predict the solubility of gases in water. The reliability of the equation of state in modelling fluid phases has been discussed elsewhere (Chapoy *et al.,* 2004 and 2005). Figures 6.12a to 6.12c illustrate the model predictions against experimental gas solubility in water for methane (Duffy *et al*., 1961 and Yarym-Agaev *et al*., 1985), carbon dioxide (Kritschewsky *et al*., 1935, Galindo *et al*., 1999 and Scott *et al*., 1980) and hydrogen sulphide (Selleck *et al*., 1952 and Burgess *et al*., 1969).

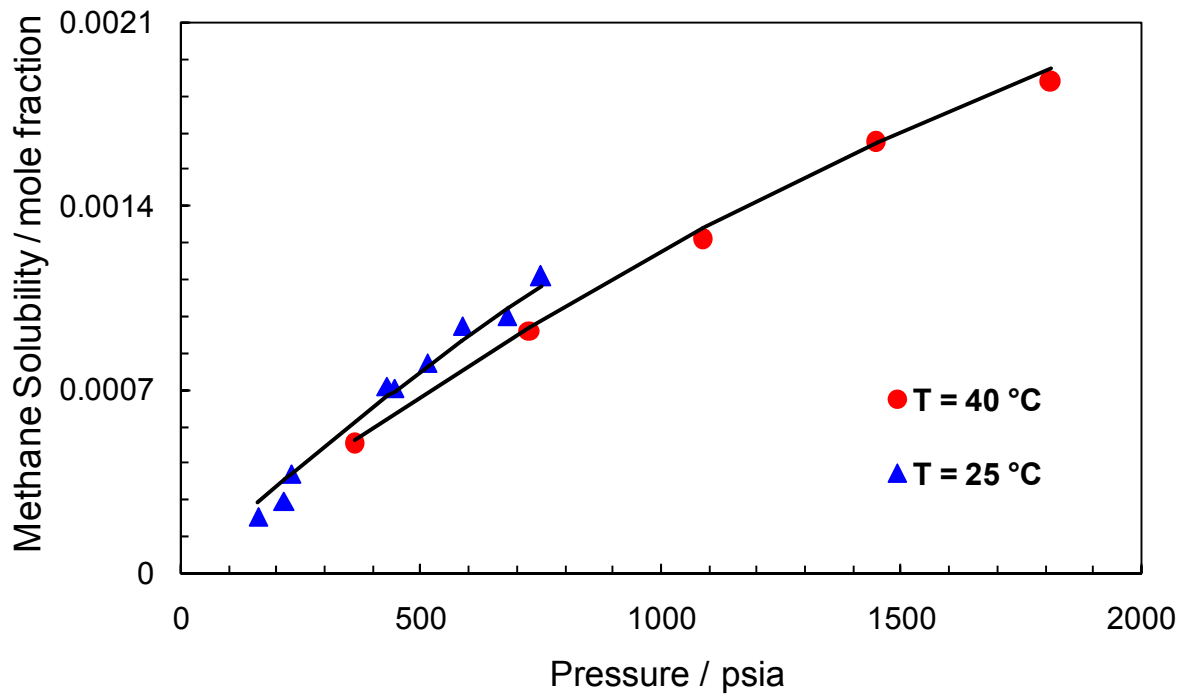

Figure 6.12a Solubility of methane in water: VPT-EoS prediction (solid lines) against experimental data ((▲) Duffy 1961 and (●)Yarym-Agaev 1985)

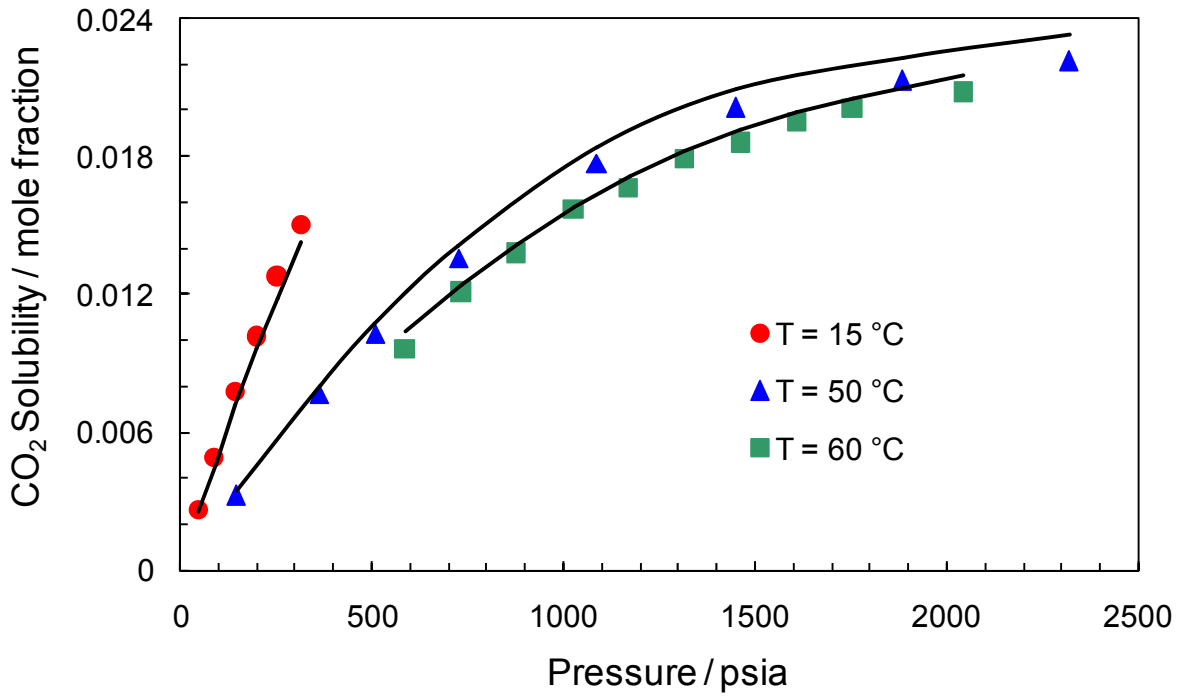

Figure 6.12b Solubility of carbon dioxide in water: VPT-EoS prediction (solid lines) against experimental data ((●) Kritschewsky 1935, (▲) Galindo 1999, (■) Scott 1980)

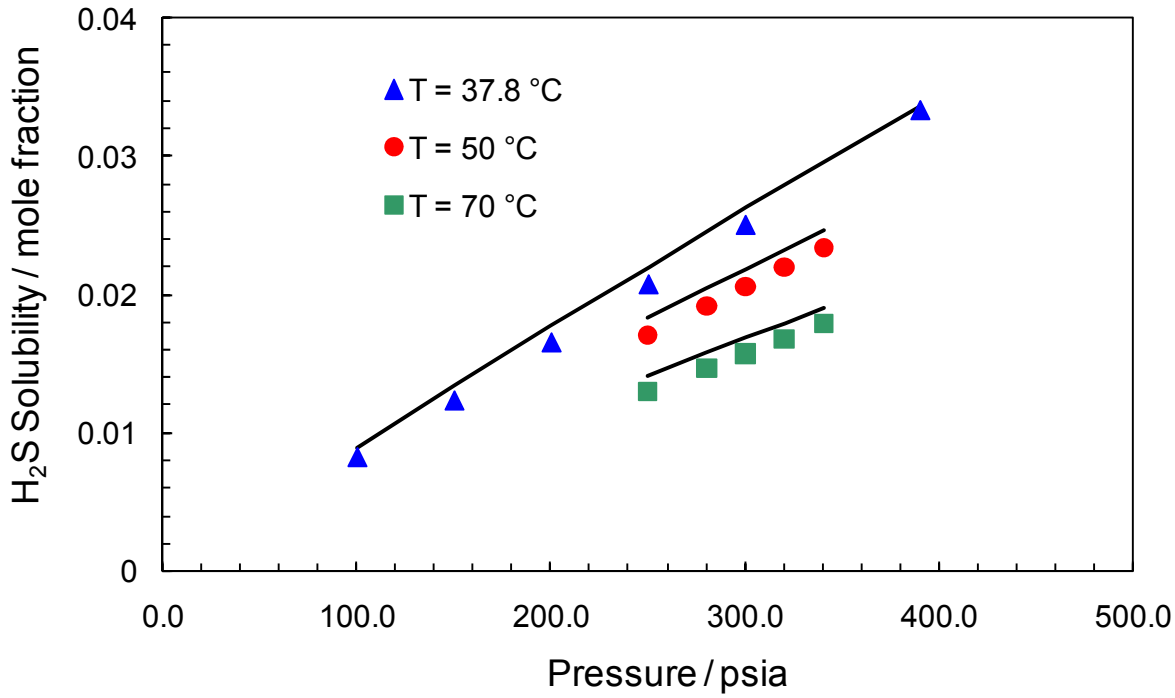

Figure 6.12c Solubility of hydrogen sulphide in water: VPT-EoS prediction (solid lines) against experimental data ((▲) Selleck 1952 and (●, ■) Burgess 1969)

6.3.4 *Firoozabadi and Ramey (1988), Argaud (1992) and Sutton (2009)*

Firoozabadi and Ramey (1988) presented one of the most popular correlations for calculating IFT between hydrocarbon (gas or liquid) and water. The difference between the densities of the two phases and the reduced temperature of the hydrocarbon phase are the two parameters used in this correlation. The proposed IFT function (Equation 6.3) versus density difference, Δρ, shows a single curve for IFT data in majority of correlated systems. The IFT function is given below:

$$IFT\ Function\ of\ FR\ Correlation \equiv \left(\frac{\sigma^{0.25}}{\Delta\rho}\right) \times T_r^{0.3125} \tag{6.3}$$

Firoozabadi and Ramey stated that the correlation required further investigation, particularly for hydrocarbon mixtures with water and the IFT calculations in hydrocarbon-brine systems. The curve generated from Equation 6.3 can be approximately represented by the following equation (Danesh 1998):

$$\sigma_{hw} = 111\left(\Delta\rho_{hw}\right)^{1.024}\left(T_r\right)^{-1.25} \tag{6.4}$$

Argaud (1992) modified the Firoozabadi and Ramey (1988) correlation by applying a corrective factor and using more experimental data to regress the correlation. A thermodynamic model (Plocker *et al.*1978) was used to calculate the difference between hydrocarbon and water densities in this modification.

Argaud (1992) mentioned that the difference in the density of phases can only consider the effect of pressure but not the chemical structure of substances so Δρ alone is insufficient to predict the interfacial tension. Accordingly, Argaud also proposed that the ratio of Parachor to molar mass of each compound as a corrective factor i.e. $(P/MW)^{\alpha}$. Exponent 'α' can be defined based on the range of density difference. The Argaud IFT function is given below (Equation 6.5):

$$IFT\ Function\ of\ Argaud\ Correlation \equiv \left(\frac{\sigma^{0.25}}{\Delta\rho}\right) \times T_r^{0.3125} / \left(\frac{P}{MW}\right)^{\alpha} \tag{6.5}$$

Argaud (1992) suggested adding a term to the formulation that can take into consideration the effect of salt. The proposed value is a function of salt type, its concentration, and temperature.

Sutton (2009) modified Firoozabadi and Ramey method by incorporating more constants and temperature in the formulation. The author replaced the critical temperature of gases with a constant for predicting the gas-water IFT. Also Sutton (2009) added a correction factor to the predicted value as a function of salt concentration ($3.44\times10^{-5}\times$salinity) to consider the effect of salt on the predicted interfacial tension.

6.3.5 *Gas-Brine IFT*

In order to extend the capability of the method developed in this work (IFT-solubility) to calculate the interfacial tension of gas-brine systems, Equation 6.1 was modified by replacing the water surface tension (WST) and solubility of gas in water with the brine surface tension (BST) and solubility of gas in brine ($S_{g\text{-}b}$), respectively (presented in Equation 6.6). Replacing the WST with the brine surface tension may not be a very accurate assumption, but due to lack of enough experimental IFT data for brine-pure gas systems in the literature, this assumption could be the best option.

$$IFT / BST = A_{I-S} \times S_{g-b} + 1 \tag{6.6}$$

The VPT equation of state (Valderrama 1990) was used for calculating solubility of gas in brine solution. The brine (NaCl solution) surface tension data which are needed in this correlation were obtained from Nasr-El-Din *et al.* (2005) at 24.1 °C and various salt concentrations. Using the assumption that the increase in surface tension of brine at each salt concentration is proportional to the temperature in Kelvin (Argaud 1992), the BST values were then calculated for the temperatures of interest.

This technique was evaluated against some experimental IFT data of gas-brine (NaCl solution) which were generated in this study to investigate the reliability of the IFT-solubility correlation for predicting IFT in gas-brine systems.

6.4 Results and Discussion

6.4.1 *Gas-Water IFT Prediction*

The predictions of the newly developed method, IFT-solubility correlation, were in good agreement with the experimental IFT of pure gases-water in the reported temperature and pressure ranges (Table 6.5). Also the obtained $A_{I\text{-}S}$ for different gases showed a clear decreasing trend from the least soluble compound (propane) to the most soluble one (hydrogen sulphide) in the aqueous phase.

To investigate the reliability of the IFT-solubility correlation for predicting the IFT of gas mixture-water systems, experimental IFT data on binary and multi-component gas mixtures were used. The compositions of the gas mixtures used in this study along with their references are reported in Table 6.6. The predicted IFT data with this technique are also compared with Firoozabadi and Ramey (1988), Argaud (1992) and Sutton (2009) methods. Figures 6.13 to 6.16 compare the IFT prediction trends and results of some of the gas-water systems among the 18 examined gas mixtures. The average absolute deviation percentages (AAD%) for each IFT predictive method form the experimental IFT data for all of the above mentioned gas mixtures are listed in Table 6.7.

Table 6.6 Compositions and references of the gas mixtures used to investigate the proposed method for prediction of gas mixture-water IFT

	Mole % of Each Compound in the Gas Mixtures						
Gas No.	Methane	Ethane	Propane	Nitrogen	Carbon Dioxide	Hydrogen Sulphide	Reference
1	-	-	-	-	70	30	Shah *et al.*, 2008
2	80	-	-	-	20	-	Ren *et al.*, 2000
3	60	-	-	-	40	-	
4	40	-	-	-	60	-	
5	20	-	-	-	80	-	
6	23.64	-	-	76.36	-	-	Yan *et al.*, 2001
7	50.09	-	-	49.01	-	-	
8	74.93	-	-	25.07	-	-	
9	-	-	-	75.03	24.97	-	
10	-	-	-	49.28	50.72	-	
11	-	-	-	24.15	75.85	-	
12	96	3	1	-	-	-	Rushing *et al.*, 2008 *
13	91.2	2.85	0.95	-	5	-	
14	86.4	2.7	0.9	-	10	-	
15	76.8	2.4	0.8	-	20	-	
16	91.2	2.85	0.95	5	-	-	
17	86.4	2.7	0.9	10	-	-	
18	76.8	2.4	0.8	20	-	-	

* IFT data are digitized from the figures (data not tabulated).

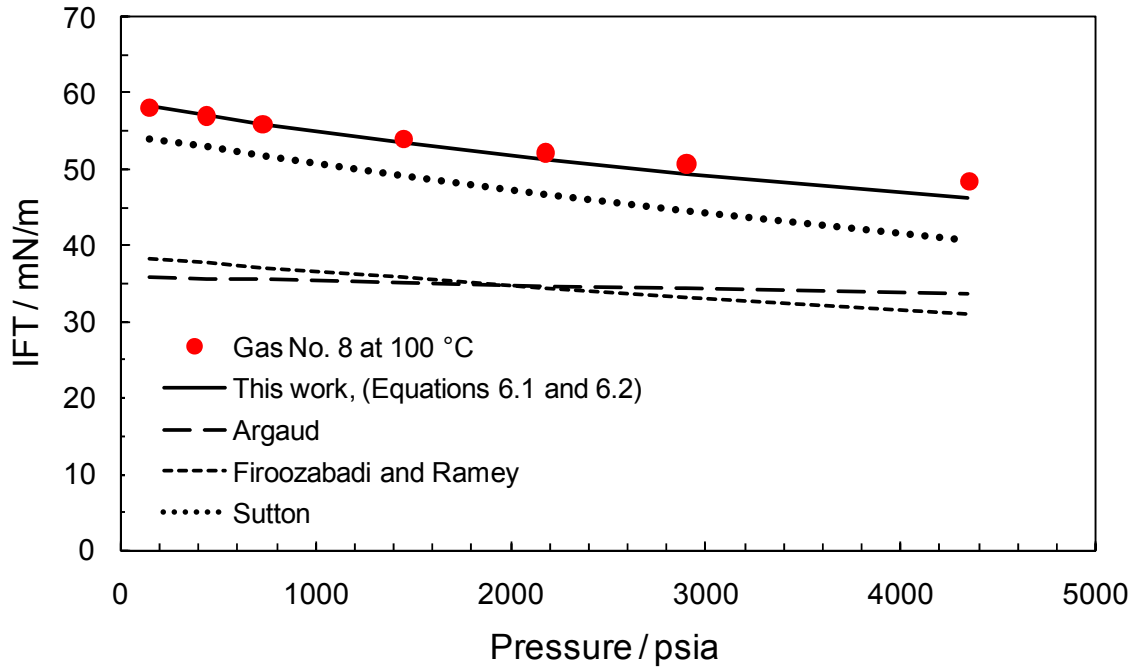

Figure 6.13 Comparison of different IFT prediction methods against experimental gas-water IFT data (gas No. 8 at 100 °C)

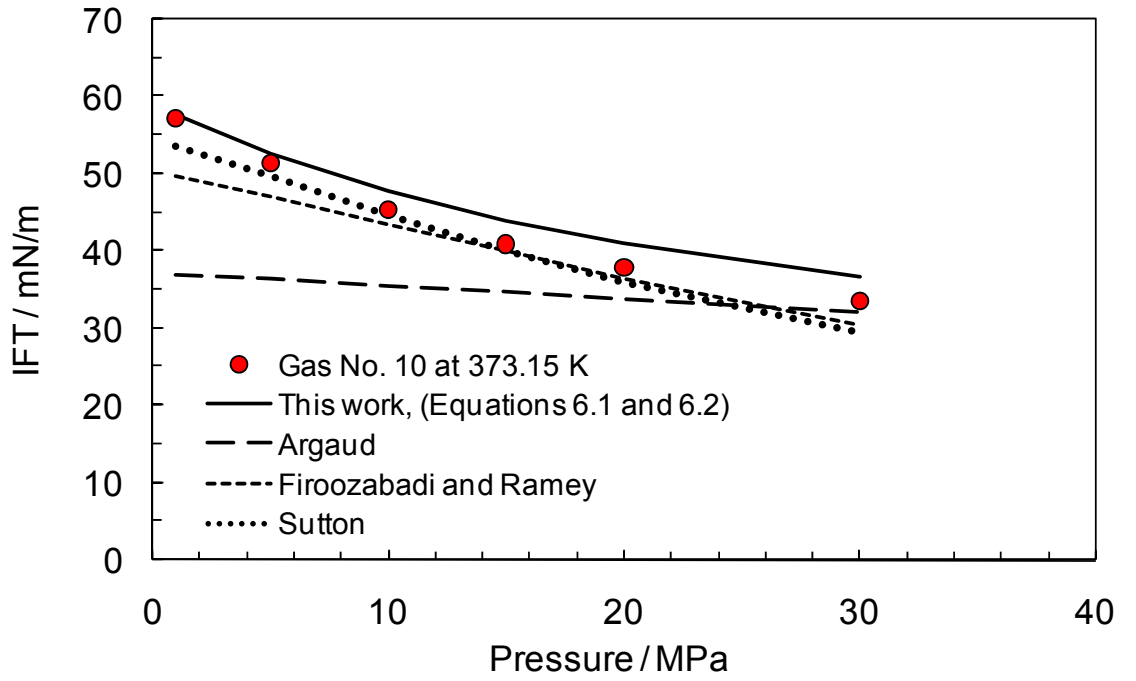

Figure 6.14 Comparison of different IFT prediction methods against experimental gas-water IFT data (gas No. 10 at 100 °C)

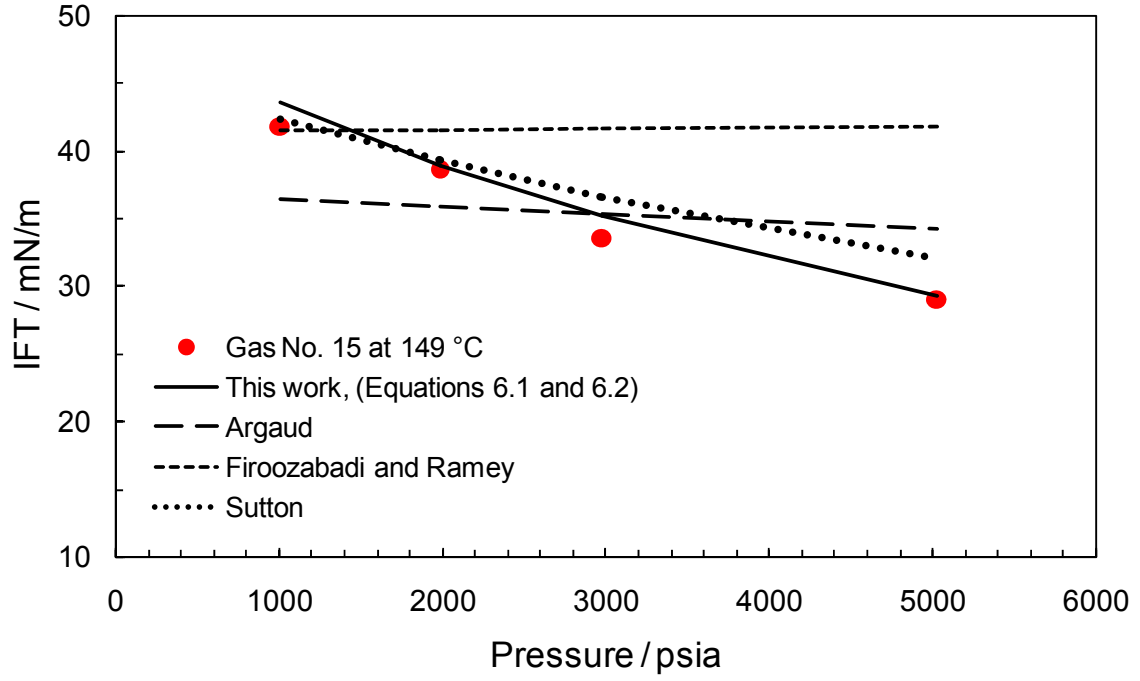

Figure 6.15 Comparison of different IFT prediction methods against experimental gas-water IFT data (gas No. 15 at 149 °C)

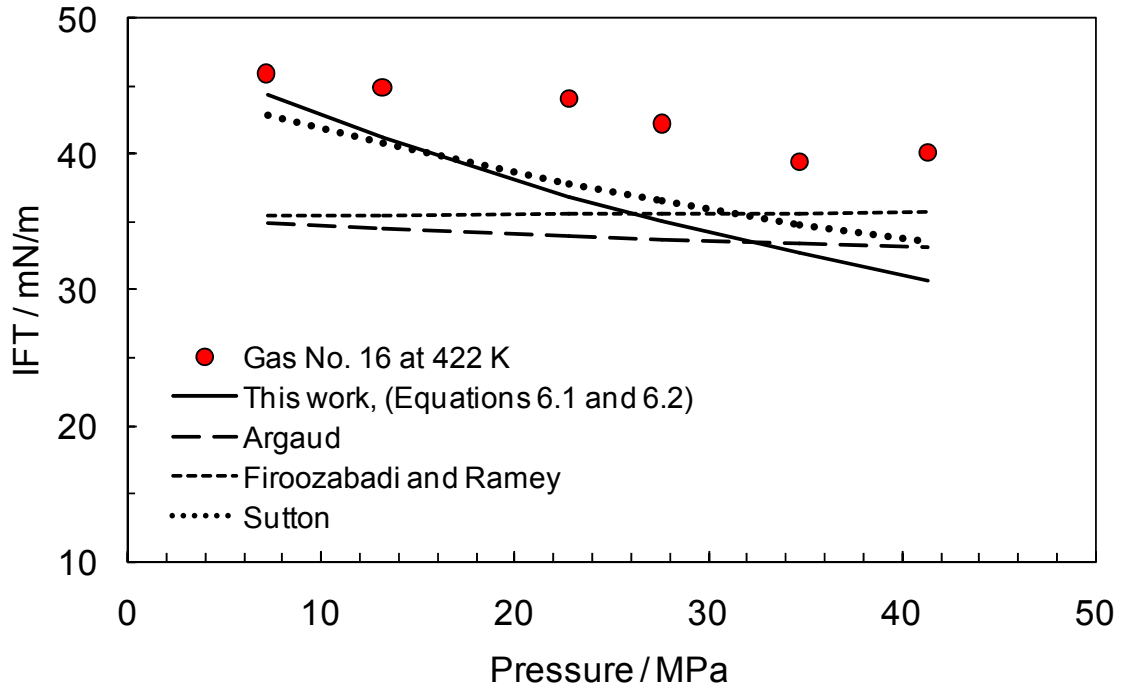

Figure 6.16 Comparison of different IFT prediction methods against experimental gas-water IFT data (Gas No. 16 at 149 °C)

Table 6.7 AAD% from experimental data for different IFT calculation methods along with the ranges of temperatures and pressures and the number of data points (Table 6.6 includes the sources of the experimental gas-water IFT data)

	AAD%						
Gas No.	IFT-Solubility Correlation (This work)	Argaud (1992)	Firoozabadi and Ramey (1988)	Sutton (2009)	No. of Data	Temperature Range / °C	Pressure Range / psia
1	7	32	95	18	13	70	72.5 – 2262
2	5	18	5	8	30	25 - 100	145 – 4350
3	7	14	10	9	30	25 - 100	145 – 4350
4	8	16	28	9	30	25 - 100	145 – 4350
5	16	32	45	15	30	25 - 100	145 – 4350
6	1	50	48	16	35	25 - 100	145 – 4350
7	1	43	39	14	35	25 - 100	145 – 4350
8	1	35	30	12	35	25 - 100	145 – 4350
9	3	36	29	10	30	25 - 100	145 – 4350
10	4	17	8	7	30	25 - 100	145 – 4350
11	4	14	28	13	30	25 – 100	145 – 4350
12	9	9	8	5	9	149 - 205	1000 - 5008
13	12	14	10	8	6	149	993 - 6061
14	8	8	6	3	4	149	2013 - 4994
15	15	10	16	8	9	149 - 205	1005 - 5016
16	14	20	17	12	6	149	1050 - 6000
17	14	23	19	13	6	149	964 – 5904
18	7	11	10	6	9	149 - 205	1979 - 4982
Average	**7.5**	**22**	**25**	**10**	**377**	-	-

As shown in the above table, the results of the method developed in this work (IFT-solubility correlation) are very promising. The calculated average absolute deviation percentage from experimental IFT data for the investigated gas mixtures-water systems is about 7% and is lower than other evaluated methods

6.4.2 *Gas-Brine IFT Prediction*

The experimental interfacial tension data for gas-brine systems were generated and reported in the experimental part of this chapter. The mentioned IFT data were used for investigating the reliability of different interfacial tension prediction methods including the IFT-solubility correlation that was introduced earlier in this chapter (Equation 6.6).

Table 6.8 reports the average absolute deviation percentages (AAD%) of each IFT predictive method from the generated experimental IFT data for methane-brine and methane-water systems. Also Figures 6.17 to 6.19 compare the IFT prediction trends and results of some of the methane-brine (water) systems at 100 °C.

Table 6.8 AAD% from experimental data (this work) for different IFT calculation methods along with the temperatures of experiments (pressure up to 15,000 psia)

IFT Systems	Temperature (°C)	IFT-Solubility Correlation (This work)	Argaud (1992)	Sutton (2009)
Methane-Brine (5 wt% NaCl)	37.8	4	20	16
	100	5	17	10
	150	10	14	14
	200	23	6	17
Methane-Brine (10 wt% NaCl)	37.8	5	22	21
	100	5	17	14
	150	7	11	14
	200	29	5	20
Methane-Water	37.8	8	20	17
	100	12	20	14
	150	25	19	16
	200	50	11	22

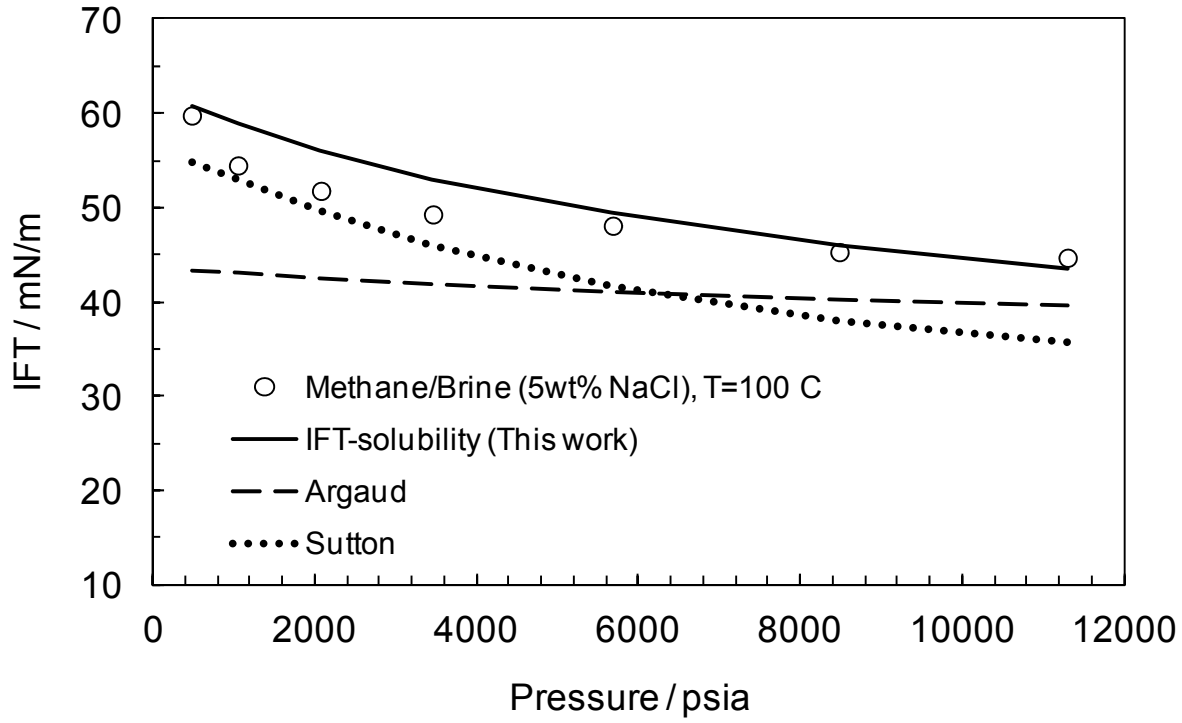

Figure 6.17 Comparison of different IFT prediction methods against experimental methane-brine (5 wt% NaCl solution) IFT data (this work) at 100 °C

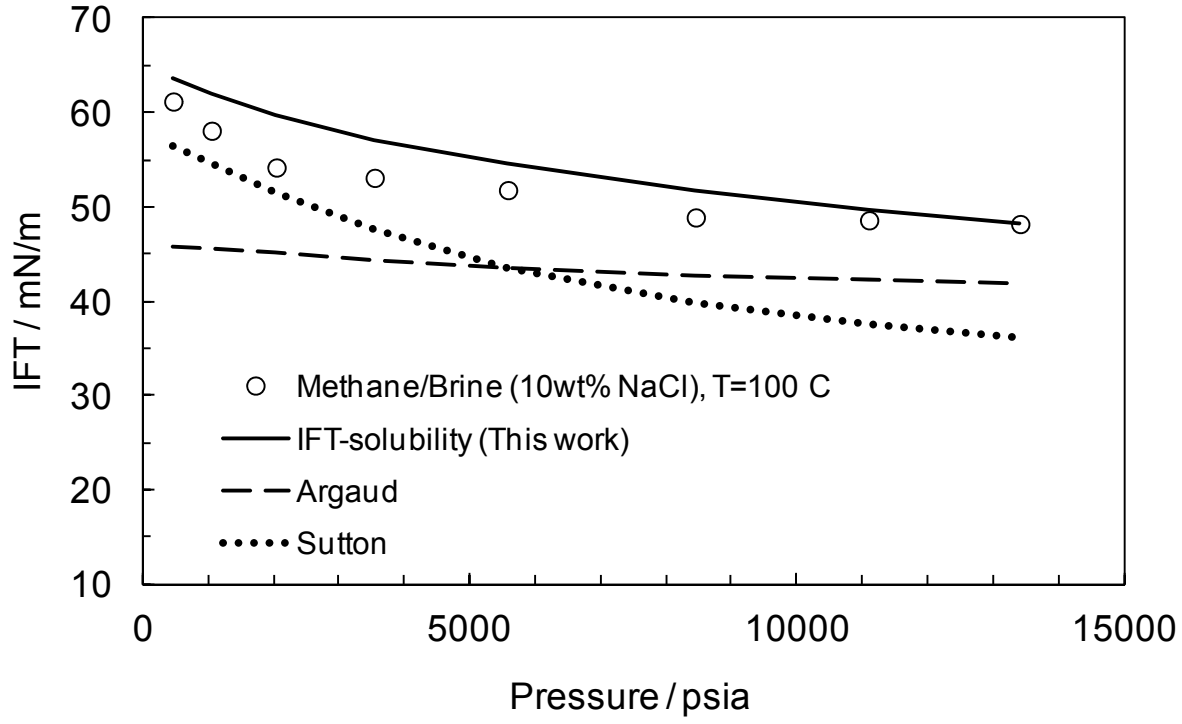

Figure 6.18 Comparison of different IFT prediction methods against experimental methane-brine (10 wt% NaCl solution) IFT data (this work) at 100 °C

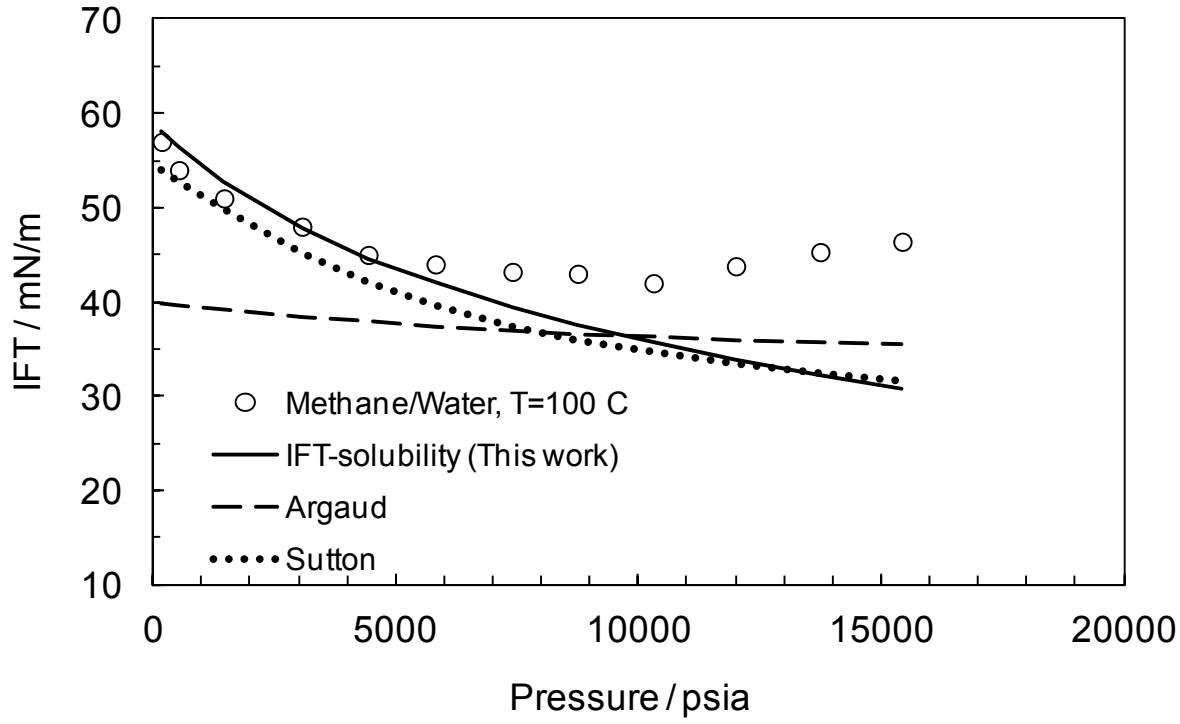

Figure 6.19 Comparison of different IFT prediction methods against experimental methane-water IFT data (this work) at 100 °C

The IFT-solubility method showed promising results in predicting IFT of the mentioned systems especially at temperatures below 200 °C. This method gave better prediction results in comparison with other techniques at the range of temperature that the coefficient of IFT-solubility correlation was tuned (up to 175 °C).

6.4.3 *Salt Effect on IFT*

The generated interfacial tension data on methane-brine (water) are plotted in Figures 6.2 to 6.4. In order to study the effect of salt closely, these series of IFT data were plotted for each temperature in separate graphs (Figures 6.20 to 6.23). As it can be clearly seen from these figures, addition of salt to water causes an increase in IFT of the study systems. By comparing these graphs, it is identified that the salt influence on IFT (or rate of increasing IFT by salt concentration) decreases at higher temperatures.

To quantify the above observation, the average of methane-brine IFT differences from the methane-water interfacial tension, ΔIFT, against salt concentrations at different temperatures are reported in Table 6.9 (the difference values were taken from Figures 6.20 to 6.23). Presence of 5 wt% NaCl in water causes an increase of about 4 to 2 mN/m at the temperature range of 37.8 to 200 °C in IFT. An increase of 8 to 4 mN/m is observed for the same range of temperature for IFT of methane and 10 wt% NaCl solutions.

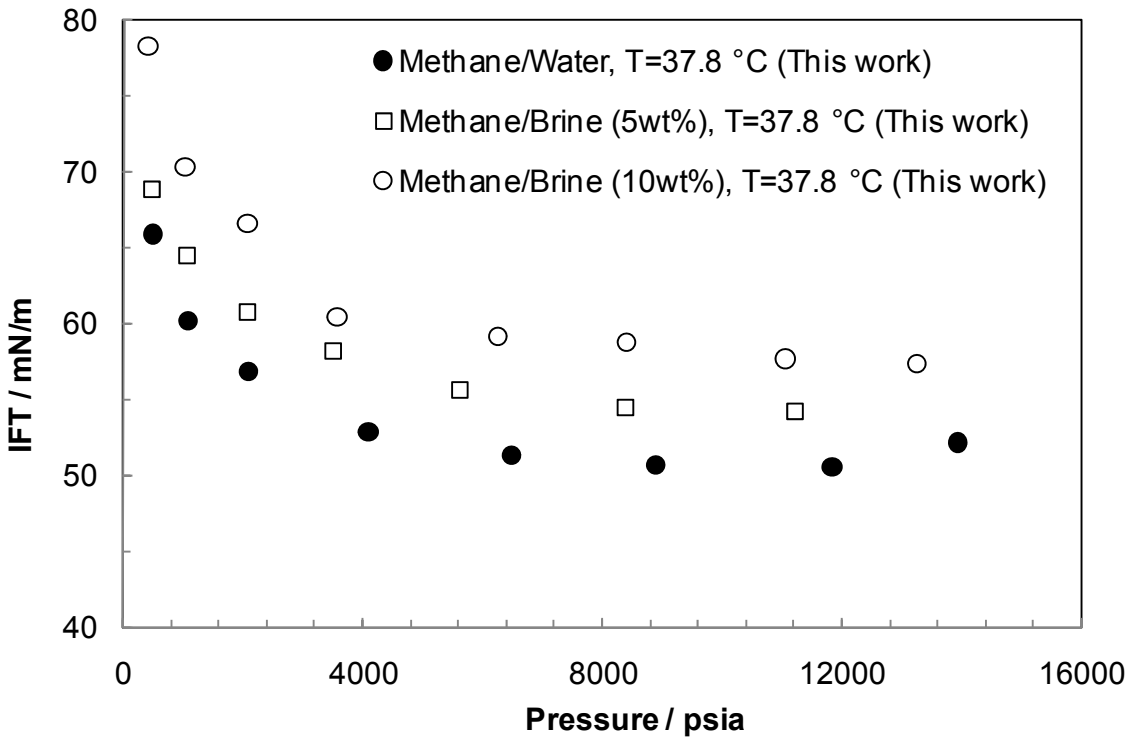

Figure 6.20 Experimental IFT data of methane-brine (water) at 37.8 °C generated in this work.

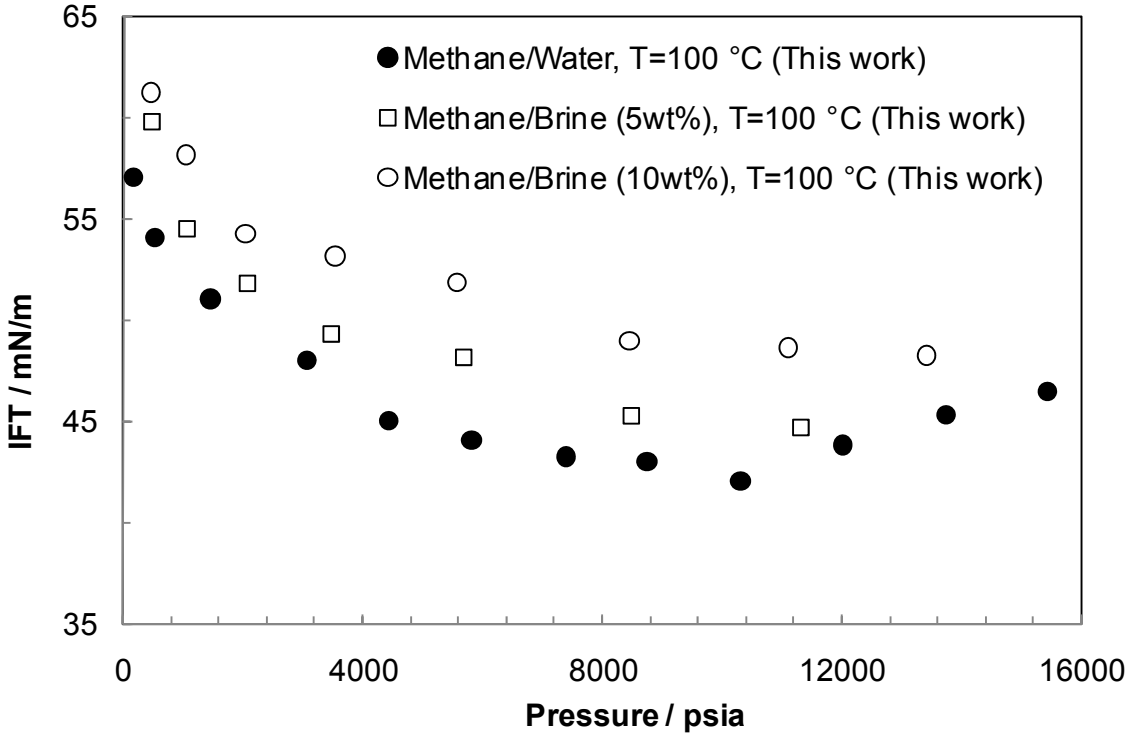

Figure 6.21 Experimental IFT data of methane-brine (water) at 100 °C generated in this work.

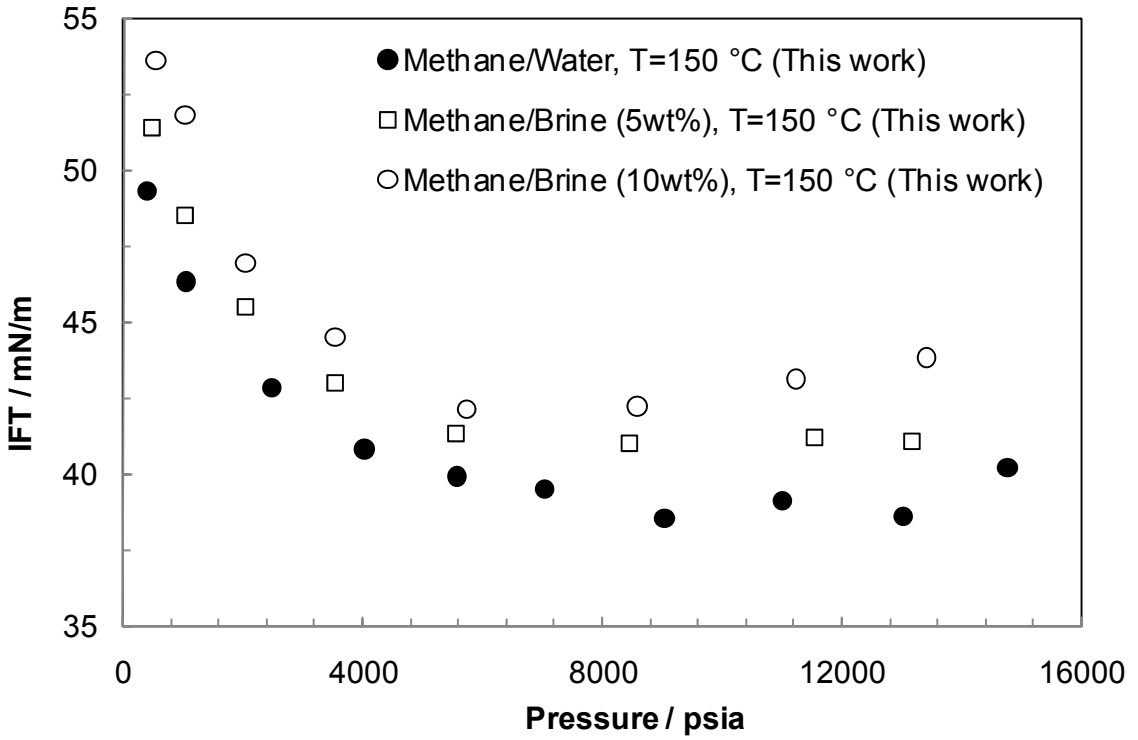

Figure 6.22 Experimental IFT data of methane-brine (water) at 150 °C generated in this work.

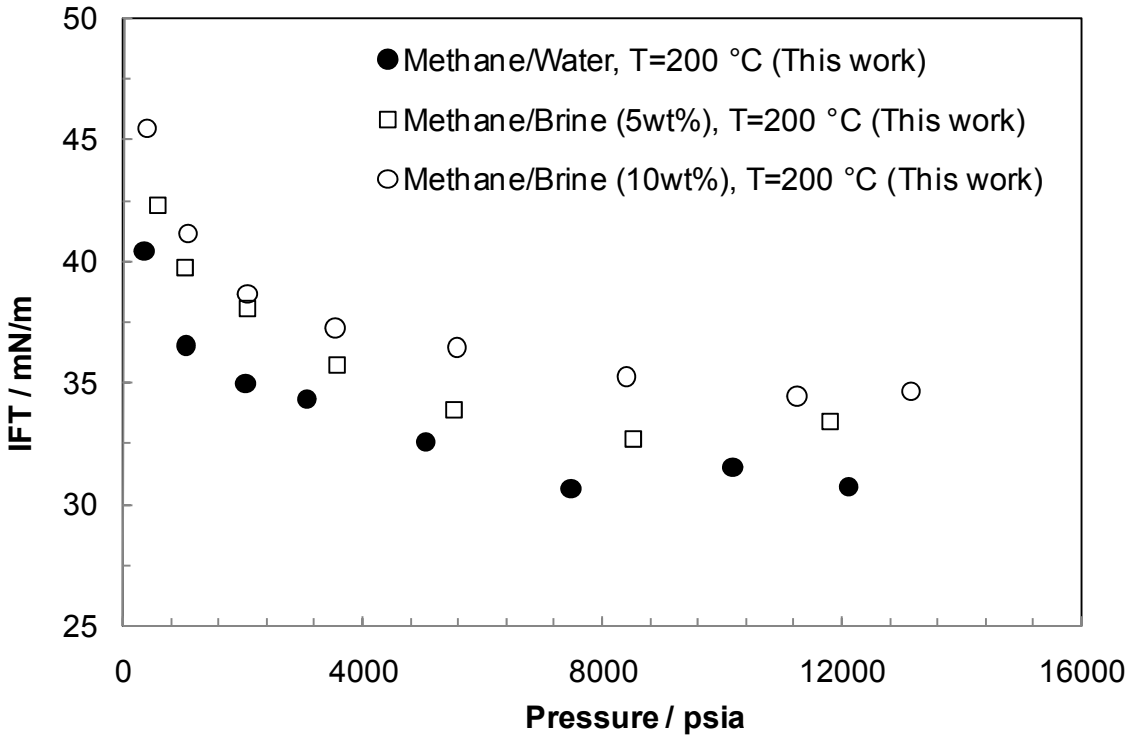

Figure 6.23 Experimental IFT data of methane-brine (water) at 200 °C generated in this work.

Table 6.9 The average of methane-brine IFT difference from the IFT of methane-water, ΔIFT, against salt concentrations at different temperatures (taken from Figures 6.19 to 6.22)

IFT Systems	Temperature (°C)	Average ΔIFT (mN/m)
Methane-Brine (5 wt% NaCl)	37.8	4
	100	3
	150	2
	200	2
Methane-Brine (10 wt% NaCl)	37.8	8
	100	6
	150	4
	200	4

One of the main reasons for the increase in the IFT of gas-brine by addition of salt is due to the density difference (Δρ) increase of the adjacent phases. The density difference (NIST web book) is plotted for the tested fluids at 200 °C in Figure 6.24. This also can be explained from the physical point of view and force balances, as the higher density difference would apply higher interfacial tension to obtain a physical balance (when the gas bubble is suspended in the heavy phase).

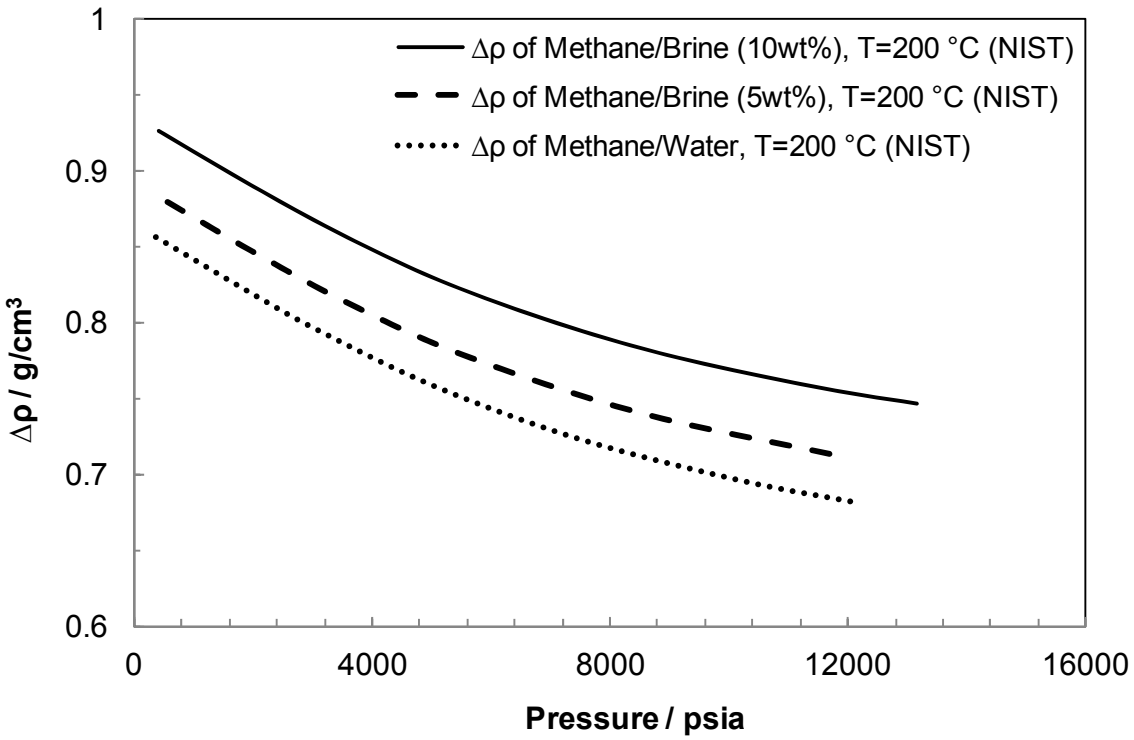

Figure 6.24 Density difference (Δρ) against pressure at 200 °C for the adjacent phases employed in interfacial tension calculation of the experimented fluids reported in present study (density data were taken form NIST)

Bubble (droplet) dimensions, d_e and d_s, (which were detailed in Chapter 2) are the other parameters that were considered in this study. The equatorial diameter (d_e) when plotted vs pressure, showed a minimum in almost all measurements. Figure 6.25 illustrates these minimums for methane-brine (water) systems at 37.8 °C. This minimum can also be observed for all data sets of brine with 5 wt% salt concentration which is depicted in Figure 6.25. These minimums were seen for other ranges of temperatures that were studied in this work. However, the observed minimum for d_s, is not as noticeable as the one for d_e and actually it remained roughly flat for the range of pressure for almost all systems and temperatures (Figure 6.26).

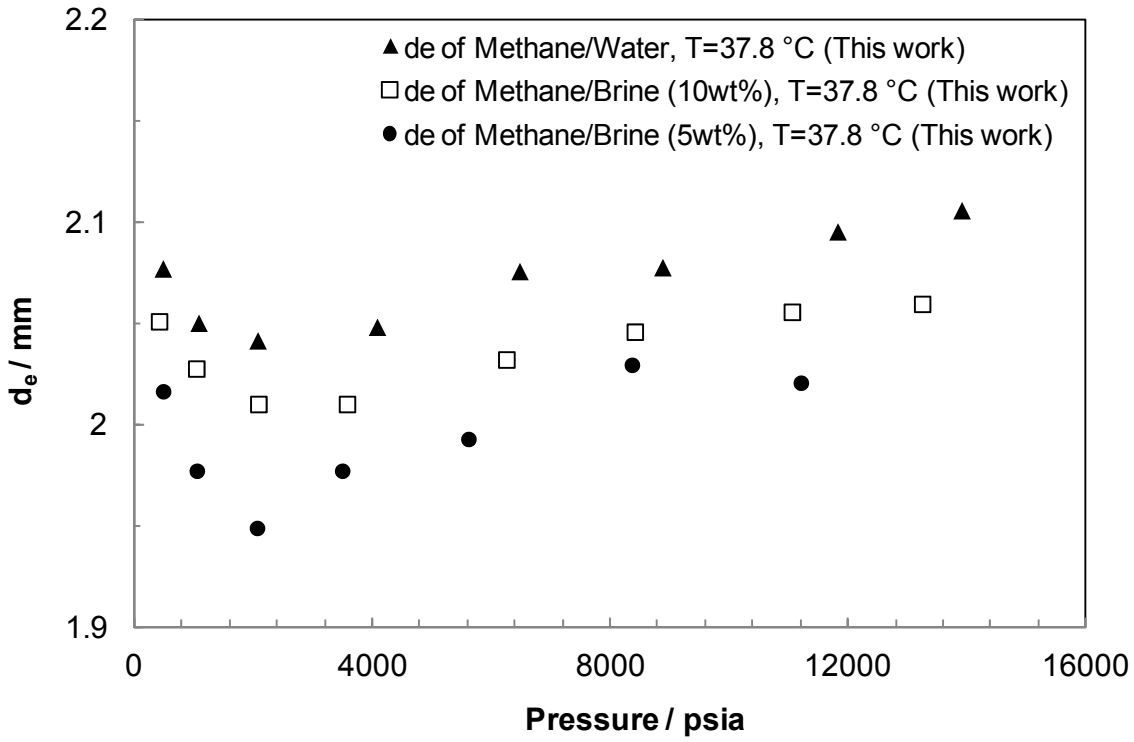

Figure 6.25 The measure equatorial diameter, d_e, against pressure during IFT measurements of methane-brine (water) systems at 37.8 °C (this work). As it can be seen, there are minimums for d_e.

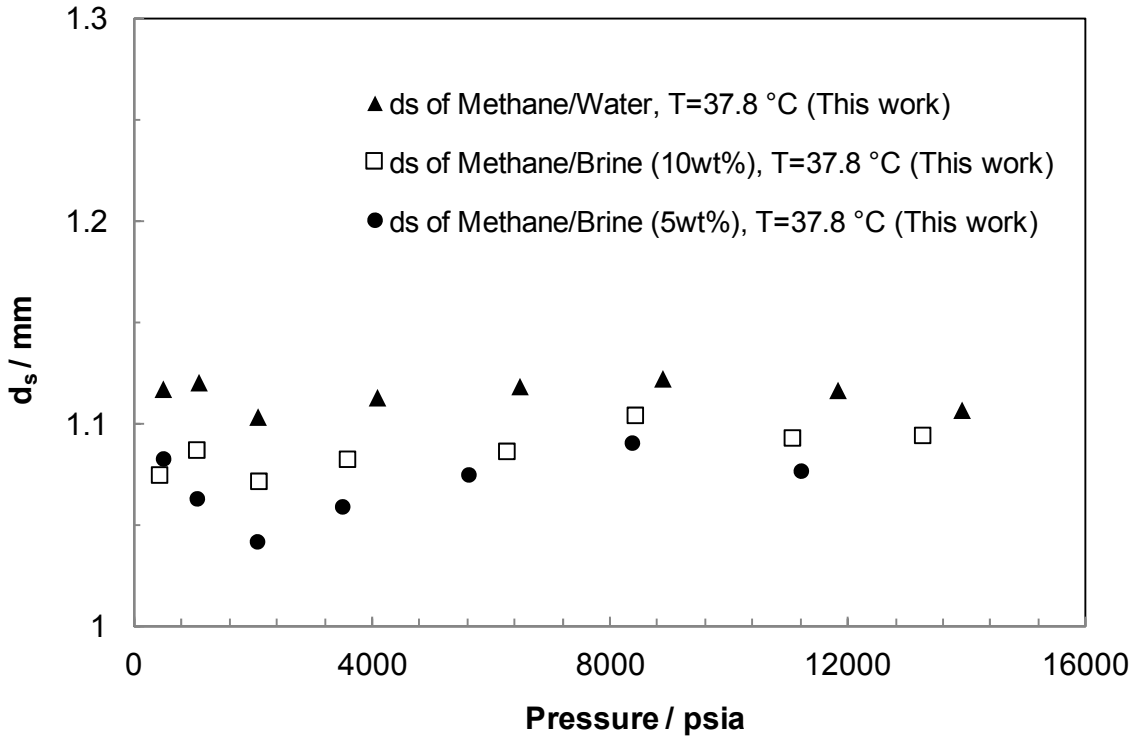

Figure 6.26 The obtained d_s values against pressure during IFT measurements of methane-brine (water) systems at 37.8 °C (this work). As it can be seen, there are minimums for d_s.

6.4.4 *A Comparison of the Two Methods*

As reported in Section 6.2.1, the pendant drop method was employed to measure methane-water IFT at 100, 150 °C. To have a cross check the interfacial tension measurement methods employed in this work (i.e. rising bubble and pendant drop methods) some IFT tests were also conducted on methane-water system at 100 and 150 °C using rising bubble technique (Figures 6.27 and 6.28).

The IFT values obtained with pendant drop method appear to be larger in comparison with rising bubble method. The difference in IFT measurements for two methods at 100 and 150 °C are about 5% and 3%, respectively.

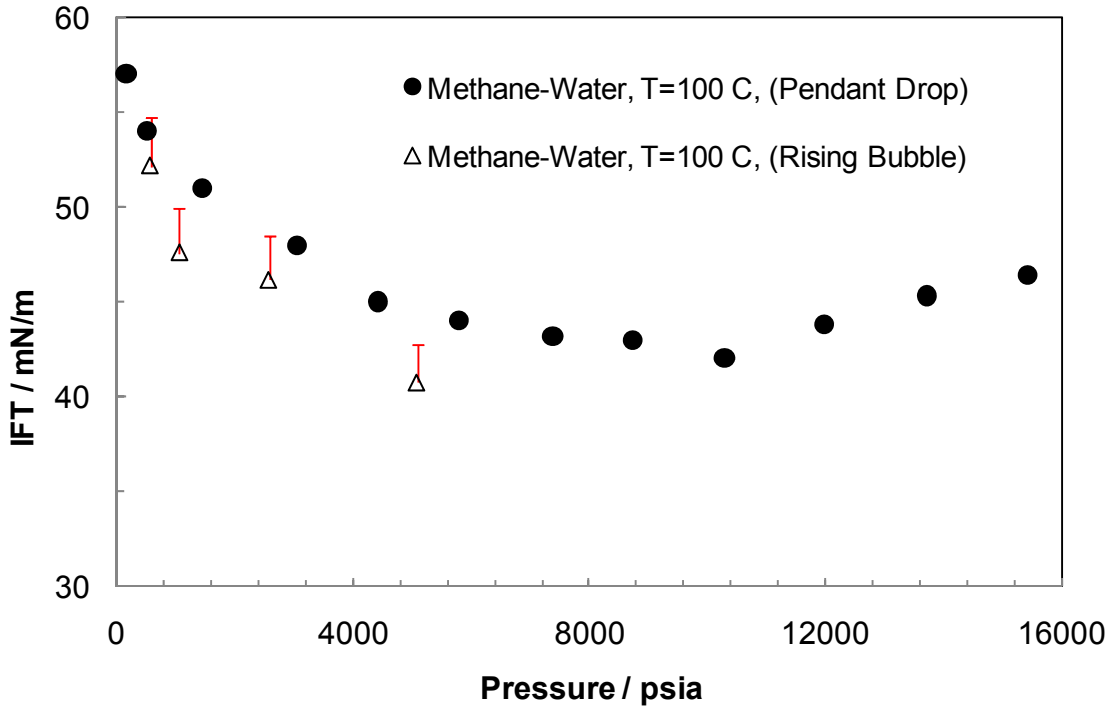

Figure 6.27 Comparison of different IFT measurements methods, pendant drop and rising bubble, for methane-water system. The IFT results obtained by rising bubble method are about 5% lower than the one with pendant drop at 100 °C.

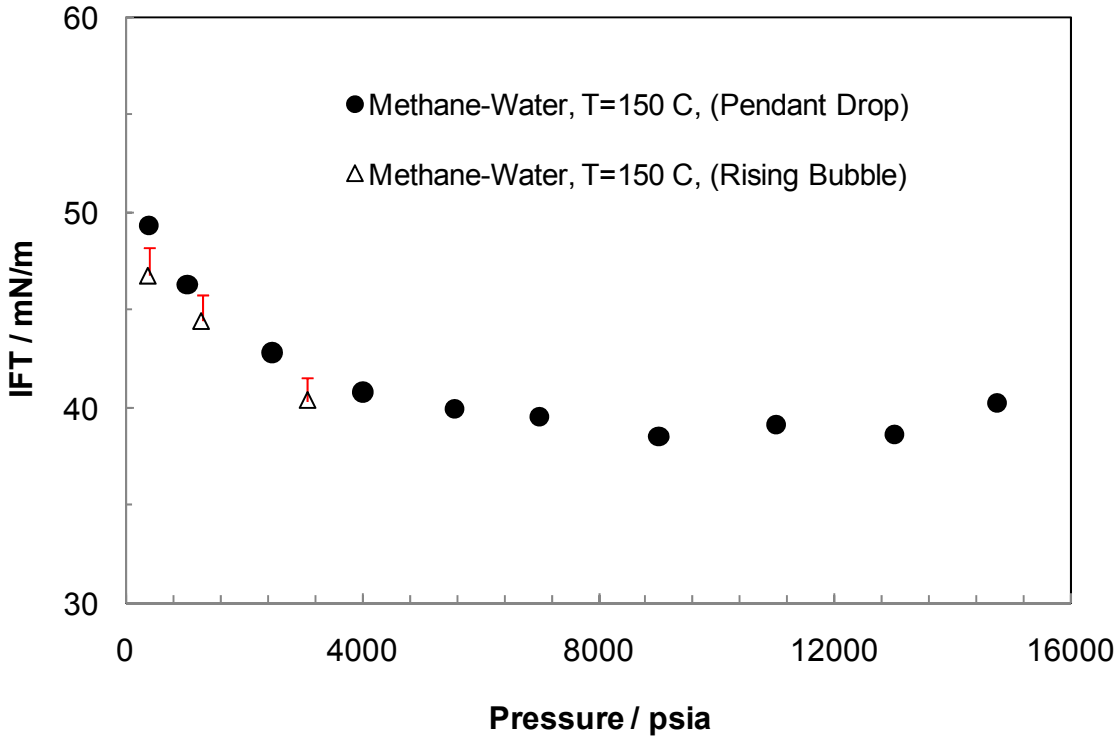

Figure 6.28 Comparison of different IFT measurements methods, pendant drop and rising bubble, for methane-water system. The IFT results obtained by rising bubble method are about 3% lower than the one with pendant drop at 150 °C.

6.5 Conclusions

It was shown that the interfacial tension of gas-water (brine) systems approaches water surface tension at zero solubility. Using this observation, a new technique (IFT-solubility correlation) was developed in this chapter to predict the IFT of gas-water (brine) systems. The common gases in petroleum industry such as methane, ethane, propane, nitrogen, carbon dioxide and hydrogen sulphide were studied. There is no limitation on the number of components as it can be simply extended to predict the IFT of gas mixtures. The required parameters are water surface tension (or brine surface tension), solubility of gas in water (or brine) and the proposed parameters ($A_{I\text{-}S}$) that relate the IFT and solubility. The results show that this method predicts the IFT of various multi-component gas-water systems with reasonable accuracy and was superior to the other investigated methods for the tested systems.

Experimental measurements of interfacial tension of methane-brine were also made as part of this study. The generated methane-brine interfacial tension data were employed to evaluate the performance of the IFT-solubility method in estimating IFT of methane-brine system with promising results.

Addition of salt to water leads to an increase in the IFT of the studied systems. The effect of salt on IFT showed a decreasing trend from the lowest temperature of experiment (37.8 °C) to the highest temperature (200 °C). For instance, an increase of about 8 mN/m in IFT was observed (at 37.8 °C and 10 wt% brine solution) while it dropped to 4 mN/m at 200 °C and the same salt concentration.

References

Abdullah, A. and Amin, R., 2009, *Experimental Investigation of Interfacial Interactions of Condensate/Brine/SC-CO2 Systems at High Pressure and High Temperature Conditions*, International Petroleum Technology Conference, SPE **13082-MS**

Argaud, M.J., 1992, *Predicting the Interfacial Tension of Brine/Gas (or Condensate) System*, paper SCA, European Core Analysis Symposium, Paris, September 14-16

Avlonitis, D., Danesh, A. and Todd, A. C., 1994, *Prediction of VL and VLL equilibria of mixtures containing petroleum reservoir fluids and methanol with a cubic EoS,* Fluid Phase Equilib., **94**, 181-216

Ayirala, S.C. and Rao, D.N., 2006, *Solubility, miscibility and their relation to interfacial tension in ternary liquid systems*, Fluid Phase Equilibria **249**, 82-91

Bachu, S. and Bennion, D.B., 2009, *Interfacial Tension between CO2, Freshwater, and Brine in the Range of Pressure from (2 to 27) MPa, Temperature from (20 to 125) °C, and Water Salinity from (0 to 334 000) mg/L*, J. Chem. Eng. Data, **54**, 765–775

Badakhshan, A. and Bakes, P., 1990, *The Influence of Temperature and Surfactant Concentration on Interfacial Tension of Saline Water and Hydrocarbon Systems in Relation to Enhanced Oil Recovery by Chemical Flooding,* unsolicited paper SPE **20295**

Bahramian, A. and Danesh, A., 2004, *Prediction of liquid–liquid interfacial tension in multi-component systems*, Fluid Phase Equilibria, 221, 197–205

Bahramian, A. and Danesh, A., 2005, *Prediction of liquid–vapour surface tension in multi-component systems*, Fluid Phase Equilibria **236**, 156–161

Bennion, D.B. and Bachu, S., 2008, *A Correlation of the Interfacial Tension between Supercritical Phase CO2 and Equilibrium Brine as a Function of Salinity, Temperature and Pressure*, SPE **114479**

Burgess, M. P. and Germann, R. P., 1969, *Physical Properties of Hydrogen Sulfide Water Mixtures*, AIChE J., **15**, 272-275

Cai, B., Yang, J., and Guo, T., 1996, *Interfacial Tension of Hydrocarbon + Water/Brine Systems under High Pressure*, J. Chem. Eng. Data, **41**, 493-496

Chapoy, A., Mohammadi, A.H. and Tohidi, B., 2005, *Experimental Measurement and Phase Behavior Modeling of Hydrogen Sulfide-Water Binary System*, Ind. Eng. Chem. Res., **44**, 7567-7574

Chapoy, A., Mohammadi, A.H., Chareton, A., Tohidi, B. and Richon, D., 2004, *Measurement and Modeling of Gas Solubility and Literature Review of the Properties for the Carbon Dioxide-Water System*, Ind. Eng. Chem. Res., **43**, 1794-1802

Chiquet, P., Daridon, J., Broseta, D. and Thibeau, S., 2007, *CO2/water interfacial tensions under pressure and temperature conditions of CO2 geological storage*, Energy Conversion and Management **48,** 736–744

Danesh, A., 1998, *PVT and Phase Behaviour of Petroleum Reservoir Fluids*, Elsevier, Amsterdam

Dittman, G. L., 1977, *Calculation of Brine Properties*, Lawrence Livermore Laboratory, http://www.osti.gov/bridge/servlets/purl/7111583-l9lvkU/native/7111583.pdf

Duffy, J. R., Smith, N.O. and Nagy, B., 1961, *Solubility of Natural Gases in Aqueous Salt Solutions. 1. Liquidus Surfaces in the System CH4–H2O–NaCl–CaCl2 at Room Temperatures and at Pressures Below 1000 Psia*, Geochim. Cosmochim. Ac., **2**, 1-2, 23-31

Firoozabadi, A. and Ramey Jr., H.J., 1988, *Surface Tension of Water-Hydrocarbon Systems at Reservoir Conditions*, J. Canadian Petroleum Tech., **27**, 41-48

Galindo, A., Gil-Villegas, A., Jackson, G. and Burgess, A.N., 1999, *SAFT-VRE: Phase behavior of electrolyte solutions with the statistical associating fluid theory for potentials of variable range*, J. Phys. Chem. B, **103**, 10272–10281

Hebach, A., Oberhof, A., Dahmen, N., Kgel, A., Ederer, H. and Dinjus, E., 2002, *Interfacial Tension at Elevated Pressures Measurements and Correlations in the Water + Carbon Dioxide System*, J. Chem. Eng. Data, **47**, 1540-1546

Herrick, C.S. and Gaines, G.L., 1973, *Surface Tension of Saturated Anhydrous Hydrogen Sulfide and the Effect of Hydrogen Sulfide Pressure on the Surface Tension of Water,* The J. of Physical Chemistry, **77**, 22

Hough, E.W., Rzasa, M. J. and Wood, B.B., 1951, *Interfacial Tension at Reservoir Pressures and Temperatures; Apparatus and the Water Methane System*, Petroleum Trans., AIME, **192**, 57-60

Ikeda, N., Aratono, M. and Motomura, K., 1992, *Thermodynamic Study on the Adsorption of Sodium Chloride at the Water/Hexane Interface,* J. of Colloid and Interface Sci., **149**, 1 208-215

Jho C, Nealon D, Shogbola S and King A.D., 1978, *Effect of pressure on the surface tension of water: Adsorption of hydrocarbon gases and carbon dioxide on water at temperature between 0 and 50°C.*, J Colloid Interface Sci., **65**, 141–63

Jennings, H.Y. and Newman, G.H., 1971, *The Effect of Temperature and Pressure on the Interfacial Tension of Water against Methane-Normal Decane Mixtures*, SPE **3071**

Kritschewsky, I.R., Shaworonkoff, N.M. and Aepelbaum, V.A., 1935, Phys. Chem. A **175,** 232–238

Kvamme, B., Kuznetsova, T., Hebach, A., Oberhof, A. and Lunde, E., 2007, *Measurements and modelling of interfacial tension for water + carbon dioxide systems at elevated pressures*, Computational Materials Science, **38**, 506–513

Lee, S.T. and Chien, M.C. H., 1984, *New Multicomponent Surface Tension Correlation Based on Scaling Theory*, Fourth Symposium on EOR, Tulsa Oklahoma, SPE/DOE, 12643

MacLeod, D.B, 1923, *On a relation Between Surface Tension, Density*, Trans. Faraday Soc., **19**, 38-43

Nasr-El-Din, H.A., Al-Otaibi, M.B., Al-Aamri, A.M. and Ginest, N., 2005, *Surface Tension of Completion Brines*, SPE International Symposium on Oilfield Chemistry, **93421-MS**

Niedrehauser, D.O. and Bartell, F.E., 1947, *A Corrected Table for Calculation of Boundary Tensions by Pendant Drop Method*, Research on Occurrence and Recovery of Petroleum, A Contribution from API Research Project, **27**, 114-146

Plocker, U. J., Knapp, H. and Prausnitz. J. M., 1978, *Calculation of high pressure vapor-liquid equilibria from a corresponding-states correlation with emphasis on asymmetric mixtures*, Ind. Eng. Chem. Proc. Des. Dev., **17**, 3, 324-322

Ren, Q., Chen, G., Yan, W. and Guo, T., 2000, *Interfacial Tension of (CO2 + CH4) + Water from 298 K to 373 K and Pressures up to 30 MPa*, J. Chem. Eng. Data, **45**, (4), 610-612

Reservoir Fluid Studies, Final Report, 1999-2002, Institute of Petroleum Engineering, Heriot-Watt University, Report No.: PVT/03/1

Rushing, J.A., Newsham, K.E., Van Fraassen, K.C., Mehta, S.A. and Moore, G.R., 2008, *Laboratory Measurements of Gas-Water Interfacial Tension at HP/HT Reservoir Conditions*, SPE **114516**

Sachs, W., and Meyn, V., 1995, *Pressure and temperature dependence of the surface tension in the system natural gas/water, Principles of investigation and the first precise experimental data for pure methane/water at 25 °C up to 46.8 MPa*, Physicochcmical and Engineering Aspects **94**, 291-301

Scott, R.L. and van Konynenburg, P.H., 1980, Philos. Trans. R. Soc. 298, 495–594

Selleck, F. T., Carmichael, L. T. and Sage, B. H., 1952, *Phase Behavior in the Hydrogen Sulfide-Water System*, Ind. Eng. Chem., **44**, 2219-2226

Schmidt, K. A. G., Folas, G. K. and Kvamme, B., 2007, *Calculation of the interfacial tension of the methane–water system with the linear gradient theory*, Fluid Phase Equilibria, **261** 230–237

Shah, V., Broseta, D., Mouronval, G. and Montel, F., 2008, *Water/acid Gas Interfacial Tensions and their Impact on Acid Gas Geological Storage*, International Journal of Greenhouse Gas Control, **2**, 594 – 604

Sun, C., Chen, G., and Yang, L., 2004, *Interfacial Tension of Methane + Water with Surfactant near the Hydrate Formation Conditions*, J. Chem. Eng. Data, **49** (4), 1023-1025

Sutton, R.P., 2009, *An Improved Model for Water-Hydrocarbon Surface Tension at Reservoir Conditions*, SPE **124968**

Valderrama JO, 1990, *A Generalized Patel-Teja Equation of State for Polar and Non-Polar Fluids and their Mixtures*, J. Chem. Eng. Jpn. **23**, 87-91

Vargaftik, N. B., Volkov, B. N. and Voljak, L. D., 1983, *International tables of surface tension water*, J. Phys. Chem. Ref. Data, **12** (3), 817-820

Wiegand, G., Franck, E. U., 1994, *Interfacial tension between water and non-polar fluids up to 473 K and 2800 bar*, Berichte der Bunsengesellschaft für physikalische Chemie, **98** (6), 809–817

Weinaug, C. F. and Katz, D. L., 1943, *Surface Tension of Methane - Propane Mixtures*, I & EC, **35**(2), 239 - 246

Yan, W, Zhao, G., Chen, G. and Guo, T., 2001, *Interfacial Tension of (Methane + Nitrogen) + Water and (Carbon Dioxide + Nitrogen) + Water Systems*, J. Chem. Eng. Data, **46**, 1544-1548

Yarym-Agaev, N.L., Sinyavskaya, R.P., Koliushko, I.I. and Levinton, LY., 1985, Zh Prikl. Khim., **58**, 165-168

CHAPTER 7

CONCLUSIONS AND RECOMMENDATIONS FOR FUTURE WORK

7.1 Introduction

In this thesis, two very important physical properties of reservoir fluids, viscosity and interfacial tension, were investigated. The present research focused on both experimental and modelling aspects of viscosity and interfacial tension for a wide variety of hydrocarbon systems including pure and multi-component alkanes and real reservoir fluids such as natural gas, gas condensate and dead oil. The effect of water, brine and mud filtrate on the above mentioned properties were also considered. A summary of the main outcomes are highlighted below.

- A series of new viscosity experimental data at HPHT conditions was generated on three binary hydrocarbons and three multi-component mixtures (Chapter 3). The results were employed to assess several viscosity prediction techniques appropriate for extreme conditions.
- The experimental viscosity data generated in this work were used to evaluate and compare the capability of viscosity prediction techniques. In addition, new/modified methods were developed and evaluated as part this work (Chapter 3).
- In order to study the influence of oil-based drilling mud filtrate (as a contaminant) on the viscosity of dead oils, viscosity measurements were conducted on three different crude oils and on various intentionally contaminated fluids (Chapter 4).
- A new approach to estimate the viscosity of original oil (uncontaminated) from contaminated samples was introduced (Chapter 4). To investigate the efficiency of this technique, the experimental viscosity data for different crudes in the original and contaminated states (with oil-based mud) were evaluated using different viscosity models (detailed in Chapter 3).
- A series of viscosity tests to quantify the effect of dissolved water on the viscosity of hydrocarbon mixtures at HPHT conditions was performed systematically (Chapter 5). For this purpose, various quantities of water (dissolved in

hydrocarbon) were added to six different hydrocarbon fluids and experiments were conducted at wide range of pressure and temperature.

- A novel technique to predict the interfacial tension of gas-water (brine) systems using the solubility of gas in water (brine) was proposed (Chapter 6). Gases such as methane, ethane, propane, nitrogen, carbon dioxide and hydrogen sulphide were employed to develop the method (named IFT-solubility correlation). The method was then generalised to estimate the IFT of gas mixture-water systems.
- New IFT experimental data on methane-brine systems were generated to study the effect of salt on interfacial tension (Chapter 6). The experiments covered wide range of pressure, temperature and salt concentrations. The reliability of the IFT-solubility correlation was examined using the IFT data for methane-brine which were reported in this thesis.

Experimental data and modelling work on viscosity and interfacial tension have been detailed in the preceding chapters of this thesis. In light of the knowledge obtained during the course of present research, some conclusions and recommendations for further work are stated below.

7.2 Experimental Results

In order to evaluate, improve and propose predictive models to calculate viscosity and interfacial tension, experimental data were gathered from open sources (Chapters 3 and 6). However, there were still some gaps in the literature for experimental data, particularly at high pressure and high temperature conditions. Viscosity experiments were therefore conducted on different reservoir fluids at high pressure and high temperature conditions (detailed in Chapter 3) and the influence of oil-based drilling mud filtrate on the viscosity of crudes was also investigated experimentally (Chapter 4). The effect of dissolved water on the viscosity of hydrocarbons at HPHT conditions was then investigated (Chapter 5). Due to limited amount of IFT data on gas-brine systems in literatures, interfacial tension measurements were made on methane-brine to evaluate the effect of salt on IFT (reported in Chapter 6). The conclusions drawn from the experimental work of this thesis are presented here.

7.2.1 *Viscosity*

Experimental viscosity data at HPHT conditions: These sets of data appear to be inadequate in the literature for various hydrocarbon mixtures. Extreme pressure and temperature conditions in hydrocarbon reservoirs result in higher costs in an oilfield development. So, generating more data on physical properties of reservoir fluids is of great importance to enable the related processes to be designed in an optimum manner.

- In order to extend the information on viscosity of hydrocarbons at high temperature and high pressure conditions and also to improve existing (and potentially propose new viscosity) models, a wide range of experiments on various fluids was conducted. The capillary tube in the HPHT set-up was used for this series of viscosity measurements (described in Chapter 2). The selected study fluids were:
    - Methane-heptane
    - Methane-decane
    - Methane-toluene
    - Natural gas
    - Gas condensate
    - Synthetic volatile oil

  Extensive viscosity data were generated at temperatures of 50, 100, 150 and 200 °C and at pressures up to 20,000 psia. The typical behaviour of hydrocarbon viscosity (increasing with an increase in pressure and a decrease in temperature) was observed over the experimental range. The results of this study are presented in Chapter 3.

Viscosity of contaminated samples: Valuable information on phase behaviour and physical properties of reservoir fluids can be obtained by sampling during the drilling operation. Oil-based mud filtrates are commonly employed in drilling operations. Since the miscibility of oil-based mud filtrate in reservoir fluids can result in contamination of the samples taken, the original fluid properties, and in particular the viscosity of samples can be drastically affected. So investigating the influence of this contaminant on viscosity would be very important.

- A mineral oil-based mud filtrate, named DMF-4, was selected to study the influence of mud filtrate on viscosity of dead oils. Viscosity measurements were performed with a rolling ball viscometer. Three different dead oils were chosen from different geographical locations:

- North Sea
- Norway
- West of Africa

Measurement technique and fluids description were detailed in Chapter 2. These crudes were intentionally contaminated with various levels (from 10 to 75 wt%) of mineral oil-based mud. The viscosity experiments were performed on the crudes, the contaminated samples and also on the filtrate in the temperature range of 20 to 72 °C at atmospheric pressure. The tests covered a viscosity range from about 1 to 1095 cP (Chapter 4).

The changes in viscosity of dead oils with the addition of mud filtrate were examined by comparing the viscosity of the original (uncontaminated) dead oil with the contaminated samples. It was observed that blending a small amount of oil-based mud filtrate with dead oil can change the viscosity of a clean sample considerably. The changes in the viscosity of the crudes, in this study when mixed with filtrate, displayed different patterns. This indicates that addition of the same amount of filtrate had various effects on the viscosity of the contaminated samples. For example, at the temperature of about 20 °C, addition of 25 wt% DMF-4 to the North Sea dead oil decreased the viscosity of the crude from 12.87 to 9.07 cP i.e., a viscosity ratio of 1.4 (viscosity of original crude/ viscosity of contaminated sample), while the ratios of decrease were much larger at 6.5 (i.e., from 47 to 305 cP) and 17.2 (from 1096 to 63.5 cP) for Norwegian and West African crudes, respectively. The generated data in this research were employed to develop a new technique for prediction of clean fluid viscosity, outlined in Chapter 4.

Influence of dissolved water on viscosity: At high temperature conditions the impact of dissolved water on viscosity is of interest in view of the facts that water is almost always part of the reservoir fluid and will be more soluble in the hydrocarbon phase at extreme conditions.

- A wide range of experiments was carried out systematically to investigate the influence of dissolved water on the viscosity of hydrocarbon mixtures at HPHT conditions. Binary mixtures of methane with *n*-heptane, *n*-decane and toluene and also three multi-component systems: gas condensate, natural gas and a synthetic volatile oil which were mixed with various amount of water (2 mole%, 5 mole%

and saturated with water) were selected. This series of experiments were planned following a previous study (Gozalpour *et al.* 2005) which reported a drastic change in viscosity with addition of water (around 5 mole%) to a synthetic volatile oil.

These experimental measurements showed the presence of water to have only a small effect on the viscosity of the three binary species studied. The effect of dissolved water on viscosity of gas condensate, natural gas and synthetic volatile oil which were saturated with water at HPHT conditions was also studied. This effect was more significant in the gas phase rather than the liquid, which could be due to the presence of more water in the gas than the liquid phase and also could be due to the fact that liquid viscosity is closer to water viscosity (reported in detail in Chapter 5). Despite the results reported in the literature (Gozalpour *et al.* 2005), no significant increase in the viscosity of saturated synthetic volatile oil with water was observed.

7.2.2 *Interfacial Tension*

Effect of salt on IFT of methane-brine: The presence of salt in the aqueous phase can change the interfacial tension between the water (brine) and the hydrocarbon phases. The addition of salt raises the interfacial tension of gas-water system. A number of data sets on IFT of gas-water systems can be found in literature. However, there are very limited IFT experimental data for gas-brine hydrocarbon systems, to investigate the effect of salt.

- Experimental interfacial tension data were generated in the salt compatible HPHT cell. The experiments were performed to quantify the effect of salt concentration on the IFT of a gas-brine system and particularly a methane-brine system. Two concentrations of sodium chloride, 5 and 10 wt%, were dissolved in water to make the brine solutions. Also IFT measurements were carried out on a methane-water system to study the effect of salt addition. The interfacial tension tests were carried out at 37.8, 100, 150 and 200 °C. The effect of salt in increasing IFT showed a decreasing trend from the lowest temperature of experiment (37.8 °C) to the highest temperature (200 °C). For instance, an increase of about 8 mN/m in IFT was observed at 37.8 °C and 10 wt% brine solution, while it dropped to 4 mN/m at 200 °C and the same concentration of salt. At each temperature, the effect of pressure on the IFT of each system decreases by increasing pressure. (Reported in Chapter 6).

7.3 Modelling Work

The proposed viscosity prediction techniques and models were evaluated against independent experimental data generated in this work as well as methods from open sources (Chapter 3). Also a new approach to retrieve the viscosity of the original fluid (clean dead oil) from a contaminated sample was introduced (Chapter 4). To predict the interfacial tension of gas-water (brine), a novel technique was presented (Chapter 6). The conclusions that can be drawn from the modelling study are outlined below.

7.3.1 *Viscosity*

Viscosity predictive methods: Several techniques to predict the viscosity of reservoir fluids are currently employed by petroleum industry. Obviously, making measurements of physical properties for various fluids under a broad range of pressure and temperature conditions would be almost impossible. Therefore, developing and evaluating predictive techniques for consistent estimation of viscosity is a growing need.

- To investigate several viscosity prediction models, the generated viscosity data (Chapter 3) were used to compare the capability of viscosity prediction techniques, including the LBC (Lohrenz *et al.* 1964), the Pedersen correlations (Pedersen *et al.* 1984, 1987) and HW2 (Al-Syabi *et al.* 2001). In addition, some new methods were developed and evaluated as part this work, which included a simple correlation incorporating the effects of temperature, pressure, molecular weight and density (TPMD), a residual viscosity correlation method (modified Fenghour) and an artificial neural network (ANN) technique (Chapter 3).

  Among the evaluated models, the Pedersen, LBC and HW2 methods showed better predictions. The ANN and TPMD can be reliable in viscosity estimation only if they are used in the range of tuned conditions and parameters such temperature, pressure and molecular weight. However, the modified Fenghour method showed prediction with acceptable accuracy for the complex fluids examined in Chapter 3.

Viscosity prediction of original fluids: Since it is a challenging and time consuming operation to obtain a contamination-free reservoir fluid sample, accurate predictive models are essential for predicting properties of original fluids from contaminated samples.

- In Chapter 4, a new technique to predict the original fluid viscosity using the viscosity of contaminated samples is introduced. Basically, this new technique was introduced to correct the viscosity prediction results of each viscosity model and was derived from the idea that the deviation of each viscosity model from experimental data for nearly identical fluid is relatively close. In this technique the experimental and predicted viscosity of contaminated sample are compared and a viscosity correction factor (VCF) is defined. If several contaminated samples are available the VCF is plotted against contamination level and the VCF for the original fluid is calculated by extrapolating the VCF to zero contamination. If only one contaminated sample is available, the calculated VCF could be used for predicting the viscosity of original fluid (in particular at low contamination levels). Alternatively, the level of contamination could be deliberately increased to calculate VCF at higher contamination levels. Again, VCF for uncontaminated sample could be calculated from plotting VCF vs. contamination level. It is worth mentioning that the above technique is applicable to all viscosity models.

  To evaluate the reliability of this method, the generated experimental viscosity data for dead oils in the original and contaminated states (detailed in Chapter 4) were compared against different viscosity models. The proposed method can improve the calculated viscosity using various predictive models (described in Chapter 3). The corrected viscosity values, using contaminated fluids, showed an acceptable accuracy and also a good agreement between the experimental viscosity data and the predicted results was achieved.

7.3.2 *Interfacial Tension*

IFT prediction of gas-water (brine): As mentioned above, performing experimental measurements on physical properties for different samples under wide range of conditions is impracticable. In addition, introducing and developing reliable interfacial tension models is needed for calculation of most reservoir processes, like water-gas contact movement, water alternating gas drive, gas-injected enhanced oil recovery and injecting and storing acid gases such as carbon dioxide and hydrogen sulphide.

- It was shown that the interfacial tension of gas-water systems approaches water surface tension at zero solubility. Based on this observation, a novel technique, named IFT-solubility correlation, was developed to predict the interfacial tension of gas-water (brine) systems, outlined in Chapter 6. The common gases in the petroleum industry such as methane, ethane, propane, an inert gas (nitrogen) and two acid gases, carbon dioxide and hydrogen sulphide were studied. There is no limitation on the number of components as the technique can be simply extended to predict the IFT of the gas mixtures. The required parameters are water (or brine) surface tension, solubility of gas in water (or brine) and the proposed parameters ($A_{I\text{-}S}$) that relate the IFT to solubility.

  As part of this study, the IFT-solubility method was evaluated against various multi-component gas-water systems and also the generated methane-brine interfacial tension data. The proposed method predicted the IFT with reasonable accuracy and was superior to the other methods investigated for the systems studied in this work.

7.4 Recommendations for Future Work

- Viscosity experiments carried out at HPHT conditions for various hydrocarbon mixtures (from different binary systems to natural gas, gas condensate and volatile oil). In order to complete the data set at HPHT conditions, performing viscosity tests on more fluid systems is recommended.
- The TMPD and ANN techniques were proposed for viscosity predictions. The correlations showed promising results in the tuned range. It is recommended, for the viscosity range of interest, to incorporate wide range of hydrocarbon systems in order to extend the capability of this technique.
- A series of experiments were performed on crude oils that were intentionally contaminated with a mineral oil-based drilling mud filtrate. More tests can be conducted employing other types of oil-based mud filtrate such as olefin, ester, and linear paraffin. It is also recommended to use heavier crude oils; that means a larger density difference between the contaminant and the dead oil studied.
- The present constants of TPDM and ANN are not appropriate for dead oil viscosity prediction. It is recommended to tune the TPDM and ANN constants for various crudes in order to apply the newly developed technique (prediction of original fluid viscosity from contaminated sample) to these correlations.

- Interfacial tension measurements were made on methane-brine (NaCl solution) system at a wide range of pressure and temperature conditions. It is recommended to perform the experiments on other gas systems and with higher concentrations of salt. Also, considering the effects of other salts such as KCl, $MgCl_2$, $CaCl_2$ and $MgSO_4$ would be of interest for the petroleum industry.
- Okasha *et al.* (2006) have reported different IFT behaviour against temperature for the IFT of dead and live oil with brine in the range of up to 3000 psig and 90 °C. Further investigation is recommended over a wider range of P & T conditions and for various hydrocarbon systems.
- Bagci *et al.* (2001) and Vijapurapu *et al.* (2004) reported IFT experimental results on brine-dead oil systems at different salinity. They reported a minimum in IFT at some salt concentrations. It is recommended to perform a systematic investigation into this effect for various systems and conditions. This would also involve a comprehensive theoretical study.
- The IFT-solubility method showed promising prediction results especially for pressures up to about 7000 psia. It is recommended to improve this method for higher pressure conditions.

References

Al-Syabi, Z., Danesh A., Tohidi, B., Todd, A.C. and Tehrani, A.D., 2001, *A residual viscosity correlation for predicting the viscosity of petroleum reservoir fluids over wide ranges of pressure and temperature*, Chemical Engineering Science, **56**, 6997–7006

Bagci, S., Kok, M. V. and Turksoy, U., 2001, *Effect of Brine Composition and Alkaline Fluid on the Permeability Damage of Limestone Reservoirs*, SPE **65394**

Gozalpour, F., Danesh, A., Fonseca, M., Todd, A.C., Tohidi, B. and Al-Syabi, Z., 2005, *Physical and Rheological Behaviour of High-Pressure/High-Temperature Fluids in Presence of Water*, SPE **94068**

Lohrenz, J., Bray, B.G. and Clark, C.R., 1964, *Calculating Viscosities of Reservoir Fluids from Their Compositions*, J. Pet. Tech. (JPT), 1171-1176

Okasha, T. M., Al-Abbad, M. A. and Al-Shiwaish, A., 2006, *Investigation of the Effect of Temperature and Pressure on Interfacial Tension and Wettability of Shu'aiba reservoir, Saudi Arabia*", GEO 2006 Middle East Conference and Exhibition, Manama, Bahrain, 27-29 March

Pedersen, K. S., Fredensland, Aa., Christensen, P. L. and Thomassen, P., 1984, *Viscosity of Crude Oils*, Chem. Eng. Sci., **39**, 1011-1016

Pedersen, K. S., and Fredenslund, Aa., 1987, *An Improved Corresponding States Model for the Prediction of Oil and Gas Viscosities and Thermal Conductivities,* Chem. Eng. Sci., **42**, 182-186

Vijapurapu, C. S. and Rao, D. N., 2004, *Compositional effects of fluids on spreading, adhesion and wettability in porous media*, Colloids and Surfaces A: Physicochem. Eng. Aspects **241**, 335–342